

Biological Synthesis of Metallic and Metal Sulfide Nanoparticles using Halophilic Archaea and Bacteria

THESIS

Submitted in partial fulfillment
of the requirements for the degree of
DOCTOR OF PHILOSOPHY

by

Pallavee Srivastava

Under the Supervision of
Prof. Meenal Kowshik



BITS Pilani
K K Birla Goa Campus

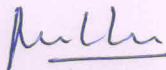


BIRLA INSTITUTE OF TECHNOLOGY AND SCIENCE, PILANI
2016

BIRLA INSTITUTE OF TECHNOLOGY AND SCIENCE, PILANI

CERTIFICATE

This is to certify that the thesis entitled Biological Synthesis of Metallic and Metal Sulfide Nanoparticles using Halophilic Archaea and Bacteria, and submitted by Pallavee Srivastava ID No 2011PHXF002G for award of Ph.D. of the Institute embodies original work done by her under my supervision.



Signature of the Supervisor

Name in capital letters: Dr. MEENAL KOWSHIK

Designation: Associate Professor

Date: 03 NOV 2016

Acknowledgements

First and foremost, I would like to express my sincere gratitude towards my mentor and supervisor, Prof. Meenal Kowshik, for your guidance throughout my Ph.D. work. You have inculcated in me the confidence and the drive required to be an independent thinker and most importantly, the perseverance needed to become a resourceful scientist. You have taught me the significance of perspective to overcome precarious scientific problems. Most importantly, you have instilled in me the importance of working in concert with fellow members of the laboratory. Thank you Ma'am, for your support both scientifically and personally, without which I would have found it difficult to bring this work to a completion.

I would like to thank Prof. Souvik Bhattacharya, current Vice-Chancellor, and Prof. Bijendra Nath Jain, past Vice-chancellor, BITS Pilani; Prof. Sasikumar Punnekkat, Director K K Birla Goa Campus; Late Prof. Sanjeev K Aggarwal and Prof. K. E. Raman Ex-director, Prof. P. K. Das, Associate Dean, ARD; and Prof. S.D Manjare, former in-charge, RCED for all their support and help.

I am sincerely thankful to my Doctoral Advisory Committee (DAC) members, Prof. Utpal Roy and Prof. Judith M. Braganca, for their helpful insights and scientific critiques that have helped me in refining my work. Thanks are also due to present and past Doctoral Research Committee (DRC) Head and members for their guidance and support. I would also like to take this opportunity to express my gratitude towards the HOD, Department of Biological Sciences, both past and present, for all their help and support.

My earnest thanks to the faculty members of Department of Biological Sciences, Prof. Srikanth Mutnuri, Prof. Dibakar Chakrabarthy, Prof. Vijayashree Nayak, Dr. Anusuya Ganguly, Dr. Sumit Biswas, Dr. Angshuman Sarkar, Dr. Veeky Baths, Dr. Malabika Biswas, Dr. Kundan Kumar, Dr. Sukanta Mondol, Dr. Indrani Talukdar, Dr. Raviprasad Aduri, and Dr. Arnab Banerjee for their timely help throughout this work.

I am grateful to Sophisticated Analytical Instrument Facility (SAIF) at IIT Bombay for their assistance in TEM, HR-TEM and SEM-EDS analysis. I would also like to thank Dr. Neha Hebalkar at ARCI, Hyderabad and Mr. Areef Sardar at NIO, Goa for assistance with TEM and SEM analysis, respectively. I am grateful to Dr. Amrita Chatterjee, Department of Chemistry, BITS Pilani, K K Birla Goa Campus for her help with spectrofluorimeter.

I thank Mr. Pratap (ARD), Mrs. Kamna Upadhyay, Mr. Mahadeo Shetkar, Mahaling Lamani and all the others who make graduate student's life easier.

I would like to express my gratitude towards Bhakti, who patiently taught me the methods to culture and maintain haloarchaea. This work would not have been possible without the support of all the research scholars of the department. I am forever thankful to Shivaraman, Vidhya, Kabilan, Raesh, Meghnath, Ram K, Arun, Rajesh, Chandrashekhar, Yogesh, Geethanjali, Mansi, Deepthi, Akriti, Jigni, Chitra, Gautam Baboo, Gautam Krishnan, Poornima, Ankush, Joseph, Rakesh, Ram, Guruprasad, Anumeha, Anant, Priya, Priyadarshini, Ansie, Angela, Divya, Om, Nupur, Starlaine, Priyanka, Lakshminarayan, Bhibudas and Merina for their timely help. Best wishes to all of you for your future, whatever it may hold.

During the course of this work, some people really left an everlasting impression on me. They not only helped me pick myself up after a major scientific setback, but also encouraged me to troubleshoot and overcome the problem, for which I am thankful to Ramya and Ajay. Archana and Shruti, you have helped me get through some really tough times. Your enthusiasm and infectious vigour for life has been a great inspiration to me. I would also like to thank Solano for being a wonderful friend over the years and helping me in my time of need.

This work would not have been possible without all the help and most importantly the friendship of our 'nano' group. Vilas and Kshipra, both of you paved way for our research and I am thankful for all your help and

support. Dr. Celisa, you have been an inspiration and true friend. The times we spent discussing practically everything under the sun, your wisdom and your precious advice is really appreciated and am thankful from the bottom of my heart for your friendship. Mansur and Ketaki, both of you have been my pillar of strength, we have been through the ups and downs together. I am forever indebted to both of you for all your advice, all the times we shared together and most importantly, I will always cherish our comradery.

I am grateful to my parents Sandhya Srivastava, and A.K. Srivastava, for always believing in me and giving me the opportunity to pursue my dreams. Both of you have taught me the importance of hard-work and perseverance, which has helped me during this work. I would also like to thank my sister, Priyanka Srivastava for bearing with me and listening to my rants when I was frustrated. But most importantly, I am forever indebted to my partner in crime, Leandro de Mello, for having blind faith in me and never letting me quit. This work is complete because of your belief in me and of course your undying support and persistence.

Pallavee Srivastava

*This work is dedicated to my life partner,
Leandro, my son, John Andre, my sister,
Priyanka and my beloved Parents...*

ABSTRACT

Microbial synthesis of nanoparticles presents an eco-friendly approach for nano-fabrication. Numerous bacteria, fungi, yeasts, and viruses have been used for biosynthesis of nanomaterials. Haloarchaea, however have not yet been exploited for the same, whilst very few halophilic bacteria have been shown to synthesise nanoparticles. In the present work, we demonstrate the synthesis of various metallic and metal sulphide nanoparticles by haloarchaea and halophilic bacteria. The haloarchaea, *Halococcus salifodinae* BK3, *H. salifodinae* BK6, *H. salifodinae* BK7, *H. salifodinae* BK11 and *H. salifodinae* BK18 were screened for their ability to synthesise nanoparticles. The halophilic bacteria screened for nanoparticles synthesis include *Halomonas aquamarina* MTCC 4661, *Halobacillus* sp. MTCC 6516, and *Idiomarina* sp. PR58-8. The haloarchaea exhibited optimum growth in NTYE, while the medium supporting optimum growth for *Idiomarina* sp. PR58-8, *Halobacillus* sp. MTCC 6516 and *H. aquamarina* MTCC 4661 was ZMB, 3.5% NTYE, and NB with 2% NaCl, respectively. Amongst the halophilic archaea screened, *H. salifodinae* BK3 and *H. salifodinae* BK6 exhibited the ability to synthesise silver nanoparticles (SNPs); *H. salifodinae* BK18 could synthesise selenium nanoparticles (SeNPs); and *H. salifodinae* BK3 could synthesise tellurium nanoparticles (TeNPs). Similarly, amongst the halophilic bacteria screened, only *Idiomarina* sp. PR58-8 could successfully synthesise SeNPs and lead (IV) sulphide nanoparticles (PbS₂NPs).

Halococcus salifodinae BK3 and *H. salifodinae* BK6 were found to be tolerant to silver nitrate and grew well up to a concentration of 0.5 mM AgNO₃. Upon adaptation to silver nitrate these isolates exhibited growth kinetics similar to that of the control. NADH dependent nitrate reductase was involved in silver tolerance, reduction, synthesis of SNPs, as evident from a metal dependent increase in enzyme activity. Silver nanoparticles synthesised by *H. salifodinae* BK3 (SNPs-BK3) exhibited face centred cubic structure with crystallite domain size of 22 nm and 12 nm, in NTYE and Halophilic Nitrate Broth (HNB), respectively. Similarly, the SNPs synthesised by *H. salifodinae* BK6 (SNPs-BK6) exhibited an average particles size of 50.3 nm and 12 nm in NTYE and HNB, respectively. The ‘as-synthesised’ SNPs exhibited antimicrobial activity against both gram-positive and gram-negative bacteria.

The intracellular synthesis of selenium nanoparticles (SeNPs) by *Halococcus salifodinae* BK18 was observed during growth in the presence of sodium selenite. Crystallographic characterisation of SeNPs by XRD, SAED and TEM exhibited rod shaped nanoparticles with hexagonal crystal lattice, a crystallite domain size of 28 nm and an aspect ratio (length: diameter) of 13:1. EDAX analysis confirmed the presence of selenium in the nano-preparation. The nitrate reductase enzyme assay and the inhibitor studies indicated the involvement of NADH-dependent nitrate reductase in SeNPs synthesis and metal tolerance. The SeNPs exhibited good anti-proliferative properties against HeLa cell lines while being non-cytotoxic to normal cell line model HaCaT. Caspase-dependent apoptosis was responsible for this anti-proliferative property, suggesting the use of these SeNPs as cancer chemotherapeutic agent.

H. salifodinae BK3 exhibited intracellular synthesis of hexagonal needle shaped tellurium nanoparticles with an aspect ratio of 1:4.4. The isolate was able to tolerate up to 5.5 mM K_2TeO_3 . The yield of tellurium nanoparticles was highest when the culture was exposed to 3 mM K_2TeO_3 , even though the isolate exhibited slightly decreased growth rate as compared to the culture growing in the absence of K_2TeO_3 . The enzyme, tellurite reductase was responsible for tellurite resistance and nanoparticle synthesis in *H. salifodinae* BK3. These tellurium nanoparticles exhibited antibacterial activities against both gram-positive and gram-negative bacteria, with higher activity towards gram-negative bacteria.

The moderate halophilic bacterium, *Idiomarina* sp. PR58-8 exhibited intracellular synthesis of SeNPs using sodium selenite as the precursor. Characterisation of SeNPs by XRD exhibited the characteristic Bragg's peak of hexagonal selenium with a crystallite domain size of 34 nm. Morphological characterisation by TEM exhibited spherical nanoparticles with a size distribution of 150-350 nm. Non-protein thiols were found to be involved in resistance/reduction of sodium selenite. The SeNPs exhibited selectivity in exerting cytotoxicity towards HeLa cell line, while being non-toxic towards HaCaT cell line. The SeNPs induced caspase-dependent apoptosis in HeLa cell lines as evident from the ROS assay, apoptotic index assay, and western blot analysis. These results suggest the application of SeNPs synthesised by *Idiomarina* sp. PR58-8 as potential anti-neoplastic agents.

Idiomarina sp. PR58-8 also exhibited the synthesis of fluorescent lead (IV) sulfide nanoparticles (PbS_2 NPs) intracelullarly. The bacterium could tolerate up to 8 mM $Pb(NO_3)_2$

during growth. A dose dependent increase in non-protein thiols in response to metal challenge suggests their involvement in growth of PbS₂ crystals and lead detoxification. Characterisation achieved by XRD, TEM, HR-TEM and EDAX exhibited spherical β-PbS₂ particles with tetragonal crystal lattice, a crystallite domain size of 2.38 nm, and an interplanar distance of 0.318 nm. A narrow symmetric emission spectrum with Gaussian distribution and an emission maximum at 530 nm was obtained when the particles were excited at 386 nm. A large Stokes' shift (7038 cm⁻¹); a relatively high quantum yield (67%); consistent fluorescence with changing micro-environment; and biocompatibility makes these nanoparticles excellent candidate for bio-imaging. The particles were internalised by the HeLa cells and evenly distributed within the cytoplasm, exhibiting their potential for *in-situ* bio-imaging applications. The 'as-synthesised' lead (IV) sulfide nanoparticles could provide expanded opportunities for targeted bio-imaging by surface modification of the particles.

This is the first study to report synthesis of nanoparticles by haloarchaea. At the same time, synthesis of PbS₂NPs by a microorganism is also reported for the first time. This is also the first study to demonstrate the bio-imaging application of a microbially synthesised lead based nanomaterial.

Brief contents

Chapter	Title	Page
1	Introduction and Review of Literature	1
2	Screening of Various Haloarchaeal and Halophilic Bacterial Cultures Capable of Synthesising Metallic or Metal Sulphide Nanoparticles	31
3	Synthesis of Silver Nanoparticles by Halophilic Archaea <i>Halococcus Salifodinae</i> BK3 and <i>H. Salifodinae</i> BK6 and their Application as Antimicrobial Agents	58
4	<i>In-vivo</i> Synthesis of Selenium Nanoparticles by <i>Halococcus salifodinae</i> BK18 and their Anti-Proliferative Properties against HeLa Cell Line	88
5	Biosynthesis of Antibacterial Tellurium Nanoparticles by the Haloarchaeon <i>Halococcus salifodinae</i> BK3	113
6	Biosynthesis of Anti-Neoplastic Selenium Nanoparticles by the Moderate Halophilic Bacterium <i>Idiomarina</i> Sp. PR58-8	136
7	Biosynthesis of Fluorescent Lead (IV) Sulphide Nanoparticles Synthesis by the Moderate Halophilic Bacterium <i>Idiomarina</i> Sp. PR58-8	155

Table of Contents

	PAGE
Thesis title page (Annexure I)	
Certificate from Supervisor (Annexure II)	
Acknowledgements	
Abstract	i
Table of contents	iv
List of tables	xi
List of figures	xiii
List of abbreviations and symbols	xxiii
Chapter 1: Introduction and Review of Literature	
1.1 Introduction	1
1.2 Nanobiotechnology	4
1.3 Properties of nanoparticles	4
1.4 Synthesis of inorganic nanoparticles	6
1.4.1 Physical methods	7
1.4.2 Chemical synthesis	7
1.4.3 Bio-inspired/ Biogenic synthesis of nanoparticles	8
1.5 Nanoparticles synthesis by microorganisms	9
1.5.1 Nanoparticle synthesis by Haloarchaea	13
1.5.2 Nanoparticles synthesis by slight and moderate halophiles	15
1.5.2.1 Halophilic bacteria and nanofabrication	15
1.5.2.2 Nanoparticles and halophilic yeast and fungi	18
1.5.2.3 Halophilic algae in nanoparticles synthesis	19
1.6 Mechanisms of metallic nanoparticles synthesis	21
1.6.1 Glutathione and related peptides in nanomaterial synthesis	22
1.6.2 Enzymes and nanoparticles synthesis	24
1.6.2.1 Oxido-reductases	24
1.6.2.2 NADH-dependent reductases	25
1.6.2.3 Nitrate Reductases (NR)	25
1.6.2.4 Enzymes of sulphate and sulphite metabolic pathway	26
1.7 Applications of biosynthesised MNPs	27
1.8 Gaps in existing research	29

1.9 Aims and objectives of the research work	30
Chapter 2: Screening of Various Haloarchaeal and Halophilic Bacterial Cultures Capable of Synthesising Metallic or Metal Sulphide Nanoparticles	
2.1 Introduction	31
2.2 Materials and Methods	32
2.2.1 Materials	32
2.2.2 Cultures and medium optimisation	32
2.2.3 Determination of MIC of metal salt	33
2.2.4 Screening of promising isolates synthesising nanoparticles	34
2.2.4.1 Screening based on colour change	34
2.2.4.2 Screening of cultures synthesising nanoparticles with no visual colour change	34
2.2.5 Statistical analysis	35
2.3 Results and discussions	35
2.3.1 Screening of haloarchaeal isolates	35
2.3.1.1 Optimisation of growth medium	35
2.3.1.2 Determination of MIC of various metals	39
2.3.1.3 Screening of promising haloarchaeal isolates for nanoparticles synthesis	42
2.3.2 Screening of halophilic bacteria	47
2.3.2.1 Optimisation of growth medium	48
2.3.2.2 Determination of MIC of various metals	50
2.3.2.3 Screening of promising halophilic bacteria for nanoparticle synthesis	55
2.4 Conclusion	57
Chapter 3: Synthesis of Silver Nanoparticles by Halophilic Archaea <i>Halococcus salifodinae</i> BK3 and <i>H. salifodinae</i> BK6 and their Application as Antimicrobial Agents	
3.1 Introduction	58
3.2 Materials and methods	60
3.2.1 Organism and culture maintenance	60
3.2.2 Silver resistance and growth kinetics studies	60
3.2.3 Biosynthesis of SNPs and process parameter optimisation	61

3.2.4 Silver estimation and yield determination	62
3.2.5 Characterisation of silver nanoparticles	63
3.2.6 Thiol assay	63
3.2.7 Nitrate reductase assay and inhibitor studies	64
3.2.8 Antimicrobial effect of SNP	65
3.2.9 Statistical analysis	66
3.3 Results and discussions	66
3.3.1 Studies on growth kinetics	66
3.3.2 Mechanism of SNPs synthesis	69
3.3.3 SNPs biosynthesis and its optimisation	76
3.3.4 Nanoparticle characterisation	81
3.3.5 Antimicrobial activity	85
3.4 Conclusion	87
Chapter 4: <i>In-vivo</i> Synthesis of Selenium Nanoparticles by <i>Halococcus salifodinae</i>	
BK18 and their Anti-Proliferative Properties against Hela Cell Line	
4.1 Introduction	88
4.2 Materials and methods	90
4.2.1 Organism and culture maintenance	90
4.2.2 Growth in presence of selenite	90
4.2.3 Estimation of selenite content	91
4.2.4 Selenium nanoparticles synthesis and optimisation of process	91
Parameters	
4.2.5 Characterisation of SeNPs	92
4.2.6 Nitrate reductase assay and inhibitor studies	93
4.2.7 Mammalian cell culture	93
4.2.8 MTT assay	94
4.2.9 Detection of intracellular reactive oxygen species (ROS)	94
4.2.10 Acridine orange and ethidium bromide (AO/EB) staining to determine apoptotic index (AI)	95
4.2.11 Western blot	96
4.2.12 Statistical analysis	96
4.3 Results and discussions	96
4.3.1 Growth in presence of selenite and selenite uptake	96

4.3.2 Selenium nanoparticles biosynthesis and characterisation	99
4.3.3 Involvement of Nitrate Reductase enzyme in selenite reduction	104
4.3.4 Antiproliferative properties of SeNPs	107
4.3.5 Mechanism of SeNPs cytotoxicity towards HeLa cell line	108
4.4 Conclusion	112
Chapter 5: Biosynthesis of Antibacterial Tellurium Nanoparticles by the Haloarchaeon <i>Halococcus salifodinae</i> BK3	
5.1 Introduction	113
5.2 Materials and methods	115
5.2.1 Determination of MIC of K ₂ TeO ₃ and growth kinetic studies	115
5.2.2 Estimation of tellurite loss from the medium	115
5.2.3 TeNPs biosynthesis and process parameter optimisation	116
5.2.4 Nanoparticles characterisation	117
5.2.5 Effect of tellurite on pigment production	117
5.2.6 Nitrate reductase assay and inhibitor studies	117
5.2.7 Tellurite reductase enzyme assay	118
5.2.8 Antimicrobial activity of the TeNPs	119
5.2.9 Statistical analysis	119
5.3 Results and discussion	120
5.3.1 Effect of potassium tellurite on growth	120
5.3.2 Tellurium nanoparticles synthesis and characterisation	123
5.3.3 Mechanism of TeNPs synthesis	128
5.3.4 Antimicrobial activity	133
5.4 Conclusion	135
Chapter 6: Biosynthesis of Antineoplastic Selenium Nanoparticles by the Moderate Halophilic Bacterium <i>Idiomarina</i> Sp. PR58-8	
6.1 Introduction	136
6.2 Materials and methods	136
6.2.1 Organism and culture maintenance	136
6.2.2 MIC determination and growth kinetics studies	137
6.2.3 Estimation of selenite content	137
6.2.4 Selenium nanoparticles synthesis and optimisation of process parameters	138

6.2.5	Characterisation of the SeNPs	138
6.2.6	Thiol assay	138
6.2.7	Mammalian cell culture	139
6.2.8	Cytotoxicity assay	139
6.2.9	Detection of intracellular ROS	139
6.2.10	Determination of AI	139
6.2.11	Western blot analysis	140
6.2.12	Statistical analysis	140
6.3	Results and discussions	141
6.3.1	Growth of <i>Idiomarina</i> sp. PR58-8 in presence of selenite oxyanion	141
6.3.2	Selenium nanoparticles (SeNPs) synthesis and their characterisation	143
6.3.3	Mechanism of SeNPs synthesis	149
6.3.4	Anti-neoplastic properties of SeNPs and its mechanism	150
6.4	Conclusion	154
Chapter 7: Biosynthesis of Fluorescent Lead (IV) Sulphide Nanoparticles Synthesis by the Moderate Halophilic Bacterium <i>Idiomarina</i> Sp. PR58-8		
7.1	Introduction	155
7.2	Materials and methods	156
7.2.1	MIC determination and growth kinetics studies	156
7.2.2	Lead uptake studies	157
7.2.3	PbS ₂ NPs synthesis and optimisation of process parameters	157
7.2.4	Characterisation of the PbS ₂ NPs	158
7.2.5	Thiol assay	159
7.2.6	Mammalian cell culture	159
7.2.7	Biocompatibility studies	160
7.2.8	Nanoparticles internalisation and bio-imaging	160
7.2.9	Statistical analysis	160
7.3	Results and discussions	161
7.3.1	Growth of <i>Idiomarina</i> sp. PR58-8 in presence of lead nitrate	161
7.3.2	Lead (IV) sulphide nanoparticles (PbS ₂ NPs) synthesis and their characterisation	164
7.3.3	Mechanism of PbS ₂ NPs synthesis	173
7.3.4	Biocompatibility studies and application of PbS ₂ NPs	175

7.4 Conclusion	178
Summary of Results and Conclusion	179
Future Scope of Work	184
References	185
Appendix I	
List of Publications and Presentations- Appendix II	
Brief Biography of the Candidate- Appendix III	
Brief Biography of the Supervisor- Appendix IV	

List of Tables

Table	Table heading	Page
Chapter 1		
Table 1.1	Various inorganic nanoparticles synthesised by some microbes	11-12
Table 1.2	The inorganic nanoparticles biosynthesised by various halophiles	20
Chapter 2		
Table 2.1	The growth kinetics parameters of the haloarchaea in various growth media	37
Table 2.2	Growth of haloarchaeal isolates at various concentrations of metal salts	41
Table 2.3	MICs of various metal salts for the five haloarchaeal isolates	42
Table 2.4	The growth kinetics parameters of all the halophilic bacteria in various growth media	50
Table 2.5	Growth of halophilic bacteria at various concentrations of metal salts	54
Table 2.6	MICs of various metal salts for the halophilic bacteria	54
Chapter 3		
Table 3.1	Instrumental conditions for FAAS measurements	62
Table 3.2	Growth kinetics parameters of <i>Halococcus salifodinae</i> BK3 and <i>H. salifodinae</i> BK6	68
Table 3.3	Optimal parameters for maximal production of SNPs by <i>H. salifodinae</i> BK3 & BK6	77
Table 3.4	SNPs yield parameters	80
Table 3.5	The 2 θ values corresponding to the characteristic Bragg's diffraction planes of SNPs	82
Table 3.6	MIC of SNPs against both gram-positive and gram-negative organisms	86
Chapter 4		
Table 4.1	SeNPs synthesis kinetics and yield parameters	106
Chapter 5		
Table 5.1	Growth kinetics parameters of <i>H. salifodinae</i> BK3 at different concentrations of K ₂ TeO ₃	125
Table 5.2	Summary of optimal parameters for maximal production of TeNPs	130
Table 5.3	TeNPs synthesis kinetics and yield parameters	131
Table 5.4	Tellurite reductase activity of the cell free extract (CFE) of <i>H. salifodinae</i> BK3 at various conditions	136
Table 5.4	MIC of the TeNPs against gram-positive and gram-negative organisms	138

Chapter 6		
Table 6.1	Growth kinetics parameters of <i>Idiomarina</i> sp. PR58-8 in presence of sodium selenite	142
Table 6.2	The yield parameters of SeNPs synthesised by <i>Idiomarina</i> sp. PR58-8	147

Chapter 7		
Table 7.1	Instrumental conditions for FAAS measurements	157
Table 7.2	Growth kinetics parameters of <i>Idiomarina</i> sp. PR58-8 in absence (control) and in presence of lead nitrate	162
Table 7.3	The yield parameters of PbS ₂ NPs synthesised by <i>Idiomarina</i> sp. PR58-8	166

LIST OF FIGURES

Figure	Figure legend	Page
Chapter 1		
Fig. 1.1	How small is nano? A comparison of various natural and man-made materials.	3
Fig. 1.2	Effect of size on photo-luminescence of CdSe QDs.	5
Fig. 1.3	Various methods for manipulation of surface chemistry and surface properties of nanoparticles to broaden the applications.	6
Fig. 1.4	Schematic of top down and bottom up approaches of MNPs synthesis.	6
Fig. 1.5	Magnetotactic bacteria (left) exhibiting the magnetosomes chain and the magnetosomes (right) with various morphologies.	9
Fig. 1.6	Pink Lake- Port Gregory, Western Australia appears pink due to carotenoid pigments in the cell membranes of the haloarchaea that inhabit it.	13
Fig. 1.7	TEM micrographs showing thin sections of (a) <i>Halobacterium</i> sp. NRC-1 and (b) SD109 (pFM104gvpC::κ1) mutant. Gas vesicles can be seen as empty oval or spindle shaped regions. SD109 (pFM104gvpC::κ1) mutant exhibits gas vesicles with altered phenotypes.	14
Fig. 1.8	TEM image of the selenium nanoparticles biosynthesised by halophilic bacteria <i>Bacillus megaterium</i> BSB12	16
Fig. 1.9	TEM micrographs (a-d) depicting the morphology of the MR-CH nanoparticles fabricated using the EPS mauran secreted by the halophilic bacteria, <i>Halomonas maura</i> .	17
Fig. 1.10	(a) SEM micrographs of the MR/PVA nanofibres fabricated using the EPS mauran (x10,000); (b) Confocal microscopy images of L292 cells attached and proliferating on MR/PVA nanofibres (merged microtracker green and DAPI stained images)	18
Fig. 1.11	General mechanisms adapted by bacteria, eukaryotes, and archaea for metal resistance.	21
Fig. 1.12	Mechanism of CdS nanocrystallite formation in <i>Schizosaccharomyces pombe</i> involves Phytochelatins (PC). (LMW- Low molecular weight; HMW- High molecular weight).	23
Fig. 1.13	Possible mechanism of gold nanoparticles synthesis by NADH-dependent reductase.	25

Fig. 1.14	Mechanism of ZnS nanoparticles synthesis by immobilized <i>Rhodobacter sphaeroides</i> .	26
Fig. 1.15	Application of nanoparticles in various fields.	28
Chapter 2		
Fig. 2.1	Growth profiles of (a) <i>Halococcus salifodinae</i> BK3, (b) <i>H. salifodinae</i> BK6, (c) <i>H. salifodinae</i> BK7, (d) <i>H. salifodinae</i> BK11, and (e) <i>H. salifodinae</i> BK18 in NTYE (NaCl Tryptone Yeast Extract), SWYE (Salt Water Yeast Extract), HB (Halophilic Broth) and Mod. Popescu (Modified Popescu et al.) media.	38
Fig. 2.2	(a) <i>Halococcus salifodinae</i> BK3 appears orange red on NTYE; (b) <i>H. salifodinae</i> BK3 turns brown black in presence of AgNO ₃ ; (c) <i>H. salifodinae</i> BK18 turns brick red in presence of Na ₂ SeO ₃ ; (d) <i>H. salifodinae</i> BK3 turns black in presence of K ₂ TeO ₃	42
Fig. 2.3	UV-visible spectra of SNPs synthesised by the haloarchaeal isolates exhibiting the characteristic peak of Ag at around 440 nm.	43
Fig. 2.4	XRD scans of SNPs synthesised by (a) <i>H. salifodinae</i> BK3; (b) <i>H. salifodinae</i> BK6; (c) <i>H. salifodinae</i> BK7 and; (d) <i>H. salifodinae</i> BK11. The crystallite domain as calculated by Debye-Scherrer formula for each SNPs sample is mentioned; ND- not determined as no major peak observed.	44
Fig. 2.5	XRD scans of SeNPs synthesised by (a) <i>H. salifodinae</i> BK3; (b) <i>H. salifodinae</i> BK6; (c) <i>H. salifodinae</i> BK7; (d) <i>H. salifodinae</i> BK11 and; (e) <i>H. salifodinae</i> BK18. Crystallite domain size as calculated by Debye-Scherrer formula for all the SeNPs samples is mentioned; ND- not determined as no major peak observed.	46
Fig. 2.6	XRD scan of TeNPs synthesised by <i>H. salifodinae</i> BK3. Crystallite domain size was calculated by Debye-Scherrer formula and was found to be 11.3 nm.	47
Fig. 2.7	Growth profile of <i>Idiomarina</i> sp. PR58-8 in ZMB, NB + 2% NaCl and 3.5% NTYE.	48
Fig. 2.8	Growth profile of <i>Halomonas aquamarina</i> MTCC 4661 in ZMB, NB + 2% NaCl and 3.5% NTYE.	49
Fig. 2.9	Growth profile of <i>Halobacillus</i> sp. MTCC 6516 in ZMB, NB + 2% NaCl and 3.5% NTYE.	49
Fig. 2.10	(a) <i>Idiomarina</i> sp. PR58-8 appears golden yellow on ZMB (b) which turns brown-black in presence of AgNO ₃ ; (c) <i>Halomonas aquamarina</i> MTCC 4661	51

	appears light orange on NB + 2% NaCl (f) which turns brown in presence of AgNO ₃ .	
Fig. 2.11	(a) <i>Idiomarina</i> sp. PR58-8; (b) <i>Halobacillus</i> sp. MTCC 6516; (c) <i>Halomonas aquamarina</i> MTCC 4661 turn brick red in presence of Na ₂ SeO ₃ .	52
Fig. 2.12	(a) ML2 appears golden yellow on ZMB and (b) turns black in presence of K ₂ TeO ₃ ; (c) <i>H. aquamarina</i> MTCC 4661 appears light orange on NB + 2% NaCl (d) which turns black in presence of K ₂ TeO ₃ .	52
Fig 2.13	<i>Idiomarina</i> sp. PR58-8 appears (a) golden yellow on ZMB and turns (b) brown when grown in presence of Pb(NO ₃) ₂ .	53
Fig. 2.14	XRD scans of SeNPs synthesised by (a) <i>Halomonas aquamarina</i> MTCC 4661; (b) <i>Halobacillus</i> sp. MTCC 6516; and (c) <i>Idiomarina</i> sp. PR58-8; Only <i>Idiomarina</i> sp. PR58-8 was able to synthesise SeNPs.	56
Fig. 2.15	XRD spectrum of PbS ₂ NPs synthesised by <i>Idiomarina</i> sp. PR58-8.	57
Chapter 3		
Fig. 3.1	Growth profile of (a) <i>H. salifodinae</i> BK3, and (b) <i>H. salifodinae</i> BK6 at varying concentrations of AgNO ₃ .	67
Fig. 3.2	(a) <i>Halococcus salifodinae</i> BK3 on NTYE plate appears orange-red; (b) BK3 turned black in presence of 0.5 mM AgNO ₃ on NTYE; Growth in halophilic nitrate broth (c) BK3 (d) BK3 + 0.05 mM AgNO ₃ (e) BK ₃ + 0.5 mM AgNO ₃ .	67
Fig. 3.3	Effect of silver nitrate on growth profiles of (i) <i>H. salifodinae</i> BK3 and (ii) <i>H. salifodinae</i> BK6 (a) in NTYE medium without AgNO ₃ (control); (b) upon first exposure to AgNO ₃ by addition of 0.5 mM AgNO ₃ in NTYE; (c) for cells adapted to AgNO ₃ upon addition of 0.5 mM AgNO ₃ in NTYE; (■) OD; (▲) Growth rate.	68
Fig 3.4	Effect of silver nitrate on the concentrations of T-SH, NP-SH and PB-SH in (a) <i>H. salifodinae</i> BK3 and (b) <i>H. salifodinae</i> BK6 exposed to 0.05 and 0.5 mM AgNO ₃ . Control= 0 mM AgNO ₃ .	71
Fig. 3.5	Effect of silver nitrate addition on the nitrite concentration of (a) <i>H. salifodinae</i> BK3 and (b) <i>H. salifodinae</i> BK6 during SNPs synthesis (day 5) and after completion of SNPs synthesis (day 10).	72
Fig. 3.6	Effect of silver nitrate addition on the nitrate reductase activity of <i>H. salifodinae</i> BK3 and <i>H. salifodinae</i> BK6 during SNPs synthesis.	72

Fig. 3.7	The effect of various inhibitors like PMSF, IAA, EDTA and sodium azide on nitrate reductase enzyme activity of <i>H. salifodinae</i> BK3 and <i>H. salifodinae</i> BK6.	74
Fig. 3.8	Effect of AgNO ₃ on growth of haloarchaeal isolates in HNB medium; (■) OD; (▲) Growth rate; Growth profile of <i>H. salifodinae</i> BK3 (a) in the absence of AgNO ₃ (control); (b) upon first exposure to 0.5 mM AgNO ₃ ; (c) for cells adapted to 0.5 mM AgNO ₃ ; Growth profile of <i>H. salifodinae</i> BK6 (d) in the absence of AgNO ₃ (control); (e) upon first exposure to 0.5 mM AgNO ₃ ; (f) for cells adapted to 0.5 mM AgNO ₃ .	75
Fig. 3.9	Optimisation of process parameters for SNPs synthesis by <i>Halococcus salifodinae</i> BK3 (a, c, e) and <i>H. salifodinae</i> BK6 (b, d, f) in both HNB and NTYE media; (a,b) Effect of AgNO ₃ concentration on SNPs synthesis at pH 7.0 and 37°C; (c, d) Effect of pH on SNPs synthesis at 37°C using 0.5 mM AgNO ₃ precursor; (e, f) Effect of temperature on SNPs synthesis at pH 7.0 using 0.5 mM AgNO ₃ precursor.	78
Fig. 3.10	Growth kinetics, SNPs accumulation and yield of SNPs by (a, b) <i>H. salifodinae</i> BK3 and (c, d) <i>H. salifodinae</i> BK6 in (a, c) NTYE medium and (b, d) HNB medium.	79
Fig. 3.11	Silver uptake by (a) <i>H. salifodinae</i> BK3, and (b) <i>H. salifodinae</i> BK6 in HNB and NTYE medium. Both the isolates accumulated Ag faster in HNB as compared to NTYE medium.	80
Fig. 3.12	UV-visible spectra of (a) SNPs-BK3 and (b) SNPs-BK6 prepared in HNB and NTYE. The spectra remained unaffected by storage for 6 months.	81
Fig. 3.13	XRD spectra of (a) SNPs-BK3 and (b) SNPs-BK6 prepared in NTYE and HNB.	82
Fig. 3.14	TEM micrographs of (a) SNPs-BK3 prepared in NTYE; (b) SNPs-BK3 prepared in HNB; (c) SNPs-BK6 prepared in NTYE; (d) SNPs-BK6 prepared in HNB.	84
Fig. 3.15	Representative TEM micrograph showing (a) triangular morphology of SNPs-BK3; and (b) disc-like morphology of SNPs-BK6; SAED pattern exhibiting the characteristic diffraction rings of fcc crystal of the (c) SNPs-BK3; (d) SNPs-BK6.	84

Fig. 3.16	EDAX spectrum of (a) SNPs-BK3 prepared in NTYE; (b) SNPs-BK3 prepared in HNB; (c) SNPs-BK6 prepared in NTYE; (d) SNPs-BK6 prepared in HNB.	85
Fig. 3.17	The antibacterial activity of (a) SNPs-BK3 and (b) SNPs-BK6 against gram-positive and gram-negative organisms. Antibiotics served as positive controls. Values are mean \pm SD (error bars) for three experiments.	86
Chapter 4		
Fig. 4.1	Growth profile of <i>H. salifodinae</i> BK18 at varying concentrations of Na ₂ SeO ₃ . MIC was found to be 6 mM.	97
Fig. 4.2	(a) <i>H. salifodinae</i> BK18 appears orange-red due to the bacterioruberin in their membrane; (b) <i>H. salifodinae</i> BK18 appears brick-red in colour due to the reduction of Na ₂ SeO ₃ to elemental Se in the growth medium; Growth of (c) BK18; (d) BK18 + 2 mM Na ₂ SeO ₃ ; (e) BK18 + 4 mM Na ₂ SeO ₃ ; (f) Media + 4 mM Na ₂ SeO ₃ , in NTYE medium.	97
Fig. 4.3	(a) Growth of <i>Halococcus salifodinae</i> BK18 in the absence (control), presence of 2 mM and 4 mM Na ₂ SeO ₃ ; (b) Decrease in the SeO ₃ ²⁻ content of the medium expressed as percentage of initial SeO ₃ ²⁻ concentration indicating SeO ₃ ²⁻ uptake by <i>H. salifodinae</i> BK18; Growth of <i>H. salifodinae</i> BK18 in relation to selenite decrease in the medium, when the initial SeO ₃ ²⁻ concentration was (c) 2 mM and (d) 4 mM. (■) OD (▲) Growth rate.	99
Fig. 4.4	Effect of selenite concentration on the yield of SeNPs at pH 7.0 and 37°C.	100
Fig. 4.5	Effect of medium pH on the yield of SeNPs at 37°C using 2 mM Na ₂ SeO ₃ precursor.	101
Fig. 4.6	Effect of incubation temperature on the yield of SeNPs at pH 7.0 using 2 mM Na ₂ SeO ₃ precursor.	101
Fig. 4.7	Growth kinetics, SeNPs accumulation and the yield of SeNPs studies for the haloarchaeon <i>H. salifodinae</i> BK18.	102
Fig. 4.8	Characterisation of the selenium nanoparticles synthesised by <i>Halococcus salifodinae</i> BK18. (a) XRD pattern exhibiting the characteristic Bragg's peak of hexagonal selenium; (b) UV-Visible spectra showing an absorption maxima at around 270nm; (c) TEM micrograph exhibiting selenium nano-rods, with few uniformly sized selenium nanospheres; (c inset) SAED pattern of the as synthesised SeNPs; (d) EDAX spectrum exhibiting the characteristic absorption band of elemental selenium.	104

Fig. 4.9	Effect of Na ₂ SeO ₃ on nitrate reduction.	105
Fig. 4.10	Effect of Na ₂ SeO ₃ on the nitrate reductase enzyme activity in the presence and absence of selenite.	105
Fig. 4.11	Effect of various inhibitors like PMSF, IAA, EDTA and sodium azide on nitrate reductase enzyme activity of <i>H. salifodinae</i> BK18.	106
Fig. 4.12	SeNPs exhibited a dose dependent increase in cytotoxicity towards HeLa cells whilst exhibiting none towards the HaCat cells. The selenium free cell material (HSBK18) and sodium selenite (SS) did not exhibit cytotoxicity towards HeLa and HaCat cell lines.	108
Fig. 4.13	ROS generation in HeLa cell lines after treatment with SeNPs/ SS/ HSBK18 represented as a percentage of ROS generated in untreated cells.	109
Fig. 4.14	(a) Representative micrographs showing HeLa cells treated with SeNPs and stained with AO/EB. The morphological characteristics of apoptotic cells such as chromatin condensation (white arrows), nuclear fragmentation (yellow arrow); cell shrinkage (blue arrow) and formation of apoptotic bodies (orange arrows) were observed; (Inset) Control cells exhibiting uniform staining indicating intact cellular and nuclear morphology; (b) HeLa cells treated with SeNPs exhibited a dose dependent increase in the apoptotic index (percent of apoptotic cells) as compared to untreated cells.	110
Fig. 4.15	Western blot analysis of HeLa cells treated with varying concentrations of SeNPs (A- 0 µg/ml; B- 30 µg/ml; C- 50 µg/ml; D- 70 µg/ml; E- 100 µg/ml). A dose dependent decrease in levels of HSP-70 and Pro-caspase 3 is suggestive of activation of caspase dependent apoptosis. The decrease in levels of Pro-PARP with a concomitant increase in levels of cleaved form of PARP, further confirms the involvement of caspase dependent apoptosis in the anti-neoplastic properties of SeNPs against HeLa cell line. β-Actin was used as a control to check equal loading of proteins.	111
Chapter 5		
Fig. 5.1	(a) Effect of 0.3 mM and 3 mM K ₂ TeO ₃ on pigment production ability of <i>H. salifodinae</i> BK3; (b) <i>H. salifodinae</i> BK3 appears orange-red (c) which turns black in presence of 3mM K ₂ TeO ₃ due to accumulation of reduced tellurium	120
Fig. 5.2	Growth profile of <i>H. salifodinae</i> BK3 at varying concentrations of K ₂ TeO ₃ . The growth was found to decrease with the increase in metal concentration. MIC was found to be 6 mM.	120

Fig. 5.3	Growth profiles of <i>Halococcus salifodinae</i> BK3 in the (a) absence of K_2TeO_3 (b) presence of 0.3 mM K_2TeO_3 and (c) presence of 3 mM K_2TeO_3 . The circles (●) represent growth as optical density and the triangles (▲) represent specific growth rates.	121
Fig. 5.4	Effect of 3 mM K_2TeO_3 on the colony size of <i>H. salifodinae</i> BK3.	122
Fig. 5.5	Uptake of tellurite from the medium by <i>H. salifodinae</i> BK3 (a) when grown in presence of 0.3 mM (76 µg/ml) and 3 mM (761.37 µg/ml) K_2TeO_3 ; (b) in relation to the growth phase at 0.3 mM K_2TeO_3 and (c) 3 mM K_2TeO_3 .	123
Fig. 5.6	Growth of <i>H. salifodinae</i> BK3 (a) in presence of K_2TeO_3 and (b) in absence of K_2TeO_3 ; (c) The media components did not result in reduction of TeO_3^{2-} in the absence of the culture.	123
Fig. 5.7	Effect of tellurite concentration on TeNPs yield at pH 7.0 and 37°C.	124
Fig. 5.8	Effect of pH on TeNPs yield at 37°C using 3 mM K_2TeO_3 precursor.	125
Fig. 5.9	Effect of temperature on TeNPs yield at pH 7.0 using 3 mM K_2TeO_3 .	125
Fig. 5.10	Growth kinetics, TeNPs accumulation and the yield of TeNPs studies for the haloarchaeon <i>H. salifodinae</i> BK18.	126
Fig. 5.11	Characterisation of the TeNPs synthesised by <i>H. salifodinae</i> BK3 (a) XRD spectrum exhibiting the characteristics Bragg's peaks of hexagonal tellurium; (b) TEM micrograph showing needle shaped particles with an average diameter of 10 nm and average length of 44 nm; (c) Selected Area Electron Diffraction (SAED) pattern of the TeNPs exhibiting the crystalline nature of the nano-preparation; (d) EDAX spectrum exhibiting the peak of pure tellurium.	128
Fig. 5.12	(a) Effect of K_2TeO_3 on the enzyme was found to be negligible as evaluated by quantification of the nitrite in the medium; (b) Effect of K_2TeO_3 on the nitrate reductase enzyme activity; (c) Effect of various inhibitors like PMSF, IAA, EDTA and sodium azide on nitrate reductase enzyme activity of <i>H. salifodinae</i> BK3 in presence of K_2TeO_3 .	130
Fig. 5.13	The tellurite reductase activity of the CFE of <i>H. salifodinae</i> BK3 grown in the presence of (a) 0.3 mM and (b) 3 mM K_2TeO_3 . In the absence of β -NADH no reduction was observed in either case, thus the absorbance did not increase.	132
Fig. 5.14	Antibacterial activity of the 'as-synthesised' TeNPs against gram-positive & gram-negative bacteria.	133

Fig. 5.15	Antibacterial activity (i) of the ‘as synthesised’ TeNPs loaded discs; (ii) Negative control (saline loaded discs) and positive control (antibiotic discs) against (a) <i>E. coli</i> ATCC 10536, (b) <i>P. aeruginosa</i> MTCC 2581, (c) <i>S. aureus</i> ATCC 6538P and (d) <i>M. luteus</i>	134
------------------	--	-----

Chapter 6

Fig. 6.1	Growth profile of <i>Idiomarina</i> sp. PR58-8 at varying concentrations of Na ₂ SeO ₃ . The growth was found to decrease with the increase in metal concentration. MIC was found to be 10 mM.	141
Fig. 6.2	<i>Idiomarina</i> sp. PR58-8 appears golden yellow when grown in Zobell marine agar (a) and Zobell marine broth (c). In presence of sodium selenite, it appears brick-red in color (b; d). Media controls with sodium selenite did not exhibit the brick-red coloration (e).	141
Fig. 6.3	Growth of <i>Idiomarina</i> sp. PR58-8 in absence (ctl), and presence of 4 mM and 8 mM Na ₂ SeO ₃ was found to be similar. Na ₂ SeO ₃ did not affect the growth negatively.	142
Fig. 6.4	Decrease in selenite concentration in the medium, expressed as percentage of the initial value, indicative of selenite uptake by <i>Idiomarina</i> sp. PR58-8.	143
Fig. 6.5	Effect of selenite concentration on the yield of SeNPs at pH 7.0 and 37°C.	144
Fig. 6.6	Effect of pH on the yield of SeNPs at 37°C using 8 mM Na ₂ SeO ₃ as the precursor.	145
Fig. 6.7	Effect of incubation temperature on the yield of SeNPs at pH 7.0 using 8 mM Na ₂ SeO ₃ as the precursor.	145
Fig. 6.8	Growth kinetics, SeNPs accumulation and the yield of SeNPs studies in presence of (a) 4 mM and (b) 8 mM Na ₂ SeO ₃ for the moderate halophilic bacterium, <i>Idiomarina</i> sp. PR58-8.	146
Fig. 6.9	(a) XRD spectrum exhibiting the characteristic Bragg's peak of hexagonal selenium; (b) UV-visible spectra with a peak at around 320 nm; (c) TEM micrograph showing spherical nanoparticles; (c inset) SAED pattern of the SeNPs corresponding to the hexagonal crystal facets; (d) EDAX spectrum with the L α , K α and K β peaks of Se.	148
Fig. 6.10	Effect of sodium selenite on the intracellular levels of total thiols (T-SH), non-protein thiols (NP-SH), and protein bound thiols (PB-SH) with respect to time.	150
Fig. 6.11	(a) SeNPs exhibited a dose-dependent decrease in cell viability towards HeLa cell lines as compared to sodium selenite (SS) and selenium free cell material	151

	(ML2); (b) SeNPs did not exhibit any significant cyto-toxicity towards HaCat cell line at the concentrations tested.	
Fig. 6.12	SeNPs exhibited a dose dependent increase in ROS which was significantly higher than the control at 15 µg/ml and above.	151
Fig. 6.13	(a) HeLa cells treated with SeNPs exhibited a dose dependent increase in the apoptotic index (percent of apoptotic cells) as compared to untreated cells. Values are mean ± SD (error bars) for three experiments. * Represents significant results (p <0.05) using ANOVA, when treated groups were compared with the untreated controls; (b) Representative micrographs showing HeLa cells treated with SeNPs and stained with AO/EB. The morphological characteristics of apoptotic cells such as chromatin condensation (white arrows), nuclear fragmentation (yellow arrow); cell shrinkage (blue arrow) and formation of apoptotic bodies (orange arrows) were observed; (Inset) Control cells exhibiting uniform staining indicating intact cellular and nuclear morphology.	152
Fig. 6.14	Western blot analysis of HeLa cells treated with varying concentrations of SeNPs (A- 0 µg/ml; B- 30 µg/ml; C- 50 µg/ml; D- 70 µg/ml; E- 100 µg/ml). β-Actin was used as control to check equal loading of proteins.	153
Chapter 7		
Fig. 7.1	Growth profile of <i>Idiomarina</i> sp.PR58-8 at varying concentrations of Pb(NO ₃) ₂ . MIC of Pb(NO ₃) ₂ was found to be 9 mM.	161
Fig. 7.2	<i>Idiomarina</i> sp. PR58-8 appears golden yellow when grown in ZMA (a) and ZMB (c). In presence of lead nitrate, it appears brown in colour (b; d). Media controls with lead nitrate did not exhibit the brown colouration (e).	161
Fig. 7.3	Growth of <i>Idiomarina</i> sp. PR58-8 in absence (ctl), and presence of 0.05, 0.5, 1 and 5 mM Pb(NO ₃) ₂ .	162
Fig. 7.4	Decrease in lead concentration in the medium, expressed as percentage of the initial value, indicative of lead uptake by <i>Idiomarina</i> sp. PR58-8.	163
Fig. 7.5	Effect of lead nitrate concentration on the yield of PbS ₂ NPs at pH 7.0 and 37°C.	164
Fig. 7.6	Effect of pH on the yield of PbS ₂ NPs at 37°C using 5 mM Pb(NO ₃) ₂ as the precursor.	165

Fig. 7.6	Effect of incubation temperature on the yield of PbS ₂ NPs at pH 7.0 using 5 mM Pb(NO ₃) ₂ as the precursor.	165
Fig. 7.8	Growth kinetics, PbS ₂ NPs accumulation and the yield of PbS ₂ NPs, when <i>Idiomarina</i> sp. PR58-8 was grown in presence of 0.5 mM Pb(NO ₃) ₂ (a) and 5 mM Pb(NO ₃) ₂ (b).	167
Fig. 7.9	XRD spectrum exhibiting the characteristic Bragg's peak of tetragonal PbS ₂ .	167
Fig. 7.10	UV-visible spectra of the PbS ₂ NPs with an absorbance maximum at 386 nm.	168
Fig. 7.11	(a) TEM micrographs of the PbS ₂ NPs exhibiting spherical particles with an average size of 6 nm. (b) HR-TEM micrograph showing spherical nanoparticles with interplanar spacing of 0.318 nm.	169
Fig. 7.12	(a) SAED pattern of the PbS ₂ NPs corresponding to the tetragonal crystal facets, where the three rings could be indexed to Bragg's planes of (1 1 1), (2 0 4) and (2 0 0); (b) FFT of a single PbS ₂ NPs obtained during HR-TEM analysis; (c) SEM micrograph of the PbS ₂ NPs used for EDAX measurements; (d) EDAX spectrum with peaks of Pb. S peaks overlap with the Pb peak.	170
Fig. 7.13	(a) The absorbance and the emission spectra of PbS ₂ NPs exhibiting an absorbance maximum at 386 nm and an emission maximum at 530 nm; (b) Effect of storage on the emission spectra of the 'as-synthesised' PbS ₂ NPs.	171
Fig. 7.14	(a) The photoluminescence spectra of the lyophilized <i>Idiomarina</i> sp. PR 58-8 exhibiting a broad peak, which disappeared on storage for 48 hrs; (b) The fluorescence spectra of PbS ₂ NPs synthesised by <i>Idiomarina</i> sp. PR58-8 in solvents such as water, PBS (pH 7.0) and DMEM.	172
Fig. 7.15	The absorbance and the emission spectra of coumarin 153 dye exhibiting an absorbance maximum at 422 nm and an emission maximum at 531 nm	172
Fig. 7.16	(a) Effect of lead nitrate on the intracellular levels of total thiols (T-SH), non-protein thiols (NP-SH), and protein bound thiols (PB-SH) with respect to time. A dose dependent increase in NP-SH was observed in response to lead stress; The increase in NP-SH concentration corresponded to the lead uptake exhibited by <i>Idiomarina</i> sp. PR58-8 in presence of (b) 0.5 mM Pb(NO ₃) ₂ and (c) 5 mM Pb(NO ₃) ₂ .	174
Fig 7.17	Effect of PbS ₂ NPs, lead free cell material (ML2) and lead nitrate (LN) on viability of HeLa cells.	175

Fig 7.18	Effect of PbS ₂ NPs, ML2 and LN on ROS generation.	175
Fig. 7.19	(a) Fluorescence micrograph of HeLa cells stained with 30 µg/ml PbS ₂ NPs. The nanoparticles exhibited red fluorescence, were evenly distributed in the cytoplasm, and did not stain the nucleus; (b) Phase contrast micrograph of HeLa cells treated with 30 µg/ml PbS ₂ NPs; (c) Fluorescence micrograph of the PbS ₂ NPs powder; (d) Phase contrast micrograph of PbS ₂ NPs powder. (e) Fluorescence micrograph of the lyophilised <i>Idiomarina</i> sp.PR58-8; (f) Phase contrast micrograph of the lyophilised <i>Idiomarina</i> sp.PR58-8	177
Fig. 7.20	Corrected total cell fluorescence of cells stained with PbS ₂ NPs synthesized by <i>Idiomarina</i> sp. PR58-8, after the subtraction of background fluorescence.	177

List of Abbreviations and Symbols

2,3-DAN- 2,3-diaminonaphthalene	DCFH-DA- 2', 7'- dichlorofluorescein diacetate
Ag- silver	DDT- dichlorodiphenyltrichloroethane
AgNO ₃ - silver nitrate	DDTC- diethyldithiocarbamate
AI- apoptotic index	DMEM- Dulbecco's modified eagle medium
ANOVA- analysis of variance	DMSO- dimethyl sulphoxide
AO/EB- acridine orange/ ethidium bromide	DTNB- 5, 5'- dithio-bis (2-nitrobenzoic acid)
ATCC- American type culture collection	E- energy band gap
Au- gold	EDAX- energy dispersive analysis of X-rays
AuNPs- gold nanoparticles	EDS- energy dispersive spectroscopy
BPEI- branched polyethyleneimine	EDTA- ethylenediaminetetraacetic acid
BSA- bovine serum albumin	EPS- exopolysaccharides
CCMV- cowpea chlorotic mottle virus	FAAS- flame-atomic absorption spectroscopy
CDW- cell dry weight	FBS- fetal bovine serum
CFE- cell free extract	fcc- face centred cubic
CFL- cell free lysate	FFT- fast Fourier transform
CLSI- clinical and laboratory standards institute	FWHM- full width half maximum
CM- complete media	GCR- bis- γ glutamyl cysteine reductase
CMV- cowpea mosaic virus	GO- grapheme oxide
CO ₂ ³⁻ - carbonate	GSH- glutathione
Cu- copper	GVNPs- gas vesicle nanoparticles
Cys- cysteine	
d- interplanar spacing	

List of Abbreviations and Symbols

H ₂ O ₂ - hydrogen peroxide	MTPs- multiply twinned particles
HB- halophilic broth	MTT- 3-(4,5-dimethylthiazol-2-yl)-2,5-diphenyltetrazolium bromide
HCO ³⁻ - bicarbonate	Na ₂ SeO ₃ - sodium selenite
HNB- halophilic nitrate broth	NCIM- national collection of industrial microorganisms
HSBK18- selenium free <i>H. salifodinae</i> BK18 cell material	NADH- nicotinamide adenine dinucleotide
HSP-70- heat shock protein 70	NB- nutrient broth
IAA- idoacetate	NED- N-(1-naphthyl) ethylene diamine hydrochloride
ICDD- international centre for diffraction data	NIR- near infrared region
K ₂ TeO ₃ -potassium tellurite	NPs- nanoparticles
LisDps- the Ferritin like protein Dps from <i>Listeria innocua</i>	NP-SH- non-protein thiols
LN- lead nitrate	NR- nitrate reductase
LSPR- localized surface plasmon resonance	NTYE- Nacl, tryptone, yeast extract
MHB- Mueller Hinton broth	OH- hydroxyl
MIC- minimum inhibitory concentration	PARP- poly(ADP-ribose) polymerase
ML2- lead/ selenium free <i>Idiomarina</i> sp. PR58-8 cell material	Pb(NO ₃) ₂ - lead nitrate
MNPs- metallic nanoparticles	PBS- phosphate buffered saline
MR- mauran	PbS ₂ NPs- lead (IV) sulphide nanoparticles
MR-CH- mauran-chitosan	PB-SH- protein bound thiol
MT- metallothionein	PbSNPs- lead (II) sulphide nanoparticles
MTCC- microbial type culture collection	PC- phytochelatin
	PMSF- phenyl methane sulphonyl fluoride

List of Abbreviations and Symbols

PVA- poly vinyl alcohol	t_d - doubling time
PVP- polyvinyl pyrrolidone	TEM- transmission electron microscopy
QDs- quantum dots	TeNPs- tellurium nanoparticles
QY- quantum yield	t_l - lag time
REMA- resazurin microtiter assay	TMV- tobacco mosaic virus
ROS- reactive oxygen species	TN- tris NaCl
RT- room temperature	TR- thioredoxin
SAED- selected area electron diffraction	T-SH- total thiol
SDS- sodium dodecyl sulphate	XRD- X-ray diffraction
SDW- sterile distilled water	ZMA- Zobell marine agar
Se- selenium	ZMB- Zobell marine broth
SeNPs- selenium nanoparticles	ZnSO ₄ - zinc sulphate
SERRS- surface enhanced resonance Raman scattering	ZoI- zone of inhibition
SNPs- silver nanoparticles	γ GC- γ -glutamyl cysteine
SNPs-BK3- silver nanoparticles from <i>H. salifodinae</i> BK3	$\Delta\nu$ - Stokes' shift
SNPs-BK6- silver nanoparticles from <i>H. salifodinae</i> BK6	λ - wavelength
SO ₄ ²⁻ - sulphate	λ_{abs} - absorbance maximum
SPR- surface plasmon resonance	λ_{em} - emission maximum
SPRI- surface plasmon resonance imaging	μ - growth rate
SS- sodium selenite	
SWYE- salt water yeast extract	

CHAPTER 1

Likewise, nanotechnology will, once it gets under way, depend on the tools we have then and our ability to use them, and not on the steps that got us there.

- K. Eric Drexler

Introduction and review of literature¹

1.1 Introduction

‘Nanotechnology’ is an interdisciplinary technology seeking to explore the unique advantages of manipulating the structure of materials at a scale of individual atoms, molecules, and their organised aggregates. It involves creation and exploitation of materials with structural features in between those of atoms and bulk materials (Rao and Cheetham 2001). ‘Nano’ translates to a billionth of a meter (Fig. 1.1). Thus, nanotechnology encompasses materials that have at least one aspect in nano-range (1-100 nm). The field of ‘nanotechnology’ was ideated with the motto ‘there’s plenty of room at the bottom’ by Richard P. Feynman in 1959 and was popularised by K. Eric Drexler in 1981. In his famous paper ‘Molecular engineering: An approach to the development of general capabilities for molecular manipulation’, Drexler suggested that development of the ability to design protein molecules would open a path to the fabrication of devices with complex atomic specifications, thereby sidestepping obstacles facing conventional microtechnology (Drexler, 1981). Even though Eric Drexler is hailed as the pioneer of this field, it was Professor Norio Taniguchi who coined the term ‘nanotechnology’ in 1974, during his studies on ultra-precision machining. ‘Engines of Creation’ (Drexler, 1986), which was published in 1986, paved the path for molecular nanotechnology and so began the field of nanotechnology.

Nanomaterials are the cornerstones of nanotechnology and nanoscience. Over the last three decades, multi-disciplinary efforts involving interaction between researchers from the fields

¹ This review of literature is published as:

1. **Srivastava P**, Kowshik M (2013) Mechanisms of metal resistance and homeostasis in haloarchaea. *Archaea* 2013:16 doi:10.1155/2013/732864 (Review article)
2. **Srivastava P**, Kowshik M (2015) Biosynthesis of nanoparticles by halophiles. In. Maheshwari DK, Saraf M (Eds). Halophiles- Biodiversity and sustainable exploitation. pp. 145-159 (Book Chapter)

of physics, chemistry, materials science, mechanics, and biology have resulted in a substantial repertoire of nanoparticles and nanomaterials with applications in myriad areas. The preference of nanoscale materials over bulk material for various applications stems from the superior properties exhibited by nanoparticles. Nanofabrication results in materials with unique size dependent optical, physico-chemical, electronic, mechanical, magnetic, and biological properties. These novel properties are a result of the large surface area to volume ratio, large surface energy, reduced imperfections, and spatial confinement of carriers/electrons. Nanomaterials can either be synthesised by a top-down approach, where the bulk materials are gradually broken down to nano-dimensions or a bottom-up approach, where the atoms or molecules are assembled into nano-structures. The top-down approach is used by various physical methods of nanomaterial fabrication such as sputter deposition, laser ablation, attrition, and pyrolysis. The chemical and biological routes of nanoparticles synthesis utilise the bottom-up approach.

Nanoparticles may be classified as organic (carbon based), and inorganic which include magnetic, metal based, and semiconductor nanoparticles. Metallic nanoparticles (MNPs) are characterised by the excitation of the surface plasmons that result in optical properties hardly achievable in other optical materials. Semiconducting nanoparticles and quantum dots (QDs) exhibit change in electronic properties with decrease in size due to quantum-confinement and increase in band gap. The magnetic moment per atom and magnetic anisotropy of the magnetic nanoparticles are distinct from their bulk counterparts due to finite size, and surface effects. Therefore, nanoparticles find application in fields such as biomedicine, bio-labelling, bio-imaging, drug delivery, photo-voltaics, solar cells, photo-catalysis, and data storage (Bera et al. 2010; Garcia 2011; Issa et al. 2013).

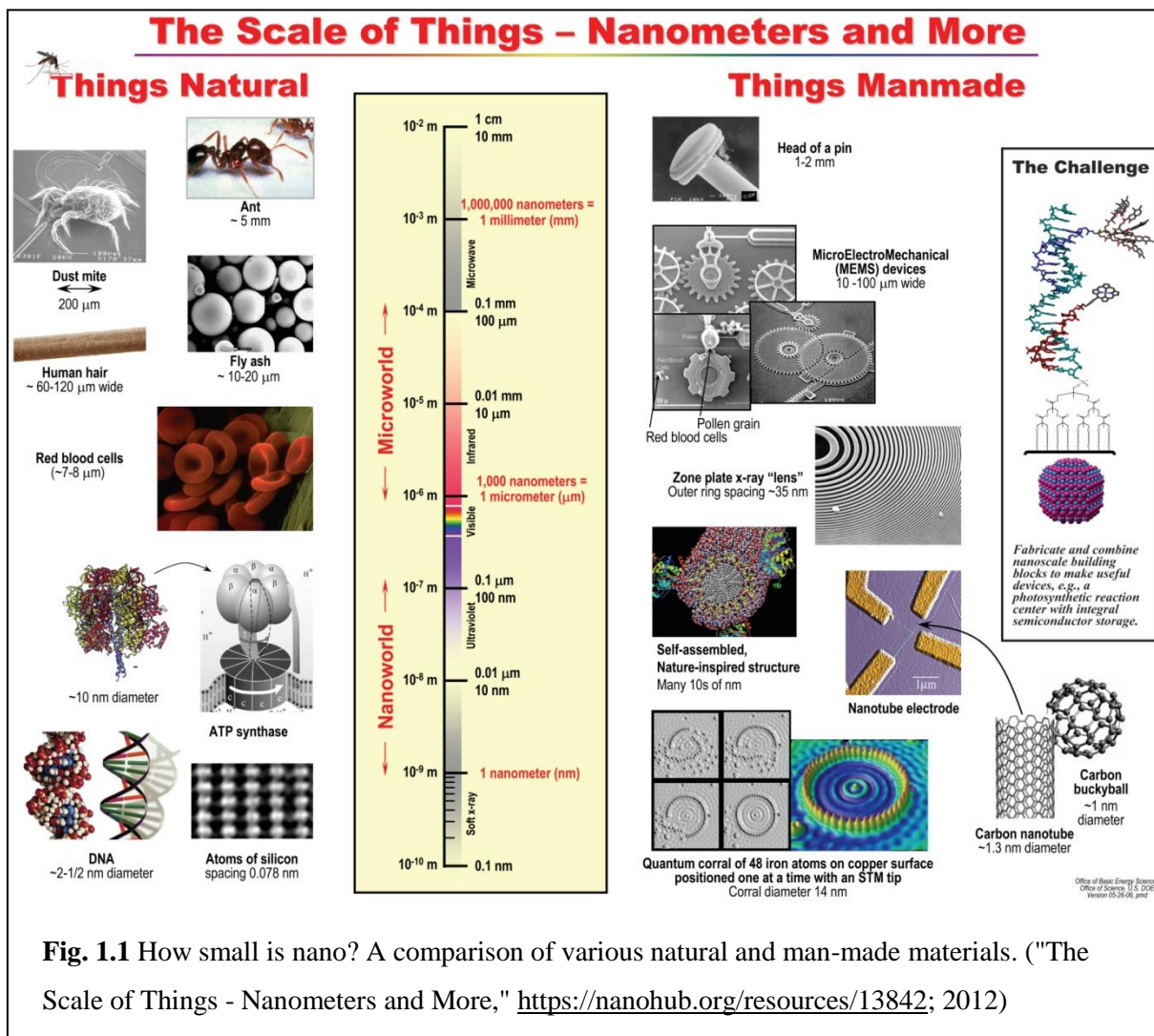


Fig. 1.1 How small is nano? A comparison of various natural and man-made materials. ("The Scale of Things - Nanometers and More," <https://nanohub.org/resources/13842>; 2012)

1.2 Nanobiotechnology

'Nanobiotechnology is creating nanofabricated materials, structures, and devices to examine and engage with biological systems on sub-cellular and molecular levels' (May and Heebner, 2005). It derives principally from nanotechnology however various other biochemical, and material principles such as those of mechanical, optical, electrical/electronic, thermal, and biological areas also contribute to this field. At the onset of nanotechnology, Feynman (1959) had said, *'A biological system can be exceedingly small. Many of the cells are very tiny, but they are very active; they manufacture various substances; they walk around; they wiggle; and they do all kinds of marvellous things- all on a very small scale. Also, they store information. Consider the possibility that we too can make a thing very small which does what we want – that we can manufacture an object that manoeuvres at that level.'* Drexler drew inspiration from protein engineering and proposed machines that work at the molecular scale to structure matter from the bottom up. Thus, the foundation of nanobiotechnology may have been laid even before the term 'nanotechnology' was coined. Some of the applications in this field include nanoscale imaging, quantum tracking, microarray chips and membranes, cellular and molecular diagnostics, theranostics, drug delivery, etc. (May and Heebner, 2005).

1.3 Properties of nanoparticles

The ever-growing interest in nanomaterial fabrication is the result of the starkly different physico-chemical properties presented by nanoparticles (both organic and inorganic) as compared to their bulk counter-parts. This difference arises due to decreased size, increased surface area and surface to volume ratio, large surface atoms, quantum/spatial confinement and reduced imperfections. In fact, structural features of nanomaterials are intermediary to those of atoms and bulk materials. As the size of the bulk material decreases, the properties instead of being composition dependent become size dependent, because the electronic structure gets altered from continuous bands to discrete electronic levels (Burda et al. 2005). The large surface to volume ratio is responsible for the novel surface dependent properties of nanoparticles which include non-linear optical behaviour, increased mechanical strength, enhanced diffusivity, high specific heat, magnetic behaviour, electric resistivity, etc. (Gleiter, 2000).

One of the important properties altered in the nano-regime includes the optical properties of the nanomaterial, which depends upon the size, shape, surface characteristics, and other variables such as doping, dielectric constant of the surrounding environment etc. The localised surface plasmon resonance (LSPR) is a characteristic of metallic nanoparticles and is defined as oscillation of electrons in the conduction band of metals upon

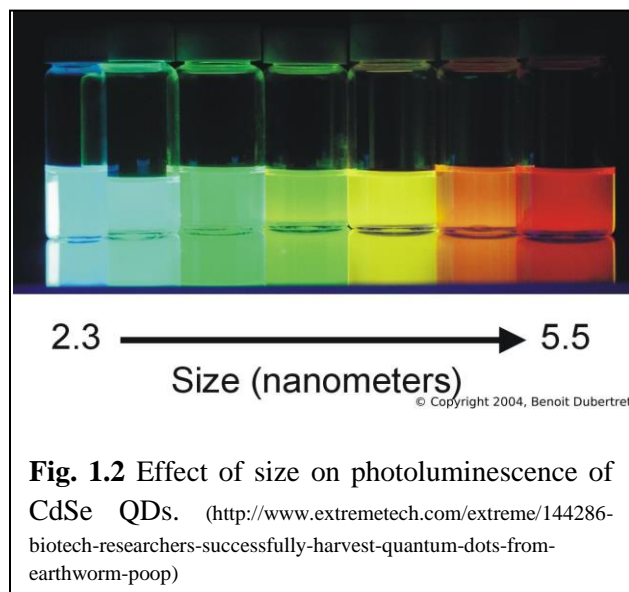
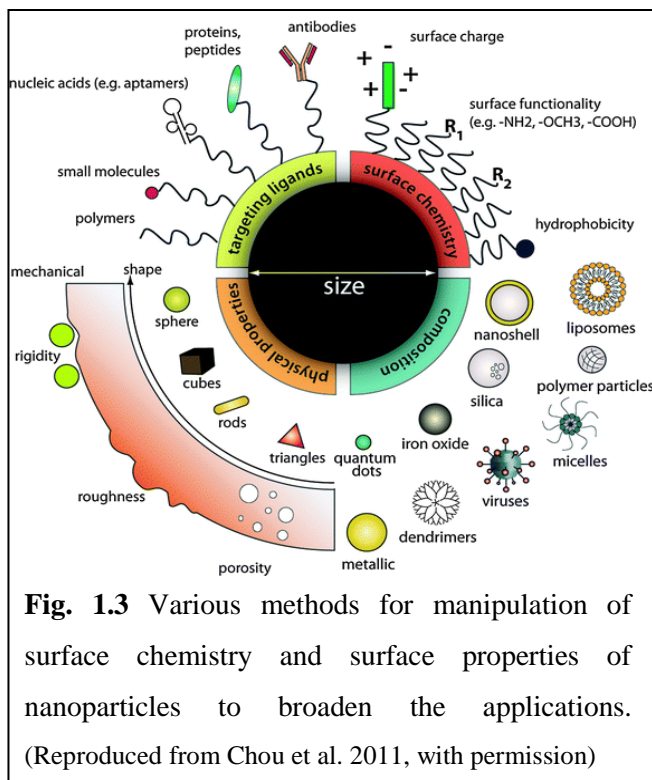


Fig. 1.2 Effect of size on photoluminescence of CdSe QDs. (<http://www.extremetech.com/extreme/144286-biotech-researchers-successfully-harvest-quantum-dots-from-earthworm-poop>)

excitation with incident radiation, resulting in sharp peaks in their spectral extinction (Hutter and Fendler 2004). The 3-dimensional quantum confinement of carriers in QDs gives rise to size dependent photo-luminescence (Fig. 1.2). The band gap in QDs further determines the frequency of emitted light, and is inversely proportional to size. Similarly, the mechanical, electrical, and magnetic properties of nanoparticles are determined by their size, and shape. These novel properties are responsible for the wide range of applications of nanomaterials, which include optical detectors, laser, sensors, imaging, phosphors, LCD display screens, solar cells, photo-catalysis, photo-electrochemistry, photo-voltaics, biomedicine, drug-delivery, etc.

The surface properties of the nanoparticles further confer pliability that enables researchers to generate multi-functional nanomaterials (Fig. 1.3). Nanoparticles can be modularly assembled using various materials to develop novel nanomaterials with desired physical and chemical properties. These materials can further be modified by altering their surface chemistry or by attaching specific targeting ligands (Chou et al. 2011). The size and the shape (sphere, rods, cubes, triangles, etc.) of the nanoparticles can be easily manipulated by the synthesis process itself. Similarly, the nanoparticles of various compositions viz., metallic, dendrimers, micelle, liposome, nanoshell, etc. can be fabricated. Based on the application, nanoparticles may be tailor-made to the desired size shape, and/or composition (Chou et al. 2011; Kango et al. 2013). A prerequisite for all the possible applications of nanoparticles is the proper surface

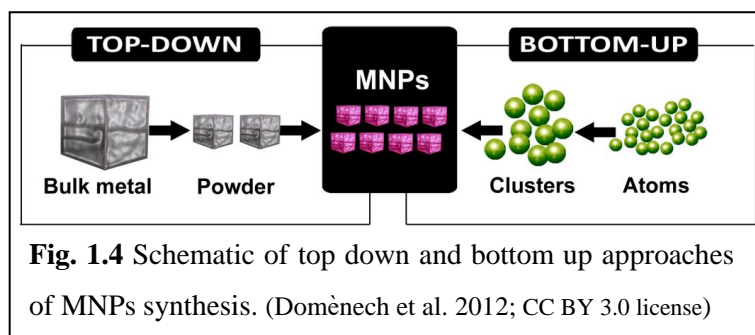


modification and/or functionalisation which determine their interaction with the micro-environment. This modification may be purely chemical or bio-chemical that may prevent agglomeration, or confer polar or non-polar properties on the nanoparticle preparation (Sperling and Parak, 2010). Functionalisation of the nanoparticles with antibodies, nucleic acids, small molecules, proteins/peptides, polymers, etc. enables targeted delivery of the nanomaterial or drugs/fluorescent dye loaded nanoparticles to the desired site

(Kango et al. 2013).

1.4 Synthesis of inorganic nanoparticles

Over the last three decades, various techniques of nanomaterial fabrication have been devised. These broadly fall in physical, chemical or bio-inspired/biogenic methods of nanofabrication. All of these



methodologies essentially rely on either of the two traditional approaches: top-down and bottom-up (Fig.1.4). However, certain techniques devised use a combination of these two approaches. The precursors for these synthetic procedures may be either in solid, liquid, or gaseous phase. Top-down approaches seek to create nanoscale objects by using larger, externally-controlled microscopic devices (microfabrication techniques) to cut, mill, and shape materials into the desired shape and size thus, directing their assembly. Bottom-up approaches

on the other hand adopt molecular components that are built up into more complex assemblies, and include chemical and biogenic methods of nanoparticle synthesis.

1.4.1 Physical methods

Physical methods of nanofabrication are based on top-down approach and result in generation of nanoparticles with good size distribution. Techniques involved in physical methods include electron beam lithography (Hu and Shaw, 1999), laser ablation (Mafune et al. 2001), inert gas condensation (Kang et al. 2011), combustion flame (Lamas et al. 2001), plasma (Rao et al. 1997), spray pyrolysis (Messing et al. 1993), electrospray (Adhikari et al. 2006), and plasma spray (Mandilas et al. 2013). Some of these size reduction processes involving solid precursors may be inexpensive however; they do not give enough control over the size, shape, and chemistry of nanoparticles. On the other hand, methods employing liquid precursors are multi-step processes, employ expensive starting materials, inadvertently use toxic precursors, and result in nano-preparations with undesirable surface chemistry. Similarly, gas-phase procedures require expensive infrastructure, and extreme conditions of temperature and pressure. The generation of hazardous by-products may also be one of the major deterrents for use of physical methods of nanofabrication (Iravani et al. 2014).

1.4.2 Chemical synthesis

The process of chemical synthesis entails a reaction between a metallic ion and an anion under desired and controlled conditions to synthesise nanoparticles. This generates nanoparticles that have high surface energies due to incomplete coordination of surface atoms resulting in agglomeration of particles. Over time these particles dissolve and are deposited again onto larger crystals in the sol. This thermodynamically driven spontaneous process occurs because larger particles are more energetically favoured than smaller particles (Ratke and Voorhees, 2002). Thus, all of these chemical methods involve capping of the synthesised nanoparticles with passivating agents such as sodium dodecyl sulphate (SDS), polyvinyl pyrrolidone (PVP), and tri-sodium citrate (Ghorbani et al. 2011). Some of the chemical synthesis methodologies include chemical reduction (Park et al. 2007), sol-gel methods (Olshavsky and Allcock, 1997), hydrothermal and solvothermal methods (Xin et al. 2010; Yan et al. 2008), etc. Although chemical synthesis yields large quantities of nanoparticles, it has numerous disadvantages. The

process uses hazardous chemicals, extreme conditions of temperature, and generates substantial environmental pollutants (Tien et al. 2008). The additional step required to passivate the nanoparticles employing hazardous capping agents is an added drawback which reduces the applicability of the nano-preparation as bio-compatibility is lost.

1.4.3 Bio-inspired/ Biogenic synthesis of nanoparticles

There is a rich and long history of gaining inspiration from nature for the design of practical materials and systems (Sarıkaya et al. 2003). Biological systems comprise of structural components which owing to the microscale of the cells are in the nano-regime. Biological systems not only present inspiration for self-assembler systems, but may also be exploited for synthesis of nanomaterials (Mann, 1993). In addition, various biological macromolecules such as proteins, DNA, and viral particles have been exploited for nanoparticle synthesis. These efforts in using biological systems for nanofabrication are in keeping with global efforts to move towards green technology, to reduce generation of hazardous waste, and to develop energy-effective production routes.

Proteins such as ferritin (Douglas et al. 1995; Wong and Mann, 1996), serrapeptase (Ravindra 2009), LisDps- the ferritin like protein Dps from *Listeria innocua* (Allen et al. 2003), nitrate reductase (Anil Kumar et al. 2007), phytochelatins and glutathiones (Brelle et al. 1999; Anil Kumar et al. 2007) have been used to synthesise inorganic nanoparticles by reduction and/or capping. These proteins may also act as templates for nanoparticles synthesis. Similarly, viral scaffolds of tobacco mosaic virus (TMV), cowpea mosaic virus (CMV), cowpea chlorotic mottle virus (CCMV), bacterial S layer, and DNA have also been used as templates for nucleation and assembly of inorganic materials (Shenton et al. 1999; Douglas and Young, 1998; Douglas et al. 2002; Hall et al. 2001; Mitchell et al. 1999). By using glutamate and aspartate on the outer layer of virus, TMV was utilised to produce iron oxides by hydrolysis, for co-crystallisation of CdS and PbS, and for the sol-gel synthesis of silica (Shenton et al. 1999). Similarly, genetically engineered Cys-TMV rods were developed that expressed cysteine (Cys) residue at the amino terminus of the coat protein. These cys-TMV rods have been successfully used for attachment of fluorescent dyes, and as bio-templates for Au, Ag, and Pd metal cluster depositions (Yi et al. 2005; Lee et al. 2005). Viral capsids were genetically

modified to express certain peptides such as A7 and J140, that act as nucleation centres for generation of ZnS and CdS nanocrystals (Lee et al. 2002; Mao et al. 2003).

Besides the biological macromolecules, the entire biological entity may be used as ‘nanofactories’ for nanomaterials synthesis. Many bacteria, yeast, fungi, algae, and viruses have been used for synthesis of various metallic, metal sulfide, metal oxide, and alloy nanoparticles, since the first report on biosynthesis of cadmium sulphide quantum dots by *Candida glabrata* and *Schizosaccharomyces pombe* in 1989 (Dameron et al. 1989). The process involved in nanoparticles synthesis by microbes is essentially bio-mineralisation and/or bio-reduction. These bio-nanofactories offer a better size control through compartmentalisation in the periplasmic space and vesicles, and the nanoparticles so obtained are stabilised as a result of capping by cellular metabolites.

1.5 Nanoparticles synthesis by microorganisms

Biological synthesis of nanoparticles using microorganisms is a clean, biocompatible, non-toxic, and an eco-friendly method. This method of nanofabrication exploits the highly structured physical and biosynthetic activities of microbial cells. Microbes when exposed to metals, overcome the toxicity using various metal resistance mechanisms. These mechanisms are a result of enzymatic detoxification of the metals, and/or extrusion of the metal through the energy-dependent ion efflux membrane transporters present in the cell. Microorganisms thereby, transform toxic metals to their non-toxic nanosized form; or the soluble form to the insoluble nanosized form, during these detoxification processes. Interactions between metals and microbes are well documented and have been exploited for various applications in the fields of bio-mineralisation, bio-leaching, and bio-remediation (Klaus-Joerger et al. 2001). Many magnetotactic bacteria are known to naturally produce nanostructured mineral crystals (Fig. 1.5) that have properties similar to chemically synthesised materials (Baumgartner et

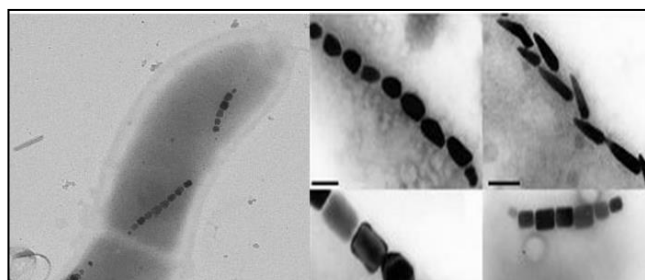


Fig. 1.5 Magnetotactic bacteria (left) exhibiting the magnetosomes chain and the magnetosomes (right) with various morphologies.

(http://2011.igem.org/wiki/images/5/56/Washington_iGEM2011_magnetotactic_bacteria_picture.jpg)

al, 2013). Such nano-factories exercise strict control over size, shape and composition by maintaining stringent control over the bio-reduction/detoxification process, and/or compartmentalisation in the periplasmic space and vesicles. Additionally, the microbially synthesised nanoparticles are usually capped by stabilising cellular metabolites produced during the process of synthesis. The rate of synthesis and the size of the nanoparticles can be manipulated to an extent by controlling parameters like pH, temperature, substrate concentration, and time of exposure of the substrate (Gericke and Pinches, 2006; Kang et al. 2008; Gurunathan et al. 2009). Various metallic, metal sulphides, metal oxide, and alloy nanoparticles have been synthesised by myriad microorganisms. The synthesis may either be an intracellular or an extracellular process depending upon the nature and the metabolic activity of the organism. Table 1.1 shows some of the organisms that have been reported for nanoparticles synthesis, their localization, and size. The forthcoming sections will describe the various halophilic organisms and their by-products that synthesise nanoparticles, the mechanisms involved, and applications of the synthesised nano-materials.

Table 1.1 Various inorganic nanoparticles synthesised by some microbes

	Organism	Type	Intra/Extracellular	Size (nm)	Shape	Application	Mechanism	Reference
BACTERIA	<i>Geobacillus</i> sp. Strain ID17	Au	Intra	5-50	Quasi-hexagonal	-	NADH-dependent reduction	Correa-Llanten et al. 2013
	<i>Serratia nematodiphilia</i>	ZnS	Extra	80	Spherical	Antimicrobial	-	Malakodi & Annadurai 2013
	<i>Pantoea agglomerans</i>	Se	Intra/Extra	100	Spherical	Antioxidant	-	Torres et al. 2012
	<i>Enetrobacter</i> sp.	Hg	Intra	2-5	Spherical	-	-	Sinha and Khare, 2011
	<i>Escherichia coli</i>	CdTe	Extra	~2-3	Spherical	Bioimaging	Protein mediated	Bao et al. 2010b
	<i>Bacillus licheniformis</i>	Ag	Extra	10-80	Spherical	-	NADH dependent NR mediated	Vaidyanathan et al. 2010
	<i>Rhodobacter sphaeroides</i>	CdS	Extra	~6.8	Spherical	-	-	Bai et al. 2009a
	<i>Lactobacillus</i> sp.	TiO ₂	Extra	~25	ND	-	Oxido-reductases	Jha et al. 2009a
	<i>Shewanella algae</i>	Pt	Intra	5	-	-	-	Konishi et al. 2007
	<i>Shewanella oneidensis</i> MR-1	UO ₂	Extra	1-5	-	-	C-type cytochrome	Marshall et al. 2006
<i>Desulfovibrio desulfuricans</i>	Pd	Surface bound	~11.5	-	Catalyst	Formate dehydrogenylase mediated reduction	Yong et al. 2002	

YEAST	<i>Rhodotorula mucilaginosa</i>	Cu	Intra	10.5	Spherical	-	-	Salvadori et al. 2014
	<i>Saccharomyces cerevisiae</i>	TiO ₂	Extra	~13	-	-	Oxido-reductase & Quinones	Jha et al. 2009a
	<i>S. cerevisiae</i>	Sb ₂ O ₃	Extra	2-10	Spherical	-	Oxido-reductase & Quinones	Jha et al. 2009b
	<i>Schizosaccharomyces pombe</i>	CdS	Extra	1-1.5	Wurtzite type hexagonal	Fabrication of diode	Phytochelatin mediated	Kowshik et al. 2002a
	<i>MKY3</i>	Ag	Extra	2-5	Hexagonal	-	-	Kowshik et al. 2002b
	<i>Torulopsis sp.</i>	PbS	Intra	2-5	Spherical	Quantum semiconductor	-	Kowshik et al. 2002c
FUNGI	<i>Aspergillus flavus</i>	Ag	Extra	3-25	Various shapes	-	NADH dependent NR	Majunath & Thiagarajan, 2014
	<i>Fusarium acuminatum</i>	Au	Extra	17	Spherical	-	NADH dependent NR	Tidke et al. 2014
	<i>Fusarium oxysporum</i>	SiO ₂	Extra	~10	Quasi-spherical	-	Cationic proteins of 21 & 24 kDa	Bansal et al. 2005
		TiO ₂	Extra	~10	Spherical	-		
	<i>Fusarium oxysporum</i>	Fe ₃ O ₄	Extra	20-50	Quasi-spherical	-	~55 kDa hydrolytic protein	Bharde et al. 2006
	<i>Verticillium sp.</i>		Extra	100-400	Cubo-octahedral	-		
<i>Fusarium oxysporum</i>	CdS	Extra	5-20	-	-	NADH and ATP dependent Sulfate reductase	Ahmad et al. 2002	

(-)- Not Determined; NR- Nitrate Reductase

1.5.1 Nanoparticle synthesis by Haloarchaea

Haloarchaea are members of the third domain of life, the Archaea, placed in order *Halobacteriales* under family *Halobacteriaceae* (Grant et al. 2001) within which a total of 50 genera and 213 species have been identified to date. These organisms require between 10-35% salt for optimum growth and are the predominant microflora of hypersaline environments (both thalassohaline and athalassohaline) such as solar salterns, salt lakes, soda lakes, salt deposits etc.



Fig. 1.6 Pink Lake- Port Gregory, Western Australia appears pink due to carotenoid pigments in the cell membranes of the haloarchaea that inhabit it. (<https://www.tumblr.com/search/haloarchaea>)

(Zafrilla et al. 2010). However, some low salt tolerant haloarchaea can be found in estuarine environments (Bochiwal 2009). Estuaries serve as interfacial mixing zones between rivers and seawaters that determine the flux of chemical species into the ocean (Shokovitz, 1976). Haloarchaea contribute to the red colouration of solar salt crystalliser ponds, salt lakes and ponds (Fig. 1.6) due to the presence of pigment α -bacterioruberin in their cell wall (Kamekura, 1993). They maintain their osmolarity by intracellular accumulation of KCl (up to 5 M) that counteracts the ionic strength of the extracellular environment (Martin et al. 1999).

Haloarchaea are known to encounter metals in their environment, but their metal tolerance has not been well documented. Eco-niches like estuaries (Ratheesh Kumar et al. 2010), and solar crystalliser ponds (Pereira et al. 2013) may contain high concentrations of metals since they serve as effective traps and ecological sinks for river borne metals (Chapman and Wang, 2001). Anthropogenic activities like urbanisation and industrialisation, including mining, agriculture, and waste disposal further contribute towards metal pollution at these sites (Ross, 1994; Tabak et al. 2005). Haloarchaea have developed various mechanisms of resistance in order to thrive under metal stress (Wang et al. 2004; Kaur et al. 2006; Bini, 2010). However, studies on metal resistance in haloarchaea are still in their infancy (Srivastava and Kowshik, 2013).

Gas vesicle nanoparticles (GVNPs) with modifications have been synthesised by genetically manipulating *Halobacterium* sp. NRC-1 (DasSarma et al. 2013; 2015a,b). GVNPs that may be engineered for various biotechnological applications are the buoyant gas vesicles widely distributed among bacteria and archaea. These organelles that naturally promote floatation are present in abundance in haloarchaea. The gas vesicles in haloarchaea are plasmid encoded with the genetic cluster *gvpMLKJIHGFEDACNO* involved in gas vesicle formation (DasSarma 1989; DasSarma and Arora 1997; DasSarma et al. 1987; Halladay et al. 1993). The proteins encoded by the gene clusters include the GvpA, J, and M of Pfam741 family, involved in gas vesicle membrane formation, and GvpF, and L, coiled-coil protein (Pfam 6386) involved in the nucleation of gas vesicles due to their self-associative properties (Jones et al. 1991; Shukla and DasSarma, 2004). Genes corresponding to these proteins have been found in other organisms as well, with the exception of *gvpC* gene, which is found only in haloarchaea, and cyanobacteria (van Keulen et al. 2005). In the haloarchaeon *Halobacterium* sp. NRC-1, the GvpC protein is hydrophilic and insertion mutations within this gene results in gas vesicles with altered shape and size (Fig. 1.7) (DasSarma et al. 1994). By genetic manipulation of *gvpC* gene, the gas vesicles may be made to express different proteins or display antigens, thereby enhancing their potential applications in the field of biotechnology. A new *Halobacterium* sp. NRC-1 derived host strain and a series of smaller, more versatile plasmid expression vectors have been constructed to obtain a significantly improved genetic system for expression of GvpC-fusion proteins. For example, active *Gaussia princeps* luciferase enzyme can be fused to GvpC that would result in the expression of the luciferase enzyme on the surface of the GVNPs (DasSarma et al. 2013). Similarly, genetically modified GVNPs have also been used for *Salmonella* antigen display in vaccine development (DasSarma et al. 2015a,b).

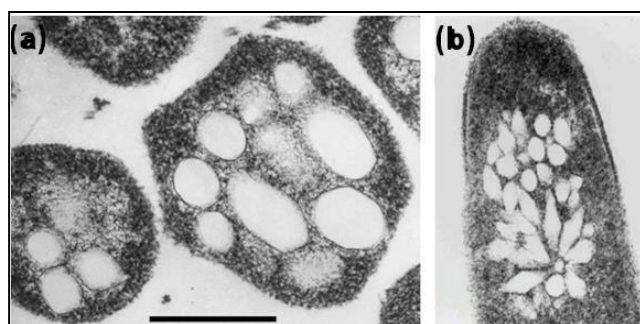


Fig. 1.7 TEM micrographs showing thin sections of (a) *Halobacterium* sp. NRC-1 and (b) SD109 (pFM104gvpC:: κ 1) mutant. Gas vesicles can be seen as empty oval or spindle shaped regions. SD109 (pFM104gvpC:: κ 1) mutant exhibits gas vesicles with altered phenotypes. (Scale bar =325 nm) (DasSarma et al. 2013; under CC BY 3.0 license)

1.5.2 Nanoparticles synthesis by slight and moderate halophiles

Halophiles are salt loving organisms that flourish in saline environments and can be classified as slightly, moderately, or extremely halophilic, depending on their sodium chloride requirements (DasSarma and DasSarma, 2012). The saline environments that halophiles inhabit include the marine and estuarine environments, solar salterns, salt lakes, brines, and saline soils. Marine environments could be good source of metal tolerant microbes as most of these organisms exist at the bottom of the sea, and contribute towards bio-geochemical cycling of inorganic elements. Besides, the marine eco-niche is continuously exposed to metallic pollution due to volcanic eruptions, natural weathering of rocks, anthropogenic activities such as mining, combustion of fuels, and industrial and urban sewage. Estuaries and solar salterns may also contain high concentrations of metals as they serve as effective traps for river borne metals (Chapman and Wang 2001). Thus, halophiles are continuously exposed to metals and could be exploited for nanoparticle synthesis.

Nanoparticles synthesis by halophiles is in its infancy and has been reported in few bacteria, yeasts, fungi, and algae. Table 1.2 gives the details of nanoparticles synthesised by few halophiles. The exopolysaccharides (EPS) secreted by the halophiles have also been exploited for synthesis of composite nanoparticles for various drug delivery applications. The exopolysaccharide Mauran, secreted by halophilic bacteria *H. maura* stabilises ZnS:Mn²⁺ QDs enhancing the biocompatibility and reducing the cytotoxicity of the QDs (Raveendran et al. 2014).

1.5.2.1 Halophilic bacteria and nanofabrication

Reports on nanoparticles synthesis by halophilic bacteria, and their metabolites are mostly confined to metallic nanoparticles. A highly silver tolerant halophilic marine bacterium *Idiomarina* sp. PR58-8 synthesises intracellular crystalline silver nanoparticles (SNPs) with an average particle size of 26 nm. Non-protein thiols (NP-SH), that are known to be expressed in

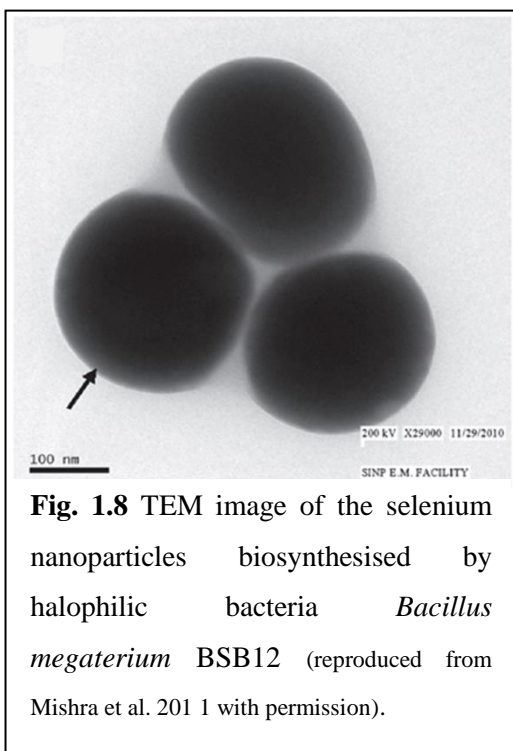


Fig. 1.8 TEM image of the selenium nanoparticles biosynthesised by halophilic bacteria *Bacillus megaterium* BSB12 (reproduced from Mishra et al. 2011 with permission).

response to metal stress, were found to be involved in metal tolerance (Seshadri et al. 2012). Similarly, a novel halophilic strain of *Pseudomonas* sp. 591786 was also reported to synthesise polydisperse intracellular SNPs with sizes ranging from 20-100 nm (Muthukannan and Karuppiah, 2011). The morphology of the gold nanoparticles (AuNPs) synthesised by the halophilic proteobacterium, *Halomomas salina* was found to be pH dependent, where alkaline pH resulted in spherical nanoparticles while nanoparticles with mixed morphology (nano-triangles and spherical) were obtained at acidic pH. The nanoparticle synthesis was extracellular and the NADH-

dependent nitrate reductase was involved in the silver reduction and nanoparticle synthesis (Shah et al. 2012). Similarly, two halophilic strains of *Bacillus megaterium*, BSB6 and BSB12, isolated from Bhitarkanika mangrove soils synthesise spherical selenium nanoparticles (SeNPs) both intracellularly and extracellularly with an average size of 200 nm (Fig. 1.8). The mechanism involved for the reduction of selenite to selenium however, remains unexplored (Mishra et al. 2011).

Two strains of halophilic bacteria *H. eurihalina* ATCC 49336 and *H. maura* ATCC 700995 convert graphene oxide (GO) to graphene sheet under both aerobic and anaerobic conditions. Reports on biological synthesis of graphene by microorganisms are rare. The microbially reduced GO sheet exhibited an increased conductivity as compared to chemically reduced GO, and was biocompatible. Such biocompatible graphene sheets may be used for green electronics, and biological applications such as detection of cancer biomarkers, encapsulation of enzymes and nanoparticles (Raveendran et al. 2013a; Myung et al. 2011).

Bacterial metabolites or products such as polysaccharides/bio-flocculants, and enzymes (eg. nitrate reductase) are also being used as reducing agents to synthesise inorganic nanoparticles. In most cases the synthesised nanoparticles are capped by reducing agents. MBSF17, a

polysaccharide bio-flocculant produced by a halophilic bacterium *Bacillus subtilis* MSBN17 could reduce silver nitrate to synthesise spherical SNPs in reverse micelles. The electrostatic forces between the amino groups of the polysaccharide MSBF17 and the silver ions in the solution were proposed to be the driving force for the formation and stabilisation of the SNPs. The carboxyl, hydroxyl, and methoxyl groups of MSBF17 form a coating on the SNPs thereby, stabilising them. These nanoparticles exhibited antimicrobial activity against a host of pathogenic organisms (Sathiyarayanan et al. 2013).

Besides the various inorganic and organic nanoparticles, the EPS of the halophilic bacteria has also been utilised for fabrication of polymer hybrid nanomaterials. The highly sulphated anionic EPS, Mauran (MR), secreted by the halophilic bacterium *H. maura*, is well characterised and has been successfully used for generation of such hybrid nanomaterials. MR exhibits characteristic viscoelastic, pseudoplastic, and thixotropic behaviour and has an ability to withstand harsh conditions, which make it an ideal candidate for material science research. The high sulphate content imparts immune-modulating, and anticancer properties to MR. Thus, MR

can be used for various biomedical applications due to their biological and physicochemical properties. MR-Chitosan (MR/CH) hybrid nanoparticles (Fig. 1.9) fabricated via the ionic-gelation technique when used for encapsulation of drugs exhibited controlled and sustained drug release, and biocompatibility (Raveendran et al. 2013b). Similarly, electrospun MR-Poly Vinyl Alcohol (MR-PVA) nanofibre membranes (Fig. 1.10) could boost the cellular adhesion, migration, proliferation, and differentiation, properties desirable for tissue engineering

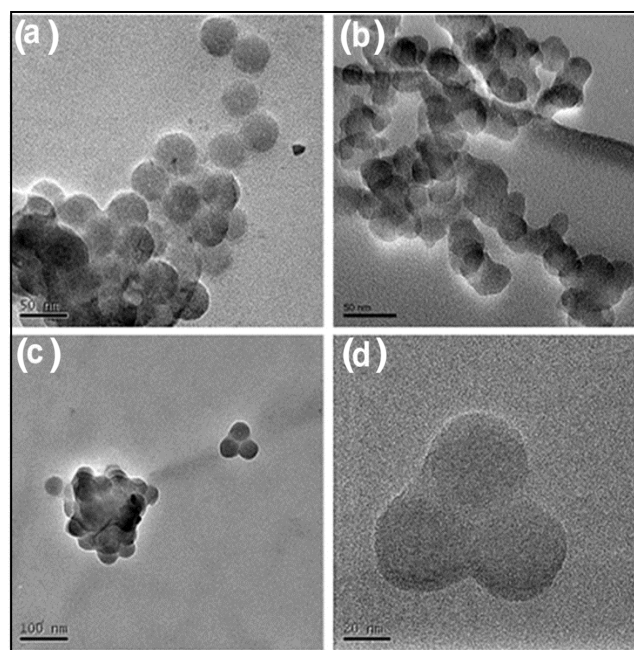
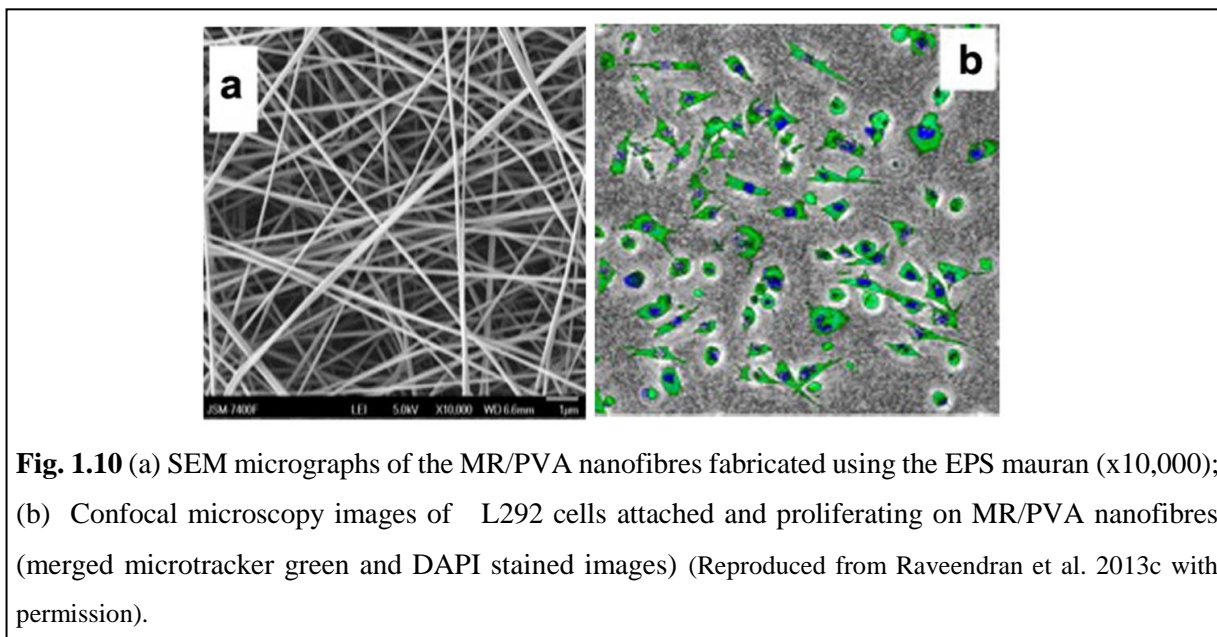


Fig. 1.9 TEM micrographs (a-d) depicting the morphology of the MR-CH nanoparticles fabricated using the EPS mauran secreted by the halophilic bacteria, *Halomonas maura* (Reproduced from Raveendran et al. 2013b with permission).

applications (Raveendran et al. 2013c). MR may be used in augmenting the biocompatibility of QDs that are usually cytotoxic. MR conjugated with ZnS:Mn²⁺ QDs resulted in a drastic increase in cell viability as compared to cell viability of bare QDs (Raveendran et al. 2014). Therefore, in addition to fabrication of polymer based nanomaterials, MR can also be used in conjugation with inorganic nanoparticles for enhancing their biological applications.



1.5.2.2 Nanoparticles and halophilic yeast and fungi

A few halophilic yeasts and fungi are known to synthesise nanomaterials. *Pichia capsulata*, a mangrove derived halophilic yeast, is capable of synthesising SNPs extracellularly (Manivannan et al. 2011). *Rhodospiridium diobovatum*, a marine yeast, could synthesise lead sulphide nanoparticles (PbSNPs) intracellularly with the help of NP-SH (Seshadri et al. 2011). Similarly, the extracellular synthesis of SNPs by the marine fungus *Penicillium fellutatum*, entails a 70 kDa protein present in the cell filtrate that acts as the reducing agent (Kathiresan et al. 2009). SNPs have also been synthesised by the halophilic fungi *Thraustochytrium* sp. and *Aspergillus niger*. SNPs synthesised by *Aspergillus niger* exhibited antibacterial activity against pathogenic bacteria which could be further enhanced by passivating them with PVA (Kathiresan et al. 2010).

1.5.2.3 Halophilic algae in nanoparticles synthesis

Currently, studies on nanoparticles syntheses by halophilic algae are on extracellular synthesis of inorganic (metallic) nanoparticles. The marine brown algae *Sargassum wightii* was found to synthesise stable AuNPs (30-100 nm), and SNPs (8-12 nm) when its extract was exposed to gold chloride and silver nitrate, respectively (Singaravelu et al. 2007; Oza et al. 2012). Similarly, various active molecules, rich in hydroxyl, and carboxyl groups, present in the extracts of *S. longifolium* could reduce silver nitrate to spherical SNPs that exhibited excellent antifungal activity (Rajeshkumar et al. 2014). The water soluble EPS extracted from the marine algae *Pterocladia capillacea*, *Jania rubins*, *Ulva faciata*, and *Colpomenia sinusa* reduced silver ions to SNPs, and also served as stabilising agents. These nanoparticles have been used to make antibacterial cotton fabrics (El-Rafie et al. 2013). EPS-gold and silica-gold bio-nanocomposites have been generated using the diatoms *Navicula atomus*, and *Diadesmis gallica*. These diatoms when grown in presence of tetrachloroaurate, reduced it to AuNPs that were associated with the diatom frustules and the EPS. The gold bio-nanocomposites find applications in the field of catalysis (Schrofel et al. 2011).

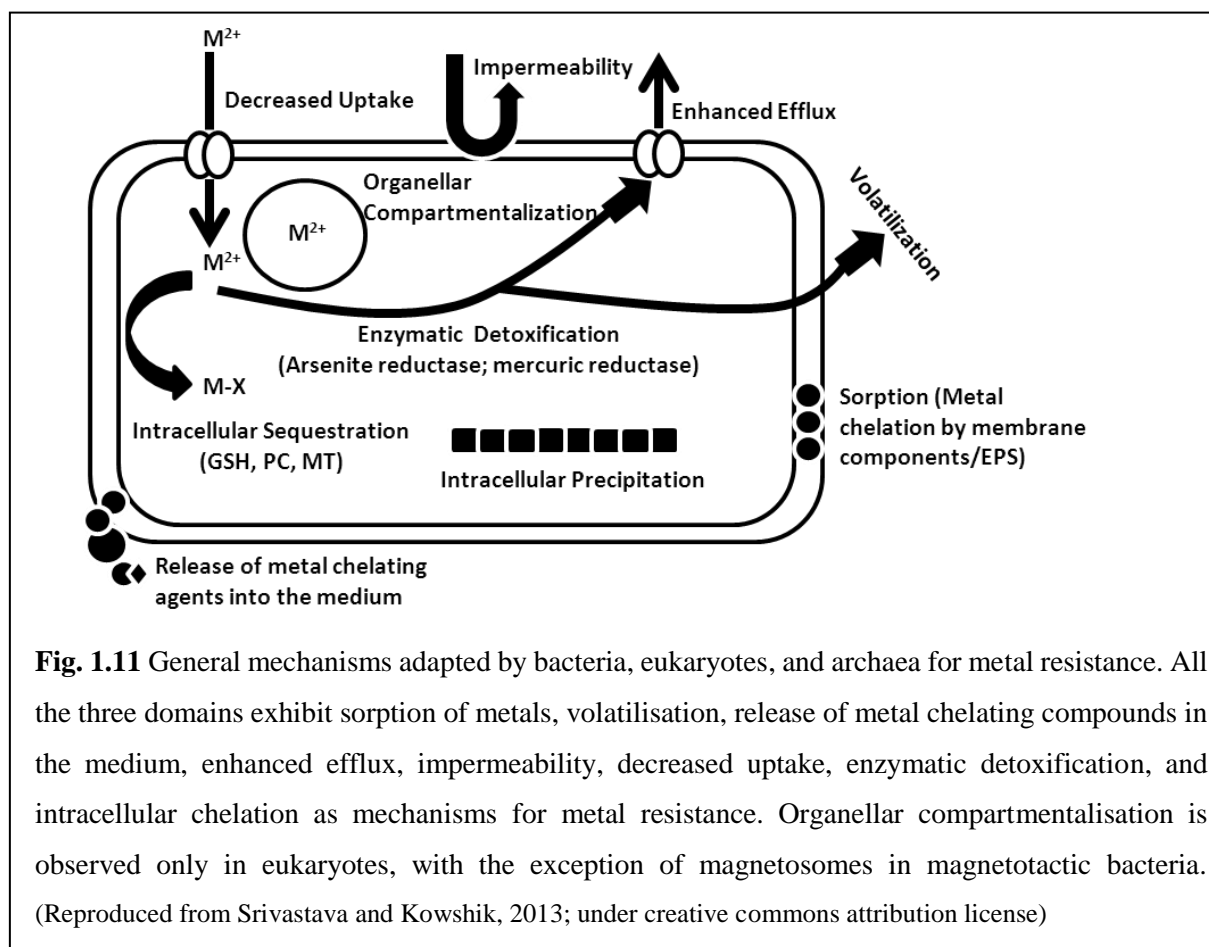
Table 1.2 The inorganic nanoparticles biosynthesised by various halophiles

Halophilic	Organisms	Type	Intra/Extra cellular	Size (nm)	Shape	Application	Mechanism	Reference
Bacteria	<i>Idiomarina</i> sp. PR58-8	Ag	Intra	26	-	-	NP-SH	Seshadri et al. (2012)
	<i>Pseudomonas</i> sp. 591786	Ag	Intra	20-100	Spherical	-	-	Muthukannan and Karuppiah (2011)
	<i>Halomonas salina</i>	Au	Extra	30-100	Anisotropic; Spherical	-	NADH-NR	Shah et al. (2012)
	<i>Bacillus megaterium</i> BSB6 & BSB12	Se	Intra; Extra	~200	Spherical	-	-	Mishra et al. (2011)
Yeast	<i>Pichia capsulata</i>	Ag	Intra	50-100	-	-	-	Manivannan et al. (2011)
	<i>Rhodospiridium diobovatum</i>	PbS	Intra	2-5	Spherical	-	NP-SH	Seshadri et al. (2011)
Fungi	<i>Penicillium fellutatum</i>	Ag	Extra	5-25	Mostly Spherical	-	70 kDa protein	Kathiresan et al. (2009)
	<i>Aspergillus niger</i>	Ag	Extra	5-35	Mostly Spherical	Antibacterial	70 kDa protein	Kathiresan et al. (2010)
Algae	<i>Sargassum wightii</i>	Ag	Extra	8-12	Planar	-	-	Singaravelu et al. (2007)
	<i>S. wightii</i>	Au	Extra	30-100	Isotropic Spheres	-	NADH-NR	Oza et al. (2012)
	<i>S. longifolium</i>	Ag	Extra	-	Spherical	Antifungal	-	Rajeshkumar et al. (2014)
	<i>Pterocladia capillacea</i> ; <i>Jania rubins</i> ; <i>Ulva fasciata</i> ; <i>Colpomenia sinusa</i>	Ag	Extra	-	-	Antibacterial	Polysaccharides	El-Rafie et al. (2013)
	<i>Navicula atomus</i> ; <i>Diadesmis gallica</i>	Au	Extra	9; 22	Spherical	-	-	Schrofel et al. 2011

(-)- Not determined; NP-SH: Non-Protein Thiols; NADH-NR: NADH-dependent Nitrate reductase

1.6 Mechanisms of metallic nanoparticles synthesis

Microbial synthesis of metallic nanoparticles involves exposing either the biomass or the cell free supernatant of the culture to metal salts. The microorganisms on encountering metal salts try to circumvent the toxicity by either preventing the influx or in the event of uptake convert the metal into a non-toxic particulate form. Owing to the size of the microbes the non-toxic particulate form of the metal is in nano-range. Mechanisms involved in nanoparticle synthesis by microorganisms may entail processes similar to metal resistance (Fig. 1.11). Metals constitute about 75% of the known elements and are ubiquitous in the biosphere. Some of these metals are directly and/or indirectly involved in all aspects of microbial growth, metabolism and differentiation, while others play no physiological role (Gadd, 1992). When present in the microenvironment, most metals exert toxicity towards microbes, which try to overcome it by elucidating various resistance mechanisms. These metal-microbe interactions involve either solubilisation or immobilisation.



Solubilisation can occur due to: (i) chemo-lithotrophic (autotrophic) and chemo-organotrophic (heterotrophic) leaching; (ii) binding with siderophores and other complexing agents; (iii) redox reactions; (iv) methylation and demethylation; and (v) biodegradation of organo-radionuclide complexes (Gadd, 2007; Gadd, 2010a).

Immobilisation can occur due to: (i) biosorption on cell walls, exo-polymers, other structural components, and derived/excreted products; (ii) precipitation as a result of metabolite release (e.g. sulphide, oxalate) or reduction; (iii) transport, accumulation, intracellular deposition, localisation, and sequestration; and (iv) adsorption and entrapment of colloids and particulates (Gadd, 2007; Gadd, 2010).

Enzymatic detoxification leading to intracellular precipitation, intracellular sequestration by peptides, organellar compartmentalisation, and release of metal chelating agents in the medium along with sorption of metals by membrane component/ EPS usually results in the toxic form of the metal being converted to immobile, non-toxic nano-particulate form (Ramezani et al. 2010). Microorganisms during the course of metabolic processes (chemo-lithotrophy), as in case of sulphate reducing bacteria, may precipitate metal salt as metal sulphide nanoparticles (Jung et al. 2002). Nanoparticles may also be synthesised by the organism for specialised functions such as magnetosomes in magnetotactic bacteria that enable them to navigate with respect to the earth's magnetic north and south poles (Bazylinski and Frankel, 2004). Reports on nanoparticles synthesis by microorganisms are numerous; however, the mechanisms involved are not well understood. Studies so far have not been able to elucidate the entire pathway, from the uptake of the metal/ metal salt by the organisms to the final fate of the metal. The metabolic complexity of viable microorganisms complicates the analysis and identification of active species in the nucleation and growth of MNPs (Kitching et al. 2015). Some of the active species including thiol (-SH) containing molecules (such as glutathione, phytochelatin, etc.), and enzymes (such as oxido-reductases, NADH- dependent reductases, etc.), that have been implicated in microbial MNPs synthesis are described in the following sections.

1.6.1 Glutathione and related peptides in nanomaterial synthesis

Glutathione (GSH; non-protein thiol) and its related peptides, metallothioneins (MT; protein bound thiol) and phytochelatins (PC; protein bound thiol) are cysteine rich metal-binding

peptides that have been known to play a major role in metal resistance, and nanoparticle synthesis. GSH is a tri-peptide with a γ -Glu-Cys-Gly structure, and is involved in various metabolic processes in bacteria and yeast. MTs are small molecular weight genetically coded polypeptides that are classified based upon the number of cysteine residues (Cobbett and Goldbrough, 2002). They typically have two cysteine rich domains that bind heavy metals through mercaptide bonds, giving these proteins a dumbbell shaped conformation comprising of a N-terminal β domain that usually binds 3 metal ions, and a C-terminal α domain that binds 4 metal ions (Cherian and Chan, 1993; Wang et al. 2006). PCs comprise of $(\gamma\text{-GluCys})_n\text{-Gly}$ where n is usually in the range of 2 to 5. They are enzymatically synthesised by PC synthase using GSH as the substrate (Glaeser et al. 1991; Rauser, 1995). The thiol group of the cysteine residue in PCs sequesters heavy metals.

Formation of these peptides occurs in response to metal stress. PC synthesis is induced most actively by Cd^{2+} , followed by Ag^+ , Bi^{3+} , Pb^{2+} , Zn^{2+} , Cu^{2+} , Hg^{2+} , and Au^{3+} . In *S. pombe*, on exposure to Cd^{2+} , PC synthases (γ -Glu-Cys dipeptidyl transpeptidase) are activated which results in synthesis of PCs (Grill et al. 1989). The thiol component of the cysteine group in PC binds to the Cd^{2+} in the cytosol to form a low molecular weight PC-Cd complex, and a high molecular weight PC-Cd- S^{2-}

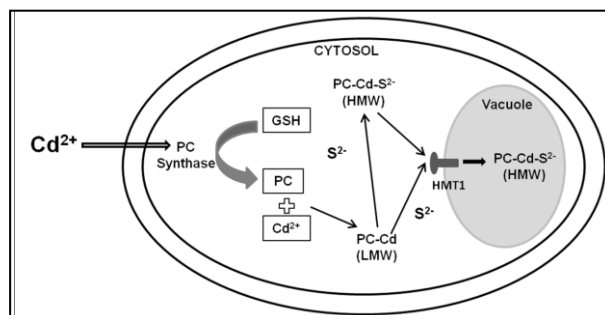


Fig. 1.12 Mechanism of CdS nanocrystallite formation in *Schizosaccharomyces pombe* involves Phytochelatins (PC). (LMW- Low molecular weight; HMW- High molecular weight)

complex (Reese et al. 1992; Speiser et al. 1992). These complexes are then transported across the vacuolar membrane by HMT1, an ATP binding cassette (ABC)-type transporter for accumulation within vacuoles (Fig. 1.12) (Ortiz et al. 1995). Thus, the CdS nanocrystallites formed are capped by these peptides. Similarly, in the yeast *C. glabrata*, 85 units of CdS were proposed to form a core that possesses a coating of 30 PC peptides (Dameron and Winge, 1990). As GSH related peptides are involved in nanoparticle synthesis, Park et al (2010) developed a recombinant *E. coli* system expressing PCs and/or MTs for *in-vivo* synthesis of various MNPs,

including certain unique materials not reported earlier. These included Au, Ag, Fe, CdSe, CdTe, SrGd, FeAg, FeCo, FeMn, CdSeZn, FeCoNi, FeCoMn and AuCdSeZn.

1.6.2 Enzymes and nanoparticles synthesis

Numerous studies have proposed the involvement of specific enzymes in reduction of metal salt to metallic and/or metal sulphide nanoparticles (Ramezani et al. 2010). Although, it has been established that certain components involved in microbial energy metabolism (Ehrlich, 1997), and/or detoxification mechanisms are associated with microbial nanoparticles synthesis, the entire pathway of nanofabrication has not been elucidated. (Gadd, 2010b). Various enzymes implicated in nanoparticles synthesis include oxido-reductases, NADH-dependent reductases, NADH-dependent nitrate reductase (NR), sulphate and sulphite reductase, hydrolases, and cysteine desulphhydrase (Ramezani et al. 2010). An initial challenge during intracellular nanoparticle synthesis is the adsorption of the metal salt onto the cell-membrane and its entry via membrane transporters. Following this, the enzyme reduces the metallic ions to form nanoparticles (Kannan et al. 2011). In case of extracellular synthesis, the microbe may secrete the enzyme into the medium where bio-reduction takes place (Bansal et al. 2004).

1.7.2.1 Oxido-reductases

Membrane bound oxido-reductases have been implicated in synthesis of TiO₂ nanoparticles by *S. cerevisiae* (Jha et al. 2009a), Ti nanoparticles by *Lactobacillus* sp. (Prasad et al. 2007), and Sb₂O₃ nanoparticles by *S. cerevisiae* (Jha et al. 2009b). Oxido-reductases are pH dependent enzymes that behave as oxidases in acidic pH, and as reductases in alkaline pH (Nelson and Cox, 2005). Jha et al. (2009a) suggested the involvement of quinones as well in the process. They proposed that the addition of metal precursors brings about tautomerisation of quinines, and low pH sensitive oxidases provide the oxygen required for the transformation of the metal salt to oxide nanoparticles.

1.6.2.2 NADH-dependent reductases

NADH-dependent reductases are a class of enzymes that require NADH for their activity. Reduction is initiated by electron transfer from NADH to the substrate, by the NADH-dependent reductases that act as electron carrier. AuNPs synthesis by *Rhodopseudomonas capsulata* was proposed to be mediated by NADH-dependent reductases (He et al. 2007). These enzymes have also been implicated in Au-Ag alloy nanoparticles synthesis by *F.*

oxysporum (Senapati et al. 2005). Similarly, membrane associated NADH-dependent reductases were found to be involved in selenite reduction and SeNPs synthesis by *Enterobacter cloacae* SLD1a-1, and *Bacillus cereus* (Losi and Frankenberger, 1997; Dhanjal and Cameotra, 2010). NADH dependent reductases from *Thermus thermophilus* HB8 exhibited tellurite reductase activity and tellurite resistance (Chiong et al. 1988) and may result in nanoparticle synthesis. More recently NADH dependent reductases were implicated in the extracellular synthesis of AuNPs by *Botrytis cinerea* (Castro et al. 2014).

1.6.2.3 Nitrate Reductases (NR)

Numerous studies including SNPs synthesis by *Aspergillus flavus* (Sangappa and Thiagarajan, 2014), *Bacillus licheniformis* (Vaidyanathan et al. 2010), *E. coli* (Lin et al. 2014), *Klebsiella pneumoniae* (Narayanan and Sakthivel, 2010), AuNPs synthesis by *H. salina* (Shah et al. 2012), *Fusarium acuminatum* (Tidke et al. 2014), and UO₂ nanoparticles synthesis by *Shewanella oneidensis* MR-1 (Marshall et al. 2006) have suggested the involvement of NADH-dependent NR in nanoparticles synthesis. The c-type cytochrome component of the NR was suggested to be the centre of metal reduction. In fact, more recently the role of c-type cytochromes in SNPs synthesis in *E. coli* was established by mutant studies. In mutants with cytoplasmic membrane-anchored tetra-heme c-type cytochrome subunit of periplasmic nitrate reductase (NapC) deletion, nanoparticle synthesis did not occur, however re-introduction of this component

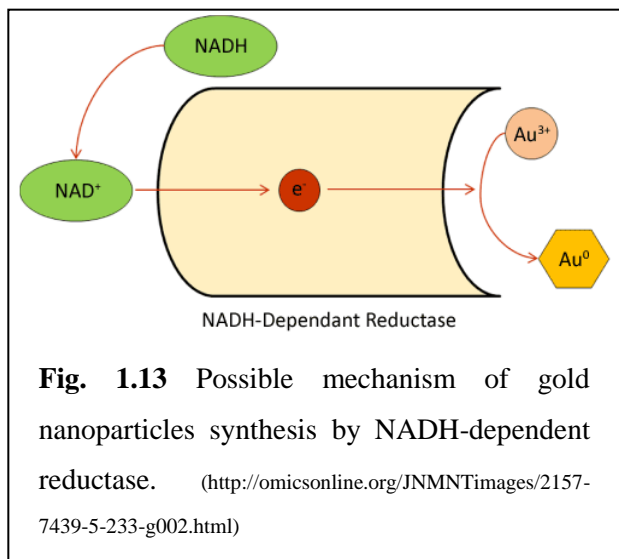


Fig. 1.13 Possible mechanism of gold nanoparticles synthesis by NADH-dependent reductase. (<http://omicsonline.org/JNMNTimages/2157-7439-5-233-g002.html>)

restored the synthesis (Lin et al. 2014). In case of fungal strains, naphthoquinones and anthroquinones act as redox centres and along with NR bring about nanoparticles synthesis (Duran et al. 2005). The purified NR enzyme extracted from the culture supernatant of *F. oxysporum* has been used for synthesis of SNPs, and this nano-preparation was found to be stabilized by the PC peptide (Anil Kumar et al. 2007).

1.6.2.4 Enzymes of sulphate and sulphite metabolic pathway

The enzymes of sulphur metabolism pathway are involved primarily in metal sulphide nanoparticles synthesis. The mechanism involved in ZnS nanoparticle synthesis by immobilised *Rhodobacter sphaeroides* using $ZnSO_4$ as the precursor has been elucidated, wherein it has been (Fig. 1.14) postulated that the sulphate (SO_4^{2-}) acts as the source of S and diffuses into the immobilised beads. Sulphate permeases facilitate the entry of SO_4^{2-} into the cells, which is further reduced to SO_3^{2-} (sulphite) by ATP sulphurylase and phosphoadenosine phosphosulphate reductase.

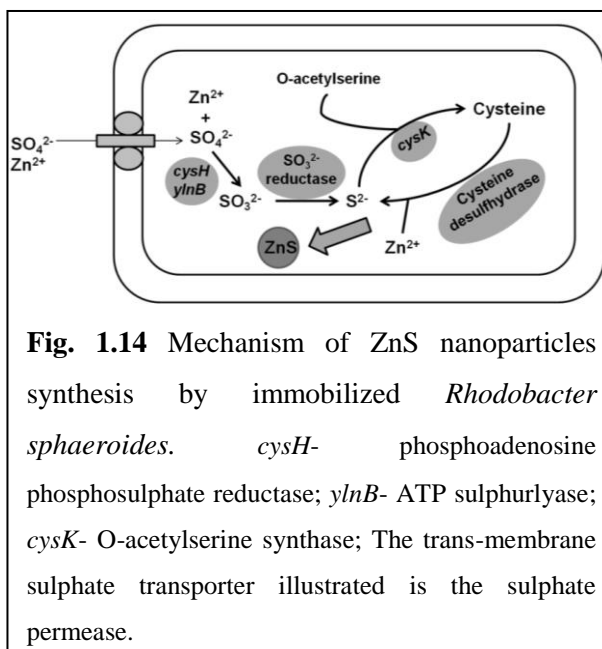


Fig. 1.14 Mechanism of ZnS nanoparticles synthesis by immobilized *Rhodobacter sphaeroides*. *cysH*- phosphoadenosine phosphosulphate reductase; *ynb*- ATP sulphurylase; *cysK*- O-acetylserine synthase; The trans-membrane sulphate transporter illustrated is the sulphate permease.

Sulphite reductase reduces the SO_3^{2-} to sulphide (S^{2-}), which reacts with O-acetylserine and assists in synthesis of cysteine via O-acetylserine thiolase. In presence of Zn, the sulphide is transferred from cysteine to Zn by cysteine desulphhydrase to form ZnS nanoparticles. The 'as-synthesised' ZnS are then extruded from the bacterial cell to circumvent the toxicity (Bai et al. 2006). Cysteine desulphhydrase was also found to be involved in CdS nanocrystal formation in *Rhodopseudomonas palustris* in the presence of $CdSO_4$ (Bai et al. 2009b).

The extracellular synthesis of CdS nanoparticles by *F. oxysporum* was attributed to the sulphate reductase elaborated by the fungi when exposed to $CdCl_2$ and Na_2SO_4 . The sulphate component is reduced by the enzyme to S^{2-} that reacts with Cd^{2+} to form the CdS nanoparticles. The enzyme has an absolute requirement of ATP and NADH for its activity (Ahmad et al. 2002).

1.7 Applications of biosynthesised MNPs

Advancements in the field of nanotechnology has the potential to revolutionise the industry, including electronics, medicine, environmental remediation, oil recovery, and consumer products (Iskandar, 2009; Kaur and Gupta, 2009; Schrofel et al. 2014; Vance et al. 2015; Cheraghian and Hendraningrat, 2016). Some of the commercially viable applications of nanoparticles include: (i) targeted drug delivery for treatment of cancers and other diseases (ii) diagnostic applications like imaging (MRI), tomography, magnetic resonance spectroscopy (iii) stain-free clothing and mattresses; (iv) polymer films as displays for laptops, cell phones, digital cameras; (v) water proof nano-coatings on mobile/cellular devices; (vi) sunscreens and cosmetics; (vii) flexible nano-lumen display; (viii) topical ointments to treat burns and wounds; (ix) ultra-light weight sports equipments, (x) in food industry for food packaging, food additive, etc. Besides these commercial applications, extensive research is being carried out to generate novel nanomaterials for applications in fields of tissue engineering (Rosenholm et al. 2016), gene delivery and therapy (Majidi et al. 2016), vaccine development (Manayani et al. 2007), data storage (Estrader et al. 2013). The nanomaterials used for these applications may be synthesised by chemical, physical, or biological methods of nanofabrication.

Biologically synthesised MNPs find application in various fields, from biomedical, to environmental remediation, to other industrially relevant applications such as, electrodes and sensors, catalytic organic synthesis, fuel cell fabrication, etc. Biologically synthesised Ag and Au MNPS have been shown to have antimicrobial, antifungal, antiviral, and/or antiparasitic applications (Duran et al. 2007; Musarrat et al. 2010; De Gusseme et al. 2011; Rajakumar et al. 2012). Similarly, biologically synthesised Au, Ag, Cu, Se, and Fe₃O₄ nanoparticles have been shown to have anticancer, and drug delivery applications (Sun et al. 2008; Valodkar et al. 2011; Amarnath et al. 2011; Luo et al. 2012). These MNPs also find applications in medical diagnostics and sensors. Some of the examples include: (i) AuNPs as human blood serum glucose sensor; (ii) SeNPs for H₂O₂ sensing; (iii) Au-Ag alloy nanoparticles for food quality evaluation sensors; (iv) AuNPs in conjugation with DNA for detection of genetic diseases (Miao 2013; Wang et al. 2010; Zheng et al. 2010; Yao et al. 2015). Few MNPs like Ag, Au, CdTe, CdSe, and CdS have been used for bio-labelling and bio-imaging applications (Sarkar et al. 2010; Bao et al. 2010a; 2010b; Fayaz et al. 2011; Pandian et al. 2011). Magnetic

nanoparticles from magnetotactic bacteria have been used in applications like magnetic solid-phase extraction for biological, food, and environmental sample preparation (Wierucka and Biziuk, 2014), environmental remediation (Tang and Lo, 2013), magnetically guided drug delivery, systemic and local chemotherapy, magnetic fluid hyperthermia for cancer treatment, bio-imaging via MRI, theranostics (Reddy et al. 2012), data storage (Estrader et al. 2013), etc.

Bio-nanofactories may be used for various bio-sorption, bio-remediation, and bio-recovery of metals that act as environmental pollutants (Hennebel et al. 2009). MNPs that are formed through this process may then be used for catalytic degradation of environmental pollutants such as dichlorodiphenyltrichloroethane (DDT), dieldrin and hexachlorobenzene, polychlorinated biphenyls, nitro-aromatic dyes etc. (Redwood et al. 2008; Gangula et al. 2011). MNPs may also be used for synthesis of organic compounds, to fabricate H₂ fuel cells, as catalyst for chemical oxidation of fuel, to improve power recovery and to fabricate electrodes and sensors (Ogi et al. 2011; Huang et al. 2014; Bindhu and Umadevi, 2014). Thus, nanoparticles find applications in numerous fields, as shown in fig. 1.15.

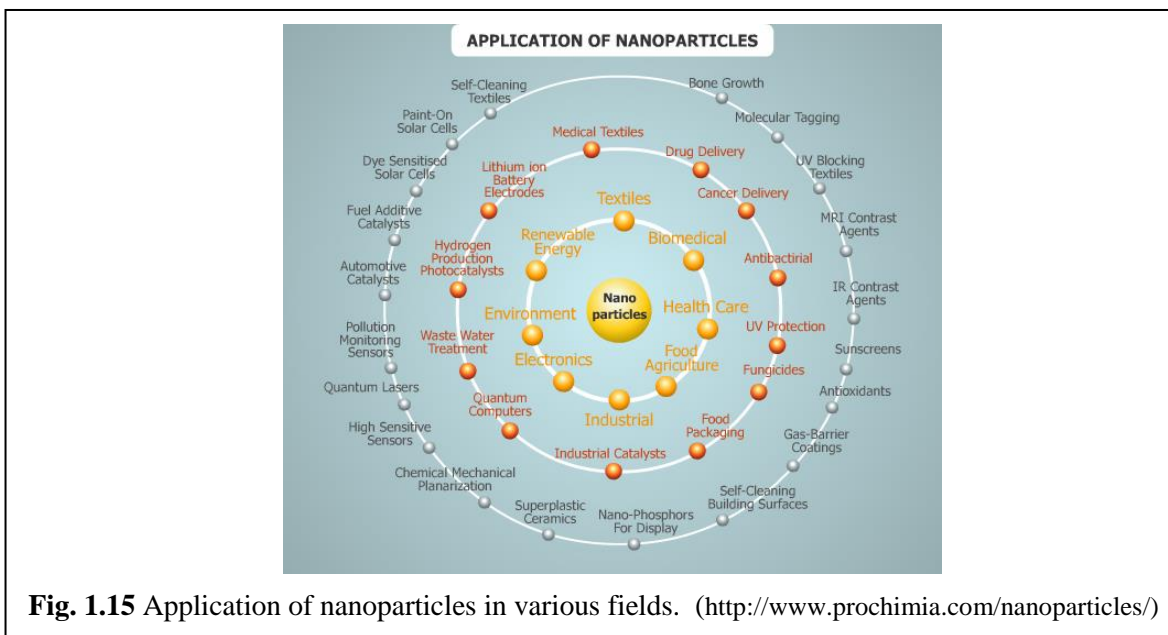


Fig. 1.15 Application of nanoparticles in various fields. (<http://www.prochimia.com/nanoparticles/>)

1.9 GAPS IN EXISTING RESEARCH

Based on the review of literature, following lacunae were found and the objectives were framed by taking the following gaps in account:

1. Numerous bacteria, fungi, yeast, algae, viruses and plants have been used for synthesis of inorganic nanoparticles in the last two decades. However, haloarchaea, have not been explored for their potential in nanoparticle synthesis. This may generate nanomaterials with unique properties that could be exploited for novel applications. Moreover, synthesis of nanoparticles by these organisms will add to the biotechnological applications of haloarchaea.
2. Haloarchaea are the predominant microflora of hypersaline eco-niches such as solar salterns, soda lakes, and estuaries. Eco-niches like estuaries, and solar crystalliser ponds may contain high concentrations of metals since they serve as ecological sinks, for metal pollution and also as effective traps for river borne metals. Although haloarchaea are known to encounter metals in their environment, their metal tolerance has not been well documented, as evident from the review of literature. Studies to further our knowledge and understanding of mechanisms that may be involved in metal resistance/tolerance in haloarchaea are essential.
3. Similarly, studies on nanoparticle synthesis by halophilic bacteria are limited. These bacteria inhabit marine environments that are a good source of metal tolerant organisms as the marine environment is continuously exposed to metals released by volcanoes, natural weathering of rocks, and also by numerous anthropogenic activities, such as mining, combustion of fuels, industrial and urban sewage, and agricultural practices. These organisms may therefore show high tolerance to heavy metals and are potential nano-factories that need to be exploited.
4. Even though microbial cells have shown a great potential for biosynthesis of inorganic nanoparticles within their orderly regulated intracellular environment, very little is known about the mechanism of nanoparticle biosynthesis. Therefore, it is difficult to control intracellular synthesis through the manipulation of biological processes, and studies on the mechanistic aspects of microbial nanoparticle synthesis are the need of the hour.

1.10 AIMS AND OBJECTIVES OF THE RESEARCH WORK

Approaches to maximise environment friendly methods of nanoparticle synthesis include microbial synthesis. The commonly used approaches for nanomaterial synthesis include physical and chemical methods which involve the use of toxic precursors and extreme conditions of temperature and pressure for synthesis (Thakkar et al. 2010; Mallick et al. 2004). The use of microbes for biosynthesis of highly structured nanoparticles was proposed as a green approach for synthesis of metal sulphide and metallic nanoparticles (Gericke and Pinches, 2006; Dameron et al. 1989). Microbes transform the toxic metals to non-toxic nano-sized form, or soluble form to insoluble nano-sized form. Various bacteria, fungi, yeast, and algae have been used for nanoparticle synthesis (Thakkar et al. 2010), but halophilic archaea remain unexplored for the same, while very few halophilic bacteria have been used as nano-factories.

Haloarchaea, belong to the third domain of life Archaea, and inhabit saline eco niches (solar salterns, estuaries) whereas, halophilic bacteria are found in solar salterns only during transitional state (Zafrilla et al. 2010). Halophilic bacteria may also be isolated from sea water. These niches especially estuaries act as sinks for various metal pollutants (Pereira et al. 2012; Kumar and Srikantawamy, 2012; Chapman and Wang, 2001). Thus, these organisms may encounter metals in their environment but their metal resistance is not well documented. The understanding of metal physiology in haloarchaea and halophilic bacteria needs more understanding and investigation.

In view of the above, and the gaps in existing literature, work was carried out with the following aims and objectives:

1. Biosynthesis and characterisation of metal sulphide and metallic nanoparticles by haloarchaea and halophilic bacteria
2. Studies on mechanistic aspects of nanoparticles synthesis and metal tolerance/resistance exhibited by haloarchaea and halophilic bacteria
3. Demonstration of applications of the synthesised nanoparticles

CHAPTER 2

Screening of Various Haloarchaeal and Halophilic Bacterial Cultures Capable of Synthesising Metallic or Metal Sulphide Nanoparticles

2.1 Introduction

The development of eco-friendly technologies in material synthesis is of considerable importance to expand their biological applications. Nanoparticle fabrication by microorganisms presents a green method for generation of bio-compatible nanomaterials. The traditional routes of nanoparticles synthesis (physical and chemical methods) employ toxic precursors, are energy intensive, expensive, require capping agents to prevent agglomeration, and produce toxic by-products (Tien et al. 2008). Besides these, the major drawback of physically/chemically synthesised nanoparticles is their incompatibility to biological systems. Thus, additional steps are required to coat the nanoparticles with bio-compatible molecules. Numerous bacteria, fungi, yeast, and viruses have been used for biosynthesis of nanomaterials (Li et al. 2011). Their cellular metabolites usually act as stabilising agents, making the synthesised nanoparticles bio-compatible. The presence of bacterial carrier matrix during microbial nanoparticles synthesis enhances the contact between the enzyme and the metal salt, producing particles with high catalytic reactivity, and greater specific surface area (Bhattacharya and Mukherjee, 2008; Simkiss and Wilbur, 1989).

Haloarchaea, inhabitants of extremely saline environments have not been explored for their potential of nanoparticles synthesis. The eco-niches inhabited by these organisms often act as effective traps for metal pollution and thus, these halophiles are exposed to varying concentrations of metal. However, studies on metal resistance mechanisms in haloarchaea are few and very preliminary (Srivastava and Kowshik, 2013). Similarly, halophilic bacteria, owing to their habitat are also exposed to high concentrations of metals, and are thus, potential nano-factories. Studies on nanoparticles synthesis by halophilic bacteria are few and do not explain the mechanism behind the process. In this work, haloarchaeal and halobacterial cultures either previously isolated in our laboratory, or obtained from microbial type culture collection (MTCC), Chandigarh, were screened for their ability to synthesise various nanoparticles. Screening allows for detection of microorganisms of interest using highly

selective procedures. Thus, in a few steps, screening results in selection of microbes that possess the desired properties while discarding all those with no value.

As the aim of this work was to screen for microbes capable of synthesising metallic or metal sulphide nanoparticles, the haloarchaeal and the halobacterial isolates were first tested for their ability to tolerate various metal salts that would act as the precursor of the end-product. Once the minimum inhibitory concentrations (MICs) were established, the ability of these microbes to synthesise nanoparticles was tested. This was achieved by a combination of techniques such as observation of visual change in culture colouration during growth, UV-visible spectroscopy to monitor plasmon resonance peaks, and/or X-ray diffraction (XRD) to determine crystal structure. The selected cultures and the nanoparticle synthesised by these cultures are described in detail in the following chapters.

2.2 Materials and Methods

2.2.1 Materials

All the chemicals and solvents utilised for the present work were of certified A.R. grade, used without any further purification, and were procured from Himedia (India) unless specified. All the glassware and accessories used were washed with distilled water, and sterilised at 15 psi, 121°C, for 15 mins. All the solutions were prepared with deionised water unless specified.

2.2.2 Cultures and medium optimisation

The haloarchaeal isolates used for this study were isolated in our laboratory previously from the Ribandar salt pans, Goa, India (Mani et al. 2012). The isolates were *Halococcus salifodinae* BK3, *H. salifodinae* BK6, *H. salifodinae* BK7, *H. salifodinae* BK11 and *H. salifodinae* BK18. They were maintained on NTYE agar plates (25% NaCl, 0.5% tryptone, 0.3% yeast extract, 2% MgSO₄.7H₂O and 0.5% KCl, 2% agar). They were also maintained in NTYE broth at 37°C, 110 rpm, and sub-cultured every 5 days. The media for growth of these haloarchaeal isolates were also optimised. For this purpose, halophilic broth (HB; Himedia M591), SWYE (salt water yeast extract), and media by Popescu et al (2009), with modifications were used. Growth curve analysis was carried out to determine the most suitable medium for growth according to Berney et al. (2006), and Breidt et al. (1994). In short, an aliquot of 1 ml was withdrawn every

24 hrs (for 10 days), starting from 0 hrs and the optical density was measured at 600 nm on UV-visible double beam spectrophotometer (Shimadzu, Japan, UV-2450). The growth kinetics parameters such as specific growth rate (μ) and doubling time (t_d) were calculated as follows:

$$\mu = \frac{[\log(OD_2) - \log(OD_1)] \times 2.303}{(t_2 - t_1)} \quad (1)$$

where, μ is the specific growth rate, OD_2 is the optical density at time t_2 , OD_1 is the optical density at time t_1 , t_1 and t_2 are time points at which respective optical densities are recorded.

$$t_d = 0.693 / \mu_{max} \quad (2)$$

where, t_d is the doubling time and μ_{max} is the maximum specific growth rate.

Lag time (t_l) was determined by the graphical method described by Breidt et al. (1994). All the experiments were carried out in triplicates.

The halophilic bacteria used for this study include *Idiomarina* sp. PR58-8, *Halomonas aquamarina* MTCC 4661, and *Halobacillus* sp. MTCC 6516. *Idiomarina* sp. PR58-8 is a marine bacterium isolated previously in our laboratory from the banks of Mandovi Estuary in Goa, India (Seshadri et al. 2012). These bacteria were maintained on Zobell marine agar (ZMA) 2216 plates and sub-cultured once every 15 days. *H. aquamarina* MTCC 4661, and *Halobacillus* MTCC 6516 were maintained at room temperature (RT), while *Idiomarina* sp. PR58-8 was maintained at 37°C. Media for growth of these organisms were optimised by growing them in nutrient broth (Himedia MM244) amended with 2% NaCl (NB + 2% NaCl), and NTYE with 3.5% NaCl (3.5% NTYE). Growth curve analysis was carried out as described above, except the aliquots were withdrawn every 2 hrs (till 48 hrs), starting from 0 hrs. All the experiments were carried out in triplicates.

2.2.3 Determination of MIC of metal salt

The MIC of silver nitrate ($AgNO_3$), sodium selenite (Na_2SeO_3), potassium tellurite (K_2TeO_3), zinc sulphate ($ZnSO_4$), and lead nitrate ($Pb(NO_3)_2$) were determined for all the haloarchaeal as well as halobacterial cultures. The metal salt solutions were prepared as 0.1 M stocks in distilled water and filter sterilised. The medium exhibiting optimal growth of the isolates was

used for this study. The isolates were grown in presence of varying concentrations of metal salts in the range of 0.05 mM to 10 mM. The various concentrations tested were, 0.05, 0.5, 1.0, 1.5, 2, 2.5, 3, 3.5, 4, 4.5, 5, 6, 7, 8, 9 and 10 mM. Negative controls (un-inoculated medium + 10 mM metal salt), and positive controls (inoculated medium) were treated, same as the test. MIC was recorded as the lowest concentration at which no growth was observed.

2.2.4 Screening of promising isolates synthesizing nanoparticles

2.2.4.1 Screening based on colour change

The isolates were grown in presence of metal salts and their ability to synthesise nanoparticles was determined by either visual observation in combination with UV-Visible spectroscopy and/or X-ray diffraction (XRD). When the cultures were grown in presence of AgNO_3 , Na_2SeO_3 , or K_2TeO_3 , colour change was used as an indicator of MNPs synthesis. The biomass was harvested ($10,000 \times \text{g}$, RT, 30 mins) and subjected to dialysis against deionised water with frequent changes of water for 24 hrs and dried overnight in an oven, at 70°C . The powder obtained after grinding was subjected to UV-visible spectroscopy and/or XRD. For UV-visible spectroscopy the nanoparticles were dissolved in appropriate solvent and spectroscopy was performed in the range of 200-800 nm on a UV-visible double beam spectrophotometer using the solvent as the blank. Crystallographic characterisation was performed using the Rigaku Mini-Flex II powder X-ray diffractometer operated at 30 kV/15 mA with $\text{Cu K}\alpha$ (1.54 \AA) as radiation source and scanning mode of $2\theta/\theta$ continuous scanning. The crystallite domain size of nanoparticles was calculated by Debye-Scherrer formula:

$$D = k\lambda / \beta \cos\theta \quad (3)$$

where λ = wavelength of X-ray applied (1.54 \AA), k = numerical constant for which the obtained value is 0.94, $\beta_{1/2}$ = full width (radians) at half maximum of the major peak and θ = Bragg angle of the major peak.

2.2.4.2 Screening of cultures synthesising nanoparticles with no visual colour change

The isolates synthesising metal sulphide nanoparticles were selected by growing the cultures in presence of ZnSO_4 , PbNO_3 , or CdSO_4 . The biomass was harvested by centrifugation at

10,000 × g, RT, for 30 mins, followed by dialysis against deionised water, with frequent changes of water for 24 hrs, and dried in a hot air oven overnight at 70°C. The sample was obtained by grinding the powder in a mortar and pestle. The nano-powder was analysed by XRD and/or UV-visible spectroscopy as described in section 2.2.4.1. All the experiments were carried out in triplicates on different days.

2.2.5 Statistical analysis

All the experiments were performed in triplicates on different days and the results were expressed as mean (\pm standard error). Statistical analysis was done using the Microsoft™ Excel 2007 software. The differences between the control and the individual experimental groups were analysed using the two-tailed Student's t-test. One-way Analysis of Variance (ANOVA) test was carried out to determine any significant difference between untreated controls and treated groups for multiple comparisons. 'p' values less than 0.05 ($p < 0.05$) were considered significant.

2.3 Results and Discussions

2.3.1 Screening of haloarchaeal isolates

The haloarchaeal isolates used for this study include *Halococcus salifodinae* BK3, *H. salifodinae* BK6, *H. salifodinae* BK7, *H. salifodinae* BK11, and *H. salifodinae* BK18. They appear as orange-red colonies on NTYE plates due to the presence of α -bacterioruberin in their membranes (Kamekura, 1993).

2.3.1.1 Optimisation of growth medium

The various media tested for growth of the haloarchaeal isolates were NTYE, SWYE, Modified Popescu et al. and HB. Haloarchaea are extreme halophiles which grow best at high salinities (3.5- 5 M of NaCl = 20% - 29.22% of NaCl) (DasSarma and Arora, 2012). The growth media used for cultivation of these isolates thus, have high NaCl concentrations with 25% NaCl (4.28 M) most commonly used (Schneegurt, 2012). However, the NaCl concentration may be lowered by substituting with other salts such as MgCl₂, CaCl₂, CH₃COONa, or Na₂S₂O₃ (Kushner, 1985). Haloarchaea also have an obligate requirement of Mg²⁺ and K⁺, as these ions play important roles in their physiology. Mg²⁺ is required by the

haloarchaeal enzymes for their activity (Madern et al. 2000), while K^+ is internalised by the cells and helps in maintaining osmolarity at such high salinities (Martin et al. 1999). As the haloarchaeal isolates used for this work were isolated from a solar saltern, the crude salt from these salt pans were used as source of Na^+ and Cl^- . Such solar salterns also contain Mg^{2+} and K^+ as a result of evaporation of sea water. Thus, all the media used for optimisation studies were selected such that NaCl was present at 25% unless substituted by other salts, Mg^{2+} was present at 2-5% and K^+ at 0.2-2%. Yeast extract was added as the complex carbohydrate source.

Table 2.1 show the various growth kinetics parameters of all five haloarchaeal isolates in four different media. The specific growth rate (μ) for all the five isolates in NTYE was between 0.92 days^{-1} to 0.99 days^{-1} , with a doubling time (t_d) of ~ 17 hrs and a lag time (t_l) of ~ 12 hrs. In HB medium, the μ ($\sim 0.81 \text{ days}^{-1}$), t_d (~ 20.6 hrs), and t_l (12 hrs) were similar to that in NTYE and the difference was insignificant ($p > 0.05$). Although, the five isolates exhibited slower growth in modified Popescu et al. medium with a μ of $\sim 0.66 \text{ days}^{-1}$, t_d of ~ 25.75 hrs, and t_l of 24 hrs, the difference when compared to that in NTYE was insignificant ($p > 0.05$). However, in SWYE, growth of *H. salifodinae* BK11 was significantly retarded ($p < 0.05$) as evident from the μ (0.39 hrs^{-1}), t_d (42.65 hrs), and t_l (38 hrs). The other four isolates, viz., *H. salifodinae* BK3, BK6, BK7, and BK18 exhibited slower growth in SWYE (μ - $\sim 0.65 \text{ days}^{-1}$, t_d - ~ 25.75 hrs, and t_l - 24 hrs) as compared to that in NTYE. Thus, the cultures exhibited optimal growth kinetics in NTYE or HB as compared to the other growth media. Fig. 2.1 shows the growth curves of the haloarchaeal isolates in various growth media. Based on these results, both NTYE and HB were suitable for studies on the haloarchaeal isolates. However, since the cost of preparing 1 L of NTYE medium (Rs. 55) is lower than preparing 1 L of HB (Rs. 2650), NTYE medium was used for further studies.

Table 2.1 The growth kinetics parameters of the haloarchaea in various growth media.

Culture	Medium	Specific Growth Rate (μ ; days ⁻¹)	Lag time (t_l ; hrs)	Doubling time (t_d ; hrs)
<i>H. salifodinae</i>	NTYE	0.99	11.52	16.9
	SWYE	0.63	24	26.4
	BK3 HB	0.81	12	20.53
	Mod. Popescu	0.65	24	25.58
<i>H. salifodinae</i>	NTYE	0.99	12	16.8
	SWYE	0.62	24	26.8
	BK6 HB	0.81	12	20.53
	Mod. Popescu	0.70	24	23.76
<i>H. salifodinae</i>	NTYE	0.92	12	18.08
	SWYE	0.65	24	25.58
	BK7 HB	0.82	12	20.28
	Mod. Popescu	0.66	24	25.2
<i>H. salifodinae</i>	NTYE	0.94	12	17.69
	SWYE	0.39	24	42.65
	BK11 HB	0.81	12	20.53
	Mod. Popescu	0.65	24	25.58
<i>H. salifodinae</i>	NTYE	0.99	11.9	16.8
	SWYE	0.66	24	25.2
	BK18 HB	0.82	12	20.82
	Mod. Popescu	0.64	24	25.98

NTYE- NaCl Tryptone Yeast Extract; SWYE- Salt Water Yeast Extract; HB- Halophilic Broth; Mod. Popescu- Modified Popescu et al. 2009 medium

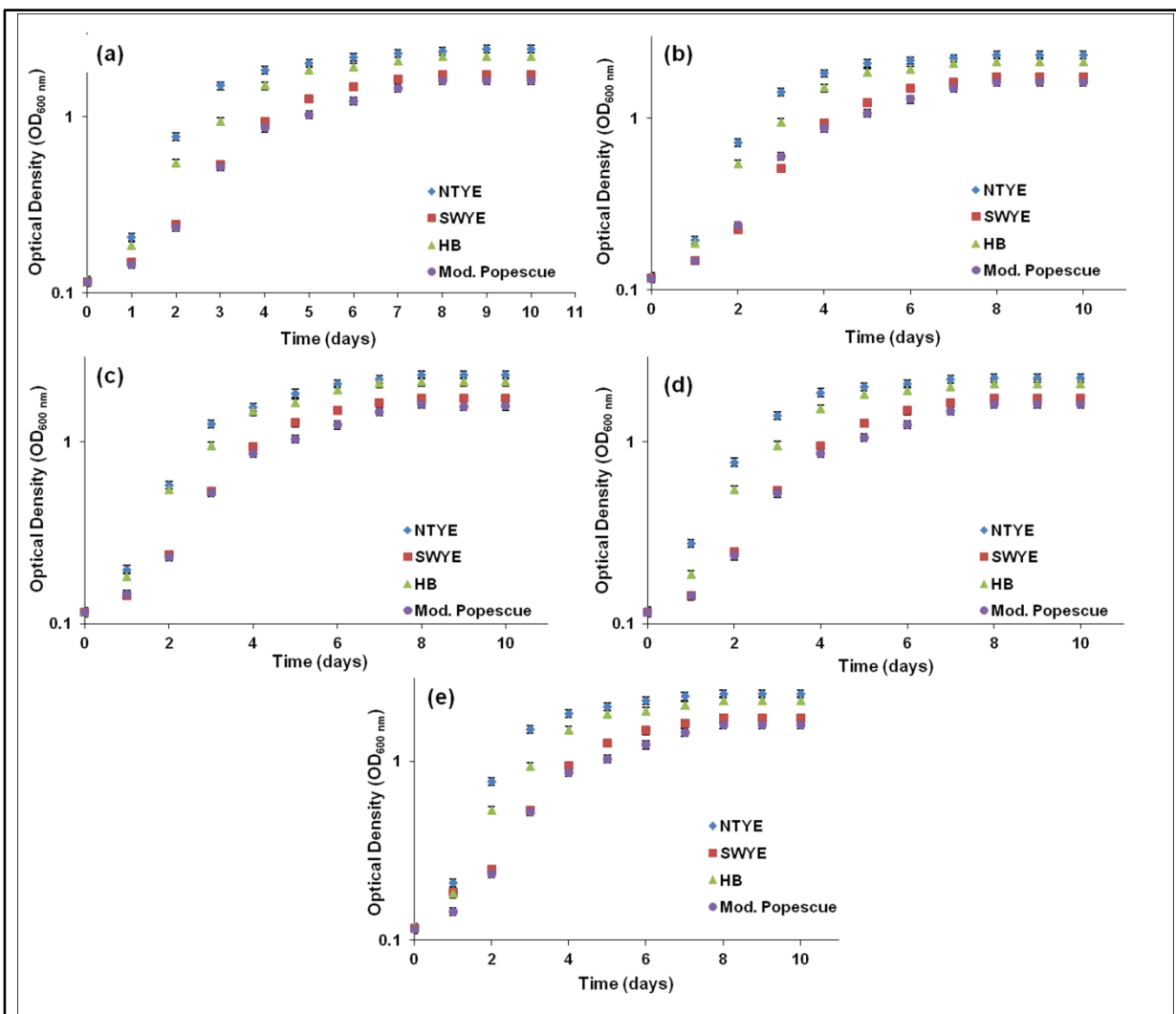


Fig. 2.1 Growth profiles of (a) *Halococcus salifodinae* BK3, (b) *H. salifodinae* BK6, (c) *H. salifodinae* BK7, (d) *H. salifodinae* BK11, and (e) *H. salifodinae* BK18 in NTYE (NaCl Tryptone Yeast Extract), SWYE (Salt Water Yeast Extract), HB (Halophilic Broth) and Mod. Popescue (Modified Popescue et al.) media. Values are mean \pm SD (error bars) for three experiments.

2.3.1.2 Determination of MIC of various metals

Minimum inhibitory concentrations (MICs) of various metal salts towards the five haloarchaeal isolates were determined by growing the isolates in presence of metal salts and visual observation of growth and changes in the colouration of culture. The medium used for this study was NTYE and the metal salts used were AgNO_3 , Na_2SeO_3 , K_2TeO_3 , ZnSO_4 , and $\text{Pb}(\text{NO}_3)_2$. Table 2.2 illustrates the growth pattern of the isolates at various metal salt concentrations. MICs of all the metals for the five isolates are given in Table 2.3.

MIC of AgNO_3

Addition of AgNO_3 to NTYE resulted in formation of a white precipitate, which dissolved immediately on mixing. At high salinities, Ag exists as soluble chloro-complexes that are bio-available for the organism (Byrne, 2002). The haloarchaeal isolates that appear orange-red (Fig. 2.2a), exhibited a brown black colouration when grown in presence of AgNO_3 (Fig. 2.2b), indicating the reduction of Ag^+ to Ag^0 . AgNO_3 was found to be toxic to haloarchaeal isolates at concentrations higher than 0.5 mM and the MIC for all five isolates was determined to be 1 mM. Therefore, all the five isolates exhibited a low level of resistance towards AgNO_3 .

MIC of Na_2SeO_3

H. salifodinae BK3, BK6 and BK7 exhibited a lower MIC value of 5 mM against Na_2SeO_3 as compared to *H. salifodinae* BK11 and BK18, which exhibited a MIC of 6 mM (Table 2.3). The addition of Na_2SeO_3 in NTYE did not show any precipitate formation. Growth in presence of Na_2SeO_3 was accompanied with generation of copious amounts of brick-red colouration (Fig. 2.2c), indicative of reduction of SeO_3^{2-} to Se^0 . Thus, all the five isolates exhibited the ability to tolerate Na_2SeO_3 .

MIC of K_2TeO_3

In presence of K_2TeO_3 , only *H. salifodinae* BK3 exhibited growth which was accompanied with the culture turning black in colour. This is indicative of TeO_3^{2-} being reduced to Te^0 . MIC of K_2TeO_3 for *H. salifodinae* BK3 was 6 mM. The other four isolates failed to grow in presence of K_2TeO_3 , even on prolonged incubation for 30 days. Therefore, only *H. salifodinae* BK3

exhibited resistance to TeO_3^{2-} oxyanion, while it exhibited toxicity towards all the other haloarchaeal isolates.

MIC of ZnSO₄

Addition of ZnSO_4 to the medium resulted in generation of small amount of white precipitate, which dissolved upon mixing. *H. salifodinae* BK3 exhibited good growth at 0.05 mM ZnSO_4 and poor growth at 0.5 and 1 mM ZnSO_4 . MIC for this isolate was 1.5 mM ZnSO_4 . *H. salifodinae* BK6 exhibited poor growth at 0.05 mM ZnSO_4 after a prolonged incubation period of 30 days, and the MIC was 1 mM ZnSO_4 . None of the other isolates exhibited growth in presence of ZnSO_4 even after prolonged incubation of 30 days. The pigmentation of both the isolates, *H. salifodinae* BK3 and BK6 remained unaffected by ZnSO_4 and the cultures retained their orange-red colour. Thus, *H. salifodinae* BK3 and BK6 exhibited low level of resistance towards ZnSO_4 , while *H. salifodinae* BK7, BK11, and BK18 were susceptible to ZnSO_4 .

MIC of Pb(NO₃)₂

Addition of $\text{Pb}(\text{NO}_3)_2$ in NTYE resulted in formation of white precipitate, which at lower concentrations (0.01, 0.05, 0.5 and 1) dissolved on mixing. However, at concentrations above 1 mM, the precipitate failed to dissolve. $\text{Pb}(\text{NO}_3)_2$ was found to be toxic to the haloarchaeal isolates, and no growth was observed even at the lowest concentration of 0.01 mM.

The cultures exhibited resistance to metal salts in the following order:

H. salifodinae BK3: $\text{K}_2\text{TeO}_3 > \text{Na}_2\text{SeO}_3 > \text{ZnSO}_4 > \text{AgNO}_3$ (least susceptible to K_2TeO_3 and most susceptible to AgNO_3)

H. salifodinae BK6: $\text{Na}_2\text{SeO}_3 \gg \text{ZnSO}_4 = \text{AgNO}_3$ (least susceptible to Na_2SeO_3 and most susceptible to $\text{ZnSO}_4/ \text{AgNO}_3$)

H. salifodinae BK7; BK11; BK18: $\text{Na}_2\text{SeO}_3 \gg \text{AgNO}_3$ (least susceptible to Na_2SeO_3 and most susceptible to AgNO_3)

Table 2.2 Growth of haloarchaeal isolates at various concentrations of metal salts.

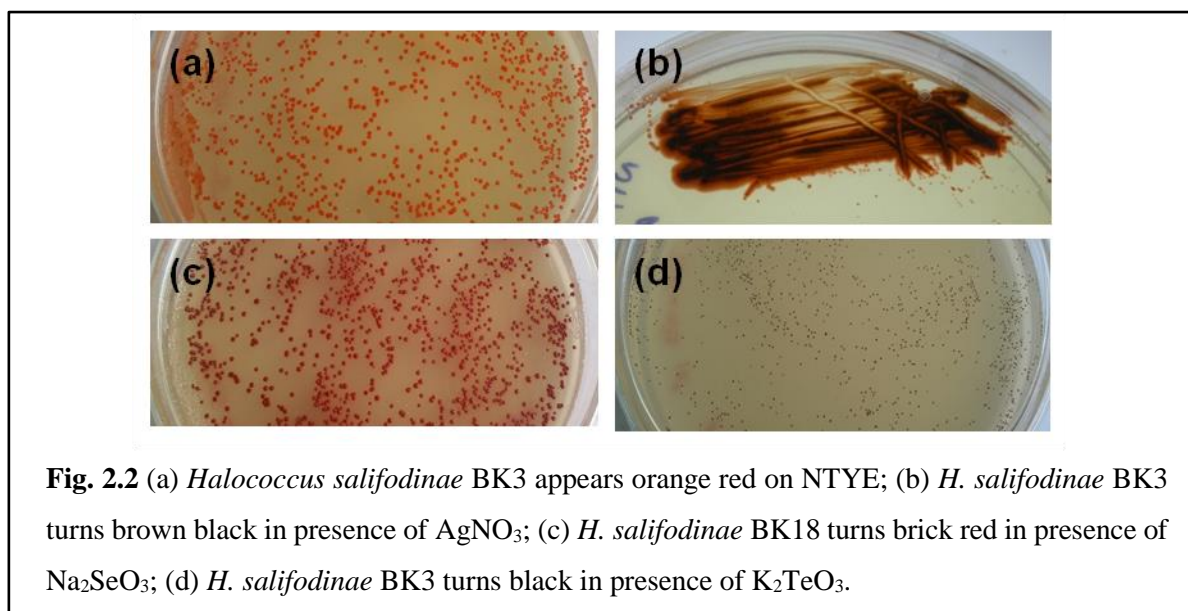
		Metal salts (mM)	0.05	0.5	1.0	1.5	2.0	2.5	3.0	3.5	4.0	4.5	5.0	6.0	7.0	8.0	9.0	10.0	
<i>H. salifodinae</i> BK3	AgNO ₃	++	+	-	-	-	-	-	-	-	-	-	-	-	-	-	-	-	
	Na ₂ SeO	+++	+++	++	++	++	++	++	++	++	++	+	-	-	-	-	-	-	
	K ₂ TeO ₃	+++	+++	+++	++	++	++	++	++	+	+	+	+	-	-	-	-	-	
	ZnSO ₄	++	+	+	-	-	-	-	-	-	-	-	-	-	-	-	-	-	-
	Pb(NO ₃) ₂	-	-	-	-	-	-	-	-	-	-	-	-	-	-	-	-	-	-
<i>H. salifodinae</i> BK6	AgNO ₃	++	+	-	-	-	-	-	-	-	-	-	-	-	-	-	-	-	
	Na ₂ SeO ₃	++	++	+	+	+	+	-	-	-	-	-	-	-	-	-	-	-	
	K ₂ TeO ₃	-	-	-	-	-	-	-	-	-	-	-	-	-	-	-	-	-	
	ZnSO ₄	+	+	-	-	-	-	-	-	-	-	-	-	-	-	-	-	-	
	Pb(NO ₃) ₂	-	-	-	-	-	-	-	-	-	-	-	-	-	-	-	-	-	
<i>H. salifodinae</i> BK7	AgNO ₃	++	+	-	-	-	-	-	-	-	-	-	-	-	-	-	-	-	
	Na ₂ SeO ₃	+++	+++	++	++	++	++	++	++	++	+	+	-	-	-	-	-	-	
	K ₂ TeO ₃	-	-	-	-	-	-	-	-	-	-	-	-	-	-	-	-	-	
	ZnSO ₄	-	-	-	-	-	-	-	-	-	-	-	-	-	-	-	-	-	
	Pb(NO ₃) ₂	-	-	-	-	-	-	-	-	-	-	-	-	-	-	-	-	-	
<i>H. salifodinae</i> BK11	AgNO ₃	++	+	-	-	-	-	-	-	-	-	-	-	-	-	-	-	-	
	Na ₂ SeO ₃	+++	+++	++	++	++	++	++	++	++	++	++	+	-	-	-	-	-	
	K ₂ TeO ₃	-	-	-	-	-	-	-	-	-	-	-	-	-	-	-	-	-	
	ZnSO ₄	-	-	-	-	-	-	-	-	-	-	-	-	-	-	-	-	-	
	Pb(NO ₃) ₂	-	-	-	-	-	-	-	-	-	-	-	-	-	-	-	-	-	
<i>H. salifodinae</i> BK18	AgNO ₃	++	+	-	-	-	-	-	-	-	-	-	-	-	-	-	-	-	
	Na ₂ SeO ₃	+++	+++	++	++	++	++	++	++	++	++	++	+	-	-	-	-	-	
	K ₂ TeO ₃	-	-	-	-	-	-	-	-	-	-	-	-	-	-	-	-	-	
	ZnSO ₄	-	-	-	-	-	-	-	-	-	-	-	-	-	-	-	-	-	
	Pb(NO ₃) ₂	-	-	-	-	-	-	-	-	-	-	-	-	-	-	-	-	-	

'+++': Good Growth; '++': Growth; '+': Poor Growth; '-': No Growth

Table 2.3 MICs of various metal salts for the five haloarchaeal isolates.

Culture	AgNO ₃ (mM)	Na ₂ SeO ₃ (mM)	K ₂ TeO ₃ (mM)	ZnSO ₄ (mM)	Pb(NO ₃) ₂ (mM)
<i>H. salifodinae</i> BK3	1.0	5.0	6	1.5	NG
<i>H. salifodinae</i> BK6	1.0	5.0	NG	1.0	NG
<i>H. salifodinae</i> BK7	1.0	5.0	NG	NG	NG
<i>H. salifodinae</i> BK11	1.0	6.0	NG	NG	NG
<i>H. salifodinae</i> BK18	1.0	6.0	NG	NG	NG

NG- No growth even at the lowest concentration tested (0.01 mM)



2.3.1.3 Screening of promising haloarchaeal isolates for nanoparticles synthesis

The MIC study helped in determining the metal salt concentration that could be used for nanoparticles synthesis. It was also helpful in screening the isolates that did not grow in presence of certain metal salts. As none of the isolates exhibited growth in presence of Pb(NO₃)₂, Pb based nanoparticles synthesis by haloarchaea was not attempted. Based on the MICs, SNPs and SeNPs synthesis was attempted using all the five isolates; and TeNPs synthesis was attempted with *H. salifodinae* BK3 only.

Silver nanoparticles (SNPs) synthesis

The haloarchaeal isolates were grown in NTYE medium in presence of 0.5 mM AgNO₃. At this concentration, due to the bio-reduction of Ag⁺ to Ag⁰, the isolates become brown-black in colour, indicative of SNPs synthesis (Fig. 2.2b). This colouration arises due to the characteristic surface plasmon resonance (SPR) of the SNPs. The biomass was harvested and dialysed against deionised water overnight, to remove all the excess Cl⁻ present due to the high salinity of the medium. The samples on drying were subjected to UV-visible spectroscopy and X-ray diffractometry to determine the crystalline facets of the synthesised nanoparticles. Medium controls with AgNO₃ did not result in reduction, and the supernatant of the culture also failed to reduce the Ag⁺ indicating that the synthesis of SNPs was a culture dependent phenomenon.

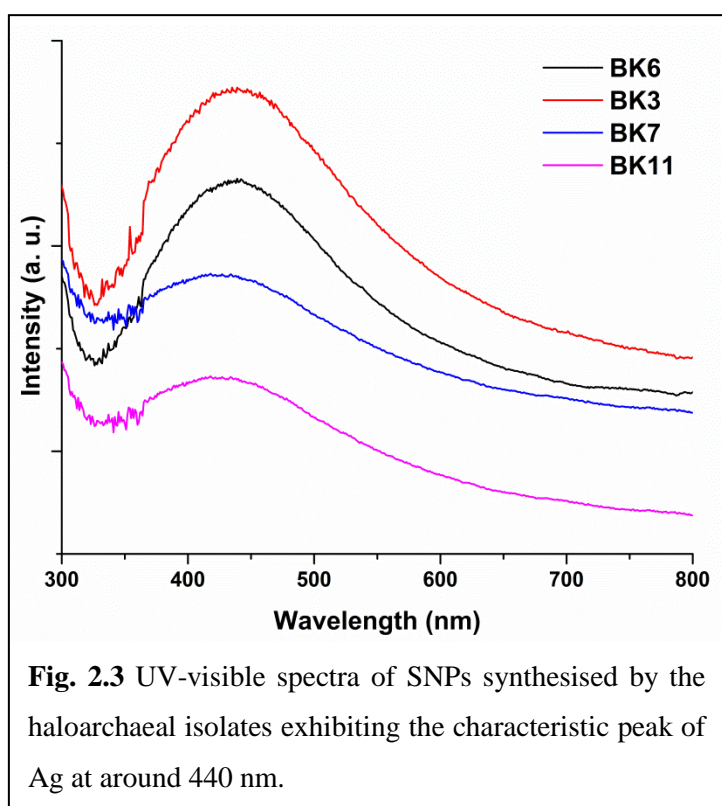
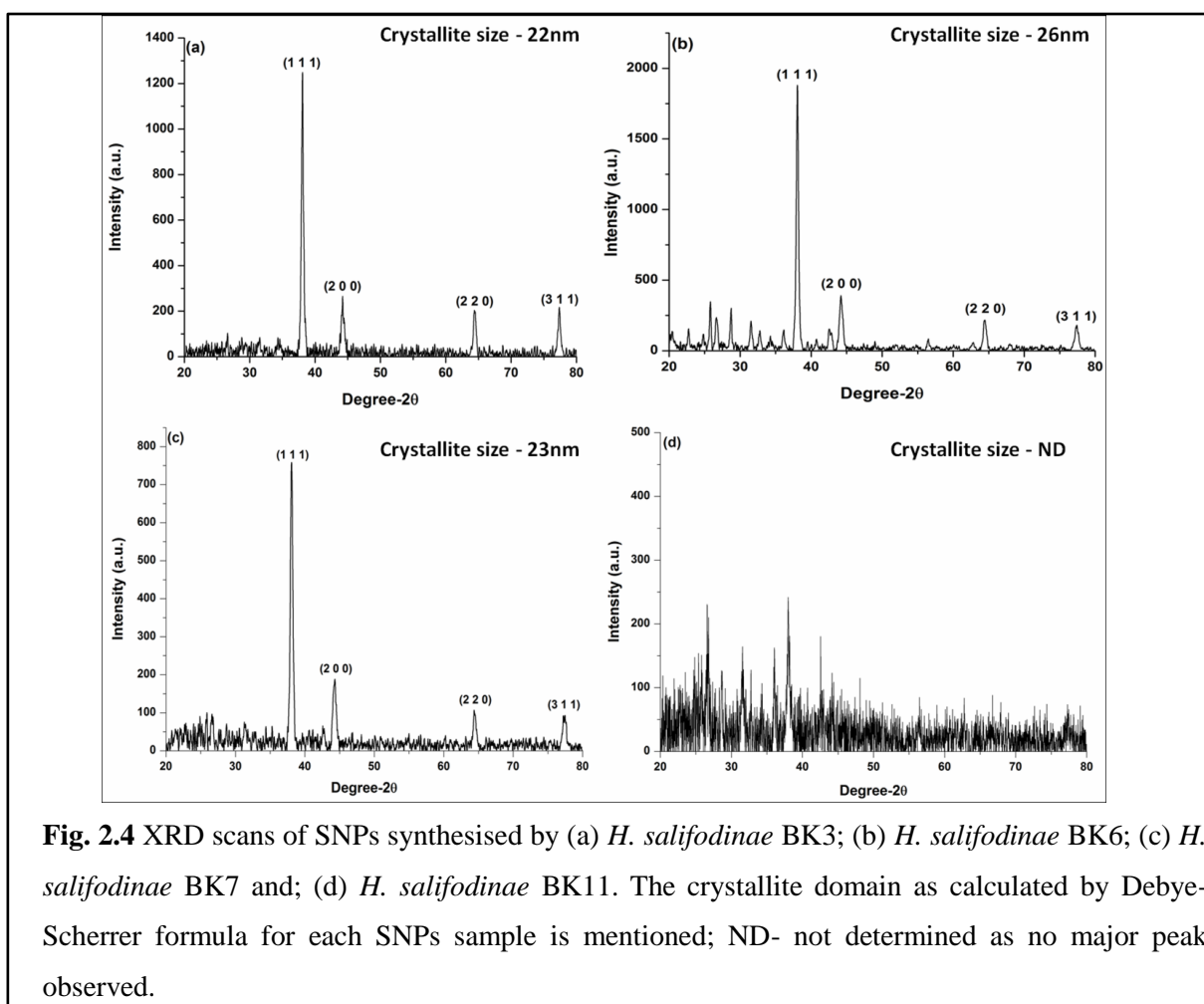


Fig. 2.3 shows the UV-visible scans of the SNPs synthesised by the haloarchaeal isolates. As is evident the characteristic broad peak arising due to the LSPR of SNPs was obtained at around 440 nm. Some anisotropy in the shape of the nanoparticles may be responsible for the asymmetry of the peak at around 380 nm (Shankar et al. 2004). The powder obtained from *H. salifodinae* BK18 did not exhibit the characteristic peak thus suggesting that although the isolate could tolerate 0.5 mM

AgNO₃, it was incapable of synthesising SNPs.

XRD analysis of the SNPs was carried out to confirm the crystalline nature of the nano-preparation. XRD scans of SNPs synthesised by *H. salifodinae* BK3 and *H. salifodinae* BK6

exhibited very little background noise and sharp peaks corresponding to face centred cubic Ag (ICDD card/file no. 04-0783). Although *H. salifodinae* BK7 was able to synthesise SNPs, the synthesis was very slow as compared to BK3 or BK6, and was observed only after prolonged incubation of 30 days. Thus, *H. salifodinae* BK7 was not used for further studies. The SNPs synthesised by *H. salifodinae* BK11 exhibited a high background noise with attenuated and/or absent Bragg's peaks of Ag. This phenomenon has been attributed to the presence of amorphous organic molecules arising from the microbial cell (Chatellier et al. 2001). Hence, this isolate was also not used for further studies. Fig. 2.4 illustrates the XRD scans of the SNPs synthesised by *H. salifodinae* BK3, BK6, BK7 and BK11. The crystallite domain sizes of the as-synthesised SNPs were calculated using the major peak at 2θ value of 38.115° corresponding to (1 1 1) facet of fcc structure. Based on the findings of UV-visible spectroscopy and XRD, isolates *H. salifodinae* BK3 and *H. salifodinae* BK6 were used for SNPs synthesis.



Selenium nanoparticles (SeNPs) synthesis

SeNPs synthesis was carried out in NTYE medium in presence of 2 mM Na_2SeO_3 . The haloarchaeal cultures were screened to determine the most suitable isolates for SeNPs synthesis. Growth of isolates was accompanied with generation of brick-red colouration indicative of SeNPs synthesis (Fig. 2.2c). The media controls, and culture supernatants failed to reduce selenite to elemental selenium, indicating that SeNPs synthesis was a culture mediated phenomenon. The nano-powders obtained on drying the dialysed biomass were subjected to XRD analysis to determine the isolates that could be used for further studies on SeNPs synthesis.

Fig. 2.5 shows the XRD scans of the SeNPs synthesised by *H. salifodinae* BK3, BK6, BK7, BK11 and BK18. Characteristic Bragg's peaks of hexagonal Se were obtained corresponding to the ICDD card no. 06-0362. However, the SeNPs synthesised by *H. salifodinae* BK18 exhibited the sharpest peaks with least background noise. The scans of SeNPs synthesised by *H. salifodinae* BK3 and BK7 show many small peaks as background noise, indicating presence of organic contaminants. The material from *H. salifodinae* BK6 did not exhibit the characteristic peaks of Se. As the SeNPs obtained from *H. salifodinae* BK18 exhibited a scan with sharp peaks and smallest crystallite domain size, the isolate was used for further studies. Besides, among the five isolates, *H. salifodinae* BK18 was found to reduce SeO_3^{2-} the fastest, which could be ascertained by the time required for red colour generation.

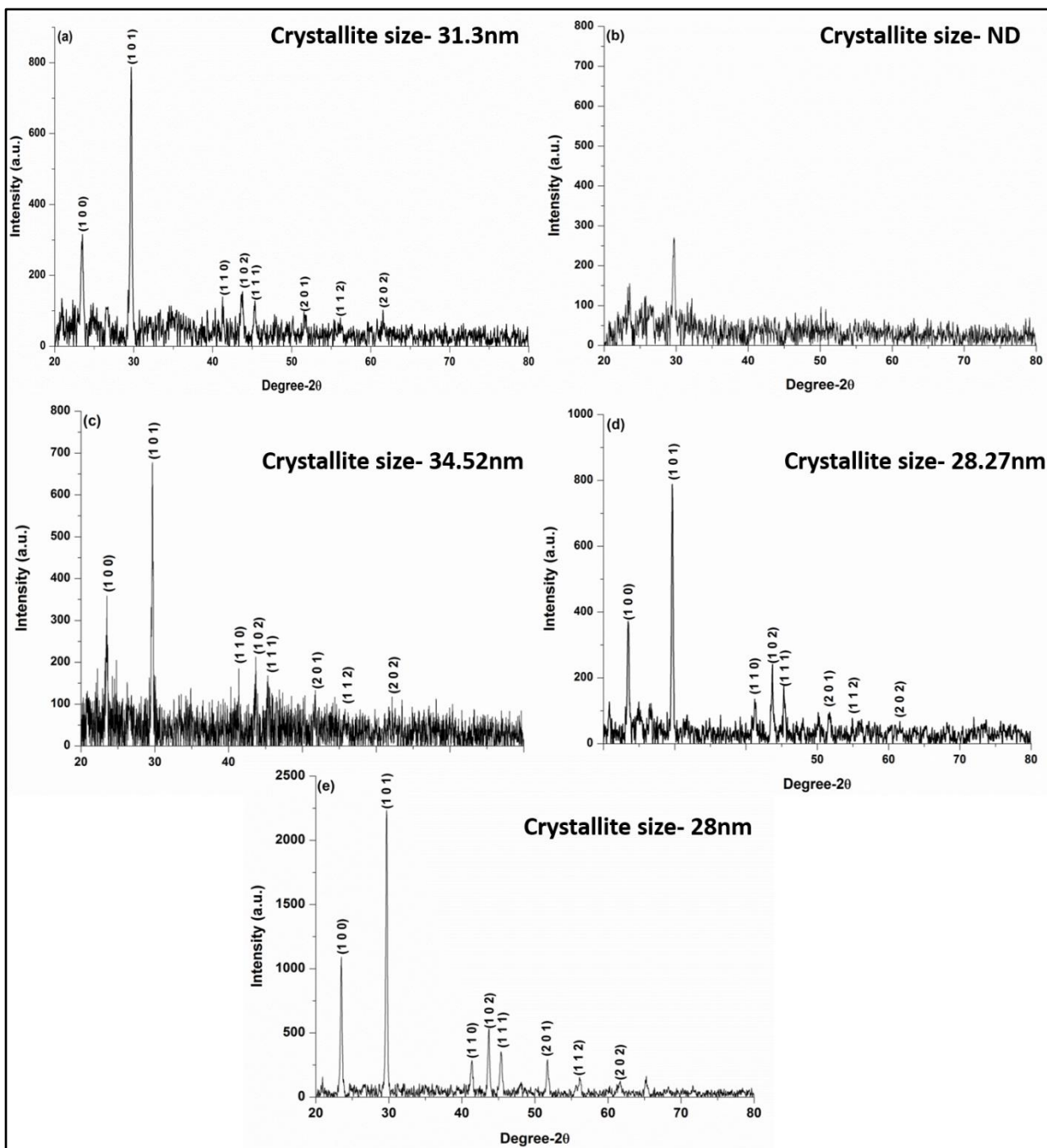
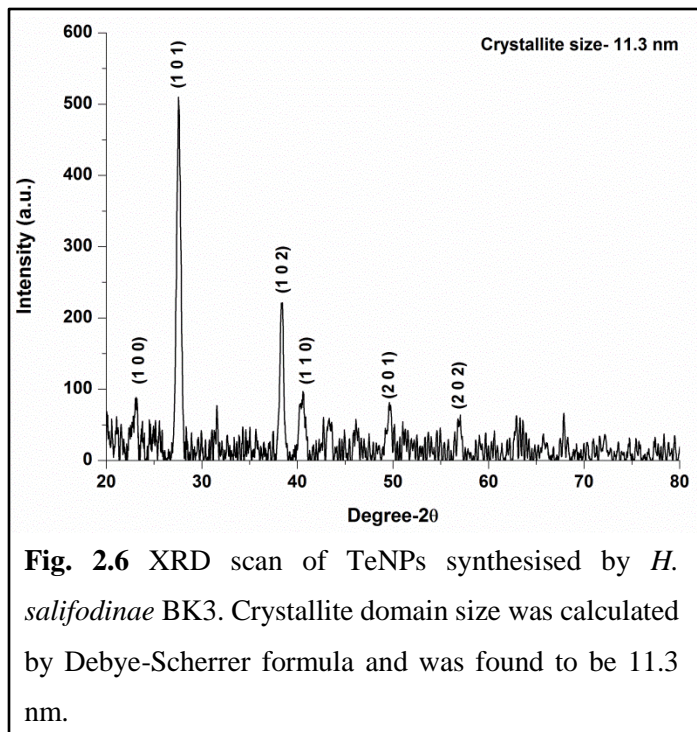


Fig. 2.5 XRD scans of SeNPs synthesised by (a) *H. salifodinae* BK3; (b) *H. salifodinae* BK6; (c) *H. salifodinae* BK7; (d) *H. salifodinae* BK11 and; (e) *H. salifodinae* BK18. Crystallite domain size as calculated by Debye-Scherrer formula for all the SeNPs samples is mentioned; ND- not determined as no major peak observed.

Tellurium nanoparticles (TeNPs) synthesis



Among all the haloarchaeal isolates tested for MIC of K_2TeO_3 , *H. salifodinae* BK3 was the only haloarchaeon capable of growing in its presence. The culture exhibited a black colouration when grown in presence of K_2TeO_3 (Fig. 2.2d) which indicates the reduction of TeO_3^{-2} to Te^0 and the formation of Te nanocrystals. The media controls, and culture supernatant did not exhibit any change in colour suggesting that the reduction, and nanoparticles

synthesis is a culture-mediated phenomenon. The sample obtained after dialysis and drying in the oven was subjected to crystallographic characterisation using X-ray diffractometry (Fig. 2.6). The spectrum obtained corresponded to the characteristic Bragg's peaks of hexagonal crystal system and was in accordance with the standard card of hexagonal tellurium (ICDD card no/ file no 36-1452). The crystallite domain size as calculated by Debye-Scherrer formula was determined to be 11.3 nm. Thus, *H. salifodinae* BK3 was used for further studies on TeNPs synthesis.

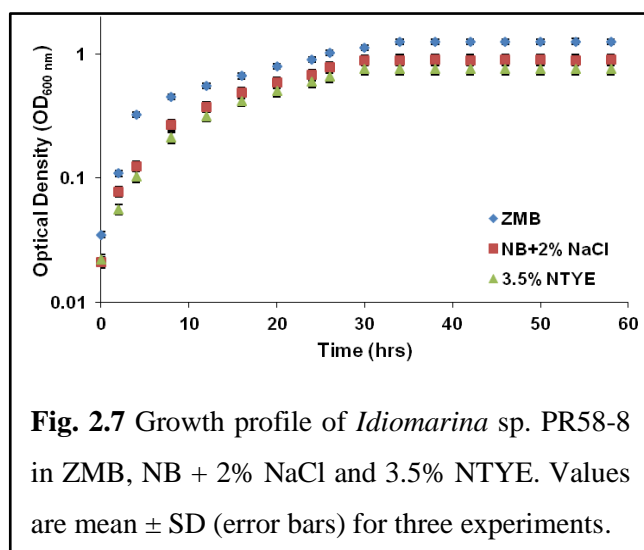
2.3.2 Screening of halophilic bacteria

Halophilic bacteria such as *Idiomarina* sp. PR58-8, *Halomonas aquamarina* MTCC 4661 and *Halobacillus* sp. MTCC 6516 were used for this study. *Idiomarina* sp. PR58-8 (henceforth addressed/designated as ML2) is a Gram-negative marine bacterium isolated previously in our laboratory from the banks of Mandovi Estuary in Goa, India (Seshadri et al. 2012). It forms golden yellow colonies on the plates. *H. aquamarina* MTCC 4661 is a Gram-negative halophilic bacterium procured from MTCC, with light orange pigmentation, while

Halobacillus sp. MTCC 6516 is a Gram-positive halophilic bacterium procured from MTCC with light pink pigmentation. All these cultures were stored as glycerol stocks at -80°C .

2.3.2.1 Optimisation of growth medium

Growth media used for optimisation studies include ZMB, NB + 2% NaCl and 3.5% NTYE. Zobell marine broth has nutrients and trace minerals required for growth of marine organisms and mimics sea water. It also has peptic digest of animal tissues and yeast extracts that act as nitrogen, amino acids, vitamins, and carbon source essential for growth of marine bacteria (Weiner et al. 1985). Similarly, nutrient broth amended with 2% NaCl provides all the essential nutrients in the form of peptic digest of animal tissues, yeast extract, and beef extract, and a salinity of 2.5% for growth of slight and moderate halophiles. NTYE amended with 3.5% NaCl also provides the salinity conditions essential for growth of slight and moderate halophiles. The halophilic bacteria were grown in these media and the growth kinetics parameters were evaluated.



ML2 is a moderate halophile, with an obligate requirement of 1% NaCl for growth and can tolerate up to 15% salinity (Seshadri et al. 2012). The growth kinetics parameters for ML2 in all three media are given in table 2.4. ML2 exhibited excellent growth in ZMB with a μ of 1.11 hrs^{-1} , a t_d of 37.46 mins, and t_l of 30 mins (Fig. 2.7). Growth of ML2 in NB + 2% NaCl (μ - 0.89 hrs^{-1} ; t_d - 46.72 mins; t_l -

50 mins) was found to be slightly slower when compared to growth in ZMB, however, the difference was found to be insignificant ($p > 0.05$). The growth of ML2 was significantly slower in 3.5% NTYE as compared to that in ZMB exhibiting a μ of 0.77 hrs^{-1} , a t_d of 54 mins, and t_l of 80 mins. Excellent growth of ML2 in ZMB may be attributed to the mineral content of the ZMB medium that mimics sea water. Thus, further studies on ML2 were carried out using ZMB medium.

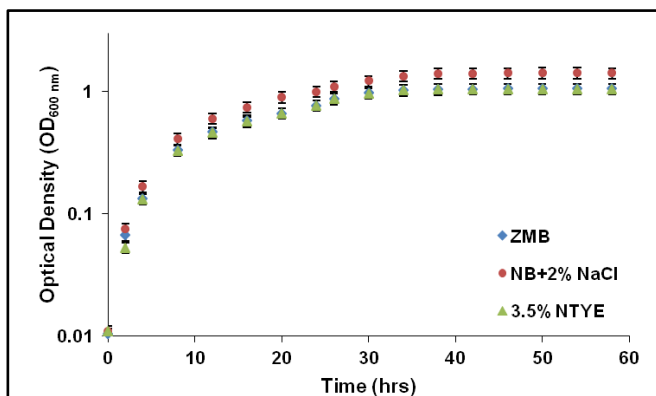


Fig. 2.8 Growth profile of *Halomonas aquamarina* MTCC 4661 in ZMB, NB + 2% NaCl and 3.5% NTYE. Values are mean \pm SD (error bars) for three experiments.

Halomonas aquamarina MTCC 4661, a slight to moderate halophilic bacterium, can grow over a range of 5%-25% salinity (Phillips et al. 2012). Table 2.4 illustrates the growth kinetics parameters for *H. aquamarina* MTCC 4661 in ZMB, NB + 2% NaCl and 3.5% NTYE. The growth kinetics parameters, μ and t_d of *H. aquamarina* MTCC 4661 in ZMB (μ - 1.28 hrs⁻¹, t_d - 32.81 mins) and NB + 2% NaCl (μ - 1.36 hrs⁻¹, t_d - 22 mins)

did not exhibit any significant difference ($p > 0.05$). However, *H. aquamarina* MTCC 4661 exhibited significantly longer lag times in ZMB (t_l - 40 mins) as compared to that in NB + 2% NaCl (t_l - 20 mins). Even though the specific growth rate (μ - 1.24 hrs⁻¹) and doubling time (t_d - 33.53 mins) of the culture in 3.5% NTYE medium remained the same, a significant increase ($p < 0.05$) in lag time (t_l - 80 mins) was observed in comparison to that in NB + 2% NaCl. The longer lag times in ZMB, and 3.5% NTYE indicates that the organism required longer time to adjust to the growth medium. Thus, NB + 2% NaCl was used for further studies on *H. aquamarina* MTCC 4661 (Fig 2.8).

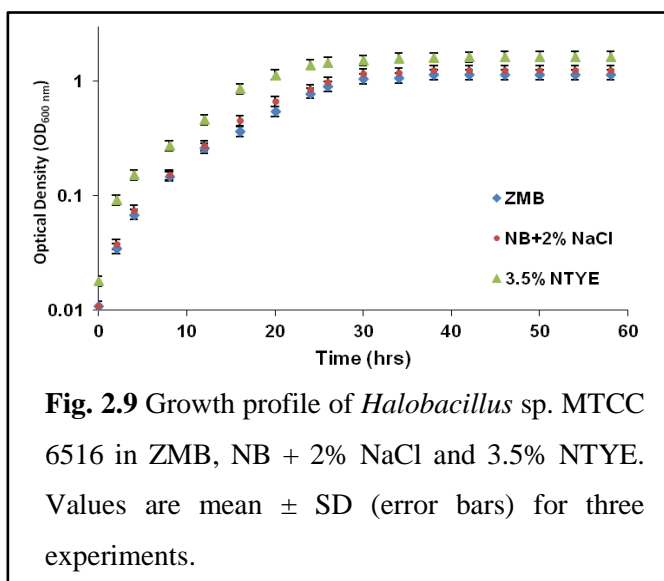


Fig. 2.9 Growth profile of *Halobacillus* sp. MTCC 6516 in ZMB, NB + 2% NaCl and 3.5% NTYE. Values are mean \pm SD (error bars) for three experiments.

Halobacillus sp. MTCC 6516 is a slight to moderate halophile exhibiting light pink pigmentation during growth on ZMB. Growth kinetics parameters of *Halobacillus* sp. MTCC 6516 in three media are presented in table 2.4. The halophilic bacteria exhibited excellent growth in 3.5% NTYE with a μ of 1.07 hrs⁻¹, a t_d of 35 mins, and a t_l of 45 mins (Fig. 2.9). These parameters were similar to

those in ZMB medium (μ - 0.92 hrs⁻¹, t_d - 45 mins; t_l - 60 mins). However, the culture exhibited the longest t_l of 108 mins in NB + 2% NaCl medium. Other parameters viz., μ (0.95 hrs⁻¹), and t_d (43 mins) for *Halobacillus* sp. MTCC 6516 in NB + 2% NaCl medium were very similar to that exhibited by the culture in 3.5% NTYE ($p>0.05$). There was no significant difference in specific growth rates ($p>0.05$) in any of the three media evaluated. Similarly, the doubling time of *Halobacillus* sp. MTCC 6516 in ZMB, and NB + 2% NaCl did not exhibit any significant difference ($p>0.05$). Based on the growth characteristics of *Halobacillus* sp. MTCC 6516 in 3.5% NTYE, this medium was used for further studies.

Table 2.4 The growth kinetics parameters of all the halophilic bacteria in various growth media.

Culture	Medium	μ (hrs ⁻¹)	t_l (mins)	t_d (mins)
<i>Idiomarina</i> sp. PR58-8 (ML2)	ZMB	1.11	30	37.46
	NB + 2% NaCl	0.89	50	46.72
	3.5% NTYE	0.77	80	54
<i>Halomonas</i> <i>aquamarina</i> MTCC 4661	ZMB	1.28	40	32.81
	NB + 2% NaCl	1.36	20	22
	3.5% NTYE	1.24	80	33.53
<i>Halobacillus</i> sp. MTCC 6516	ZMB	0.92	60	45
	NB + 2% NaCl	0.95	108	43
	3.5% NTYE	1.07	45	35

ZMB- Zobell Marine Broth; NB + 2% NaCl- Nutrient Broth amended with 2% sodium chloride; 3.5% NTYE- 3.5% NaCl Tryptone Yeast Extract; Medium highlighted in grey were used for further studies on nanoparticles synthesis.

2.3.2.2 Determination of MIC of various metals

The MICs of various metals against the three halophilic bacteria were determined by growing the isolates in presence of metal salts and visual observation of growth and changes in the colouration of the culture during growth. MIC against ML2 was determined in ZMB, while

that against *H. aquamarina* MTCC 4661 was determined in NB + 2% NaCl, and against *Halobacillus* sp. MTCC 6516 was determined in 3.5% NTYE medium. The growth pattern of the halophilic bacteria in presence of metal salts is presented in table 2.5. Table 2.6 shows the MICs of various metal salts against the three halophilic bacteria.

MIC of $AgNO_3$

Amongst the three halophilic bacteria used for this study, ML2 exhibited the maximum resistance towards $AgNO_3$, with a MIC of 10 mM. The growth in presence of this metal salt was accompanied by the culture turning brown-black in colour (Fig. 2.10), indicative of reduction of Ag^+ to Ag^0 . *H. aquamarina* MTCC 4661 exhibited a low level of resistance towards $AgNO_3$ with a MIC of 0.5 mM, and the growth was found to be retarded at 0.05 mM. $AgNO_3$ was found to be extremely toxic to *Halobacillus* MTCC 6516 as the organism failed to grow at 0.05 mM $AgNO_3$ even after prolonged incubation of 30 days. The addition of $AgNO_3$ to ZMB, NB + 2% NaCl, and 3.5% NTYE at higher

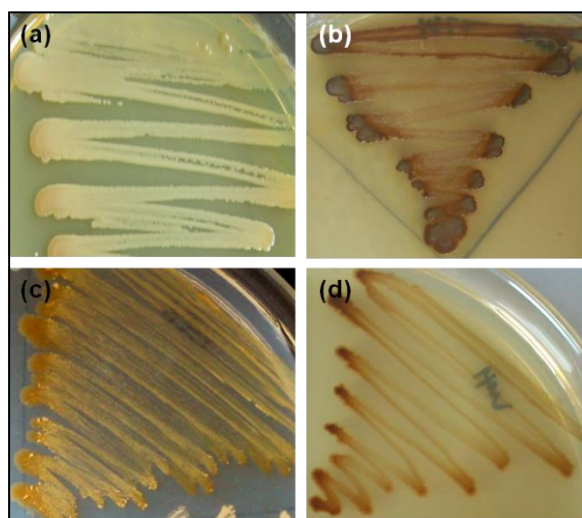


Fig. 2.10 (a) *Idiomarina* sp. PR58-8 appears golden yellow on ZMB (b) which turns brown-black in presence of $AgNO_3$; (c) *Halomonas aquamarina* MTCC 4661 appears light orange on NB + 2% NaCl (f) which turns brown in presence of $AgNO_3$.

concentrations (>1 mM) resulted in generation of white precipitate of chloro-complexes of silver ($AgCl^0$, $AgCl^{2-}$, $AgCl_3^{2-}$, $AgCl_4^{3-}$). At 3 mM and lower concentrations of $AgNO_3$ the white precipitate dissolves on vigorous mixing, however, at concentrations above 3 mM some residual white precipitate was observed. Such chloro-complexes formed below 3.5% salinity are lipophilic and are easily transported across the cellular membranes of the microbes, making them bio-available (Byrne, 2002). Thus, the high MIC value of $AgNO_3$ obtained is not due to the un-availability of the metal, but is in fact the true MIC value.

MIC of Na_2SeO_3

All the three halophilic bacteria used for this study were able to tolerate Na_2SeO_3 . Growth was accompanied by the culture turning brick-red in colour (Fig. 2.11). The reduction of SeO_3^{2-} to Se^0 is responsible for the generation of this colour. Amongst the three halophilic bacteria, ML2, and *H. aquamarina* MTCC 4661 exhibited a high level of resistance towards Na_2SeO_3 with a MIC of 10 mM, and 7 mM, respectively. MIC of Na_2SeO_3 against *Halobacillus* MTCC 6516 was 4.5 mM. Thus, all the three halophilic bacteria were found to be resistant to Na_2SeO_3 .



Fig. 2.11 Brick red appearance during growth in presence of Na_2SeO_3 of (a) *Idiomarina* sp. PR58-8; (b) *Halobacillus* sp. MTCC 6516; (c) *Halomonas aquamarina* MTCC 4661.

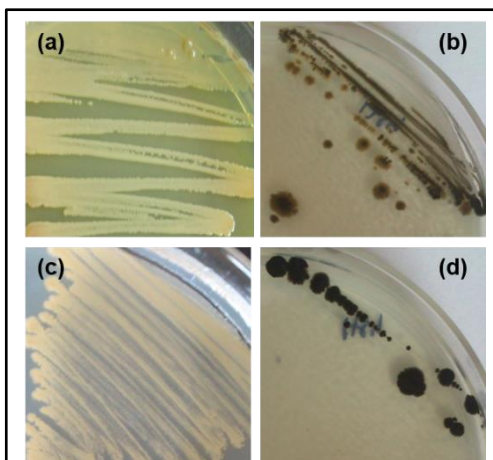
MIC of K_2TeO_3 

Fig. 2.12 (a) ML2 appears golden yellow on ZMB and (b) turns black in presence of K_2TeO_3 ; (c) *H. aquamarina* MTCC 4661 appears light orange on NB + 2% NaCl (d) which turns black in presence of K_2TeO_3 .

ML2 and *Halobacillus* MTCC 6516 exhibited a low level of resistance towards K_2TeO_3 , as evident from the MIC, which was 1 mM. The growth in presence of K_2TeO_3 was delayed and accompanied by the culture turning black in colour (Fig. 2.12). This change in colour is suggestive of the reduction of TeO_3^{2-} to Te^0 . K_2TeO_3 was toxic to *H. aquamarina* MTCC 4661 and the culture failed to grow even at 0.01 mM K_2TeO_3 after prolonged incubation of 30 days. Thus, ML2 and *Halobacillus* MTCC 6516 were resistant to K_2TeO_3 , while *H. aquamarina* MTCC 4661 was found to be susceptible to K_2TeO_3 .

MIC of ZnSO₄

The halophilic bacteria exhibited delayed growth in presence of ZnSO₄. MIC of ZnSO₄ against ML2, *H. aquamarina* MTCC 4661, and *Halobacillus* MTCC 6516 was 4.5 mM, 2 mM, and 0.5 mM, respectively.

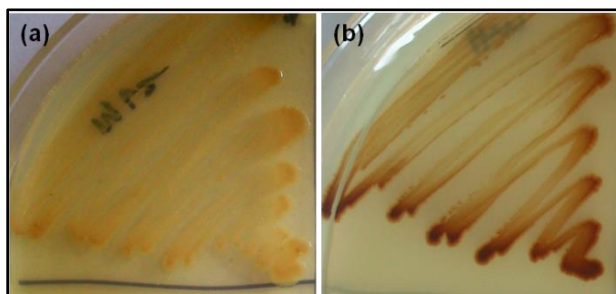
MIC of Pb(NO₃)₂

Fig 2.13 *Idiomarina* sp. PR58-8 appears (a) golden yellow on ZMB and turns (b) brown when grown in presence of Pb(NO₃)₂.

ML2 exhibited a high level of resistance against Pb(NO₃)₂ as was evident from the MIC value which was 9 mM. The growth in presence of Pb(NO₃)₂ was accompanied by the culture turning brown in colour (Fig. 2.13). MIC of Pb(NO₃)₂ for both, *H. aquamarina* MTCC 4661 and *Halobacillus* MTCC 6516 was 2.5 mM, however, the growth

was very poor and slow. Addition of Pb(NO₃)₂ in all the three growth media resulted in generation of white precipitate (PbCl₂) which dissolved on vigorous mixing. The growth medium ZMB contains excess Cl⁻ ions, which causes the dissolution of the PbCl₂ to form lead-chloro complexes (PbCl₃⁻, PbCl₄²⁻), which are lipophilic and thus bio-available (Byrne, 2002)

The cultures exhibited resistance/tolerance in varying degrees to other metal salts in the following order:

ML2: AgNO₃ = Na₂SeO₃ > PbNO₃ >> ZnSO₄ > K₂TeO₃ (least susceptible to AgNO₃/Na₂SeO₃ and most susceptible to K₂TeO₃)

H. aquamarina MTCC 4661: Na₂SeO₃ >> PbNO₃ ~ ZnSO₄ > AgNO₃ (least susceptible to Na₂SeO₃ and most susceptible to AgNO₃)

Halobacillus sp. MTCC 6516: Na₂SeO₃ > PbNO₃ >> K₂TeO₃ > ZnSO₄ (least susceptible to Na₂SeO₃ and most susceptible to ZnSO₄)

Table 2.5 Growth of halophilic bacteria at various concentrations of metal salts.

		Metal salts (mM)	0.05	0.5	1.0	1.5	2.0	2.5	3.0	3.5	4.0	4.5	5.0	6.0	7.0	8.0	9.0	10.0	
<i>Idiomarina</i> sp. PR58-8 (ML2)	AgNO ₃	+++	+++	+++	+++	++	++	++	++	++	++	++	++	+	+	+	+	-	
	Na ₂ SeO	+++	+++	+++	+++	+++	+++	+++	+++	+++	+++	+++	+++	+++	++	+	+	+	-
	K ₂ TeO ₃	++	+	-	-	-	-	-	-	-	-	-	-	-	-	-	-	-	-
	ZnSO ₄	+++	+++	++	++	+	+	+	+	+	+	-	-	-	-	-	-	-	-
	Pb(NO ₃) ₂	+++	+++	+++	+++	++	++	++	++	++	++	++	++	++	++	+	+	-	-
<i>Halomonas</i> <i>aquamarina</i> MTCC 4661	AgNO ₃	+	-	-	-	-	-	-	-	-	-	-	-	-	-	-	-	-	-
	Na ₂ SeO ₃	++	++	++	++	++	++	++	++	++	+	+	+	+	-	-	-	-	-
	K ₂ TeO ₃	-	-	-	-	-	-	-	-	-	-	-	-	-	-	-	-	-	-
	ZnSO ₄	+++	++	++	+	-	-	-	-	-	-	-	-	-	-	-	-	-	-
	Pb(NO ₃) ₂	+	+	+	+	+	-	-	-	-	-	-	-	-	-	-	-	-	-
<i>Halobacillus</i> sp. MTCC 6516	AgNO ₃	-	-	-	-	-	-	-	-	-	-	-	-	-	-	-	-	-	-
	Na ₂ SeO ₃	++	++	++	++	++	+	+	+	+	+	-	-	-	-	-	-	-	-
	K ₂ TeO ₃	+	+	-	-	-	-	-	-	-	-	-	-	-	-	-	-	-	-
	ZnSO ₄	+	-	-	-	-	-	-	-	-	-	-	-	-	-	-	-	-	-
	Pb(NO ₃) ₂	+	+	+	+	+	-	-	-	-	-	-	-	-	-	-	-	-	-

'+++': Good Growth; '++': Growth; '+': Poor Growth; '-': No Growth

Table 2.6 MICs of various metal salts for the halophilic bacteria.

Culture	AgNO ₃ (mM)	Na ₂ SeO ₃ (mM)	K ₂ TeO ₃ (mM)	ZnSO ₄ (mM)	Pb(NO ₃) ₂ (mM)
<i>Idiomarina</i> sp. PR58-8 (ML2)	10	10	1	4.5	9
<i>Halomonas aquamarina</i> MTCC 4661	0.05	7	NG	2	2.5
<i>Halobacillus</i> sp. MTCC 6516	NG	4.5	1	0.5	2.5

NG- No growth even at the lowest concentration tried (0.01 mM)

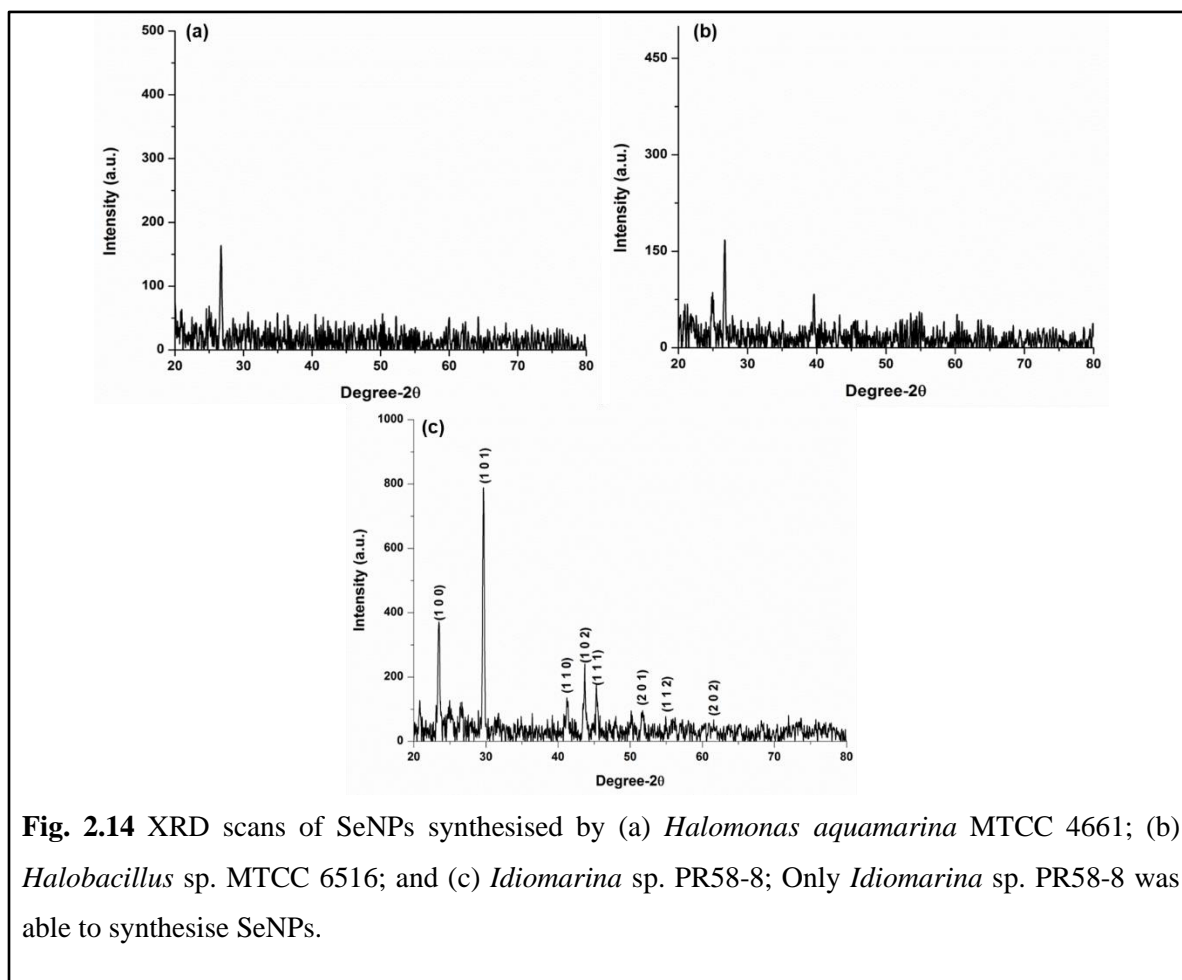
2.3.2.3 Screening of promising halophilic bacteria for nanoparticle synthesis

The metal salt concentration required for nanoparticle synthesis was determined by the MIC studies. ML2 exhibited intrinsic resistance to AgNO_3 , Na_2SeO_3 , and $\text{Pb}(\text{NO}_3)_2$, and was therefore used for SeNPs synthesis and lead based nanoparticles synthesis. SNPs synthesis by this bacterium has already been reported previously (Seshadri et al. 2012). *H. aquamarina* MTCC 4661 exhibited low resistance towards AgNO_3 , ZnSO_4 , and $\text{Pb}(\text{NO}_3)_2$. Besides, the growth of this halobacterium in presence of these metals was retarded, thus SNPs, Zn based, and Pb based nanoparticle synthesis were not attempted. Similarly, *Halobacillus* sp. MTCC 6516 exhibited low resistance towards K_2TeO_3 , ZnSO_4 , and $\text{Pb}(\text{NO}_3)_2$, and thus the corresponding nanoparticles synthesis was not carried out. SeNPs synthesis however was attempted with *H. aquamarina* MTCC 4661 and *Halobacillus* sp. MTCC 6516.

SeNPs synthesis

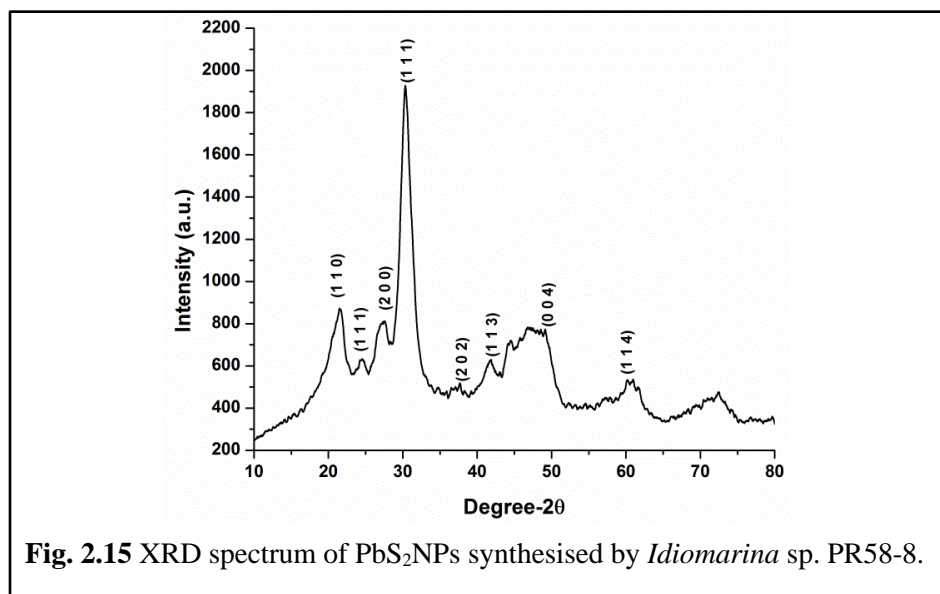
SeNPs synthesis by ML2 was carried out in ZMB medium in presence of 8 mM Na_2SeO_3 . SeNPs synthesis by *H. aquamarina* MTCC 4661 was carried out in NB + 2% NaCl medium in presence of 6 mM Na_2SeO_3 , while 3.5% NTYE and 4 mM Na_2SeO_3 were used for SeNPs synthesis by *Halobacillus* sp. MTCC 6516. Generation of brick-red colouration (Fig. 2.8) was used as an indicator of reduction of SeO_3^{2-} to Se^0 and SeNPs synthesis. The synthesis was found to be a culture dependent phenomenon as the media controls, and culture supernatants failed to reduce the SeO_3^{2-} to Se^0 . The biomass was harvested once the synthesis was over, and dialysed against deionised water overnight with frequent changes of water and dried in the oven. The nanoparticles thus obtained were subjected to crystallographic characterisation by XRD. The halophilic bacteria capable of synthesising SeNPs were selected for further studies.

Fig. 2.14 shows the XRD scans of nanoparticles synthesised by *H. aquamarina* MTCC 4661, *Halobacillus* sp. MTCC 6516, and ML2. XRD analysis exhibited characteristic Bragg's peak of hexagonal selenium (ICDD card no. 06-0362) with ML2. The crystallite domain size as calculated by Debye-Scherrer formula was found to be 34.52 nm. Even though both *H. aquamarina* MTCC 4661 and *Halobacillus* sp. MTCC 6516 exhibited brick red colouration, the characteristic peaks of selenium were absent. Thus, ML2 was used for SeNPs synthesis and further studies.



Lead (IV) sulfide nanoparticles (PbS₂NPs) synthesis

Amongst the three halophilic bacteria tested for their ability to synthesise lead based nanomaterials, only ML2 exhibited a high level of intrinsic resistance towards $\text{Pb}(\text{NO}_3)_2$. Pb based nanoparticles were synthesised by growing ML2 in ZMB medium with 5 mM $\text{Pb}(\text{NO}_3)_2$. In presence of $\text{Pb}(\text{NO}_3)_2$, ML2 turned brown in colour (Fig. 2.11). The biomass was harvested, and dialysed against deionised water overnight with frequent changes of water. The nanopowder was obtained by drying the dialysed biomass in a hot air oven. XRD analysis of the ‘as synthesised’ nanoparticles exhibited the characteristic Bragg’s peak of tetragonal lead (IV) sulfide (PbS_2) corresponding to ICDD card No. 20-0596 (Fig. 2.15). The crystallite domain size was found to be 2.38 nm. Thus, ML2 was used for PbS_2 NPs synthesis and further related studies.



2.4 Conclusion

The screening of halophilic archaea and bacteria was carried out to determine the most suitable cultures for metal and metal sulphide nanoparticle synthesis. Halophilic archaea, *Halococcus salifodinae* BK3, *H. salifodinae* BK6, *H. salifodinae* BK7, *H. salifodinae* BK11, and *H. salifodinae* BK18, and halophilic bacteria, *Idiomarina* sp. PR58-8, *Halomonas aquamarina* MTCC 4661, and *Halobacillus* sp. MTCC 6516 were used for this study. First the medium for optimum growth for each culture was determined. All the five haloarchaea exhibited optimum growth in NTYE medium as was evident from their specific growth rates, doubling times, and lag times. The medium supporting optimum growth for *Idiomarina* sp. PR58-8 was ZMB, for *Halobacillus* sp. MTCC 6516 was 3.5% NTYE, while that for *H. aquamarina* MTCC 4661 was NB + 2% NaCl. The MICs of various metals in the respective medium was successfully determined for all the haloarchaeal isolates and the halophilic bacteria. Amongst the halophilic archaea screened *H. salifodinae* BK3 and *H. salifodinae* BK6 exhibited the ability to synthesise SNPs; *H. salifodinae* BK18 could synthesise SeNPs; and *H. salifodinae* BK3 could synthesise TeNPs. Similarly, amongst the halophilic bacteria screened, only *Idiomarina* sp. PR58-8 could successfully synthesise SeNPs and PbS₂NPs. Thus, these cultures were used for synthesis and applications of metal and metal sulphide nanoparticles.

CHAPTER 3

Synthesis of Silver Nanoparticles by Halophilic Archaea *Halococcus salifodinae* BK3 and *H. salifodinae* BK6 and their Application as Antimicrobial Agents¹**3.1 Introduction**

Silver (Ag) is a transition metal belonging to group 11 (IB) of the periodic table along with copper (Cu), gold (Au), and roentgenium (Rg). Pure silver is lustrous, soft, very ductile, malleable, and an excellent conductor of heat and electricity. It is present in nature as minerals such as argentite (Ag_2S), which usually occurs associated to other sulphides of Cu or Pb; cerargirite (AgCl); proustite ($3\text{Ag}_2\text{S}.\text{Ag}_2\text{S}_3$); pirargirite ($3\text{Ag}_2\text{S}.\text{Sb}_2\text{S}_3$); stefanite ($5\text{Ag}_2\text{S}.\text{Sb}_2\text{S}_3$) and native silver. It is present at 0.08 ppm in the earth's crust. Unlike copper which is an essential trace element, silver has no known biological role. Historically, Ag was used for making jewellery, utensils, monetary currency, dental alloy, photography, explosives, etc. (Chen and Schluesener 2008). The use of silver as an antiseptic to manage open wounds and burns is also well known. Besides these applications, other uses of silver and its compounds include, brazing and soldering, catalysis to produce ethylene oxide and formaldehyde, in electronic industry as electrical switches, photovoltaic cells, batteries, and mirrors and glasses as reflective surfaces. Silver nanoparticles (SNPs) have received considerable attention due to their attractive physicochemical properties such as high electrical and thermal conductivity, surface enhanced Raman scattering, chemical stability, catalytic activity, and non-linear optical behaviour (Vo-Dinh, 2008; Olenin et al. 2008). The large effective scattering cross section of individual SNPs makes them ideal candidates for molecular labelling where surface-enhanced resonance Raman scattering (SERRS) or surface plasmon resonance imaging (SPRI) techniques may be used for detection (Graham et al. 2009; Paul et al. 2011).

¹ This work is published as: (1) **Srivastava P**, Braganca J, Ramanan SR, Kowshik M (2013) Synthesis of silver nanoparticles using haloarchaeal isolate *Halococcus salifodinae* BK3. *Extremophiles* 17:821-831; (2) **Srivastava P**, Braganca J, Ramanan SR, Kowshik M (2013) Green synthesis of silver nanoparticles by haloarchaeon *Halococcus salifodinae* BK6. *Advanced Materials Research* 938:236-241.

Silver in its various chemical forms is known to be a potent antimicrobial agent (Catauro et al. 2004) and SNPs exhibit strong toxicity against microbes (Furno et al. 2004). The decreased particle size and increased specific surface area enables rapid dissolution of ions than the equivalent bulk material, thereby enhancing toxicity of SNPs. Once the particles start to dissolve or degrade *in situ*, SNPs readily interact with bio-molecules and biological receptors and can reach sub-cellular locations leading to potentially higher localised concentrations of ions. Further, these nanoparticles generate reactive oxygen species (ROS), and interact with, and potentially disturb the functioning of bio-molecules such as proteins, enzymes, and DNA (Hwang et al. 2008; Feng et al. 2008; Reidy et al. 2013).

Various chemical (polyol process, precursor injection method, etc.), physical (evaporation-condensation, thermal-decomposition, and arc discharge), and biological methods have been used for synthesis and fabrication of mono- and/or poly-dispersed SNPs. Chemical route of SNPs synthesis is the simplest, and large quantities of nanoparticles are generated. However, major drawbacks of chemical synthesis include the generation of hazardous by-products, and the requirement of capping agents like PVP, poly(N-isopropyl acrylamide) like surfactants, alkylthiols, and branched polyethyleneimine (BPEI) which are toxic and reduce the applicability of SNPs (Guo et al. 2007, Vasiliev et al. 2009). Physical methods yield large quantities of SNPs in a single process, however, the use of extreme conditions of temperature and pressure, and the overall instrumentation expenses are disadvantageous (Tran et al. 2013). The highly structured physical and biosynthetic activities of microbial cells present a green alternative for benign synthesis of SNPs (Gericke and Pinches 2006). Microbially synthesised SNPs are usually capped by the stabilising cellular metabolites produced during the process of synthesis.

SNPs have been successfully synthesised by a plethora of microorganisms with properties similar to chemically synthesised nanoparticles. Various fungi (Mukherjee et al. 2003; Kathiresan et al. 2010), yeast (Kowshik et al. 2003; Manivannan et al. 2011), bacteria (Lengke et al. 2007; Shah et al. 2012), and algae (Rajeshkumar et al. 2014) have been reported to biologically synthesise SNPs both intracellularly and extracellularly. However, there are no reports on nanomaterial synthesis by haloarchaea. In this work, we report for the first time,

nanoparticle synthesis by halophilic archaea (haloarchaea), member of the third domain of life, Archaea.

The reduction of Ag^+ to colloidal silver by microorganisms in aqueous solutions is a stepwise process. First various complexes of Ag^+ are reduced to metallic silver atoms (Ag^0). This is followed by the agglomeration of Ag^0 into oligomeric clusters (Sharma et al. 2008). It is these clusters that eventually lead to the formation of colloidal Ag nanoparticles (Kapoor et al 1994; Sharma et al. 2008). The low molecular weight peptide, GSH and proteins like metallothioneins and phytochelatins, enzymes such as oxidoreductases, NADH-dependent reductases, nitroreductases, NADH-dependent NRs, and cysteine desulphhydrases have been shown to be responsible for nanocrystal formation in yeast, bacteria, and fungi (Sweeney et al. 2004; Mokhtari et al. 2008; Bai et al. 2009; Ahmad et al. 2003; Shahverdi et al. 2007; Ramezani et al. 2010). In this study we report the intracellular synthesis of silver nanoparticles by two haloarchaeal isolates, *Halococcus salifodinae* BK3 and *H. salifodinae* BK6. We demonstrate the involvement of NADH-dependent NRs in metal tolerance, silver reduction and nanoparticle synthesis.

3.2 Materials and Methods

3.2.1 Organism and culture maintenance

H. salifodinae BK3 and BK6 were previously isolated and characterised in the laboratory by Mani et al. (2012). They were maintained on NTYE plates. They were also maintained in NTYE broth at 37°C, 110 rpm, and sub-cultured every 5 days.

3.2.2 Silver resistance and growth kinetics studies

The effect of silver on the growth of haloarchaeal isolates was determined in the presence of AgNO_3 in the concentration range of 0.05 mM to 1 mM. Silver nitrate was prepared as 0.1 M stock solution and sterilised by filtration. The silver resistance studies were performed by growing *H. salifodinae* BK3 and BK6 in the presence of 0.05 mM AgNO_3 . The culture was adapted to silver in NTYE by sub-culturing it in increasing concentrations of silver salt. To study the effect of metal on the growth kinetics of *H. salifodinae* BK3, and BK6, 100 ml NTYE supplemented with 0.5 mM/1 mM AgNO_3 was inoculated with 1% culture adapted to silver

and incubated at 37°C, 110 rpm. A 1 ml aliquot of culture was withdrawn at intervals of 24 hrs and absorbance was measured at 600 nm on UV-visible double beam spectrophotometer. Inoculated medium without AgNO₃ served as positive control, and un-inoculated medium with AgNO₃ served as negative control. Similarly, the growth profile of both the isolates in nitrate broth (0.5% peptic digest of animal tissue, 0.3% beef extract and 0.1% potassium nitrate) amended with 25% NaCl, 0.5% KCl and 2% MgSO₄.7H₂O (Halophilic Nitrate Broth; HNB) was also determined. Specific growth rate, doubling time and lag time were calculated as described in section 2.2.2.

3.2.3 Biosynthesis of SNPs and process parameter optimisation

H. salifodinae BK3, and *H. salifodinae* BK6 (2%, OD= 0.6) were inoculated in NTYE medium with requisite amount of AgNO₃ and incubated at 37°C, 110 rpm in the dark for nanoparticle synthesis. The accumulation and reduction of silver was followed by visual observation of biomass turning brown-black, which is a convenient indication of the formation of silver nanoparticles. The cells were harvested by centrifugation (10,000 × g, 20 mins, RT). The pellet obtained was washed twice with sterile distilled water (SDW) and dialysed against deionised water for 24 hours, with change of water once every two hours. The sample was sonicated (Microson™ Sonicator) at 0°C for 15 mins each, at 3 RPS (40 W) followed by centrifugation at lower speed (10,000 × g, 30 mins) to separate the cell debris and then high speed (22,000 × g, 1 hr) to collect the nanoparticles. The nanoparticle powder was obtained by drying the pellet at 60°C for 12 hours. Appropriate controls (un-inoculated medium + AgNO₃ and culture supernatant + AgNO₃) were run simultaneously. Similarly, SNPs were also synthesised in HNB medium.

Process parameters such as medium pH, incubation temperature and AgNO₃ concentration were varied to determine the optimal conditions for maximum yield of SNPs. *H. salifodinae* BK3, and BK6 were grown in NTYE/HNB with varying pH, or varying AgNO₃ concentrations, or incubation temperatures and the yield of SNPs was determined as mentioned in section 3.2.4. The following parameters were tested for optimising the process:

pH	4.5	5.0	5.5	6.0	6.5	7.0	7.5	8.0	
AgNO₃ conc. (mM)	0.05	0.1	0.15	0.2	0.3	0.4	0.5	0.6	0.7
Temperature (°C)	20	25	30	35	37	40	45		

3.2.4 Silver estimation and yield determination

Flame-atomic absorption spectroscopy (FAAS), Shimadzu AA-700 was used to determine the silver concentration in the supernatant and the cell pellet after exposure to AgNO_3 . Instrumental conditions for FAAS measurement are summarised in Table 3.1. For process parameter optimisation, both the culture supernatant and the cell pellet were harvested followed by digestion with nitric acid. The samples were diluted appropriately and analysed by FAAS.

Table 3.1 Instrumental conditions for FAAS measurements

Element	Silver
BGC mode	BGC-D2
Wavelength	328.1 nm
Lamp current	10 mA
Slit width	0.7 nm
Flame type	Air-C ₂ H ₂
C₂H₂ flow rate	2.2 L/min
Burner height	7 mm

SNPs synthesis was subsequently carried out at optimised conditions in both HNB and NTYE media in triplicates. 5 ml samples were withdrawn every 24 hrs, and the supernatant was separated from the cell pellet (12,000 × g; 30 mins). The supernatants, and cell pellets were prepared by nitric acid digestion, appropriately diluted, and analysed by FAAS. One set of the cell pellets was dried and weighed to determine the respective cell dry weight (CDW). The yield per gram of CDW was calculated as: $Y = P/B$ where, Y is the yield (mg/g CDW), P is the weight/mass of the product obtained and B is the CDW. The yield per mg of substrate added was determined as: $SY = Q/S$ where, SY is the yield (mg/mg of Ag added), Q is the mass/weight of Ag taken up by the cells (mg) and S is the mass/weight of Ag (substrate) provided to the cells for SNPs synthesis.

3.2.5 Characterisation of silver nanoparticles

The excitation spectra of the SNPs dried powder (prepared in NTYE, and HNB), suspended in distilled water was recorded in the range of 200-800 nm using UV-visible double beam spectrophotometer with distilled water as the blank. Crystallographic characterisation was performed as described in section 2.2.4.1. The lattice parameters for fcc crystal system were calculated according to the formula:

$$\frac{1}{d^2} = \frac{(h^2+k^2+l^2)}{a^2} \quad (4)$$

where (h k l) is (1 1 1).

The morphology of the nanoparticles powder was determined using transmission electron microscopy (TEM). The SNPs synthesised in NTYE and HNB were dispersed in water by sonication at 0°C for 15 mins each, at 3 RPS (40 W). The colloidal solution of SNPs thus obtained, was drop-coated on carbon-coated copper TEM grids. The TEM images were obtained using Philips (Model- CM200) transmission electron microscope (resolution 2.4 Å), which was operated at an accelerating voltage of 190 keV. Selected area electron diffraction (SAED) studies were also carried out using the TEM. The elemental composition of the nanoparticles was determined by energy dispersive X-ray analysis (EDAX) using JEOL, JSM-5800LV scanning electron microscope equipped with EDX and operated at 20 keV. The sample powders were deposited on a carbon tape before mounting on a sample holder and gold coated for EDAX.

3.2.6 Thiol assay

H. salifodinae BK3, and *H. salifodinae* BK6 cells (0.5 g wet weight) grown in presence of 0.05 mM, and 0.5 mM AgNO₃ were suspended in TN buffer (50 mM Tris, 4 M NaCl). The suspension was sonicated at 0°C for 5 cycles of 2 mins each, at 3 RPS (40 W). Cell debris was removed by centrifugation at 10,000 × g, at 4°C for 20 mins, and the supernatant (Cell free extract- CFE) was stored at -20°C for thiol assay. Cells grown in the absence of AgNO₃ served as the negative control. Total thiol (T-SH), non-protein thiol (NP-SH), and protein bound thiol (PB-SH) were estimated using 5,5'-dithio-bis (2-nitrobenzoic acid) (DTNB; Sigma) according to Sedlak and Lindsay (1968). For determination of T-SH, 79% methanol (Merck), 0.03 M

Tris (pH 8.2) and 0.1 mM DTNB were added to 50 μ l of CFE, and incubated at RT for 15 mins. The mixture was centrifuged at $1,700 \times g$, for 15 mins, and absorbance was recorded at 412 nm against a reagent blank. Reduced GSH (Sigma) was used as the standard. For determination of NP-SH, 500 μ l of CFE, 400 μ l of milli Q water and 5% TCA were gently mixed for 12 mins and centrifuged at $1,700 \times g$, for 15 mins. Tris (0.16 M; pH 8.9) and DTNB (0.1 mM) were added to 200 μ l of the supernatant and absorbance was measured at 412 nm within 3 mins of addition of DTNB. PB-SH was determined by subtracting the NP-SH from the T-SH. Total cellular proteins were estimated by Bradford's method (Bradford, 1976) using bovine serum albumin (BSA) as standard. The T-SH and PB-SH were normalised to the total protein content of the cells. The assay was carried out in triplicates.

3.2.7 Nitrate reductase assay and inhibitor studies

The cultures *H. salifodinae* BK3 and *H. salifodinae* BK6 were grown in HNB broth, with 0 (control), 0.05 and 0.5 mM AgNO_3 at 37°C , 110 rpm for 10 days. Both positive (inoculated medium with 0.05 and 0.5 mM KNO_3), and negative (un-inoculated medium with 0.5 mM AgNO_3) controls were run simultaneously. Culture was centrifuged at $10,000 \times g$, for 20 mins at RT. 100 μ l of Griess Ilosvays reagent and 2.6 ml distilled water were added to 300 μ l of culture supernatant, incubated at RT for 30 mins, and the absorbance of the resultant coloured product was recorded at 548 nm using UV-visible double beam spectrophotometer. The standard curve was prepared using NaNO_2 . The assay was performed in triplicates.

The NR enzyme activity of *H. salifodinae* BK3, and *H. salifodinae* BK6 was measured according to Harley (1993) by determining the amount of nitrate reduced within 2 mins by the CFE, on addition of substrate mixture (25 mM potassium phosphate buffer, 10 mM KNO_3 , and 0.05 mM ethylene diamine tertra acetic acid (EDTA) (pH 7.3)). 100 μ l CFE of *H. salifodinae* BK3, and *H. salifodinae* BK6, grown in presence of 0.05 and 0.5 mM AgNO_3 was added to the substrate mixture along with 0.2 mM β -nicotinamide adenine dinucleotide (reduced form; β -NADH). The reaction was stopped after 2 mins by addition of 0.15 mM sulphanilamide solution in 3 mM HCl (Qualigens), followed by 0.19 mM N-(1-naphthyl) ethylene diamine hydrochloride (NED) solution, with proper mixing. Absorbance of the resultant coloured product was recorded at 540 nm. 0.05mM, and 0.5 mM KNO_3 were used as positive controls. For negative control, the substrate mixture was inactivated by boiling the CFE for 10 mins,

and the nitrite content was subtracted from that of the test, to give total amount of nitrite produced by the enzyme in 2 mins. All the assays were performed in triplicates.

Phenyl methane sulphonyl fluoride (PMSF), EDTA, sodium azide, and idoacetate (IAA) were used for the inhibitor study. *H. salifodinae* BK3, and *H. salifodinae* BK6 were grown in the absence of inhibitor (Negative control), in presence of 10 mM inhibitor, and in presence of 10 mM inhibitor along with 0.5 mM AgNO₃. Culture grown in presence of 0.5 mM AgNO₃ in the absence of the inhibitor served as positive control. Further, the NR activity of the CFE obtained from cells grown in presence of 0.5 mM AgNO₃ was determined in presence of 10 mM inhibitor. The study was carried out in triplicates for each inhibitor. The percentage of inhibition of NR enzyme activity was determined by the formula:

$$\% \text{ inhibition} = 100 - \{(NR_I \times 100)/NR_{AI}\} \quad (5)$$

where, NR_I is NR activity in the presence of the inhibitor and NR_{AI} is the NR activity in the absence of the inhibitor.

3.2.8 Antimicrobial effect of SNPs

Disk diffusion method was employed to determine the antimicrobial activity of the SNPs synthesised by both *H. salifodinae* BK3, and *H. salifodinae* BK6. The test organisms used were gram-negative *Escherichia coli* ATCC 10536 and *Pseudomonas aeruginosa* MTCC 2582, and gram-positive *Staphylococcus aureus* ATCC 6538P and *Micrococcus luteus* NCIM 2170. A stock solution of 20 mg/mL SNPs synthesised in HNB was prepared in SDW, and the suspension was sonicated for proper dispersal. Sterile disks of 6 mm diameter were loaded with SNPs suspension to give a concentration of 10 and 50 µg/disc. Log phase bacterial cultures (~ 10⁶ CFU/mL) were swabbed on Mueller Hinton agar, impregnated with the sample loaded disks and incubated at 37°C for 18 hrs. The antibacterial activity was determined by measuring the zone of inhibition (ZoI), which is a fast and inexpensive method. The ZoI obtained due to SNPs was compared to that obtained due to the antibiotic streptomycin (25 µg/disc) and gentamicin (30 µg/disc) which served as positive controls; saline served as the negative control. The assay was performed in triplicates.

The minimum inhibitory concentration (MIC) of the SNPs synthesised by both *H. salifodinae* BK3, and BK6 was also determined according to the standard guidelines of CLSI, against *E. coli* ATCC 10536, *P. aeruginosa* MTCC 2582, *S. aureus* ATCC 6538P, and *M. luteus* NCIM 2170. 100 μ l/well of double strength MH broth (MHB) was added in a 96-well microtiter plate along with appropriate dilutions of the SNPs prepared in deionised water. 10 μ l of 0.1% resazurin sodium salt (Sigma-Aldrich) was added to each well, followed by exponential phase bacterial cells ($\sim 10^6$ CFU/ml), and the volume was made up to 200 μ l using SDW. The plate was incubated in the dark at 37°C, for 24 hrs on a shaking incubator. The lowest concentration of the SNPs at which no blue to pink colour change was observed was recorded as the MIC. Appropriate controls were subjected to similar treatments. All experiments were carried out in triplicates.

3.2.9 Statistical analysis

The statistical analysis was carried out as described in section 2.2.5.

3.3 Results and Discussion

3.3.1 Studies on growth kinetics

Silver nitrate was found to be toxic to both *H. salifodinae* BK3, and *H. salifodinae* BK6 above concentrations of 0.5 mM. At 0.05 mM AgNO₃, both the isolates exhibited growth similar to the unexposed controls (Fig. 3.1 a,b). MIC of AgNO₃ for both the isolates was 1 mM, as the cultures did not exhibit growth at this concentration (Fig 3.1). In presence of 0.5 mM AgNO₃, both the isolates exhibited slow growth, and the pigmentation of the culture changed from orange-red to brown-black, indicating the reduction of Ag⁺ to metallic silver (Ag⁰) (Fig. 3.2). During the first contact with AgNO₃, the cultures in NTYE medium exhibited a retarded growth (Fig. 3.3). However, on repeated growth in medium containing 0.05 mM to 0.5 mM AgNO₃ (three subcultures) the organism adapted to growth in presence of silver. The growth profile of Ag adapted *H. salifodinae* BK3 (Fig. 3.3ic) was similar to that of control (Fig. 3.3ia). The specific growth rate (μ) of *H. salifodinae* BK3 exposed to AgNO₃ for the first time was 0.27 days⁻¹, which increased to 0.67 days⁻¹ (p<0.05) for cells adapted to AgNO₃ (Table 3.2). Similarly, AgNO₃ adapted *H. salifodinae* BK6 cells exhibited a significantly higher μ of 0.69 days⁻¹ (p<0.05) as compared to 0.28 days⁻¹ for cells exposed to AgNO₃ for the first time (Fig.

3.3ii). The lower growth rate and prolonged lag phase are indicative of longer adaptation periods required by the isolates encountering AgNO_3 for the first time. Adaptation by repeated sub-culturing with increasing concentrations of AgNO_3 enables the microorganism, in this case the haloarchaea, to adjust to the metal stress. A similar tolerance to metal toxicity and metal uptake by adaptation has been shown in other microorganisms i.e., bacteria (Appanna et al. 1996; Xia et al. 2008), yeast (Domnez et al. 2001), and fungi (Ge et al. 2011).

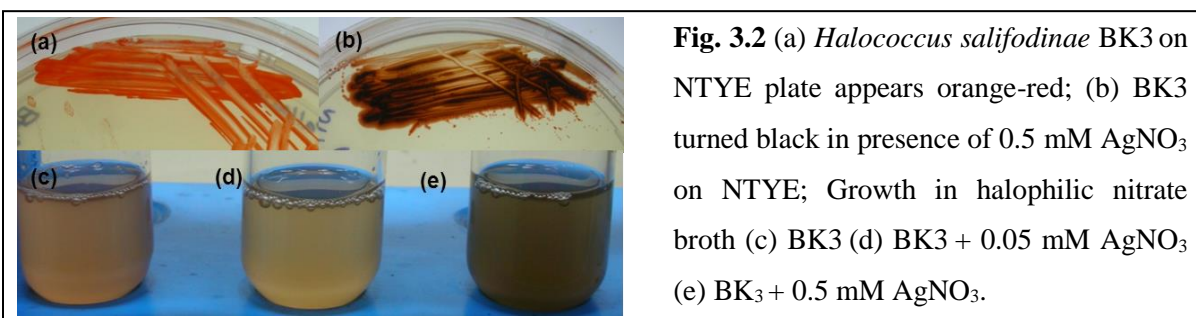
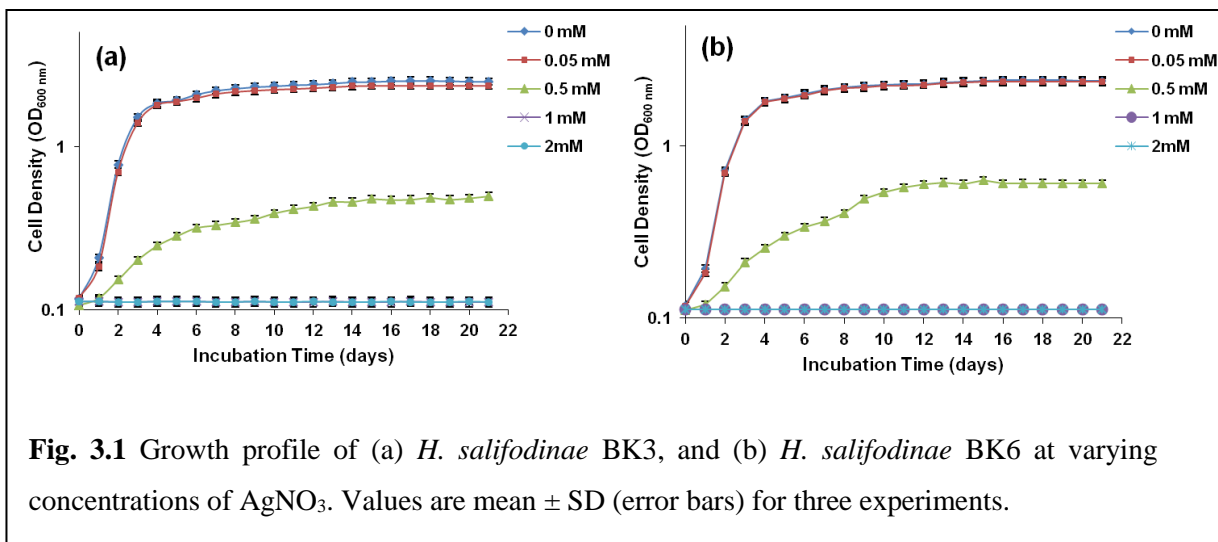
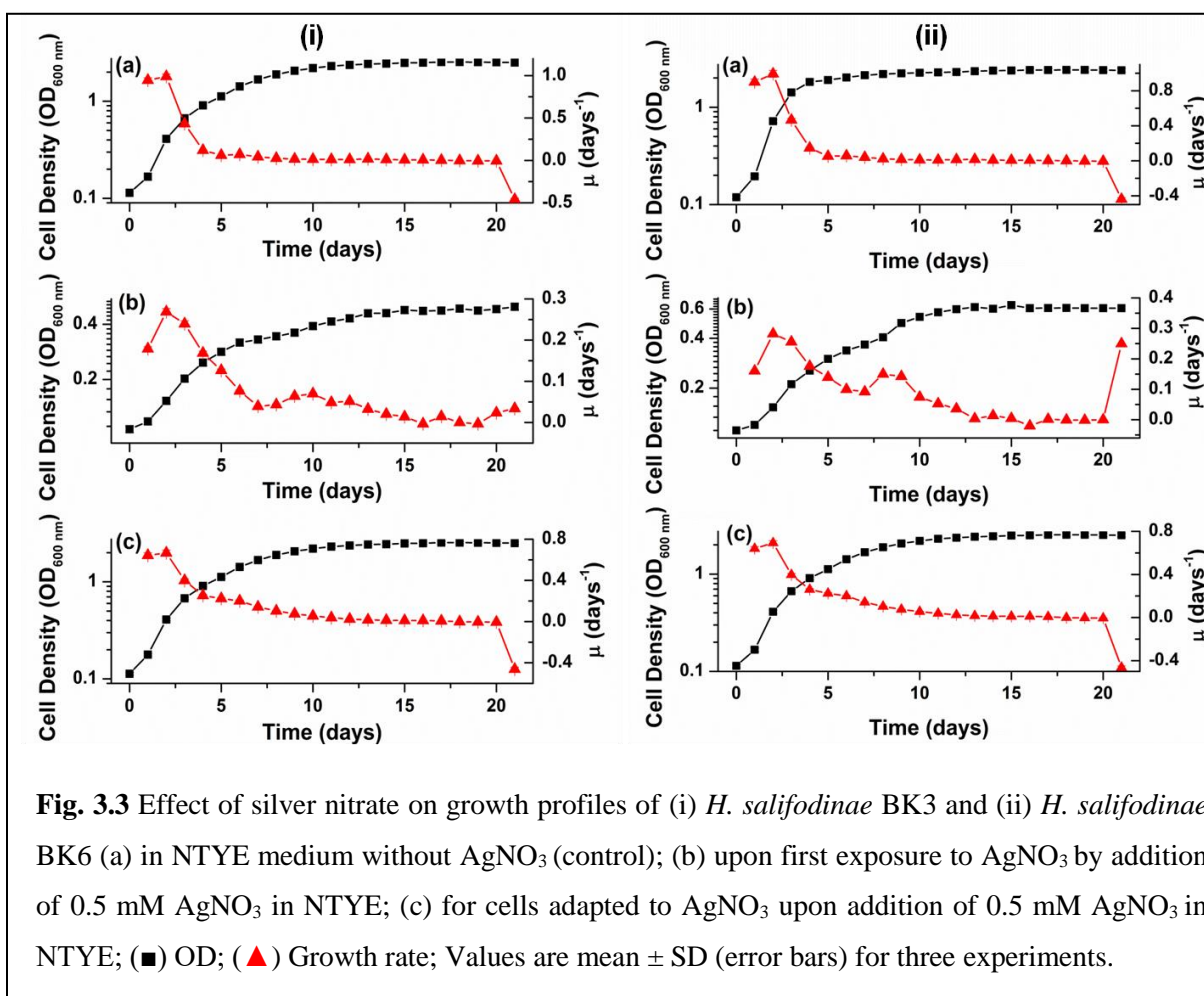


Table 3.2 Growth kinetics parameters of *Halococcus salifodinae* BK3 and *H. salifodinae* BK6.

Medium		μ (days ⁻¹)		t_l (hrs)		t_d (hrs)	
		BK3	BK6	BK3	BK6	BK3	BK6
Control		0.99	0.99	11.52	12	16.9	16.8
NTYE	Silver adapted	0.67	0.69	12.48	14.4	25.1	24.02
	Silver exposed	0.27	0.28	19.2	19.2	61.9	58.97
Control		0.99	0.99	10.56	12	16.9	16.82
HNB	Silver adapted	0.87	0.98	11.52	11.52	19.2	16.94
	Silver exposed	0.32	0.37	14.4	21.6	51.5	45.58

μ - specific growth rate; t_l - lag time; t_d - doubling time



The haloarchaeal isolates, *H. salifodinae* BK3, and *H. salifodinae* BK6 were capable of reducing toxic, colourless, soluble Ag^+ to brown-black, insoluble elemental (Ag^0) form as SNPs intracellularly. Various organisms have been shown to synthesise SNPs which is accompanied by the brown-black colouration of the medium (Kowshik et al. 2003; Shankar et al. 2004; Basavaraja et al. 2008), that arises due to the excitation of surface plasmon vibrations typical of SNPs (Mulvaney 1996). Media controls without the culture did not precipitate silver, thus confirming that synthesis of SNPs was a culture dependent phenomenon. Likewise, NP synthesis was not observed when AgNO_3 was added to the supernatant of *H. salifodinae* BK3/*H. salifodinae* BK6 grown both in the presence, and absence of AgNO_3 for 72 hrs. Certain organisms like yeast, bacteria, and fungi have been shown to overcome metal stress and synthesise MNPs when the metal is introduced into the medium during the mid-log phase of growth (Kowshik et al. 2003; Bai et al. 2009; Hariharan et al. 2012). The AgNO_3 when added to the mid-log phase of either *H. salifodinae* BK3 or *H. salifodinae* BK6 prevented further growth of the haloarchaea and did not result in SNPs synthesis. However, when these cells were inoculated in fresh NTYE medium, the organisms resume growth, suggesting that the addition of AgNO_3 during mid-log phase does not kill the haloarchaeon, only inhibits their growth. On the other hand, addition of AgNO_3 at the time of inoculation allows the haloarchaeal cells to adapt to the toxic Ag^+ , resulting in growth and synthesis of SNPs. A similar phenomenon has been reported in bacteria in response to metal stress, where addition of metal any time after lag phase is bacteriostatic, while addition at the time of inoculation allows the bacteria to overcome metal stress (Williams et al. 1996; Walker and Houston, 1981). SNPs synthesis by the marine bacterium, *Idiomarina* sp. PR58-8 also requires the addition of AgNO_3 at the time of inoculation (Seshadri et al. 2012). The addition of the metal salt at the time of inoculation is advantageous, especially during the scale-up of the SNPs synthesis process, as the need for growth phase monitoring is eliminated.

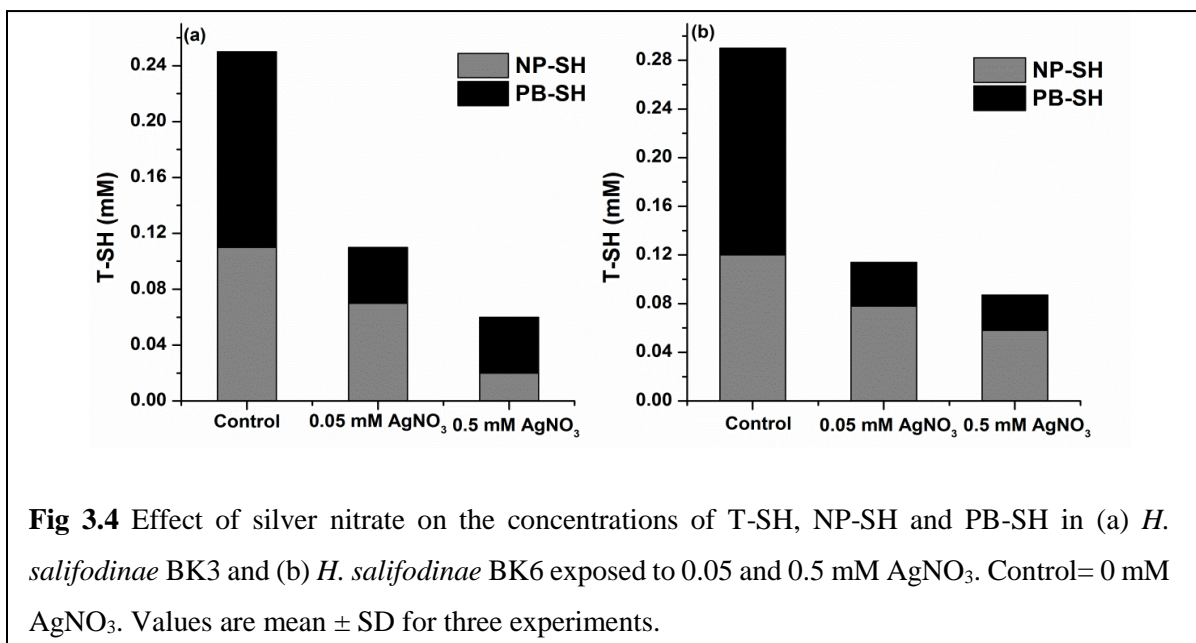
3.3.2 Mechanism of SNPs synthesis

Organisms are known to tolerate metal stress by increasing the cellular pools of thiol compounds, resulting in formation of a thiolate-metal complex, which neutralises the toxicity of the metals and traps them inside the cells. These thiol compounds include the NP-SH glutathione (Avery et al. 2001), and the PB-SH MTs and PCs (Winge et al. 1985; Kneer et al.

1992). In certain fungi and yeast, heavy metal exposure results in an increased synthesis of PCs or MTs thereby exhibiting an increased PB-SH (Münger et al. 1987; Hayashi and Mutoh 1994; Borrelly et al. 2002). However, in some fungi and bacteria, exposure to heavy metal causes the sulphur in the proteome to be utilised for synthesis of GSH instead of sulphur rich proteins (Speiser et al. 1992), thereby decreasing the levels of PB-SH and increasing the NP-SH levels within the cell (Guimarães- Soares et al. 2007; Seshadri et al. 2011). Haloarchaea have γ -glutamyl cysteine (γ GC) (Newton and Javor 1985; Malki et al. 2009) which is analogous to GSH, and is involved in maintaining a reducing environment within the cell, overcoming oxidative and disulphide stress, and detoxification of xenobiotics (Fahey 2001). However, its role in metal resistance of haloarchaea has not been investigated. To determine the role of thiols in conferring metal resistance in both *H. salifodinae* BK3, and *H. salifodinae* BK6, thiol assay was performed on cells grown in the presence, and absence of AgNO_3 .

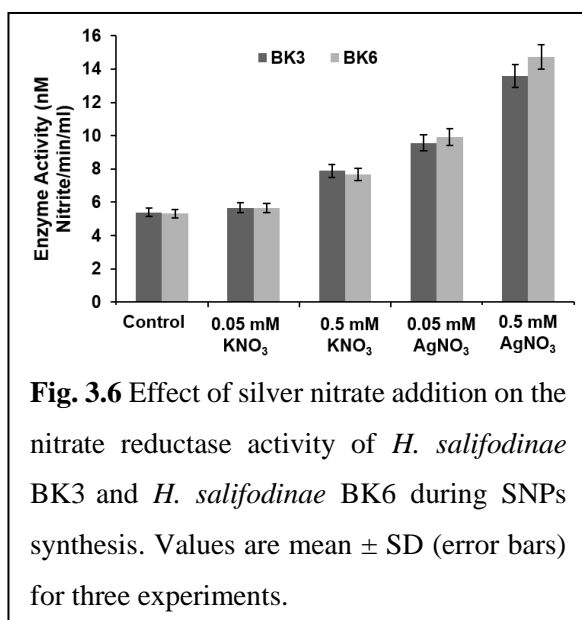
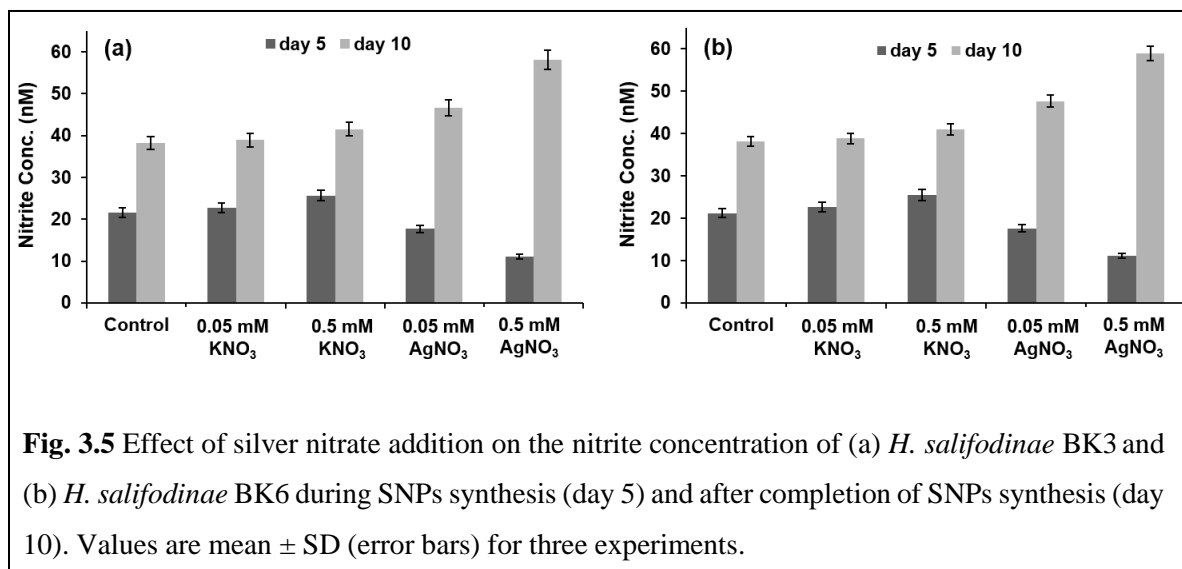
On exposure to AgNO_3 , both *H. salifodinae* BK3, and *H. salifodinae* BK6, exhibited a concentration dependent decrease in T-SH, NP-SH and PB-SH (Fig. 3.4). The thiol contents were normalised to the total protein content of the respective samples. In presence of 0.05 mM AgNO_3 , a 60%, 35% and 75% decrease in concentration of T-SH, NP-SH, and PB-SH, respectively, as compared to the control (*H. salifodinae* BK3 cells grown in the absence of AgNO_3), was observed. Similarly, in case of *H. salifodinae* BK3 cells grown in presence of 0.5 mM AgNO_3 , the concentration of T-SH, NP-SH, and PB-SH decreased by 81%, 86% and 76%, respectively. *H. salifodinae* BK6 grown in presence of 0.05 and 0.5 mM AgNO_3 also exhibited a similar decrease in T-SH, NP-SH and PB-SH as compared to unexposed controls (Fig. 3.4b). A similar observation of decrease in NP-SH, and PB-SH in *Articulospora tetracladia* exposed to copper was made by Miersch et al. (2001) during studies on the influence of Cd^{2+} , Cu^{2+} , and Zn^{2+} on growth and thiol production. Here, the reduced levels of GSH and PCs were attributed to the participation of Cu in Fenton reaction, resulting in the oxidation of the thiols accompanied with an imbalance in their synthesis/recycling and consumption/degradation. In haloarchaea, γ GC is maintained in its reduced form by the enzyme bis- γ glutamyl cysteine reductase (GCR), which is analogous to glutathione reductase (Sundquist and Fahey 1989). Heavy metal ions of Zn^{2+} , Cu^{2+} , Hg^{2+} , and arsenite have been shown to inhibit GCR in *Halobacterium halobium* (Sundquist and Fahey 1989). A similar inhibition of GCR by Ag^+ may be responsible for a concentration dependent decrease in the

NP-SH and T-SH, in both *H. salifodinae* BK3, and *H. salifodinae* BK6. Thus, thiol compounds were not involved in SNPs synthesis and metal resistance in these organisms.



The reduction of silver ions to its metallic form in bacterial, and fungal systems has also been shown to involve enzymatic detoxification by enzymes like nitrate reductase (NR), where toxic metal form is converted to non-toxic nano-particulate form (Ahmad et al. 2003; Durán et al. 2005; Kalimuthu et al. 2008; Vaidyanathan et al. 2010). Both, *H. salifodinae* BK3, and BK6 were found to be NR positive as indicated by the pink colour development on addition of Griess Ilosvays reagent. The reduction of nitrate to nitrite is catalysed by NR using NADH as the electron donor, however in the presence of silver the electron is shuttled from NADH to reduction of silver ions (Deepak et al. 2011). In case of *H. salifodinae* BK3, the nitrite concentration within the cell at the time of inoculation was 0.68 nM. On day 5, the nitrite concentration for cells grown in presence of 0.05 mM and 0.5 mM AgNO₃ decreased by 18% and 49%, respectively (Fig. 3.5a), as compared to the control (cells grown in the absence of AgNO₃). However, after complete reduction of silver (day 10), the nitrite concentration of cells grown in presence of 0.05 mM, and 0.5 mM AgNO₃ increased by 22% and 52%, respectively, with respect to the control (cells grown in the absence of AgNO₃). Similarly, for *H. salifodinae* BK6 grown in presence of 0.05 mM, and 0.5 mM AgNO₃, a decrease in nitrite concentration of 17% and 46%, respectively was observed on day 5, which increased by 25% and 54% as

compared to control, on day 10 (Fig. 3.5b). Thus, it may be postulated that after complete reduction of silver, the nitrate reduction resumes, and the NR activity increases with increase in the metal concentration.



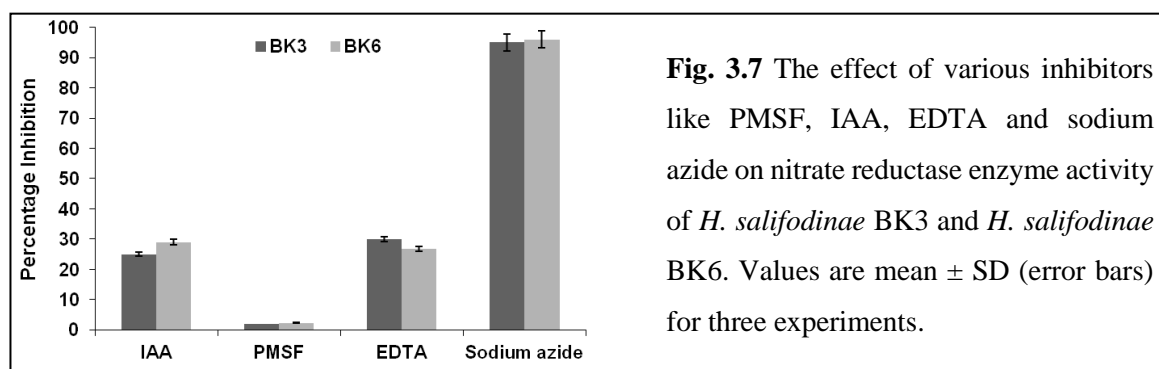
This was confirmed by estimation of NR enzyme activity (Fig. 3.6). *H. salifodinae* BK3 CFE exhibited a two-fold (9.6 nmols nitrite/min/ml) and a three-fold (13.6 nmols nitrite/min/ml) increase in NR enzyme activity at 0.05 mM, and 0.5 mM AgNO₃, respectively, as compared to the control (0 mM AgNO₃; 5.4 nmols nitrite/min/ml). Likewise, *H. salifodinae* BK6 exhibited an NR enzyme activity of 5.3 nmols nitrite/min/ml which in presence of 0.05 mM, and 0.5 mM AgNO₃ exhibited a two-

fold (9.9 nmols nitrite/min/ml) and a threefold (14.7 nmols nitrite/min/ml) increase, respectively, suggesting an upregulation of NR activity in presence of AgNO₃. A similar up-regulation of NADH-dependent NR during silver nitrate treatment was reported by Babu et al. (2011), in a global transcriptomic study of *Bacillus cereus* ATCC 14579 in response to AgNO₃ stress. In order to verify whether the upregulation in the activity of NR was due to the silver

ions or the nitrate component of AgNO_3 , the NR enzyme assay was performed by spiking the growth medium with 0.05 mM, and 0.5 mM KNO_3 . The NR enzyme activity of *H. salifodinae* BK3 was 1.7 times lower (5.7 nmols nitrite/min/ml, and 7.9 nmols nitrite/min/ml for 0.05 mM, and 0.5 mM KNO_3 , respectively) as compared to the activity of the cells grown in presence of 0.05 mM, and 0.5 mM AgNO_3 . The enzyme activity of the cells grown in presence of 0.05 mM KNO_3 was found to be similar to that of control (cells grown in the absence of AgNO_3), which may be explained by the negligible increase in the overall nitrate concentration of the medium. The higher NR enzyme activity exhibited by the cells grown in presence of 0.05 mM and 0.5 mM AgNO_3 , suggest that the upregulation is due to the silver component of AgNO_3 and not the nitrate. Likewise, the enzyme activity of *H. salifodinae* BK6 in presence of 0.05 mM, and 0.5 mM KNO_3 was found to be 1.06 times (5.7 nitrite/min/ml) and 1.5 times (7.9 nmols nitrite/min/ml) lower, respectively, as compared to the activity of the cells grown in presence of AgNO_3 (0.05 mM and 0.5 mM). Only a negligible increase in the nitrite content of the cells was observed for cells grown in presence of KNO_3 (Fig 3.6a, b). Thus, the enzymatic detoxification by NADH-dependent NR may be responsible for silver resistance and SNPs synthesis in both *H. salifodinae* BK3 and *H. salifodinae* BK6.

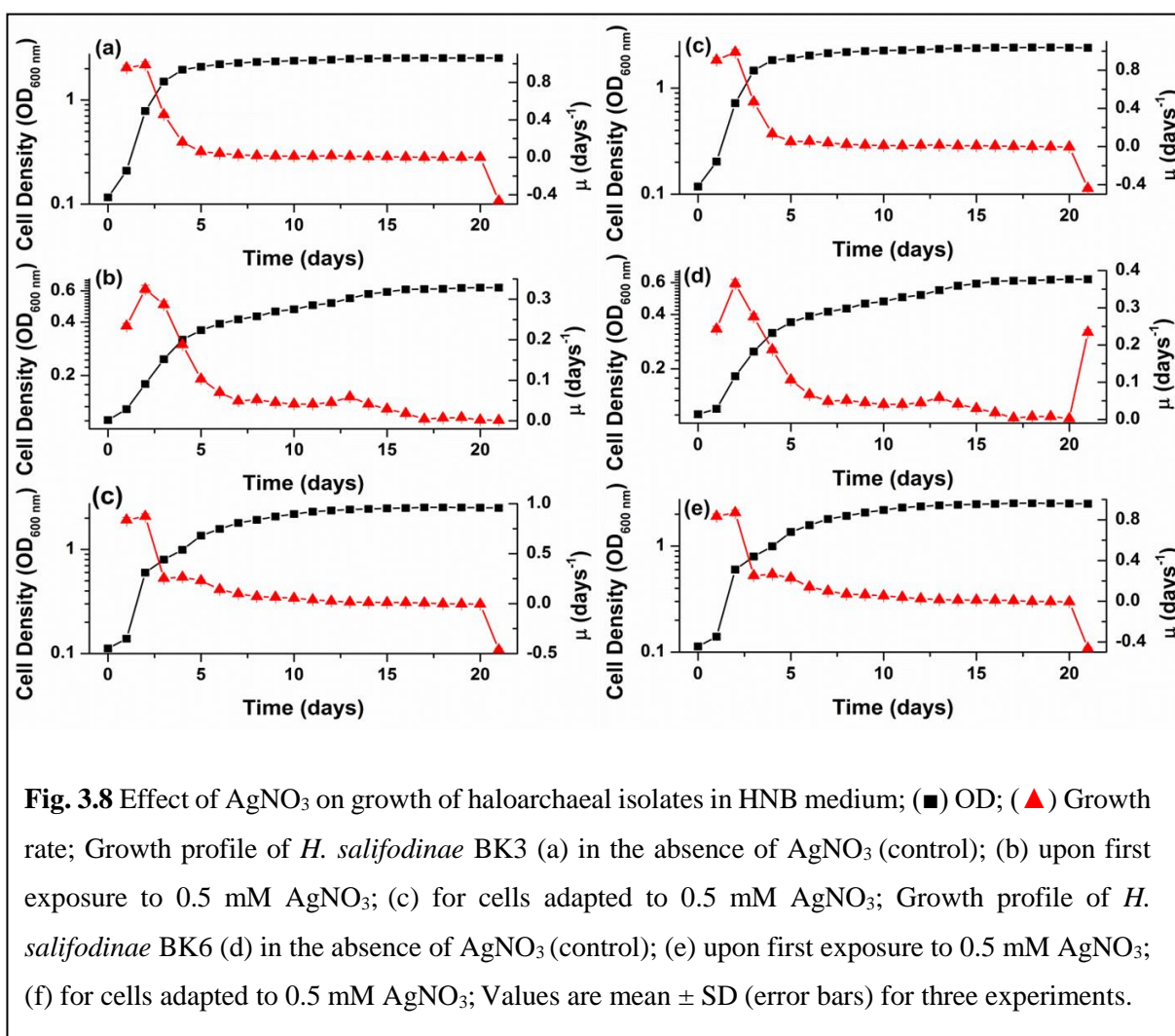
The role of NR in metal resistance and nanoparticle synthesis was further confirmed by enzyme inhibitor studies using sodium azide, PMSF, EDTA and IAA. These compounds are well known enzyme inhibitors specific for certain enzymes. PMSF is a serine protease inhibitor (Michaud et al. 1993), IAA a cysteine peptidase inhibitor (Knap and Pratt, 1991), EDTA a metallopeptidase inhibitor (Auld, 1995) while, sodium azide is a known nitrate reductase inhibitor (Amy and Garrett, 1974). In the absence of any metal stress both the isolates *H. salifodinae* BK3 and *H. salifodinae* BK6 were able to grow in presence of 10 mM concentration of all the inhibitors, growth being slightly delayed only in case of IAA. In presence of AgNO_3 and the inhibitors growth of both the isolates remained unaffected, with the exception of sodium azide. Sodium azide inhibited growth of BK3 and BK6 in presence of AgNO_3 . Similarly, the SNPs synthesis was significantly affected ($p < 0.05$) during growth in presence of sodium azide. Although EDTA and IAA exhibited an inhibition of SNPs synthesis, it was found to be insignificant ($p > 0.05$) as compared to sodium azide. In presence of metal stress, enzyme inhibitors affected both growth and SNPs synthesis in the following order, Sodium azide \gg EDTA \geq IAA \gg PMSF. Similar observations were made by Vaidyanathan

et al. (2010) during studies on silver nanoparticle synthesis by *Bacillus licheniformis*. They postulated the involvement of enzyme NR in SNPs synthesis based upon the inhibition of nanoparticle synthesis exhibited by the known inhibitor of NR, sodium azide. The NR activity of the CFE of *H. salifodinae* BK3 cells in presence of 10 mM inhibitor and 0.5 mM AgNO₃ was found to be 0.3 nmols nitrite/min/ml (for sodium azide), 10.2 nmols nitrite/min/ml (for IAA), 13.3 nmols nitrite/min/ml (for PMSF) and 9.5 nmols nitrite/min/ml (for EDTA), as compared to the control (cells grown in the presence of 0.5 mM AgNO₃ and with no inhibitor) which exhibited a NR activity of 13.6 nmols nitrite/min/ml. Similarly, *H. salifodinae* BK6 grown in presence of sodium azide exhibited lowest enzyme activity (0.6 nmols nitrite/min/ml) as compared to the cells grown in the presence of 0.5 mM AgNO₃ with no inhibitor (14.7 nmols nitrite/min/ml). Fig. 3.7 shows the enzyme activity in the presence of inhibitor as a percentage of that in controls where inhibitor was not added but silver nitrate was present. The NR activity of CFE of cells grown in the absence of AgNO₃ and any inhibitor was found to be 5.4 and 5.3 nmols nitrite/min/ml for *H. salifodinae* BK3, and *H. salifodinae* BK6, respectively. Although the involvement of other factors (or enzymes etc.) cannot be ruled out, our results suggest the involvement of the enzyme NR in nanoparticle synthesis and silver nitrate tolerance. Therefore, the NR mediated tolerance and detoxification of silver in haloarchaeal isolates *H. salifodinae* BK3, and *H. salifodinae* BK6 may represent a metal resistance mechanism that has not been exhibited earlier in haloarchaea.



SNPs synthesis by *H. salifodinae* BK3 and *H. salifodinae* BK6 was also obtained using nitrate broth amended with 25% NaCl, 0.5% KCl, and 2% MgSO₄ (HNB) as the growth medium. Growth kinetics studies using this medium (Fig. 3.8) showed that although there was a decrease in the growth rate of both the isolates in presence of silver nitrate, the affect was lower

as compared to growth in NTYE (Table 3.1). The doubling time of silver adapted *H. salifodinae* BK3 in presence of 0.5 mM AgNO₃ in HNB was found to be 1.3 times (19.2 hrs) lower than the doubling time in NTYE (25.1 hrs). The specific growth rate (0.87 days⁻¹) taken together with the lag phase (11.52 hrs) and doubling time of silver adapted *H. salifodinae* BK3 thus indicate the HNB to be a medium for faster growth of the organism in presence of silver nitrate and production of SNPs. Similarly, the specific growth rate was found to be higher, and lag time and doubling time lower, for *H. salifodinae* BK6 in HNB as compared to NTYE. The SNPs synthesis in HNB was intracellular with brown colouration of the cells. Media controls without culture did not precipitate silver indicating that SNPs synthesis was a culture dependent phenomenon.



3.3.3 SNPs biosynthesis and its optimisation

Growth of both *H. salifodinae* BK3, and BK6 in presence AgNO_3 was accompanied with the change in culture colouration to brown black. In order to determine the optimal conditions for synthesis, the haloarchaeal isolates were grown at various medium pH, incubation temperature, and AgNO_3 concentration in both NTYE, and HNB media. Following synthesis at these conditions, the nanoparticles were extracted and their yield determined. The SNPs synthesised by *H. salifodinae* BK3 are designated as SNPs-BK3, while that synthesised by *H. salifodinae* BK6 are designated as SNPs-BK6.

AgNO₃ concentration

A concentration range of 0.05 mM to 0.7 mM AgNO_3 was used to determine the optimum concentration for SNPs synthesis. The yield at all the concentrations was not affected by the medium used however, the synthesis occurred faster in HNB. Both the cultures exhibited a similar trend of SNPs synthesis at all the concentrations. Maximum SNPs synthesis was obtained in presence of 0.5 mM AgNO_3 with a yield of ~ 3.26 mg/g CDW (Fig. 3.9a, b). The yield of SNPs at 0.6 mM AgNO_3 was very similar to that of 0.5 mM AgNO_3 , with no significant difference ($p < 0.05$), however the growth was slightly delayed. The yield of SNPs at lower concentrations of AgNO_3 (0.05, 0.1, 0.15, 0.2, 0.3, and 0.4 mM) was found to be proportional to the substrate concentration. At 0.7 mM AgNO_3 , the yield was ~0.75 mg/g CDW, which was significantly lower ($p < 0.05$) when compared to the yield at 0.5 mM AgNO_3 . This may be attributed to the increase in toxicity at higher concentration of AgNO_3 . Although the organisms were able to grow and synthesise SNPs at 0.7 mM AgNO_3 , both growth and SNPs synthesis were negatively affected. Thus, a concentration of 0.5 mM AgNO_3 was used for SNPs synthesis by *H. salifodinae* BK3/BK6 in NTYE/HNB.

Medium pH

The SNPs synthesis by *H. salifodinae* BK3, and BK6 was evaluated in NTYE and HNB between pH 4.5- pH 8.0. A similar trend of SNPs synthesis was exhibited by both the haloarchaea (Fig. 3.9c, d). The medium used for the optimisation did not affect the yield of the SNPs however the synthesis was faster in HNB. Maximum yield of ~ 3.26 mg/g CDW was obtained at pH 7.0. At a pH of 4.5, the haloarchaeal cultures failed to grow even in the absence

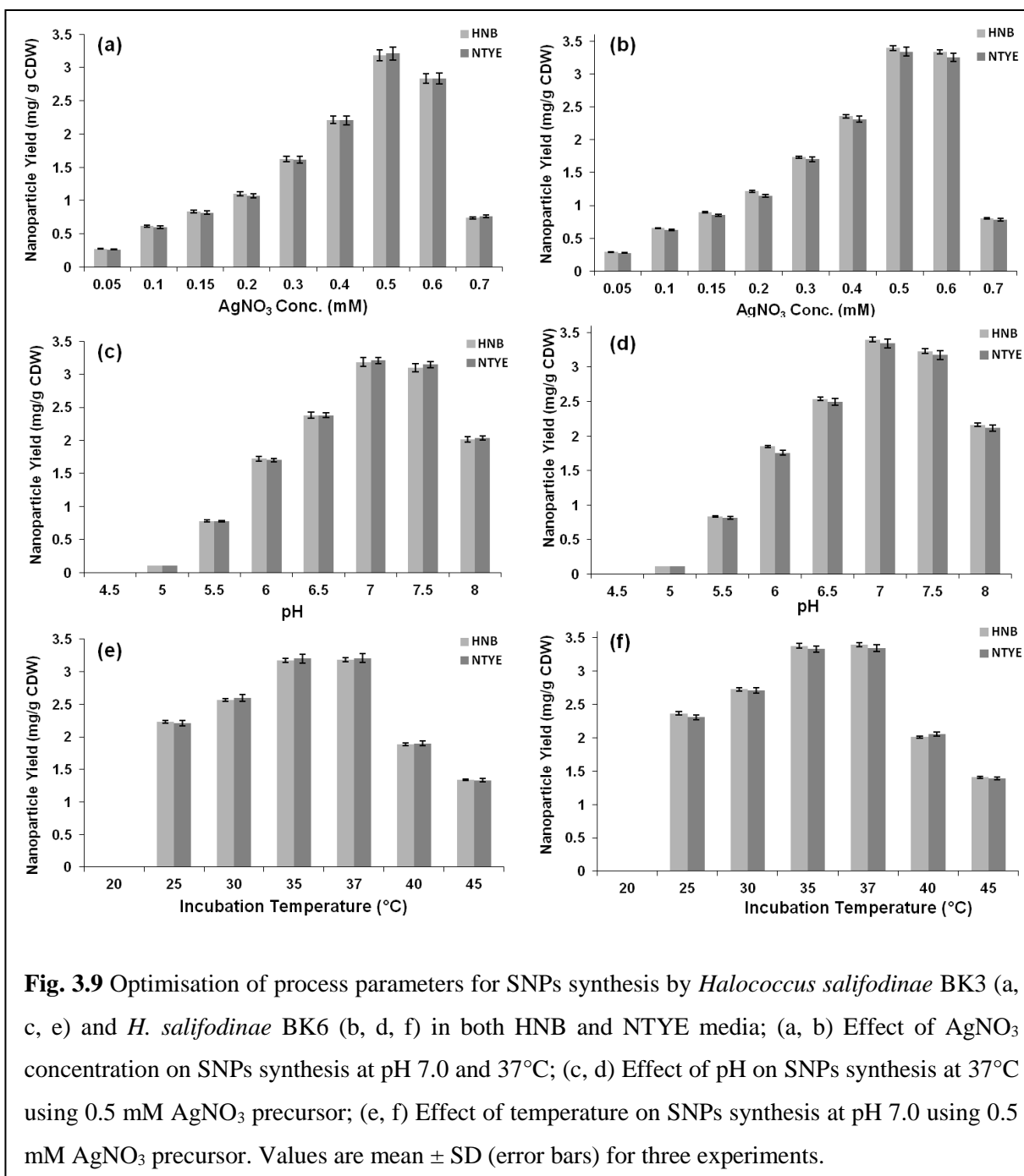
of AgNO₃. At pH of 5.0 and 5.5, the growth of haloarchaeal cultures in the absence of AgNO₃ was very poor, therefore when grown in presence of 0.5 mM AgNO₃ the yield of SNPs was significantly lower ($p < 0.05$) as compared to that at pH 7.0. The pH range for growth of *Halococcus* is 6.0-9.5, with the optimum at pH 7.0 (Grant, 2015). Thus, as the pH increased from 6.0 to 6.5, the yield also increased. Yield of SNPs at pH 7.5 was ~ 3.15 mg/g CDW, which was not significantly different ($p > 0.05$) than the yield obtained at pH 7.0. However, pH 8.0 significantly lowered the yield of SNPs, which may be attributed to the pH changing to alkaline. Based on these results, SNPs synthesis was carried out at pH 7.0.

Incubation temperature

A temperature range of 20°C to 45°C was tested to determine the optimum temperature for SNPs synthesis. The yield at all the temperatures evaluated was not affected by the medium used however, the synthesis occurred faster in HNB. Likewise, *H. salifodinae* BK3 and BK6 exhibited a similar trend of SNPs synthesis at all the temperatures. The optimum range of incubation temperature for growth of *Halococcus* is 30°C to 40°C (Grant, 2015). Maximum SNPs synthesis was obtained at 35°C, and 37°C with a yield of ~ 3.26 mg/g CDW (Fig. 3.9e, f). The haloarchaeal isolates did not exhibit growth at 20°C even in the absence of AgNO₃. As the temperature increased from 25°C to 37°C, the yield of SNPs also increased albeit the difference in yield between 30°C, 35°C, and 37°C was insignificant ($p > 0.05$). The haloarchaeal cultures show a slow growth at 45°C, and therefore, the yield of SNPs was also lower. Thus, SNPs synthesis by both the cultures in NTYE/HNB carried out at 37°C temperature.

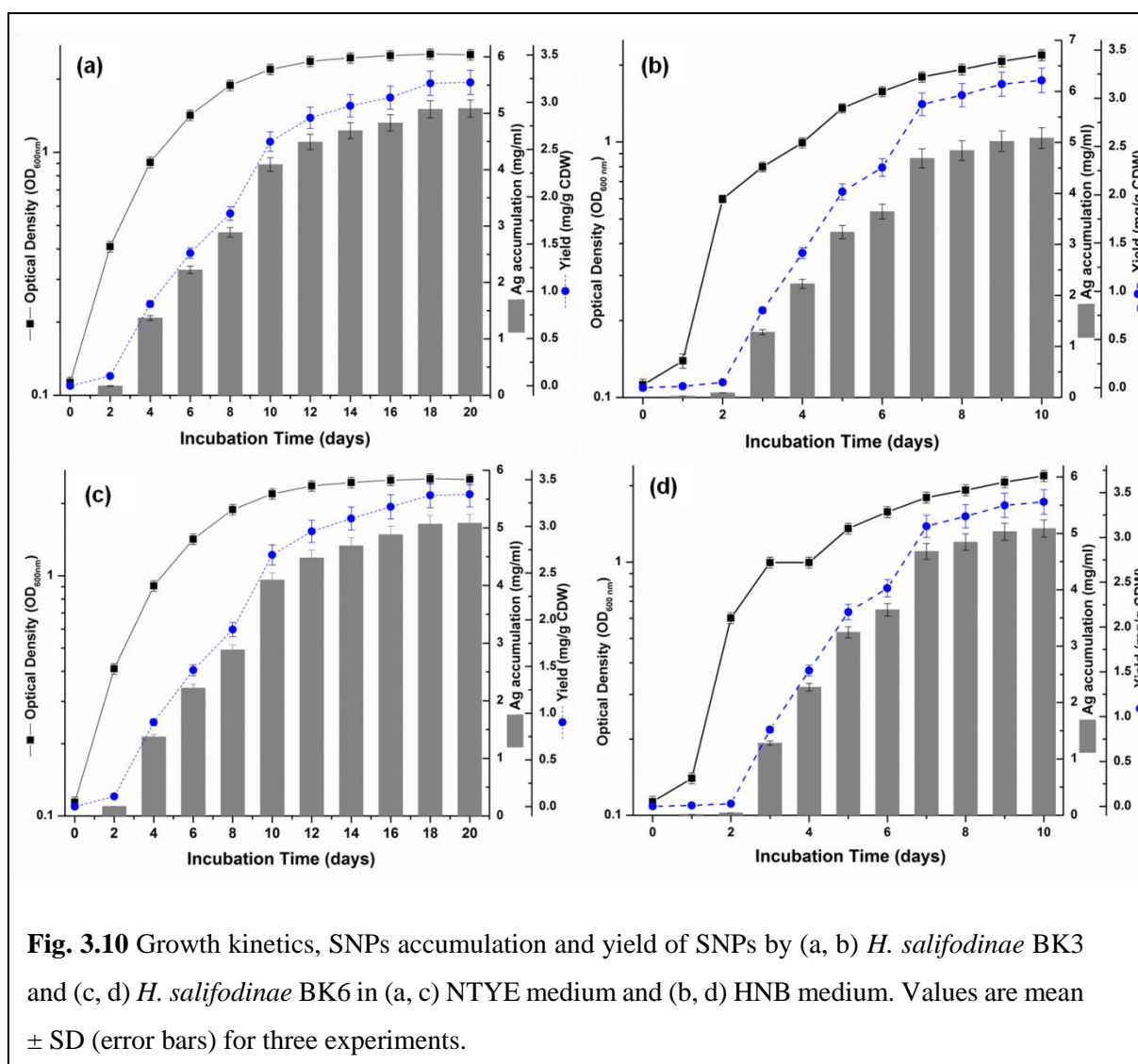
Table 3.3 Optimal parameters for maximal production of SNPs by *H. salifodinae* BK3 & BK6.

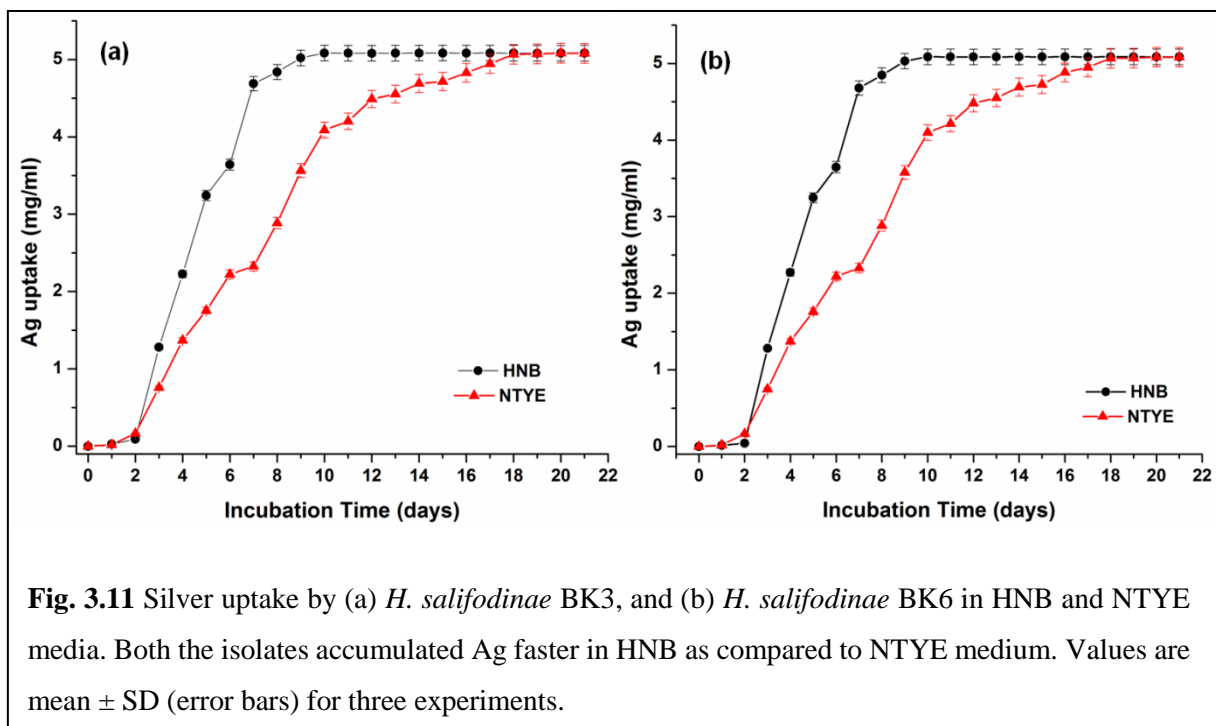
Parameters	HNB	NTYE
Time of AgNO ₃ addition	T= 0 hrs	T= 0 hrs
Medium pH	7.0- 7.5	7.0- 7.5
AgNO ₃ concentration	0.5 mM	0.5 mM
Incubation temp	35- 37°C	35- 37°C



Based on the above results, further studies on SNPs synthesis by *H. salifodinae* BK3 and BK6 were carried out at 37 °C, pH 7.0 using 0.5 mM AgNO₃ as the precursor in HNB, and NTYE media. The time course of silver accumulation, growth, and yield of SNPs is illustrated in Fig. 3.10. In NTYE medium, Ag accumulation for both *H. salifodinae* BK3, and BK6 started from mid-exponential phase (day 4) and continued up to late stationary phase (day 20).

Approximately 94.2 % Ag was taken up by both the isolates with a residual 0.313 mg/ml Ag in the medium (Fig. 3.11a). Beyond this incubation time no further Ag uptake was observed. However, HNB medium was found to be more efficient in Ag uptake. The Ag accumulation in this medium by both the isolates commenced from mid exponential phase (day 3) and was completed by the early stationary phase (day 10). In HNB medium, both the cultures accumulated ~95% of the Ag provided (Fig. 3.11b) by the day 10, whereas, in NTYE only 76% was taken up by this time.





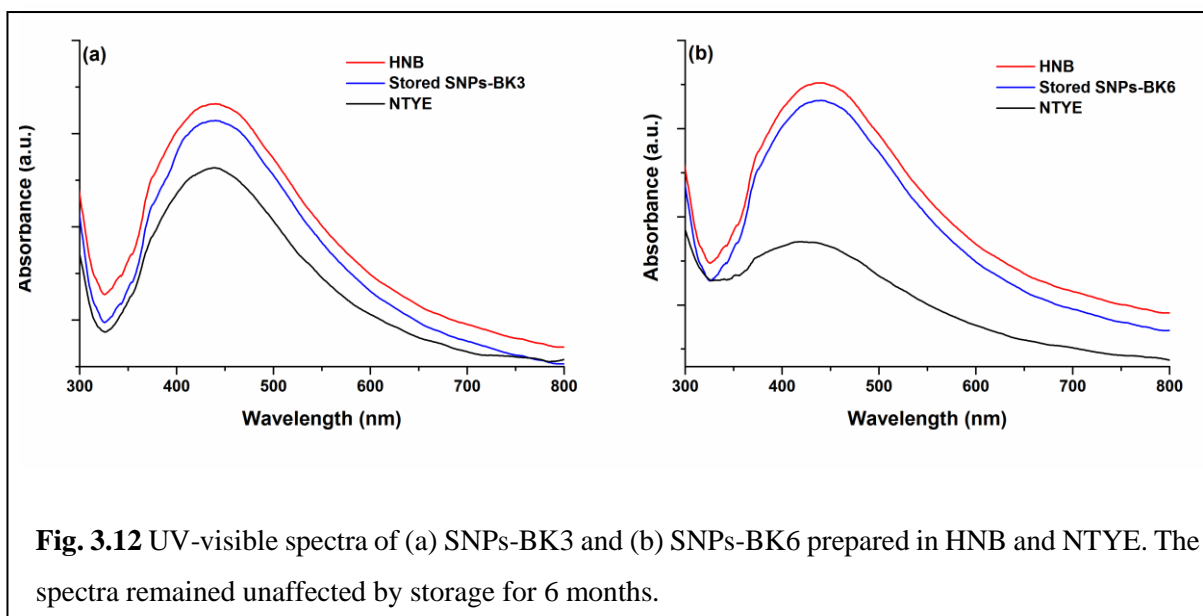
The silver adapted *H. salifodinae* BK3, and BK6 were used for SNPs synthesis, as they exhibited a higher specific growth rate as compared to the culture exposed to AgNO_3 for the first time. The yield with respect to substrate concentration and biomass were estimated over the course of SNPs synthesis. Maximum yield (3.185 mg/g CDW; 0.943 mg/mg Ag) for SNPs-BK3 in HNB medium was obtained on day 10 exhibiting an efficiency of 94.27%. However, in NTYE medium BK3 exhibited the maximum yield (3.21 mg/g CDW; 0.942 mg/g Ag) of SNPs-BK3 on day 20 with an efficiency of 94.23%. Similarly, for BK6, in NTYE the maximum yield of SNPs-BK6 obtained was 3.396 mg/mg CDW or 0.943 mg/mg Ag on day 20 and the maximum yield in HNB was 3.342 mg/mg CDW or 0.943 mg/g Ag on day 10. Table 3.4 summarises the various yield parameters of SNPs synthesis by *H. salifodinae* BK3, and BK6.

Table 3.4 SNPs yield parameters

Yield Parameters	<i>H. salifodinae</i> BK3		<i>H. salifodinae</i> BK6	
	NTYE	HNB	NTYE	HNB
Y (mg/g CDW)	3.210	3.185	3.342	3.396
MY (mg/mg Ag)	0.942	0.943	0.943	0.943
Efficiency (%)	94.23	94.27	94.24	94.36

3.3.4 Nanoparticle characterisation

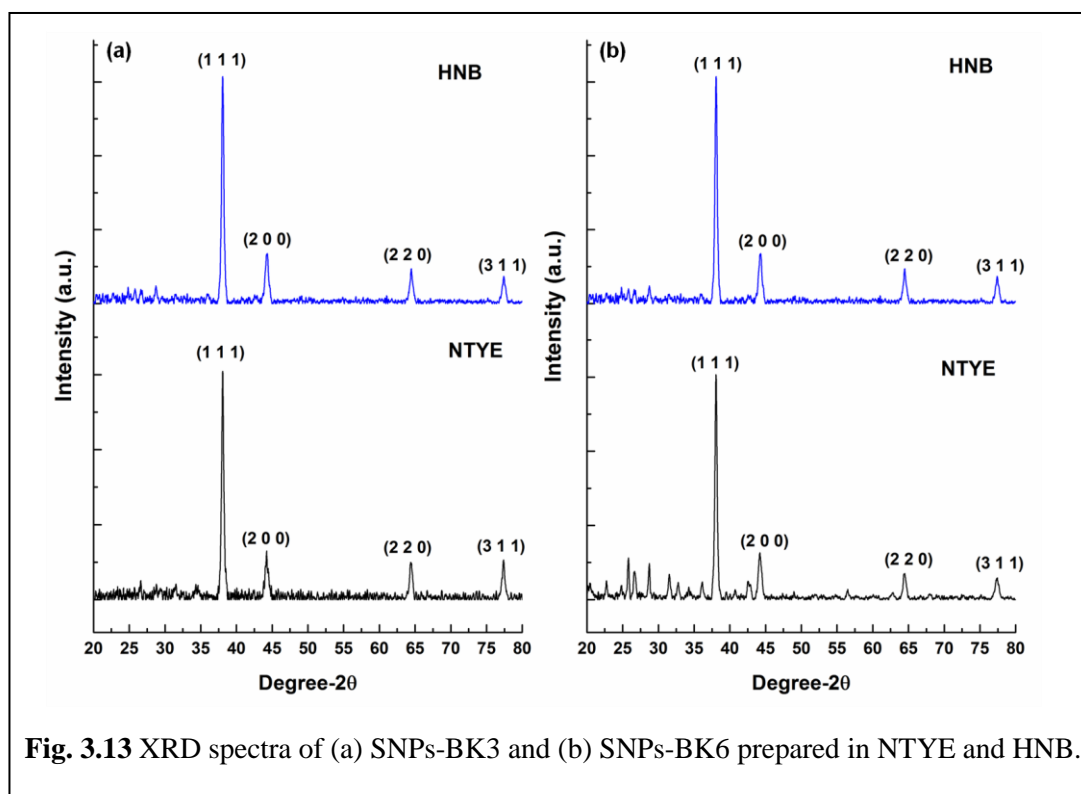
Silver nanoparticles exhibit LSPR at visible and near-infrared frequencies leading to sharp peaks in their spectral extinction (Hutter and Fendler 2004). The frequency (i.e., absorption maxima or colour), and intensity of the surface plasmon absorption bands are characteristic of the type of material and are highly sensitive to the size, shape, and size distribution of the nanostructures, as well as the environment that surrounds them (Underwood and Mulvaney, 1994). The extinction is the result of collective excitation of conducting electrons due to strong interaction between the metallic nanoparticles and the incident electromagnetic radiation (Mie, 1908). As illustrated in Fig. 3.12 (a,b), the UV-visible spectra of the SNPs-BK3 and SNPs-BK6 synthesised in NTYE, and HNB exhibit a strong, but broad, surface plasmon peak at ~ 440 nm. The absorption band was found to be slightly asymmetrical which indicates the presence of an additional weaker component at about 380 nm. This may be due to some anisotropy in the shape of the ‘as-synthesised’ SNPs. Shankar et al. (2004) also made similar observations for SNPs formed on reduction with geranium root broth. A long tailing on the large-wavelength side may be due to small amount of particle aggregation. The SNPs preparations in solution were found to be stable even after 6 months of synthesis as is evident from the absorption profile (Fig. 3.12a,b).



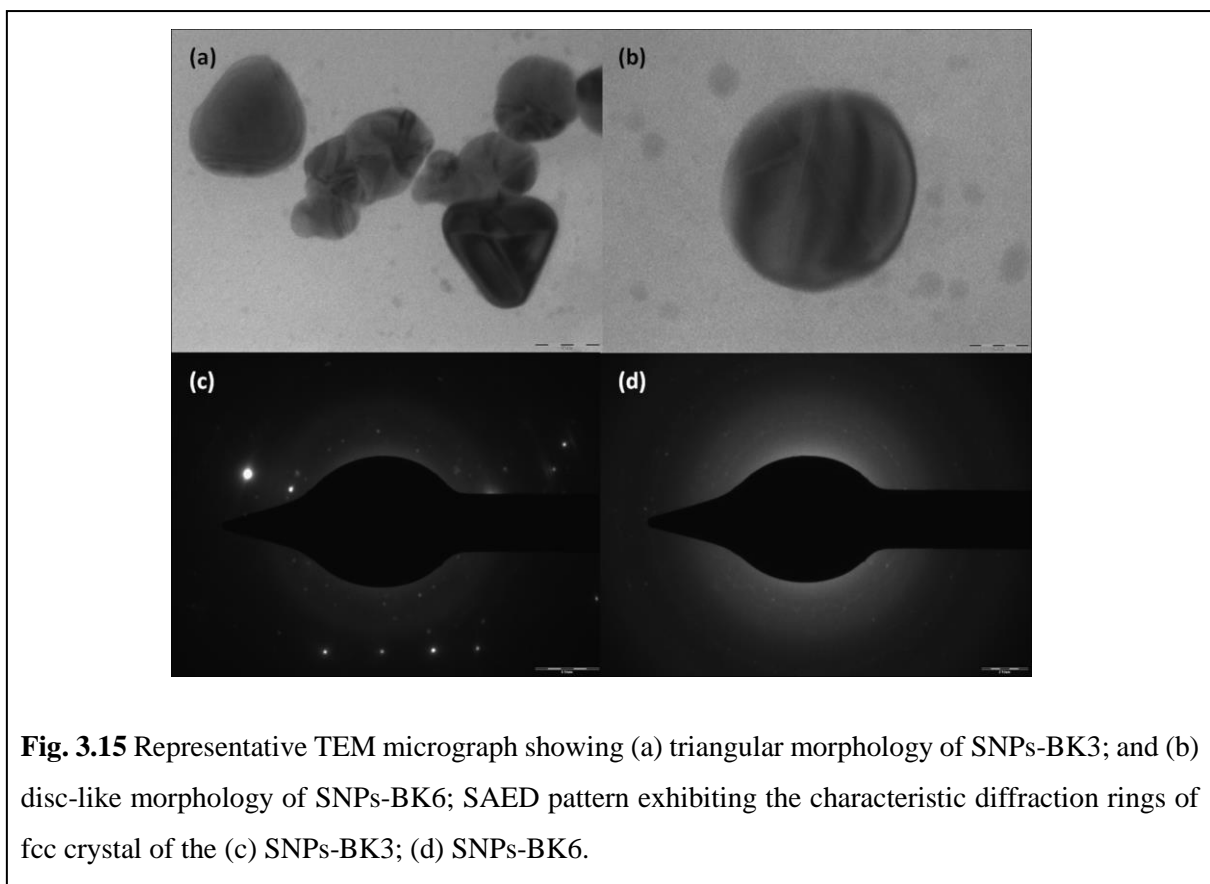
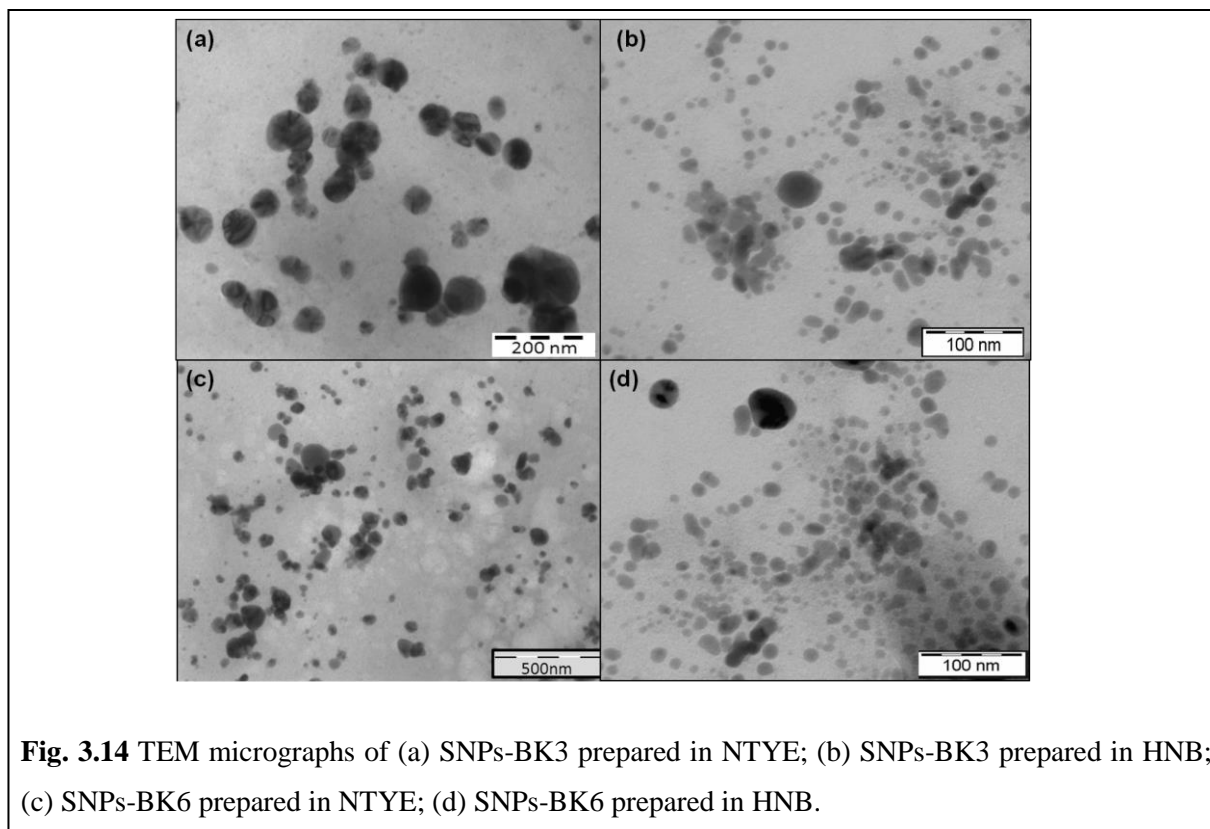
Powder XRD was carried out for the ‘as-synthesised’ SNPs to determine the crystalline nature of the particles. The XRD profiles of SNPs-BK3 and SNPs-BK6 synthesised in NTYE and HNB (Fig. 3.13) exhibited the characteristic Bragg’s peaks of fcc silver that could be indexed to ICDD (international centre for diffraction data) card no.04-0783 (fcc Silver 3C, syn). The 2θ values corresponding to the (1 1 1), (2 0 0), (2 2 0) and (3 1 1) planes for SNPs-BK3 and SNPs-BK6 are presented in table 3.5. The crystallite domain size was calculated using line width of the (1 1 1) plane and was found to be 22 nm, and 12 nm for SNPs-BK3 synthesised in NTYE, and HNB, respectively. Similarly, the crystallite domain size of 26 nm, and 12 nm, was obtained for SNPs-BK6 synthesised in NTYE, and HNB, respectively. The lattice parameter for SNPs-BK3 and SNPs-BK6 in both NTYE and HNB was 0.216 nm.

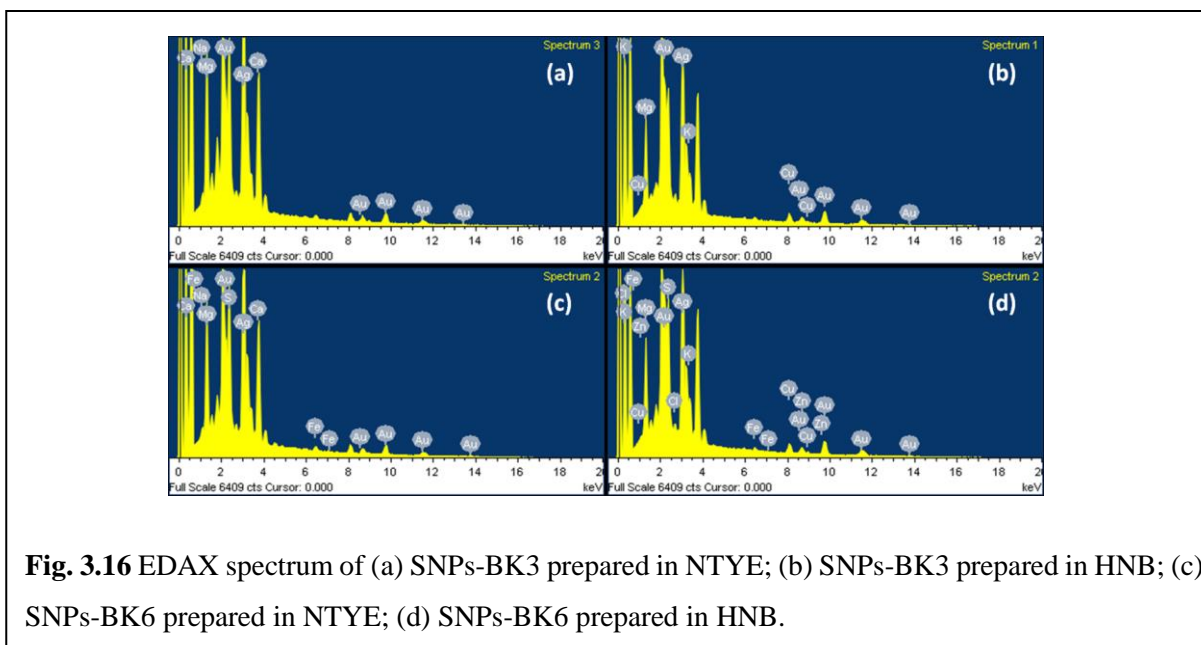
Table 3.5 The 2θ values corresponding to the characteristic Bragg’s diffraction planes of SNPs

Diffraction plane	SNPs-BK3		SNPs-BK6	
	NTYE	HNB	NTYE	HNB
(1 1 1)	38.08°	38.08°	38.06°	38.08°
(2 0 0)	44.18°	44.20°	44.20°	44.20°
(2 2 0)	64.78°	64.38°	64.40°	64.38°
(3 1 1)	77.44°	77.34°	77.42°	77.36°



TEM analysis of the SNPs synthesised by *H. salifodinae* BK3, and *H. salifodinae* BK6 in NTYE, and HNB was carried out to further understand the morphology and the size distribution. The TEM images are shown in Fig. 3.14. The SNPs were predominantly spherical in shape with a few being triangular, prismatic, or disc-like (Fig. 3.15a,b). Contrast was observed within the physical boundaries of majority of the SNPs in both cases due to twinned or multiply twinned nanocrystals. Multiply twinned particles (MTPs) formation is widespread in transition metals having fcc crystal lattice, upon size reduction in nanometer scale (Marks 1994), and is a result of joining along twin boundaries of tetrahedral subunits sharing axis of five-fold symmetry (Hofmeister 1999; Nepijko et al. 2000). Presence of flat disc like particles may be responsible for the out-of plane SPR excitation which can be assigned to 380 nm of UV-visible spectra. Similar observations have been made by Shankar et al. (2004). Average particle size for SNPs-BK3 synthesised in NTYE was ~50.3 nm, and the range was 20 nm to 100nm. The particle size of SNPs-BK3 synthesised in HNB was much smaller, and was in the size range of 2 nm to 20 nm, with an average particle size of 12nm. Very few particles of ~40 nm were observed. The micrographs also exhibit that ‘as-synthesised’ SNPs are well dispersed with no copious agglomeration. SNPs-BK6 synthesised in HNB also exhibited a smaller size distribution between 2- 20 nm with an average particle size of 12 nm, which corresponds well with the XRD data. However, SNPs-BK6 synthesised in NTYE exhibited an average particle size of 50.3 nm. The SAED analysis further confirmed their crystalline nature and exhibited the diffraction rings typical of fcc crystals (Fig. 3.15c,d). The EDAX spectrum of SNPs synthesised in NTYE and HNB exhibited a peak corresponding to silver at around 3.4 keV (Fig. 3.16). The maximum peak located on the left of the spectrum at 0.2 keV corresponds to carbon. Besides the major component Ag, peaks of Copper (Cu) and Gold (Au) were also obtained which are contributions of the sample holder and gold coating, respectively.





3.3.5 Antimicrobial activity

The extensive use of antibiotics as antimicrobial agents has resulted in organisms acquiring resistance against them, causing the clinical strains to become more potent infectious agents (Farrar 1985; Monroe and Polk 2000). Therefore, there is need for producing antimicrobial agents that overcome this obstacle and efficiently kill bacteria. SNPs have been shown to be more efficient than silver salts in mediating antimicrobial activity with lower propensity to induce microbial resistance (Kim et al. 2007; Rai et al. 2009). The exact mechanism of action of SNPs though is still not fully understood. Some studies suggest the nano-particulate form of SNPs to be responsible for the antibacterial action (Hwang et al. 2008; Sondi et al. 2004; Danilcauk et al. 2006; Kim et al. 2007), whilst others attribute the antimicrobial activity of the SNPs to the release of Ag^+ ions that result in damage to DNA, and proteins (Feng et al. 2008; Matsumura et al. 2003; Morones et al. 2005).

In this study, the antimicrobial effect of the SNPs synthesised in HNB by *H. salifodinae* BK3, and *H. salifodinae* BK6 was determined by disk diffusion method. The SNPs diffuse into the agar medium and are responsible for growth inhibition of the test organisms. A dose dependent increase in sensitivity towards SNPs synthesised by either of the haloarchaeal isolates was observed for all the four test organisms (Fig. 3.17). The ZoI were correlated to the antibiotic activity (streptomycin and gentamicin). The MIC of the SNPs was determined by the two-fold

serial dilution method in MH-broth (Table 3.6). The MIC of the SNPs-BK3 against *E. coli* ATCC 10536, and *P. aeruginosa* MTCC 2581 was 3 $\mu\text{g/ml}$, and 4.5 $\mu\text{g/ml}$, respectively. Similarly, the MIC for SNPs-BK6 against *E. coli* ATCC 10536, and *P. aeruginosa* MTCC 2581 was 3.25 $\mu\text{g/ml}$, and 4.25 $\mu\text{g/ml}$, respectively. However, the MIC against gram-positive, *S. aureus* ATCC 6538P, and *M. luteus* NCIM 2170 were higher and exhibited a value of 7.5 $\mu\text{g/ml}$, and 9 $\mu\text{g/ml}$, respectively for SNPs-BK3 and SNPs-BK6. Thus the ‘as-synthesised’ SNPs were found to have antibacterial activity against both gram-positive and gram-negative bacteria and therefore, are promising candidates for antimicrobial agents. Similar antimicrobial activity of biologically synthesised SNPs against gram-positive and gram-negative bacteria has been reported by Furno et al. (2004), Morones et al. (2005) and Kim et al. (2011).

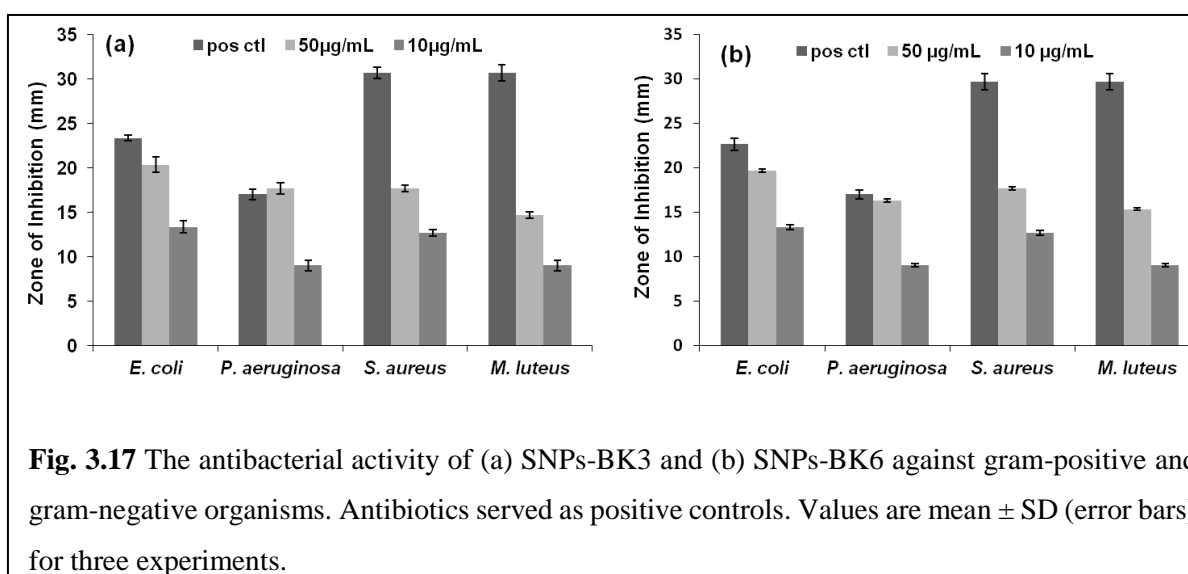


Table 3.6 MIC of SNPs against both gram-positive and gram-negative organisms.

Organism	MIC ($\mu\text{g/ml}$)	
	SNPs-BK3	SNPs-BK6
<i>E. coli</i> ATCC 10536	3	3.25
<i>P. aeruginosa</i> MTCC 2581	4.5	4.25
<i>S. aureus</i> ATCC 6538P	7.5	7.5
<i>M. luteus</i> NCIM 2170	9	9

3.4 Conclusion

We have successfully synthesised silver nanoparticles using haloarchaeal isolates *Halococcus salifodinae* BK3, and *H. salifodinae* BK6. The SNPs-BK3 were around 50 nm, and 12 nm when prepared in NTYE, and HNB, respectively. The average particle size of 53 nm, and 12 nm were obtained for SNPs-BK6 synthesised in NTYE, and HNB, respectively. In both cases, the NPs had fcc crystalline structure with spherical morphology. The nanoparticle preparations were found to be stable with almost negligible aggregation even after 6 months of synthesis. The concentration dependent increase in NR activity in presence of silver nitrate and the negligible NR enzyme activity, along with inability of the haloarchaeal isolate to grow in presence of NR inhibitor, sodium azide, confirms the involvement of the enzyme in metal resistance, and silver nanoparticle synthesis. The obtained *in-vivo* reduction of silver ions and subsequent formation of silver nanoparticles speak in favour of environment friendly synthetic protocol for the synthesis and stabilisation of metal nanoparticles. Thus, these strains can be used for nanoparticle synthesis as well as bioremediation of heavy metal polluted environments, as the nanoparticle synthesis is intracellular.

CHAPTER 4

In-vivo* Synthesis of Selenium Nanoparticles by *Halococcus salifodinae* BK18 and their Anti-Proliferative Properties against HeLa Cell Line¹*4.1 Introduction**

Selenium (Se) is a chalcogen metalloid that belongs to group 16 (VIA) of the periodic table. It is chemically similar to sulphur, and tellurium and exists in four oxidation states, -2 (Se^{-2}), 0 (Se^0), +4 (SeO_3^{2-}), and +6 (SeO_4^{2-}). Organic forms of selenium and other salts have been studied for their biological effects, and semi-conductor properties. Elemental selenium is present in various allotropic forms, viz., red amorphous, black vitreous, three (α , β , γ) of red crystalline forms, and grey/black crystalline hexagonal form (Cherin and Unger, 1967; Takahashi, 1982). The grey/black hexagonal crystal of selenium is the most stable form (Cherin and Unger, 1967; Takahashi, 1982). Se is present as a trace element in representative species from all three domains of life: Bacteria, Archaea, and Eukarya (Shisler et al. 1998; Hamilton, 2004). It supports expression of various seleno-proteins like glutathione peroxidase and thioredoxin reductases, through tRNA mediated incorporation of seleno-cysteine (Allan et al. 1999). At human nutritional doses, Se is essential for an optimum immune response, and affects both the innate and acquired immune systems (Arthur et al. 2003). It also promotes cell cycle progression, and prevents cell death by quenching any reactive oxygen species (ROS) and redox regulation at nutritional doses. However, at supra-nutritional doses Se induces cell cycle arrest and apoptosis (Zeng, 2009). Se and its compounds are known for anticarcinogenic/antitumorigenic and antimetastatic properties via differential expression of redox-active proteins, regulating inflammatory and immune responses, inducing cell cycle arrest and apoptosis, and prevent angiogenesis (Whanger, 2004; Rayman, 2005; Chen et al. 2013). Se also exhibits chemopreventive properties at higher doses, essentially by blocking angiogenesis (Lu and Jian, 2001; Rayman, 2005).

¹ This work is published as: **Srivastava P**, Braganca JM, Kowshik M (2014) In vivo synthesis of selenium nanoparticles by *Halococcus salifodinae* BK18 and their anti-proliferative properties against HeLa cell line. *Biotechnology Progress* 30:1480-1487

Elemental selenium (Se^0) nanoparticles (SeNPs) have gained attention due to their unique biological activities and low toxicity (Chen et al. 2008). Besides, selenium of smaller dimensions is of interest specifically in semiconductor industry, due to their unique electrical and optical properties stemming from quantum confinement (Tam et al. 2010). SeNPs have been widely used in electrical rectifiers, photocells, photographic exposure meters, xerography etc., due to their high photoconductivity, excellent spectral sensitivity, and large piezoelectric, thermo-electric, and non-linear optical response (Greenwood and Eamshaw, 1997). It is also used in the glass industry to eliminate bubbles, and remove undesirable tints produced by iron (Johnson et al. 1999). SeNPs have been synthesised chemically by processes like solvothermal, sonochemical, laser ablation, and microwave enhanced reactions (Lu et al. 2002; Gedanken, 2004; Jiang et al. 2003; Gao et al. 2008). However, these routes of synthesis are usually tedious; require environmentally challenging techniques, elevated temperatures, and long-growth times; result in low yields; and invariably use toxic chemicals and radiations (Li et al. 2007; Ingle et al. 2009).

Even though various bacteria and archaea were reported for their capability to grow anaerobically, by linking the oxidation of organic substrates or H_2 to the dissimilatory reduction of selenium oxyanions (Oremland and Stolz, 2000; Stolz and Oremland, 1999), these organisms were not recognised as nano-factories. Oremland et al. (2004) were the first to examine the selenium nanospheres formed as a result of the bio-reduction by the selenium respiring bacteria. They extracted the nanospheres, purified them, and characterised the SeNPs by UV-visible spectroscopy and XRD. Subsequently several studies have exhibited SeNPs synthesis by various bacteria (Shakibaie et al. 2010; Lampis et al. 2014), and fungi (Sarkar et al. 2011; Zare et al. 2013), both intracellularly and extracellularly. However, there have been no studies on SeNPs synthesis by haloarchaea. Although a novel strictly anaerobic, hyperthermophilic, facultative organotrophic archaeon, *Pyrobaculum arsenaticum* was reported to utilise Se oxyanion as the terminal electron acceptor during respiration, characterisation of the final red coloured selenium based product was not carried out (Huber et al. 2000).

The knowledge on mechanisms employed by various selenite/selenate resistant microorganisms for respiration of Se oxyanion is cursory. Nevertheless, for a better

understanding attempts are being made to explore the chemical reactions occurring in these media. The respiratory arsenate reductase was found to be involved in selenite reduction in *Bacillus selenitireducens* strain MLS10 (Stolz, 2003). Similarly, periplasmic nitrite reductases were found to be essential for generation of SeNPs in *Rhizobium* sp. strain B1, and *Azospira oryzae* (Hunter and Kuykendall, 2007; Hunter, 2007), while hydrogenase I was found to be responsible for selenite reduction in *Clostridium pasteurianum* (Yanke et al. 1995). Nitrate reductase (NR) was found to confer basal resistance to selenium oxyanions in *E. coli*, and reduced selenite to non-toxic elemental selenium (Avazeri et al. 1997).

In this study we report the biological synthesis of SeNPs by the haloarchaeon *Halococcus salifodinae* BK18. Characterisation of the SeNPs and their application as a potential chemotherapeutic agent has been demonstrated.

4.2 Materials and Methods

4.2.1 Organism and culture maintenance

Halococcus salifodinae BK18 was maintained on NTYE plates at RT and sub-cultured every 30-45 days. It was also maintained in NTYE broth at 37°C, 110 rpm and sub-cultured every five days.

4.2.2 Growth in presence of selenite

The isolate was grown in presence of different concentrations of sodium selenite (Na_2SeO_3 ; 0.05 mM-10 mM with an increment of 0.5 mM) to determine the MIC. The effect of selenite on growth of *H. salifodinae* BK18 was determined in presence of 2 mM and 4 mM Na_2SeO_3 . Growth was evaluated by quantifying the total protein content of the biomass grown in presence of different concentrations of Na_2SeO_3 , which was prepared as 0.1 M stock solution in SDW, and sterilised by filtration. NTYE medium was inoculated with 1% culture and supplemented with respective concentrations of Na_2SeO_3 at zero hr. The flasks were incubated at 37°C, 110 rpm. A 1ml aliquot of culture was withdrawn every 24 hrs and the protein content of cells was determined using Bradford's method (Bradford, 1976) with BSA as the standard. Protein content of culture grown in absence of Na_2SeO_3 (positive control) was compared with that of culture grown in presence of Na_2SeO_3 to determine the effect of selenite stress on

growth. Un-inoculated medium with Na_2SeO_3 served as the negative control. The growth kinetics parameters such as specific growth rate (μ ; days^{-1}), lag time (t_l ; hrs) and doubling time (t_d ; hrs) were determined as described in section 2.2.2. The assay was performed in triplicates.

4.2.3 Estimation of selenite content

The ability and time course of selenite reduction in the medium by *H. salifodinae* BK18 was determined spectrophotometrically by the method described by Watkinson (1966) with some modifications. Briefly, NTYE medium was inoculated with 1% inoculum and different concentrations of Na_2SeO_3 , viz., 2 mM, and 4 mM, were added to the respective flasks. Starting from 0 hr, every 24 hrs, 1 ml aliquot was withdrawn, centrifuged ($10,000 \times g$; 20 mins), and the supernatant was used for selenite content determination. Appropriate controls (negative control: un-inoculated medium with 4 mM Na_2SeO_3 ; positive control: inoculated medium) were similarly processed. For determination of selenite content, to 10 ml of 0.1 M HCl, 0.5 ml of 0.1 M EDTA, 0.5 ml of 0.1 M NaF, and 0.5 ml of 0.1 M disodium oxalate were added and mixed. Sample supernatant (250 μL) was subsequently added to the above mixture, followed by 2.5 ml of 0.1% 2,3-diaminonaphthalene (2,3-DAN). The solution was mixed and the tubes were incubated at 40°C for 40 mins. Following incubation, the mixture was cooled to room temperature, and the selenium-2,3-DAN complex was extracted with 6 ml cyclohexane by shaking the tubes vigorously for 1 min. To further accelerate the phase separation, tubes were centrifuged at $3,000 \times g$ for 10 mins. Absorbance of the organic phase was measured at 377 nm on UV-visible double beam spectrophotometer using a 1-cm-path length cuvette. All the experiments were carried out in triplicates. Calibration curves were obtained using 0 to 5 mM Na_2SeO_3 solution.

4.2.4 Selenium nanoparticles synthesis and optimisation of process parameters

In a typical synthesis of SeNPs, a requisite amount of Na_2SeO_3 was added to 500 ml of NTYE medium inoculated with 2% *H. salifodinae* BK18, and the flask was incubated in an incubator shaker at 37°C , 110 rpm. The reduction and thus synthesis of SeNPs was followed by visual observation of medium turning brick-red, which indicates the reduction of SeO_3^{2-} to Se^0 . The cells were harvested by centrifugation ($10,000 \times g$, 20 mins, RT). The biomass along with the SeNPs was washed twice with SDW and dialysed against deionised water overnight. The cells

were subjected to wet heat sterilisation in a laboratory autoclave at 121°C, 15 psi for 20 mins. The resulting solution was centrifuged at 10,000 × g, RT, for 20 mins. The pellet was re-suspended in SDW and sonicated at 0°C for three cycles of 1 min each at three RPS (40 W). The solution was centrifuged (10,000 × g, RT, 20 mins), and the pellet was washed with conc. H₂SO₄ to purify the SeNPs. The pellet obtained after centrifugation was subjected to drying at 70°C for 12 hrs. To determine the yield (both per gram of cell dry weight and molar) and efficiency, the selenium nanoparticles were converted to selenite by oxidation according to Kessi and Hanselmann (2004), and the selenite was quantified according to Watkinson (1966). The yield per gram of cell dry weight (CDW) was determined as described in section 3.2.4. The molar yield was determined as: $MY = Q/S$ where, MY is the molar yield (mM/mM selenite), Q is the moles of selenite taken up by the cells (mM) and S is the moles of Na₂SeO₃ provided for the SeNPs synthesis (mM).

Conditions such as medium pH, incubation temperature and Na₂SeO₃ concentration were varied to determine the conditions for maximum yield of SeNPs. *H. salifodinae* BK18 was grown in NTYE at following conditions and the yield of SeNPs was determined as mentioned above.

pH	4.5	5.0	5.5	6.0	6.5	7.0	7.5	8.0
Na₂SeO₃ conc. (mM)	0.05	0.5	1.0	2.0	3.0	4.0	5.0	5.5
Temperature (°C)	20	25	30	35	37	40	45	

4.2.5 Characterisation of SeNPs

The excitation spectra of the SeNPs suspended in ethanol was recorded in the range of 200-800 nm using UV-visible spectrophotometer. Ethanol was used as the blank. XRD measurement of the nanoparticles and calculation of the crystallite domain size by the Debye-Scherrer formula was carried out as described in section 3.2.5. TEM, SAED, and EDAX analysis of the ‘as-synthesised’ SeNPs were carried out as described in section 3.2.5. The lattice parameters were determined using the formula for hexagonal crystal system:

$$\frac{1}{d^2} = \frac{4}{3} \left(\frac{h^2 + hk + k^2}{a^2} \right) + \frac{l^2}{c^2} \quad (6)$$

where, (h k l) are Braggs diffraction planes.

4.2.6 Nitrate reductase assay and inhibitor studies

H. salifodinae BK18 was grown in 10 ml HNB with 0, 2, and 4 mM Na₂SeO₃ at 37°C, 110 rpm for 7 days. Un-inoculated medium with Na₂SeO₃ served as the negative control for the assay. After incubation, the supernatant was collected by centrifugation at 10,000 × g for 20 mins, at RT. The nitrite concentration in the supernatant was estimated using Griess Illosvays reagent as described previously in section 3.2.7. The standard curve was prepared using 0-0.5 μM NaNO₂. All the experiments were carried out in triplicates.

The NR enzyme activity was determined using the method described by Harley (1993). The cells were grown in presence of 2 mM, and 4 mM Na₂SeO₃ and the CFE were prepared as described in section 3.2.6. The CFE was used to determine the NR enzyme activity as described in section 3.2.7. The amount of nitrite generated within 2 mins of addition of substrate mixture to CFE was read at 540 nm. KNO₃ (2 mM, and 4 mM) was used as positive control. One set of reaction mix was boiled to stop the enzyme activity, and the nitrite content of these tubes was subtracted from the nitrite content of the test, to give total amount of nitrite produced by the enzyme in 2mins. Thus, the NR activity was the net increase in nitrite concentration in 2mins, and was expressed as nM nitrite/min/ml.

PMSF, EDTA, sodium azide, and IAA were used for the inhibitor study. *H. salifodinae* BK18 was grown in the absence of the inhibitor (negative control), in presence of 10 mM inhibitor and in presence of 10 mM inhibitor along with 4 mM Na₂SeO₃. For positive control, the culture was grown in the presence of 4 mM Na₂SeO₃ alone. Further, the NR activity of the CFE obtained from cells grown in presence of 4 mM Na₂SeO₃ was determined in the presence of 10 mM inhibitor. The study was carried out in triplicates for each inhibitor. The percentage inhibition of NR enzyme activity was determined using the equation (5) as mentioned in section 3.2.7:

4.2.7 Mammalian cell culture

The cell lines used for this study were the human epidermal keratinocyte (HaCaT) and the human epithelial cervical adenocarcinoma (HeLa). Both the cell lines were maintained in

Dulbecco's modified eagle medium (DMEM) supplemented with 10% fetal bovine serum (FBS) and antibiotics (Complete media- CM). The cells were maintained at 37°C in a humidified 5% CO₂ incubator (Sanyo, Japan) and sub-cultivated according to standard cell culture protocols (Freshney, 2005).

4.2.8 MTT assay

Cytotoxicity of the SeNPs was evaluated by the MTT (3-(4,5-dimethylthiazol-2-yl)-2,5-diphenyltetrazolium bromide) assay towards HeLa, and HaCaT cell lines. The purple MTT dye is converted to pink formazan by actively metabolising human cells. Exponentially growing cells (2×10^4 cells/ well) were seeded in 24-well plates supplemented with CM. After 24hrs of growth the cells were exposed to varying concentrations of SeNPs (10-150 µg/ml) dispersed in DMEM, and incubated for 24 hrs. 30 µl MTT (5 mg/ml) was added to each well and the plates were further incubated at 37°C for 4 hrs in the dark. The media was aspirated carefully without disturbing the cells after 4 hrs and the formazan crystals were dissolved by adding 300 µl DMSO (dimethyl sulphoxide). The absorbance was measured at 570 nm and 630 nm using UV-visible spectrophotometer. The experiment was performed in triplicates on three different days. Selenium-free cell material (HSBK18) and sodium selenite (SS) were also evaluated for their cytotoxicity towards HeLa, and HaCaT cell lines. The cell viability (%) relative to cells unexposed to the SeNPs was calculated as:

$$\% \text{ cell viability} = \left(\frac{A_{\text{test}}}{A_{\text{control}}} \right) \times 100 \quad (7)$$

where, A_{test} is absorbance of the cells exposed to SeNPs, and A_{control} is the absorbance of cells unexposed to SeNPs.

4.2.9 Detection of intracellular reactive oxygen species (ROS)

Intracellular ROS was estimated using 2',7'-dichlorofluorescein diacetate (DCFH-DA), a fluorescent probe that readily diffuses through the cell membrane in to the cellular cytoplasm, where it is enzymatically hydrolysed to non-fluorescent DCFH. The oxidation of DCFH to highly fluorescent 2',7'-dichlorofluorescein provides a quantitative estimate of ROS formation (Kim et al. 2010; Mukherjee et al. 2012). The ROS studies were carried out in HeLa cell line alone as the SeNPs were found to be cytotoxic against this cell line. Exponentially growing

cells (5×10^4 cells/ well) were seeded in 24-well plates supplemented with CM. After 24 hrs of growth the cells were exposed to varying concentrations of SeNPs (10- 150 $\mu\text{g/ml}$) dispersed in DMEM and incubated for 24 hrs. Following exposure, the cells were washed with 500 $\mu\text{l/well}$ of PBS. DCFH-DA (20 μM) was added to all the wells and the plate was incubated in the dark at 37°C for 30 mins. The fluorescence was measured using a spectrofluorometer (JASCO FP-6300) at an excitation wavelength of 485 nm, and an emission wavelength of 530 nm. HSBK18 and SS were also evaluated for their ability to generate ROS in HeLa cell line. 1 μM hydrogen peroxide (H_2O_2) was used as a positive control. All the experiments were performed in triplicates on different days.

4.2.10 Acridine orange and ethidium bromide (AO/EB) staining to determine apoptotic index (AI)

Exponentially growing HeLa cells (2×10^5 cells/ well) were seeded in 6-well plates and allowed to grow for 24 hrs. The cells were then treated with varying concentration of SeNPs (10- 150 $\mu\text{g/ml}$) for a further 24 hrs. After trypsinisation the cells were washed with PBS and stained with AO/EB dye mixture as follows. To 25 μl of cell suspension, 1 μl dye mix containing 100 mg/ml of AO (Sd-fine) and 100 mg/ml EB (Sd-fine) in 1 X PBS, was added. Post staining, the cells were observed immediately at $40 \times$ of the epi-fluorescence microscope (Olympus BX41) using the FITC and TRITC filters. A minimum of 300 cells were counted and the apoptotic and viable cells were differentiated based on the type of fluorescence and state of chromatin condensation. Viable cells show uniform green nuclei with organized structure, while apoptotic cells may either have patchy green nuclei with condensed chromatin or orange to red nuclei with fragmented chromatin depending on the stage of apoptosis (Crucic et al. 2012). The experiments were performed in triplicates on different days. Apoptotic index (AI) was calculated as follows:

$$AI = \left(\frac{T_A}{T_C} \right) \times 100 \quad (8)$$

where, T_A is the total number of apoptotic cells; T_C is the total number of cells counted

4.2.11 Western blot

HeLa cells treated with various concentrations of SeNPs (0, 30, 50, 70, and 100 $\mu\text{g/ml}$) at 37°C, for 24 hrs were washed three times in PBS (pH 7.5). The cells were trypsinised, and lysed by addition of 1.0 ml lysis buffer (0.1 % Triton X-100, 1 mM EDTA, 1 mM PMSF, 20 mM Tris-HCl, pH 7.4) and incubating on ice for 25 mins. The total cellular proteins were obtained by centrifuging the cell lysates at 4°C (16,000 \times g, 20 mins). The protein concentrations were quantified by Lowry's method using BSA as control (Lowry et al. 1951). The total cellular proteins were separated on SDS-PAGE, transferred to PVDF membranes and blocked with 5% non-fat milk in transfer buffer (Tris base, glycine, SDS and methanol) for 1 hr at RT. The membranes were then incubated overnight at 4°C with the corresponding primary antibodies diluted in 5% non-fat milk with Tris-buffered saline containing Tween-20 (TBST). The following dilutions were used: anticaspase 3, 1:1000 (Biolegend), antiHsp 70, 1:1000 (Biolegend), and antiPARP, 1:1000 (BD Pharmingens). Subsequently, the membranes were washed with TBST, and incubated for 1 h at room temperature with horse radish peroxidase conjugated secondary antibody at a dilution of 1:2000, and specific proteins were visualised on X-ray films by enhanced chemiluminescence detection. β - Actin was used as the standard to check equal protein loading.

4.2.12 Statistical analysis

Statistical analysis was carried out as described in section 2.2.5.

4.3 Results and Discussions

4.3.1 Growth in presence of selenite and selenite uptake

MIC of sodium selenite (Na_2SeO_3) was determined by growing BK18 in presence of 0.05 to 10 mM Na_2SeO_3 , at increments of 0.5 mM. The culture could tolerate up to 5.5 mM Na_2SeO_3 and the MIC was 6 mM. At concentrations of up to 2 mM Na_2SeO_3 , growth was similar to that of unexposed control cells (Fig. 4.1). However, at concentrations above 2 mM Na_2SeO_3 , growth rate of *H. salifodinae* BK18 decreased with the increase in Na_2SeO_3 concentration, and ceased completely at 6 mM Na_2SeO_3 . Growth in Na_2SeO_3 was accompanied with generation of brick-red precipitate. The growth kinetics studies performed in presence of 2 mM and 4 mM

Na_2SeO_3 exhibited good growth with brick-red colouration due to reduction of selenite to elemental selenium (Fig. 4.2).

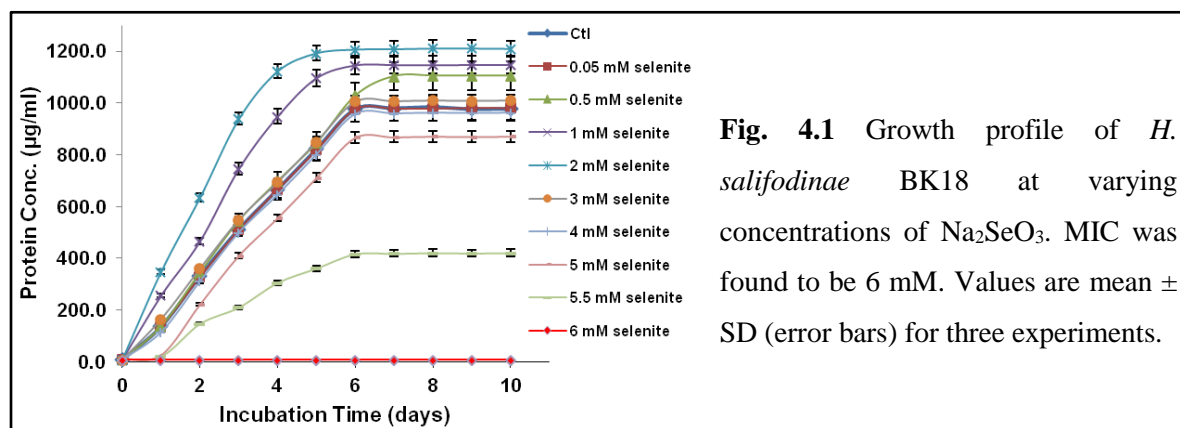


Fig. 4.1 Growth profile of *H. salifodinae* BK18 at varying concentrations of Na_2SeO_3 . MIC was found to be 6 mM. Values are mean \pm SD (error bars) for three experiments.

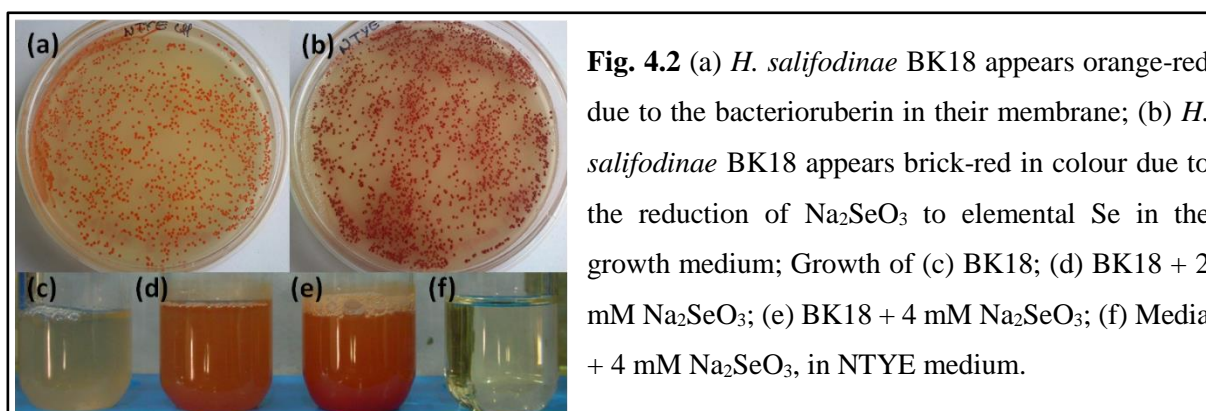


Fig. 4.2 (a) *H. salifodinae* BK18 appears orange-red due to the bacterioruberin in their membrane; (b) *H. salifodinae* BK18 appears brick-red in colour due to the reduction of Na_2SeO_3 to elemental Se in the growth medium; Growth of (c) BK18; (d) BK18 + 2 mM Na_2SeO_3 ; (e) BK18 + 4 mM Na_2SeO_3 ; (f) Media + 4 mM Na_2SeO_3 , in NTYE medium.

H. salifodinae BK18 grows with a lag time (t_l) of 11.9 hrs, a doubling time (t_d) of 16.8 hrs and a maximum specific growth rate (μ) of 0.99 days^{-1} . The copious amounts of brick-red precipitate formed in presence of Na_2SeO_3 interfered with the absorbance measurements at 600 nm, giving a false positive result. Therefore, growth was evaluated by determining the total protein concentration of the cells with the premise that, the cell number is proportional to the total protein concentration. Lower concentration of Na_2SeO_3 , i.e. 2 mM, enhanced the growth of *H. salifodinae* BK18 (Fig. 4.3a) and the lag phase reduced to 6 hrs as compared to the 11.9 hrs for the control (without Na_2SeO_3). However, at 4 mM Na_2SeO_3 , *H. salifodinae* BK18 exhibited a μ of 0.94 days^{-1} , a t_d of 17.68 hrs, and a t_l of 12.37 hrs, which were very similar to the growth kinetics parameters of unexposed controls ($p > 0.05$). *H. salifodinae* BK18 when provided with 2 mM Na_2SeO_3 exhibited better growth kinetics which may be attributed to the element selenium being a trace element. Studies have shown that selenium exhibits varying

effects on the growth of bacteria depending upon the species and the concentration of selenium used. Usually, low concentrations of selenium are known to enhance growth of bacteria and high concentrations are detrimental (Penas et al. 2012).

The kinetics of selenite reduction in the medium as a result of cellular metabolism by *H. salifodinae* BK18 (Fig. 4.3b) was determined and co-related to the growth of the isolate in presence of selenite. At the beginning of the stationary phase, *i.e.* on day five, the selenite concentration in the medium was 0.23 mM indicating a decrease of ~90% (1.77 mM) of the 2 mM Na₂SeO₃ initially added to the medium (Fig. 4.3c). For the haloarchaeal isolate grown in presence of 4 mM Na₂SeO₃, by the end of exponential phase, *i.e.* on day six, 2.62 mM Na₂SeO₃ was taken up, leaving 1.38 mM (~36%) of selenite in the medium (Fig. 4.3d). However, by the end of stationary phase, only 0.042 mM and 0.476 mM Na₂SeO₃ remained unutilised in the media, during growth in presence of 2 mM, and 4 mM Na₂SeO₃, respectively. Thus, the selenite concentration was found to decrease from early exponential phase up to late stationary phase due to the metabolic activity of the haloarchaeal isolate. These results are in contrast to the findings of Kessi et al. (1999), where selenite uptake by the phototrophic bacterium *Rhodospirillum rubrum* was observed only at the beginning of stationary phase. Similarly, they reported the reduction of the selenite to red elemental selenium only when the cells transitioned from exponential to stationary phase. However, in our study the reduction of the selenite to red elemental selenium was observed at the beginning of the early exponential phase and continued up to early stationary phase, without any further reduction during the late stationary phase. A similar selenite uptake and reduction of selenite during early exponential phase by the bacterium *Bacillus cereus* grown in presence of Na₂SeO₃ was observed by Dhanjal and Cameotra (2010), during their study on the aerobic biogenesis of selenium nanospheres by *B. cereus*. The selenite concentration in the un-inoculated media controls with 4 mM Na₂SeO₃ did not exhibit any change and remained constant throughout the experiment (Fig. 4.3b).

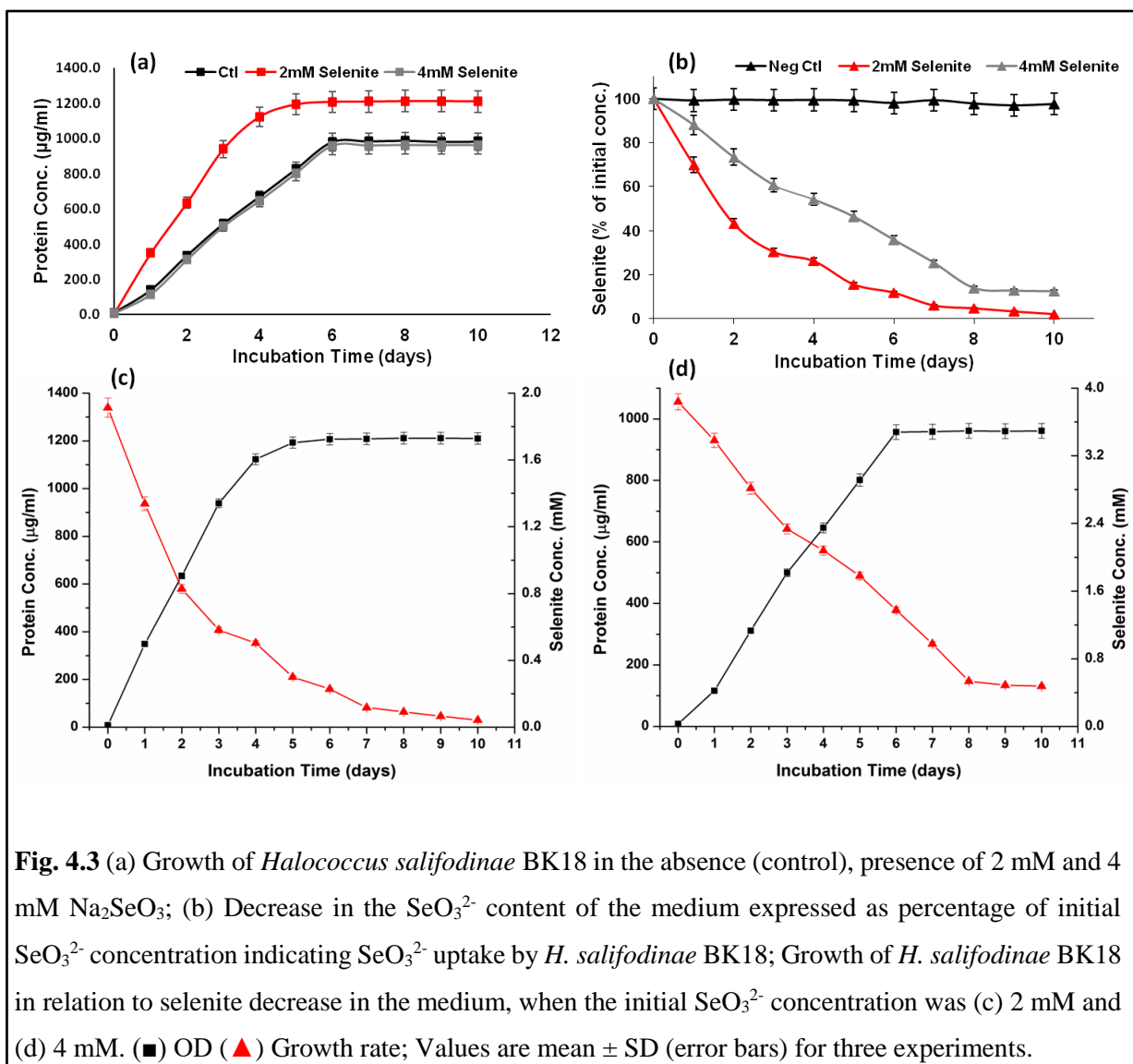
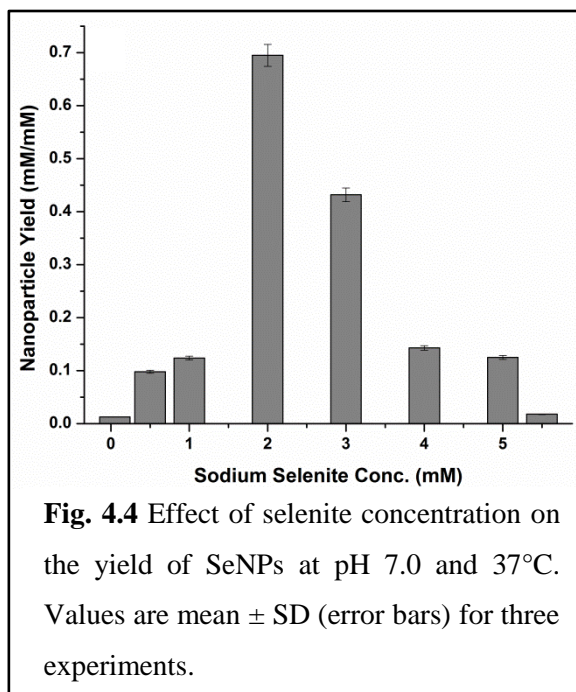


Fig. 4.3 (a) Growth of *Halococcus salifodinae* BK18 in the absence (control), presence of 2 mM and 4 mM Na_2SeO_3 ; (b) Decrease in the SeO_3^{2-} content of the medium expressed as percentage of initial SeO_3^{2-} concentration indicating SeO_3^{2-} uptake by *H. salifodinae* BK18; Growth of *H. salifodinae* BK18 in relation to selenite decrease in the medium, when the initial SeO_3^{2-} concentration was (c) 2 mM and (d) 4 mM. (■) OD (▲) Growth rate; Values are mean \pm SD (error bars) for three experiments.

4.3.2 Selenium nanoparticles biosynthesis and characterisation

The SeNPs synthesis was found to be a culture dependent phenomenon as mentioned in previous sections. Growth of *H. salifodinae* BK18 in presence Na_2SeO_3 was accompanied with the biomass turning brick-red in colour. In order to determine the optimal conditions for synthesis, the haloarchaeal isolate was grown at various pH, temperature, and Na_2SeO_3 concentration in NTYE media. Following synthesis at these conditions, the nanoparticles were extracted and their yield determined.

Na₂SeO₃ concentration

A concentration range of 0.05 mM to 5.5 mM Na₂SeO₃ was tested to determine the optimum concentration needed for maximal SeNPs synthesis (Fig. 4.4). At concentrations lower than 2 mM Na₂SeO₃, the yield of SeNPs obtained was very low (~0.1 mM/mM selenite added). The low yield may be attributed to the presence of low concentration of Na₂SeO₃. Maximum yield of 0.697 mM/ mM Na₂SeO₃ was obtained at 2 mM Na₂SeO₃. Although the growth of *H. salifodinae* BK18 was not affected by presence of 3 mM and 4 mM Na₂SeO₃ (Fig.

4.1), the yield of SeNPs was affected exhibiting a molar yield of only 0.432 mM/ mM selenite and 0.143 mM/ mM selenite, respectively. The difference in yield of SeNPs when 2 mM and 3 mM Na₂SeO₃ were added was insignificant ($p > 0.05$), however the yields obtained at 4 mM, 5 mM and 5.5 mM Na₂SeO₃ were significantly lower ($p < 0.05$) as compared to that obtained at 2 mM Na₂SeO₃. Higher concentrations of 5 mM and 5.5 mM Na₂SeO₃, negatively affected both growth rate and yield of SeNPs. This suggests that at concentrations above 4 mM Na₂SeO₃, the oxyanion exerts its toxic effects on the haloarchaeal isolates which may be responsible for low yields. As maximum yield of SeNPs was obtained at 2 mM Na₂SeO₃, this concentration was used for further studies on SeNPs synthesis.

Medium pH

The SeNPs synthesis was carried out at varying pH (4.5-8.0) to determine the optimum pH for maximum yield. Optimal growth and maximum yield of 0.697 mM/ mM selenite, was obtained at pH 7.0 (Fig. 4.5). *H. salifodinae* BK18 failed to grow at pH 4.5 even in the absence of Na₂SeO₃. The haloarchaeon exhibited poor growth at pH of 5.0 and 5.5 in the absence of

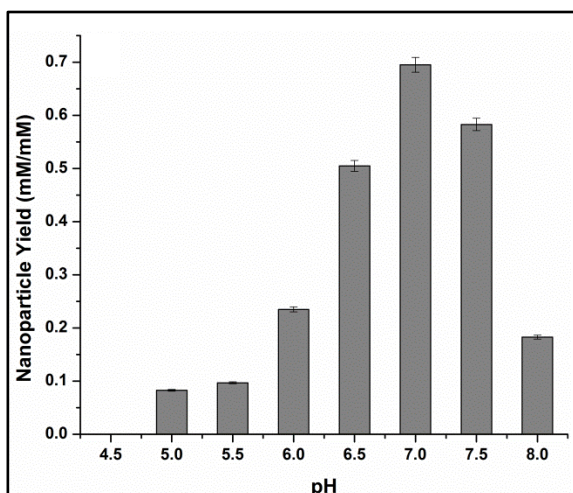


Fig. 4.5 Effect of pH on the yield of SeNPs at 37°C using 2 mM Na₂SeO₃ precursor. Values are mean ± SD (error bars) for three experiments.

SeNPs synthesis was carried out at pH 7.0.

Incubation Temperature

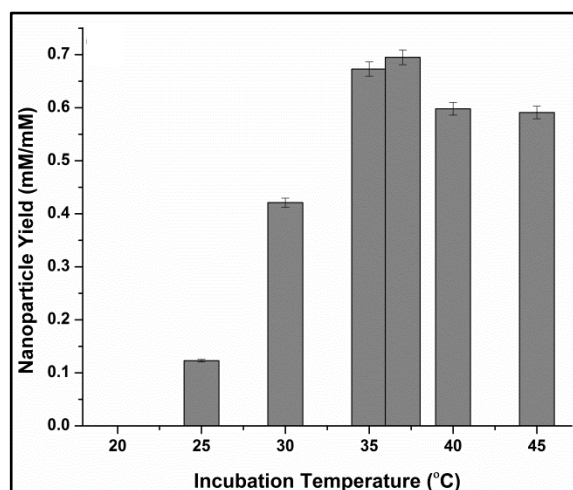


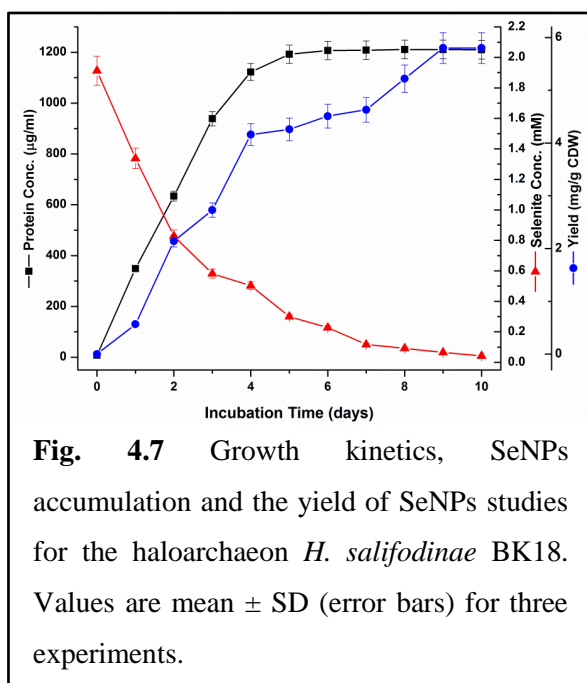
Fig. 4.6 Effect of incubation temperature on the yield of SeNPs at pH 7.0 using 2 mM Na₂SeO₃ precursor. Values are mean ± SD (error bars) for three experiments.

Na₂SeO₃, therefore, when grown in presence of 2 mM Na₂SeO₃ the yield of SeNPs was significantly lower ($p < 0.05$) as compared to that at pH 7.0. The pH range for growth of *Halococcus* is 6.0-9.5, with the optimum at pH 7.0 (Grant, 2015). Therefore, as the pH increased from 6.0 to 6.5, there was a corresponding increase in yield. At pH 7.5, yield of SeNPs was 0.583 mM/ mM Na₂SeO₃, which was not significantly different ($p > 0.05$) from that at pH 7.0. However, the yield of SeNPs was significantly lowered at the alkaline pH of 8.0. Based on these results,

A temperature range of 20°C to 45°C was tested to determine the optimum temperature for SeNPs synthesis by *H. salifodinae* BK18. Maximum SeNPs synthesis was obtained at 35, and 37°C with a yield of 0.673 mM/ mM and 0.697 mM/ mM selenite, respectively (Fig. 4.6). The haloarchaeal isolate did not grow at 20°C even in the absence of Na₂SeO₃. As the temperature increased from 25°C to 37°C, the yield of SeNPs also increased, albeit the difference in yield between 30, 35, and 37°C was insignificant ($p > 0.05$). The optimum range of temperature for growth of *Halococcus* is 30°C to 40°C

(Grant, 2015). *H. salifodinae* BK18 exhibited slow growth at 45°C, and therefore, the yield of SeNPs was also lower. Thus, SeNPs synthesis by *H. salifodinae* BK18 was carried out at 37°C.

Maximum yield of SeNPs synthesis was obtained at 2 mM Na₂SeO₃, pH 7.0, and temperature of 37°C (Table 4.1).



The time course of SeNPs accumulation, selenite loss from the medium and the growth is shown in Fig. 4.7. As mentioned in section 4.3.1, *H. salifodinae* BK18 exhibited an increase in μ (specific growth rate) to 1.21 days⁻¹, in presence of 2 mM Na₂SeO₃ as compared to the μ of the isolate in the absence of Na₂SeO₃. Both molar yield and the yield with respect to the biomass were estimated during the synthesis. *H. salifodinae* BK18 exhibited SeNPs accumulation from the early exponential phase. The yield was initially determined by

growing the haloarchaeal cells in presence of 2 mM Na₂SeO₃, and extracting the SeNPs by wet heat sterilisation to give a crude SeNPs preparation. The yield of crude unpurified SeNPs was 0.934 mM/ mM Na₂SeO₃. However, after purification (acid-wash), yield was 0.697 mM/mM Na₂SeO₃, exhibiting a loss of 23.7% during the process of purification. Maximum yield (5.8 mg/g CDW; 0.697 mM/mM of Na₂SeO₃ added) was obtained on day 9, exhibiting an efficiency of 70%. Table 4.2 summarises the various kinetic and yield parameters of SeNPs synthesis by *H. salifodinae* BK18.

Table 4.1 SeNPs synthesis kinetics and yield parameters.

Kinetics parameters	Values	Yield parameters	Values
μ (days ⁻¹)	1.12	Y (mg/g CDW)	5.8
t_d (hrs)	14.85	MY (mM/mM)	0.697
t_i (hrs)	8.9	Efficiency (%)	70

The selenium nanopowder obtained after biosynthesis was subjected to crystallographic characterisation by X-ray diffraction (Fig. 4.8a). Characteristic Bragg's peaks corresponding to the (1 0 0), (1 0 1), and (1 0 2) facets of hexagonal selenium (ICDD card no.06-0362) were obtained. The crystallite domain size was found to be 28.27 nm. The lattice parameters a and b were calculated for hexagonal system for the plane (1 0 1) and found to be 0.436 nm and 0.493 nm, respectively. The UV-visible spectral characterisation of the synthesised SeNPs revealed an absorption band between 200 to 300 nm with a maximum at around 270 nm (Fig. 4.9b) indicating the formation of selenium nanoparticles (Praharaj et al. 2006; Fesharaki et al. 2010). Rod shaped nanoparticles with an average length of 129 nm, average diameter of 10 nm, and an aspect ratio of 13:1 were observed during the morphological characterisation of SeNPs by TEM. Some spherical SeNPs of uniform size distribution with an average diameter of 9 nm were also observed (Fig. 4.9c). Most studies on biological syntheses of SeNPs have reported spherical SeNPs (Oremland et al. 2004; Dhanjal and Cameotra, 2010; Sarkar et al. 2011; Prasad et al. 2012). However, Srivastava and Mukhopadhyay (2013), in their study on selenium nanoparticle biosynthesis by the bacterium *Zooglea ramigera*, reported generation of spherical nanoparticles that acted as seed for growth of trigonal Se nanorods due to their high free energy. The Ostwald ripening process has been attributed to be responsible for the growth of SeNPs in to larger particles, which due to their in-stability dissolve and precipitate out as trigonal Se nanorods (Jeong and Xia, 2005; Wang et al. 2010; Srivastava and Mukhopadhyay, 2013). A similar phenomenon may be responsible for the presence of rod shaped nanoparticles with a few spherical particles. The SAED pattern of the SeNPs further confirmed their crystalline nature and exhibited the diffraction rings typical of hexagonal crystals (Fig. 4.6c inset). The elemental analysis by EDAX exhibited absorption bands at 1.5, 11.2 and 12.5 keV, confirming the presence of elemental selenium (Fig.4.8d). Additional weaker peaks of S and O obtained may be attributed to the bio-molecules that may be involved in capping of the biogenic SeNPs.

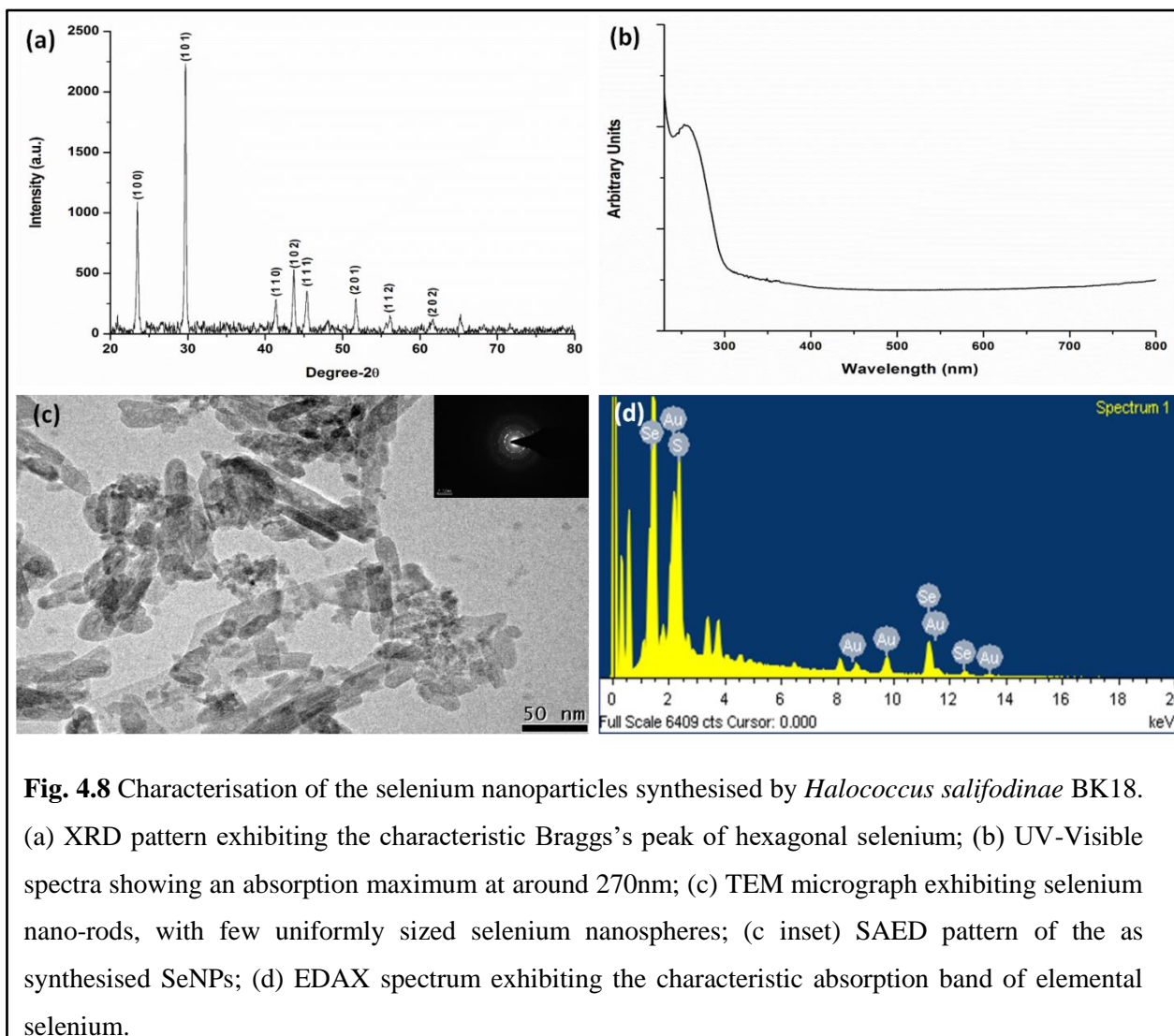
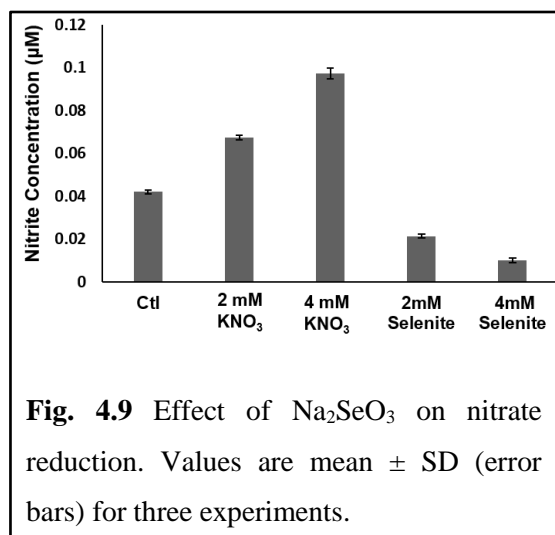


Fig. 4.8 Characterisation of the selenium nanoparticles synthesised by *Halococcus salifodinae* BK18. (a) XRD pattern exhibiting the characteristic Bragg's peak of hexagonal selenium; (b) UV-Visible spectra showing an absorption maximum at around 270nm; (c) TEM micrograph exhibiting selenium nano-rods, with few uniformly sized selenium nanospheres; (c inset) SAED pattern of the as synthesised SeNPs; (d) EDAX spectrum exhibiting the characteristic absorption band of elemental selenium.

4.3.3 Involvement of Nitrate Reductase enzyme in selenite reduction

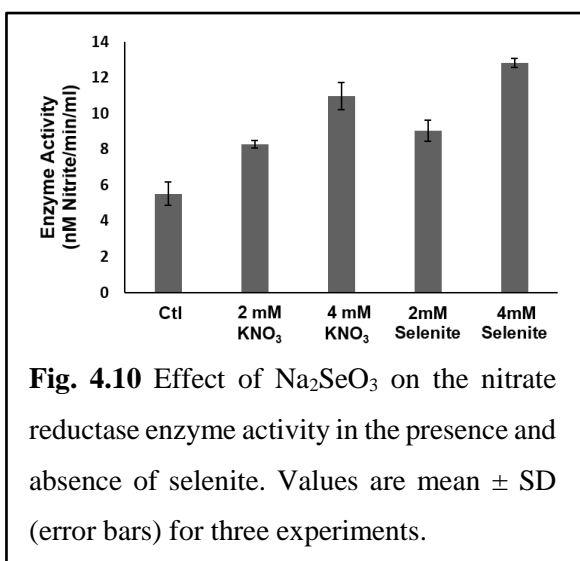
Although microorganisms have been reported to tolerate toxic concentrations of selenate and selenite, the mechanism of this tolerance is poorly understood. Selenite being more toxic than selenate to the cells (Dong et al. 2003), the detoxification of this oxyanion is a feature of diverse microorganisms. Various enzymes like periplasmic nitrite reductase (Hunter and Kuykendall, 2007; Hunter, 2007), intracellular nitrate reductase (Avazeri et al. 1997), hydrogenase I (Yanke et al. 1995), arsenate reductase (Afkar et al. 2003), oxido-reductases and membrane associated reductases (Dhanjal and Cameotra, 2010) have been implicated in the selenite reduction. Some recent studies have also suggested the presence of

NADH/NADPH dependent selenate reductases that bring about the reduction of both selenate and selenite to Se^0 (Hunter and Manter, 2009; Etezzad et al. 2009).



The pink colouration obtained on the addition of Griess-Illosvays reagent to the cell free medium confirmed the nitrate reductase activity of *H. salifodinae* BK18. Fig. 4.9 shows the amount of nitrite present in the medium after the growth of the culture in presence of 2 mM and 4 mM KNO_3 , and 2 mM and 4 mM Na_2SeO_3 . The nitrite concentration in presence of 2 mM and 4 mM KNO_3 was 0.07 and 0.1 μM , respectively, while the nitrite content of the medium after

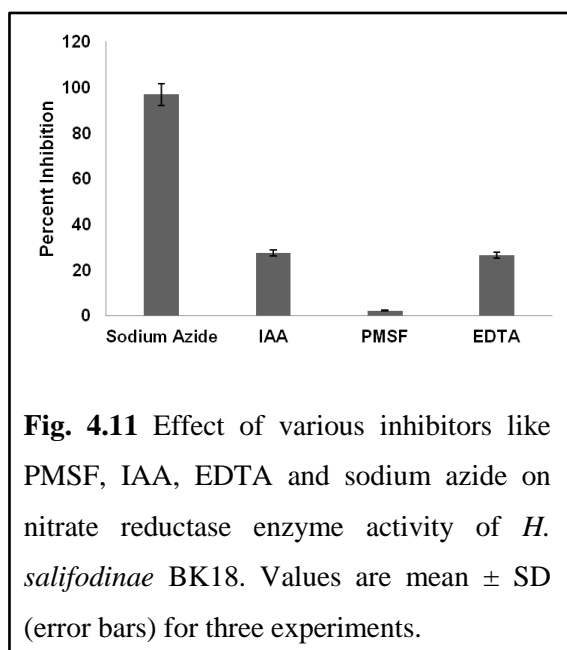
the growth of the culture in presence of 2 mM and 4 mM Na_2SeO_3 was 0.02 and 0.01 μM , respectively. The decrease in the nitrite concentration in presence of Na_2SeO_3 may be due to the involvement of the enzyme nitrate reductase in SeO_3^{2-} reduction. This suggests the inhibition of the enzyme NR by selenite.



To rule out the possibility of inhibition of the enzyme NR by Na_2SeO_3 , nitrate reductase enzyme assay was performed using the CFE of *H. salifodinae* BK18 grown in presence of 2 mM and 4 mM Na_2SeO_3 with 2 mM and 4 mM KNO_3 as positive control. The CFE of the un-induced control cells exhibited a specific enzyme activity of 5.5 nM Nitrite/min/ml. The CFE of the cells obtained from selenite treated haloarchaeal cell exhibited a dose-dependent increase in

NR enzyme activity (Fig. 4.10). CFE of 2 mM Na_2SeO_3 treated cells exhibited an activity of 9.01 nM Nitrite/min/ml, which was 64% higher than the untreated control ($p < 0.05$). For CFE

of 4 mM Na_2SeO_3 treated cells, the NR enzyme activity was 12.82 nM Nitrite/min/ml, which was 133% higher than the enzyme activity exhibited by the CFE of untreated cells ($p < 0.05$). The enzyme activity of CFE of the cells grown in presence of 2 mM and 4 mM KNO_3 was found to increase by 50% and 99% respectively. This increase is due to the increase in the substrate for the enzyme NR. The dose dependent increase in NR enzyme activity of the CFE of selenite treated cells indicates that selenite does not inhibit the NR enzyme, and that the enzyme gets diverted to reduction of selenite instead of nitrate. To further confirm the role of NR in selenite reduction, inhibitor studies were performed.



Four compounds used for the inhibitor studies included PMSF, IAA, EDTA and sodium azide. These compounds are well known enzyme inhibitors specific for certain enzymes (Michaud et al. 1993; Knap and Pratt 1991; Auld, 1995; Amy and Garrett, 2007). Except for IAA, the other inhibitors had no effect on the growth of *H. salifodinae* BK18. IAA was found to delay the growth slightly. Similarly, when the isolate was grown in the presence of 4 mM Na_2SeO_3 and either one of the inhibitors (PMSF, IAA, EDTA), the SeNPs synthesis remained

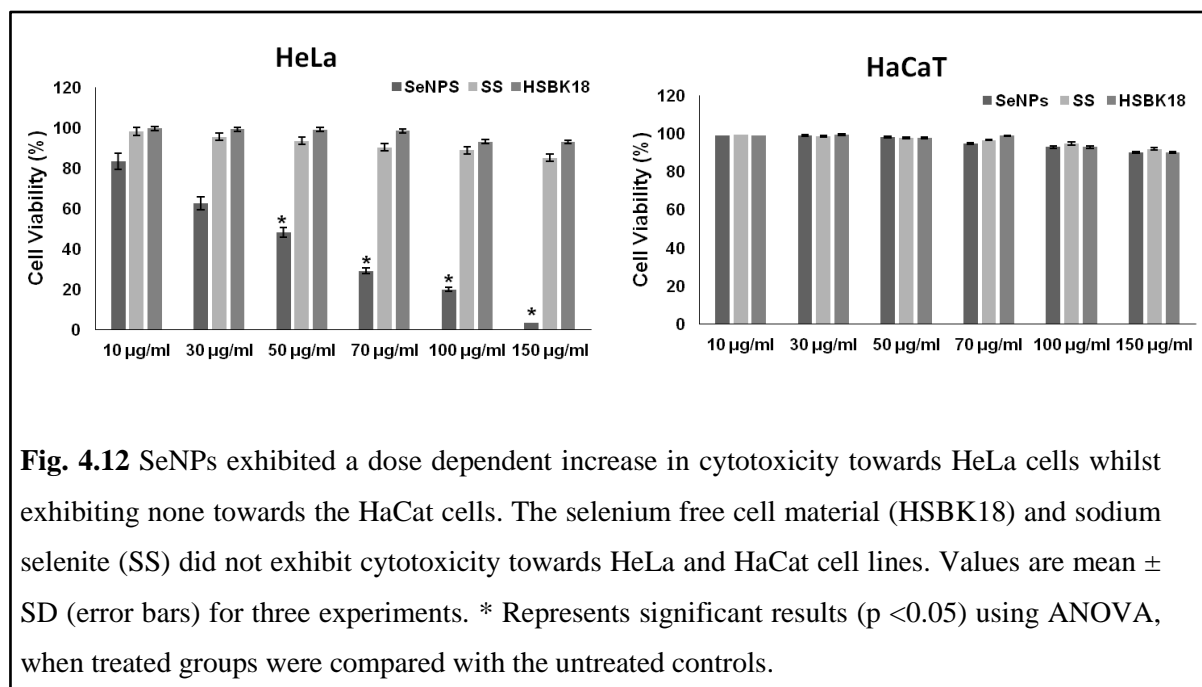
unaffected. However, when the isolate was grown in presence of 10 mM Sodium azide and 4 mM Na_2SeO_3 both, growth and SeNPs synthesis was negligible. The effect of inhibitors on the SeNPs synthesis in presence of Na_2SeO_3 was in the order of Sodium azide \gg IAA = EDTA $>$ PMSF, with sodium azide being most inhibitory and PMSF being least inhibitory. Sodium azide exhibited a 96.8% inhibition in enzyme activity as compared to the control (Fig. 4.11). Sodium azide is a known inhibitor of nitrate reductase enzyme (Amy and Garrett, 1974), therefore, the inability of the haloarchaeon to grow in presence of this inhibitor and selenite, is suggestive of the involvement of NR in selenite tolerance and nanoparticles synthesis.

4.3.4 Anti-proliferative properties of SeNPs

Selenium compounds like selenite, selenate, Se-methionine, Se-cysteine and methylselenocysteine are known to be anticarcinogenic and cancer-chemopreventive (Rikiishi, 2007). Recently, elemental nano-selenium has attracted substantial attention due to its excellent biological activity and low toxicity, and is being touted as the new anticancer and chemopreventive agent (Zhang et al. 2008; Luo et al. 2012; Sun et al. 2014). Several studies have shown the dose-dependent cytotoxic effect of the red elemental nano-selenium towards various cancer cell lines like A375 (human melanoma cell line), HepG2 (hepatocellular carcinoma cell line), MCF-7 (breast adenocarcinoma cell line), MDA-MB-231 (human breast carcinoma), HeLa (human cervical carcinoma cell line), HK-2 (human kidney cell line) and human ileocecal adenocarcinoma, HCT-8 cells (Chen et al. 2008; Luo et al. 2012; Zheng et al. 2010; Sun et al. 2014; Gao et al. 2014). These nanoparticles have also been shown to augment the anti-proliferative properties of chemotherapeutic drugs like adriamycin (Tan et al. 2009), doxorubicin (Ramamurthy et al. 2013) and irinotecan (Gao et al. 2014). Few reports have exhibited lower toxicity and selectivity of nanoselenium towards normal cells (Chen et al. 2008; Luo et al. 2012).

The SeNPs biosynthesised by *H. salifodinae* BK18 were evaluated for their anti-proliferative properties on HeLa and HaCaT (human epidermal keratinocyte) cell lines. The HeLa cell line was treated as the cancer model cell line and the HaCaT cell line as a substitute for normal primary cultures (Bonifas et al. 2010). HaCaT cells were immortalised by growing human epidermal keratinocytes at lower calcium concentration and higher temperature (Boukamp et al. 1988; Bonifas et al. 2010). *H. salifodinae* BK18 biosynthesised SeNPs were found to be cytotoxic towards HeLa cells in a dose-dependent manner (Fig. 4.12). However, this trend of dose-dependent cytotoxicity was not observed in HaCaT cells (Fig. 4.12). Even at a concentration of 150 μ g/ml SeNPs, 90% cell viability was observed for HaCaT cells. This difference in susceptibility of the cancer cells to SeNPs as compared to the normal cells may be attributed to the difference in the antioxidant enzyme regulation, particularly thioredoxin (TR) in cancer cells (Fang et al. 2000). TR when overexpressed (as in cancer cells) leads to the increase in selenide generation which causes an increase in oxidative stress due to redox cycling. At the same time, the increased TR also inhibits lipooxygenases thereby removing

essential fatty acid growth factors from cancer cells, and causing cell death (Fang et al. 2000). Selenium free cell material (HSBK18) and sodium selenite (SS) did not exhibit cytotoxicity towards both HeLa and HaCaT cell lines. Thus, the SeNPs are anti-proliferative against cancer cell line while being non-toxic to normal model cell line HaCaT and may be used as potential cancer chemotherapeutic agent.



4.3.5 Mechanism of SeNPs cytotoxicity towards HeLa cell line

Mechanisms involved in the anticancer activity of nanoselenium are not yet fully elucidated. However, there are few studies indicating apoptosis as one of the mechanisms responsible for the cytotoxicity of nanoselenium against cell lines such as, A357 human melanoma cells (Chen et al. 2008), LNCaP prostate cancer cells (Kong et al. 2011), MCF-7, and MDA-MB-231 breast cancer cells (Vekariya et al. 2010). Nanoselenium has also been shown to inhibit the growth of HeLa, human cervical cancer cells and MDA-MB-231 cells through the induction of S-phase arrest (Luo et al. 2012).

To understand the mechanisms involved in SeNPs cytotoxicity towards HeLa cell line, ROS studies were carried out using the fluorescent probe DCFH-DA. An increase in ROS generation is responsible for oxidative damage of mitochondria, nucleic acids, and lipids which results in cell death due to apoptosis (Wu et al. 2012). SeNPs treated cells exhibited a

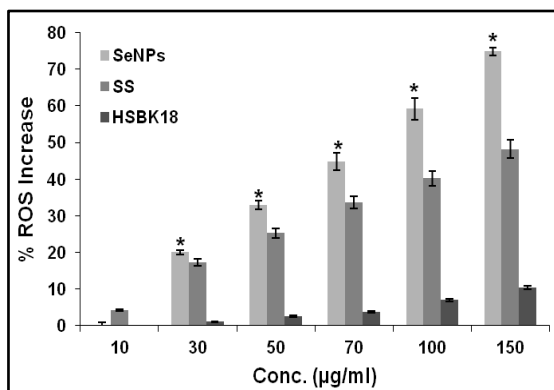


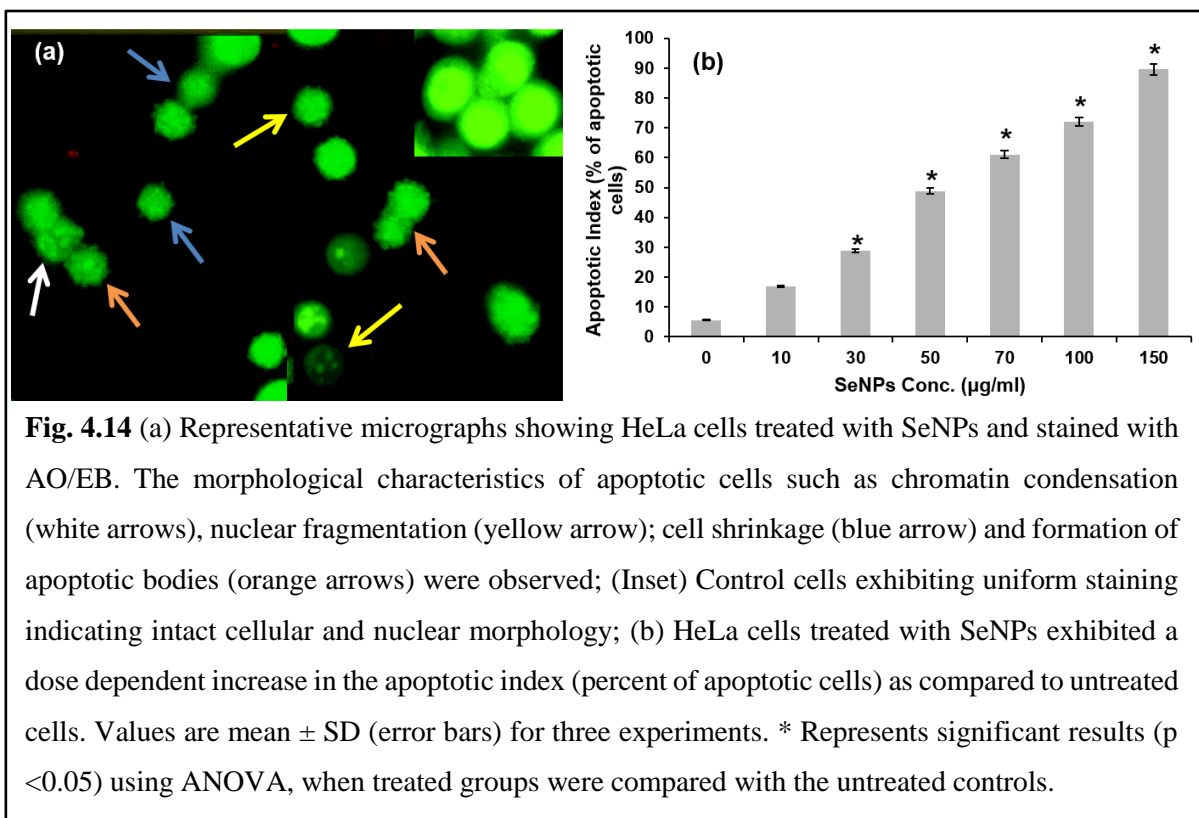
Fig. 4.13 ROS generation in HeLa cell lines after treatment with SeNPs/ SS/ HSBK18 represented as a percentage of ROS generated in untreated cells. Values are mean \pm SD (error bars) for three experiments. * Represents significant results ($p < 0.05$) using ANOVA, when treated groups were compared with the untreated controls.

significant increase ($p < 0.05$) in ROS levels as compared to unexposed controls. This increase in ROS was dose dependent (Fig. 4.13) and maximum increase (75%) in ROS was observed at a concentration of 150 $\mu\text{g/ml}$ of SeNPs. This suggests that SeNPs cause oxidative damage in HeLa cells leading to apoptosis and cell death. Both HSBK18 and SS did not exhibit a significant increase ($p > 0.05$) in ROS generation as compared to SeNPs, however SS resulted in a significant increase in ROS ($p < 0.05$) as compared to unexposed control. At a concentration of 50 $\mu\text{g/ml}$ SS exhibited ~25% increase in ROS as compared to the unexposed controls. SS is a known chemotherapeutic agent, however the

effective dose to achieve cell death is much higher, which is usually toxic to the normal cells (Rikiishi, 2007; Zhang et al. 2008; Zeng, 2009). Nano-preparations of Se offer equal efficacy in anticancer activity at lower doses, without eliciting any toxicity towards normal cells (Zhang et al. 2008).

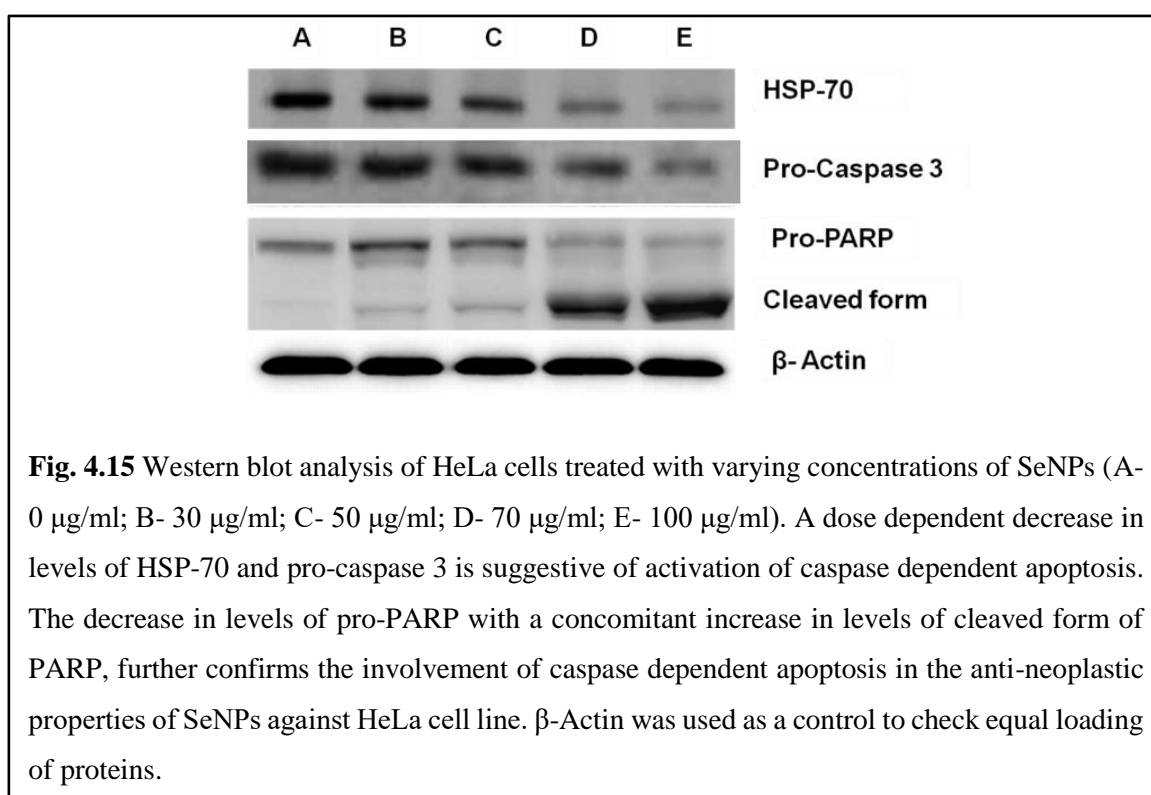
Apoptosis induction by SeNPs was further confirmed by acridine orange/ethidium bromide (AO/EB) staining. This is a quick and easy method to determine the apoptotic morphology as well as to estimate the apoptotic index (AI) (Ribble et al. 2005). AI is a measure of the percentage of apoptotic cells within the overall population of cells (Soini et al. 1998). AO stains live cells green, while EB stains non-viable cells red. Viable cells are stained uniformly green, while apoptotic cells exhibit fluorescent green patches representing chromatin condensation. The cells treated with SeNPs exhibited morphological characteristics of apoptotic cells such as cell shrinkage, chromatin condensation, nuclear fragmentation, and formation of apoptotic bodies (Fig. 4.14a). Apoptotic cells and the total number of cells were counted and AI was determined (Fig. 4.14b). A dose dependent increase in AI was observed

on SeNPs treatment. The AI was found to be significantly higher ($p < 0.05$) for cells treated with 30, 50, 70, 100, and 150 $\mu\text{g/ml}$ as compared to untreated controls. Cells treated with 10 $\mu\text{g/ml}$ exhibited only 16.8% cell death.



To further understand the mechanism of SeNPs cytotoxicity towards HeLa cell line, the expression of apoptotic markers, pro-caspase-3, poly(ADP-ribose) polymerase (PARP), and heat shock protein-70 (HSP-70) was determined by western blot analysis. Caspases are a group of intracellular proteases that exist as inactive pro-enzymes and are activated by proteolytic cleavage resulting in the deliberate disassembly of the cell into apoptotic bodies (Thornberry et al. 1998). In response to a pro-apoptotic signal, such as UV-light or chemotherapy, proteins upstream of pro-caspase-3 cleave it resulting in generation of active form of caspase-3. HeLa cells treated with SeNPs exhibited a dose dependent decrease in expression of pro-caspase 3 as compared to untreated controls (Fig. 4.15), suggesting the activation of apoptotic pathway. This was confirmed by determining the expression of pro-PARP and cleaved PARP, as the activated form of caspase-3 catalyses the cleavage of pro-PARP. As seen in Fig. 4.15, the expression of pro-PARP was found to decrease with the increase in SeNPs concentration,

while the cleaved-PARP was found to be upregulated. At the same time, HSP-70 was found to be downregulated with the increase in SeNPs concentrations (Fig. 4.15). This further confirms the activation of apoptotic pathway, as HSP-70 is known to protect cells against caspase dependent apoptotic cell death (Sabirzhanov et al. 2012). A similar decrease in the expression levels of pro-caspase-3, and pro-PARP and an increased expression of cleaved PARP was observed in prostate cancer cell line, LNCaP, in response to chemically synthesised SeNPs treatment (Kong et al. 2011). Thus, the western blot analysis indicates the activation of caspase-dependent apoptosis in HeLa cells treated with SeNPs synthesised by *H. salifodinae* BK18.



4.4 Conclusion

In this study, we report the biosynthesis of selenium nanoparticles by the halophilic archaeon *Halococcus salifodinae* BK18. The selenium nanorods were found to possess hexagonal crystalline facets, with an aspect ratio of 13:1. In presence of 2mM Na_2SeO_3 , the isolate exhibited enhanced growth, while in presence of 4mM Na_2SeO_3 the growth was similar to the control. The increase in the nitrate reductase enzyme activity in presence of Na_2SeO_3 and its

inability to grow in the presence of the enzyme inhibitor sodium azide implies the involvement of nitrate reductase in detoxification of the selenite. These SeNPs exhibited cytotoxicity towards the human cervical cancer cell line, HeLa, while being non-cytotoxic towards the normal primary cell substitute, human epidermal keratinocyte cell line, HaCaT. The increase in ROS and AI in SeNPs treated HeLa cells suggested the induction of apoptosis resulting in cell death. The concomitant decrease in the expression of HSP-70, pro-caspase 3, and pro-PARP, along with an increase in cleaved PARP expression suggests the activation of caspase dependent apoptotic pathway. These SeNPs may therefore be used as potential chemotherapeutic agents.

CHAPTER 5

Biosynthesis of Antibacterial Tellurium Nanoparticles by the haloarchaeon *Halococcus salifodinae* BK3¹**5.1 Introduction**

Tellurium (Te) is a metalloid that belongs to group 16 (VI A) of the periodic table, along with oxygen (O), sulphur (S), selenium (Se), and polonium (Po). It is a trace element present at 0.005 ppm level in the earth's crust. Unlike its other group members such as O, S, and Se, that find biological use, Te has no known biological function. However, in rare cases, fungi grown in presence of sodium tellurite (Na_2TeO_3) and in absence of S, have exhibited the formation of Te-containing amino acids (tellurocysteine, tellurocystine and telluromethionine) and proteins (Chasteen and Bentley, 2003). In nature, Te occurs in four oxidation states, partially soluble oxyanions Te (+VI)/ TeO_4^{2-} and Te (+IV)/ TeO_3^{2-} , elemental Te^0 , and the metal tellurides (Te^{2-}) like CdTe. Occurrence of Te in its elemental form is rarest, and is usually found as telluride of gold and/or other metals. Tellurium is most commonly used in the rubber industry as a vulcanising agent, in the manufacture of steel as an alloying element, and along with selenium in electronic industry (Naumov, 2010). Prior to the advent of antibiotics, tellurite was used for the treatment of leprosy, tuberculosis, dermatitis, cystitis, eye infections, and as an antibacterial agent in growth media (Taylor, 1999, Summers and Jacoby, 1977).

More recently, nanoparticles of tellurium have gained importance due to their unique properties such as photoconductivity, catalytic activity towards hydration and oxidation reactions, high piezoelectronic, thermoelectronic, and non-linear optical responses (Ufimtsev et al, 1997; Liu et al, 2003). Nano-scaled Te compounds such as CdTe/ZnTe, CdSeTe, CdHgTe, have been shown to have great potential for use in solar-cells, and as QDs for bio-imaging (Tang et al, 2006; Law et al, 2009; Chen et al, 2010). Elemental tellurium nanoparticles (TeNPs) are fabricated majorly through chemical solution phase methods, where $\text{TeO}_4^{3-}/\text{TeO}_3^{2-}$ is reduced to Te^0 employing reducing agents such as hydrazine, ethylene glycol, sodium borohydride, formamide etc. (Mayers and Xia, 2002a; Mayer and Xia, 2002b; Xi et al,

¹ This work is published as: **Srivastava P**, Nikhil EV, Braganca JM, Kowshik M (2015) Anti-bacterial TeNPs biosynthesized by haloarchaeon *Halococcus salifodinae* BK3. *Extremophiles* 19:875-884

2005). However, these procedures usually employ extreme temperatures for synthesis and calcination, and expensive stabilisers and capping agents (Lan et al, 2007; Lin et al, 2008; Kurimella et al, 2013). Therefore, biological entities may serve as substitutes for nanofabrication as the process would occur at ambient temperature and without the need of a capping agent (Shankar et al, 2004).

Bacteria such as *Bacillus selenitireducens*, *Bacillus* Sp. BZ, *Sulfurospirillum barnesii*, *Pseudomonas fluorescens* K27, *Rhodobacter capsulatus*, and *Shewanella oneidensis* have been shown to synthesise tellurium nano-rods and irregular nanospheres (Baesman et al, 2007; Zare et al, 2012; Basnayake et al, 2001; Borghese et al, 2004; Klonowska et al, 2005). Studies on resistance to tellurates and tellurites in other bacteria such as *E. coli*, *P. aeruginosa*, *Enterobacter* sp. YSU, *Roseococcus thiosulfatophilus*, *Erythrobacter litoralis*, and *Erythromicrobium ramosum* have reported the generation of black precipitates indicative of nano Te^0 , however, none of these organisms have been exploited for TeNPs synthesis (Turner et al, 1999; Summers and Jacoby, 1977; Jasenec et al, 2009; Yurkov et al, 1996). Although there are reports on TeNPs synthesis by bacteria, TeNPs biosynthesis by haloarchaea is not yet reported.

Microbial synthesis of inorganic metal based nanomaterials entails the metal resistance/tolerance mechanism elicited by the microorganism in response to metal stress. Generally, the resistance to Te oxyanion involves physical removal from the vicinity of the cells either through volatilisation (as dimethyl telluride) or through reductive precipitation (as Te^0) (Basnayake et al, 2001; Borghese et al, 2004; Klonowska et al, 2005). Microorganisms responsible for the reduction of Te oxyanion in to Te^0 in nano-dimensions may be considered as biological nano-factories. The mechanism of Te resistance in gram-negative bacteria has been shown to be plasmid mediated, while that of gram-positive is poorly understood (Turner et al, 1995). Activation of the plasmid mediated resistance mechanism requires an upregulation or a mutation, which occurs in response to the presence of TeO_3^{2-} in the vicinity of the microbial cell. Thus, it may not represent the primary microbial metal resistance mechanism, indicating presence of other Te resistance determinants (Taylor, 1999). However, very little is known about how these determinants work and none of them have been clearly established as resistance mechanisms for bacteria. As compared to bacterial systems, there is even lesser

knowledge about tellurite/tellurate resistance in haloarchaea (Srivastava and Kowshik, 2013), or for that matter in archaea as well (Bini, 2010). Three haloalkaliphilic archaea, viz, *Natronococcus occultus*, *Natronobacterium magadii* and *N. gregoryi* have been reported to be resistant to high levels of TeO_3^{2-} , but, the reduced Te was not characterised (Pearion and Jablonski, 1999).

This study reports the intracellular synthesis of needle shaped TeNPs by the haloarchaeon *Halococcus salifodinae* BK3 in presence of 3 mM K_2TeO_3 . Growth kinetics studies exhibited a high level of intrinsic resistance to tellurite. The nanoparticles were found to be antibacterial against both gram-positive and gram-negative organisms, with a better activity against gram-negative organisms.

5.2 Materials and Methods

5.2.1 Determination of MIC of K_2TeO_3 and growth kinetic studies

H. salifodinae BK3 was grown in presence of varying concentrations of potassium tellurite (K_2TeO_3 ; Molychem) to determine the minimum inhibitory concentration (MIC). A concentration range of 0.1-10 mM was used for this study.

Parameters of growth kinetics like specific growth rate (μ), doubling time (t_d) and lag time (t_l) were determined according to Berney et al. (2006) and Breidt et al. (1994), respectively as described in section 2.2.2. In brief the isolate was grown in the presence of 0.3 mM, and 3 mM K_2TeO_3 , and an aliquot of 1 ml was withdrawn every 24 hrs. The absorbance was measured at 600 nm on UV-visible double beam spectrophotometer. Inoculated medium without K_2TeO_3 and un-inoculated medium with 3 mM K_2TeO_3 were used as positive and negative controls, respectively. The experiment was performed in triplicates on different days.

5.2.2 Estimation of tellurite loss from the medium

The tellurite loss from the medium was determined by the colorimetric method using diethyldithiocarbamate (DDTC) as described by Turner et al. (1992). In brief, NTYE medium was inoculated with 2% culture along with 0.3 mM or 3 mM K_2TeO_3 and incubated at 37°C, 110 rpm for 10 days. An aliquot of 500 μl was withdrawn every 24 hrs and centrifuged at $10,000 \times g$ for 5 mins to pellet down the cells. To 100 μl of supernatant, 0.3 M Tris- NaCl

(TN) buffer (pH 7.0) and 2 mM DDTC reagent were added, and the absorbance read at 340 nm to determine the amount of tellurite remaining in the medium. Appropriate positive and negative controls were analysed simultaneously. The assay was carried out in triplicates.

5.2.3 TeNPs biosynthesis and process parameter optimisation

The biosynthesis of TeNPs was carried out by inoculating *H. salifodinae* BK3 in to NTYE medium (2%, OD = 0.6), to which requisite amount of K_2TeO_3 was added at time zero. The culture was incubated at 37°C, 110 rpm. The reduction of TeO_3^{2-} to Te^0 and TeNPs synthesis was allowed for 10 days during which the biomass turned black. The biomass was harvested by centrifugation at $10,000 \times g$ for 30 mins, followed by two washes with deionised water. Subsequently, the biomass was dialysed with frequent changes (once every two hours) of water overnight to remove the ions. The sample was sonicated at 0°C for 15 min, at 3 RPS (40 W). The cell debris was separated from the nanoparticles by first centrifuging the samples at lower speed ($10,000 \times g$, 15 mins) to pellet the cell debris, followed by centrifugation at high speed ($22,000 \times g$, 1 hr) that pellets the TeNPs. The suspension obtained after dialysis was dried in a hot air oven at 70°C, and ground in a mortar and pestle to obtain the nanopowder. Media controls and culture supernatant, both containing 3 mM K_2TeO_3 were also evaluated for TeNPs synthesis.

The process parameters such as medium pH, incubation temperature, and K_2TeO_3 concentration were varied to determine the conditions for maximum yield of TeNPs. *H. salifodinae* BK3 was grown in NTYE with varying conditions as mentioned below:

pH	5.0	5.5	6.0	6.5	7.0	7.5	8.0
K_2TeO_3 conc. (mM)	0.5	1	2	3	4	5	5.5
Temperature (°C)	25	30	35	37	40	45	

The yield was determined by a spectrophotometric method described by Molina et al (2010). A calibration curve of Te^0 was prepared in the concentration range of 10 μM to 10 mM. The Te^0 was obtained by incubating K_2TeO_3 (10 μM - 10 mM) with 3.5 mM $NaBH_4$ for 10 mins at RT. The absorbance was recorded using a UV- visible double beam spectrophotometer at 500 nm. *H. salifodinae* BK3 was allowed to synthesise TeNPs at various conditions of temperature, pH, or K_2TeO_3 concentration and the nanoparticles were extracted and purified. The TeNPs

were then suspended in water and their absorbance was read spectrophotometrically. The molar yields of TeNPs at various conditions were recorded in mM/mM K_2TeO_3 and calculated as described in section 4.2.4. The experiments were carried out in triplicates on different days.

Biosynthesis was carried out at the optimised conditions and the molar yields and yield per gram of CDW were determined over the period of synthesis. TeNPs synthesis was carried out in 1 L medium inoculated with *H. salifodinae* BK3 along with the optimised concentration of K_2TeO_3 . 3 ml aliquots were withdrawn every 24 hours, of which 1 ml was used for growth kinetic analysis, 1 ml was used for determination of CDW and 1 ml was used for yield determination. The molar yield (MY) was calculated as mentioned above. The yield per gram of CDW was calculated as described in section 3.2.4 to determine the efficiency of the process. The experiment was carried out in triplicates on different days.

5.2.4 Nanoparticles characterisation

XRD, TEM, SAED, and EDAX analysis of the ‘as-synthesised’ TeNPs were carried out as described in section 3.2.5. The lattice parameters were determined as described in section 4.2.5.

5.2.5 Effect of tellurite on pigment production

Stationary phase *H. salifodinae* BK3 (8-10 days) grown in the presence of 0.3 mM, and 3 mM K_2TeO_3 , and in the absence of K_2TeO_3 (control) were used to determine the effect of tellurite on pigment production. The biomass was harvested by centrifugation at $10,000 \times g$ for 20 mins, at RT. The pellet obtained was dispersed in acetone and the mixture was vortexed. The solution was sonicated at $0^\circ C$ for 15 min, at 3 RPS (40 W) till the entire pigment was extracted in the solvent. The supernatant was separated from the colourless cell debris by centrifugation ($10,000 \times g$ for 20 mins). The supernatant was scanned between 350-650 nm using UV-visible double beam spectrophotometer.

5.2.6 Nitrate reductase assay and inhibitor studies

The involvement of NADH-dependent nitrate reductase (NR) in TeNPs synthesis and tellurium resistance was determined as described previously in section 3.2.7. Briefly, *H. salifodinae* BK3 was grown in HNB in the presence of 0.3 mM and 3 mM K_2TeO_3 at $37^\circ C$,

110 rpm for 10 days. KNO_3 (0.3 and 3 mM) was used as the positive control and un-inoculated medium with 3 mM K_2TeO_3 served as negative control. The CFE of *H. salifodinae* BK3 was prepared as described in section 3.2.6. 100 μl CFE of *H. salifodinae* BK3 (0.5 g wet weight) grown in presence of 0.3 mM and 3 mM K_2TeO_3 was added to the substrate mixture containing 10 mM KNO_3 , along with 0.2 mM β -NADH. The reaction was stopped after 2 mins by addition of 0.15 mM sulphanilamide solution in 3 mM HCl (Qualigens), followed by 0.19 mM NED solution. The solution was mixed properly and the absorbance of the coloured product was recorded at 540 nm. For negative control, CFE was boiled to destroy enzyme activity and the nitrite content was determined. The nitrite content of the negative control so obtained was subtracted from that of the test, to give total amount of nitrite produced by the enzyme in 2 mins. The effect of NR inhibitor, sodium azide, on nanoparticle synthesis by *H. salifodinae* BK3 was evaluated as described in section 3.2.7. All the studies were performed in triplicates.

5.2.7 Tellurite reductase enzyme assay

Crude extracts (CFE) of *H. salifodinae* BK3 grown in presence of K_2TeO_3 were prepared to determine the tellurite reductase enzyme activity. The CFE of *H. salifodinae* BK3 prepared as described in section 3.2.6, served as the crude enzyme extract. The tellurite reductase activity of the crude extract was assayed according to Chiong et al. (1988). The reaction mixture (1 ml) comprised of 10 mM Tris (pH 7.5), 1 mM K_2TeO_3 , 1 mM NADH and the crude extract. The reduction of the tellurite was measured by recording an increase in absorbance at 500 nm (A_{500}). Boiled crude extract served as negative control. The assay was carried out in the absence of NADH to determine the dependence of the enzyme on NADH. The amount of crude enzyme which resulted in an increase of 0.001 units of $A_{500} \text{ min}^{-1} \text{ ml}^{-1}$ was denoted as 'One unit' of enzymatic activity. Specific activity was expressed as units/mg of protein. The total protein content of the cells was determined by Bradford's method (Bradford, 1976). The reaction was also carried out in presence of 1% SDS, 4 mM β -mercaptoethanol, and at temperatures of 37°C, 70°C, and 100°C for 15 mins, independently to determine the nature of the reducing moiety. All the experiments were performed in triplicates.

5.2.8 Antimicrobial activity of the TeNPs

The Kirby-Bauer disk susceptibility method was used to determine the antimicrobial property of the TeNPs. The gram-negative organisms, *E. coli* ATCC 10536, *E. coli* NCIM 2574, *Pseudomonas aeruginosa* MTCC 2581, and gram-positive *Staphylococcus aureus* ATCC 6538P, and *Micrococcus luteus* were tested for their susceptibility to the synthesised TeNPs. The TeNPs were suspended in deionised water at a final concentration of 10 mg/ml, and appropriate volumes were loaded on the disks to give the following concentrations- 10, 50 and 100 µg Te /disc. Log phase cultures ($\sim 10^6$ CFU/ml) were swabbed on a Mueller-Hinton (MH) agar plate, and the nanoparticle impregnated sterile disks were placed on them. The plates were incubated at 37°C, for 18 hrs, following which the ZoI was recorded. Antibiotic discs of tetracycline (10 µg/disc) and ciprofloxacin (30 µg/disc) served as positive control, and the saline loaded disks served as negative control.

The MIC of the TeNPs against *E. coli* ATCC 10536, *E. coli* NCIM 2574, *P. aeruginosa* MTCC 2581, *S. aureus* ATCC 6538P and *M. luteus* NCIM 2170 was determined by the resazurin microtiter assay (REMA) (LiPuma et al, 2009), as per standard CLSI methods. 100 µl/well of double strength MH broth was added in a 96-well microtiter plate along with appropriate dilutions of the TeNPs prepared in deionised water. 10 µl of 0.1% resazurin sodium salt (Sigma-Aldrich) was added to each well, followed by exponential phase bacterial cells ($\sim 10^6$ CFU/ml), and the volume was made up to 200 µl using sterile distilled water. The plate was incubated in the dark at 37°C, for 24 hrs on a shaking incubator at 110 rpm. The lowest concentration of the TeNPs at which no blue to pink colour change was observed was recorded as the MIC. Appropriate controls were subjected to similar treatments. All experiments were carried out in triplicates.

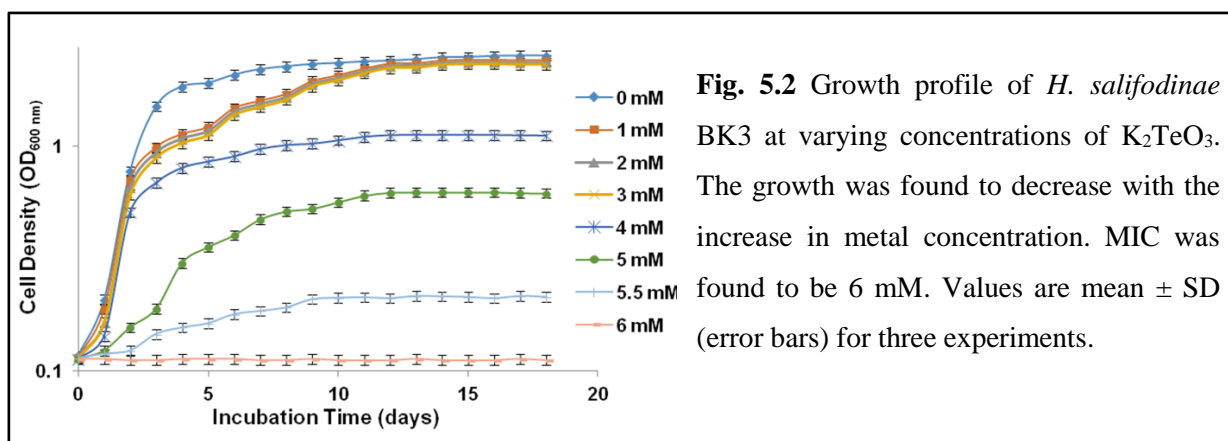
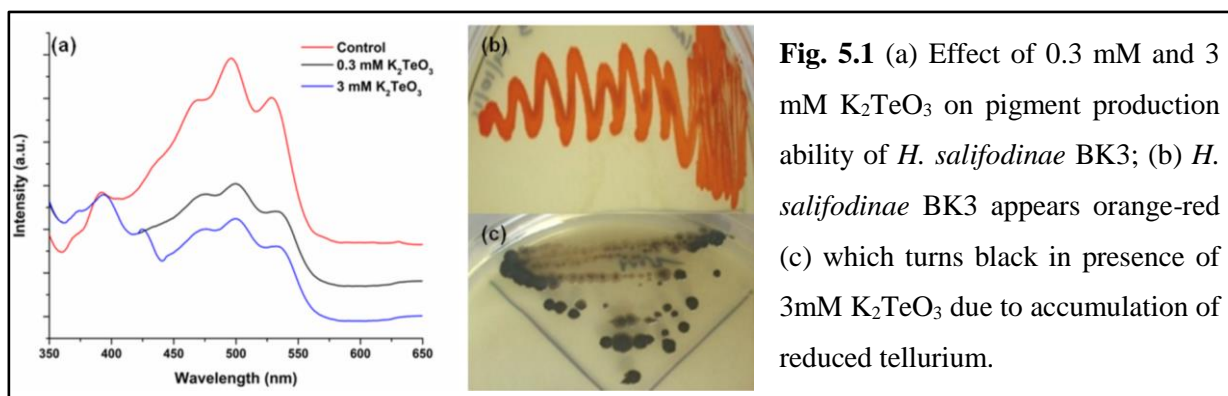
5.2.9 Statistical analysis

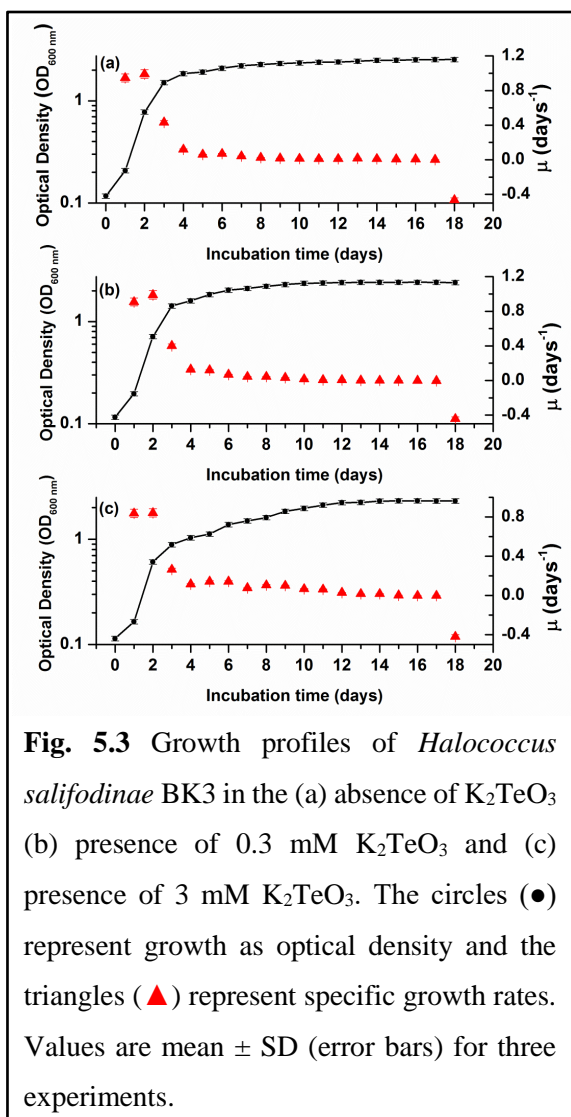
The statistical analysis was carried out as described in section 2.2.5.

5.3 Results and Discussions

5.3.1 Effect of potassium tellurite on growth

The haloarchaeal isolate *H. salifodinae* BK3, during growth in presence of potassium tellurite, exhibited a decrease in pigmentation with the increase in TeO_3^{2-} concentration (Fig. 5.1a). At concentrations above 0.2 mM K_2TeO_3 , *H. salifodinae* BK3 turned black which may be attributed to the reduction of tellurite to elemental tellurium (Fig. 5.1b, c). The growth profiles of *H. salifodinae* BK3 exposed to 1 mM, 2mM and 3 mM K_2TeO_3 were similar to that of unexposed control (cells grown in the absence of K_2TeO_3 ; Fig. 5.2). Concentrations above 3 mM K_2TeO_3 negatively affected the growth of *H. salifodinae* BK3, and no growth was observed at 6 mM or above. MIC of K_2TeO_3 for *H. salifodinae* BK3 was 6 mM.





The effect of K_2TeO_3 on the growth of *H. salifodinae* BK3 was evaluated by growing the isolate in presence of 0.3 mM and 3 mM K_2TeO_3 (Fig. 5.3). *H. salifodinae* BK3 exhibited a maximum specific growth rate (μ) of 0.99 days^{-1} and a lag time (t_l) of 11.8 hrs. In presence of 0.3 mM K_2TeO_3 , the haloarchaeon exhibited growth kinetics parameters very similar to that of control (cells grown in the absence of K_2TeO_3 ; Table 5.1), with no significant difference ($p > 0.05$). At 3 mM K_2TeO_3 , a slight decrease in the μ and an increase in t_l to 14.4 hrs of *H. salifodinae* BK3 were observed, however the difference was insignificant ($p > 0.05$). The blackening of the biomass due to intracellular accumulation of Te^0 was more pronounced for the cells grown in presence of 3 mM K_2TeO_3 , which could be attributed to the availability of higher tellurite

concentration. A decrease in the colony size in presence of 3 mM K_2TeO_3 as compared to control was also observed (Fig. 5.4). This decrease in colony size may arise due to the toxicity exerted by the increased tellurite concentration.

Table 5.1 Growth kinetics parameters of *H. salifodinae* BK3 at different concentrations of K_2TeO_3

<i>H. salifodinae</i> BK3	μ (days^{-1})	t_l (hours)	t_d (hours)
Control (0 mM K_2TeO_3)	0.99	11.8	16.8
0.3 mM K_2TeO_3	0.99	12	16.8
3 mM K_2TeO_3	0.74	14.4	22.48

μ - maximum specific growth rate; t_l - lag time; t_d - doubling time

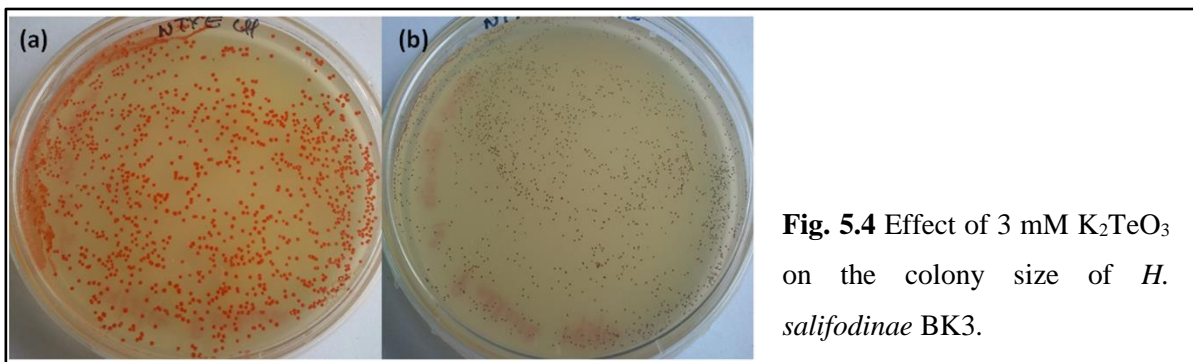


Fig. 5.4 Effect of 3 mM K_2TeO_3 on the colony size of *H. salifodinae* BK3.

The loss of tellurite from the medium as a result of growth of *H. salifodinae* BK3 was correlated to the growth of the isolate in the presence of 0.3 mM and 3 mM K_2TeO_3 (Fig. 5.5). Un-inoculated medium with 3 mM K_2TeO_3 exhibited negligible loss of tellurite from the medium. Tellurite uptake by *H. salifodinae* BK3 was observed from early exponential phase to the late stationary phase, with no effect on the growth rate at 76 $\mu\text{g/ml}$ (0.3 mM) and with a very slight decrease in growth rate at 761 $\mu\text{g/ml}$ (3 mM) K_2TeO_3 . In case of *H. salifodinae* BK3 grown in presence of 76 $\mu\text{g/ml}$ K_2TeO_3 , at the beginning of the stationary phase, *i.e.* on day 3, the tellurite concentration in the medium was 19.03 $\mu\text{g/ml}$, indicating an uptake of ~75% of the tellurite provided. Similarly, by the end of the exponential phase, *i.e.* on day 4, 545 $\mu\text{g/ml}$ of the 761 $\mu\text{g/ml}$ tellurite provided, was taken up by the haloarchaeon leaving ~28 % in the medium. In both the cases the haloarchaeon was able to take up 97% of the K_2TeO_3 provided by the end of the stationary phase (day 10). In a study by Borghese et al (2004), on the effects of the tellurite oxyanion on growth characteristics of the phototrophic bacterium *Rhodobacter capsulatus*, the tellurite uptake was observed during the exponential phase alone, and the oxyanion was found to negatively affect the growth rate of the culture. As *H. salifodinae* BK3 exhibited uptake of tellurite from the early exponential phase, for nanoparticles synthesis, tellurite was added at the time of inoculation. This eliminates the requirement for monitoring of growth phase of the haloarchaea which is advantageous for TeNPs synthesis.

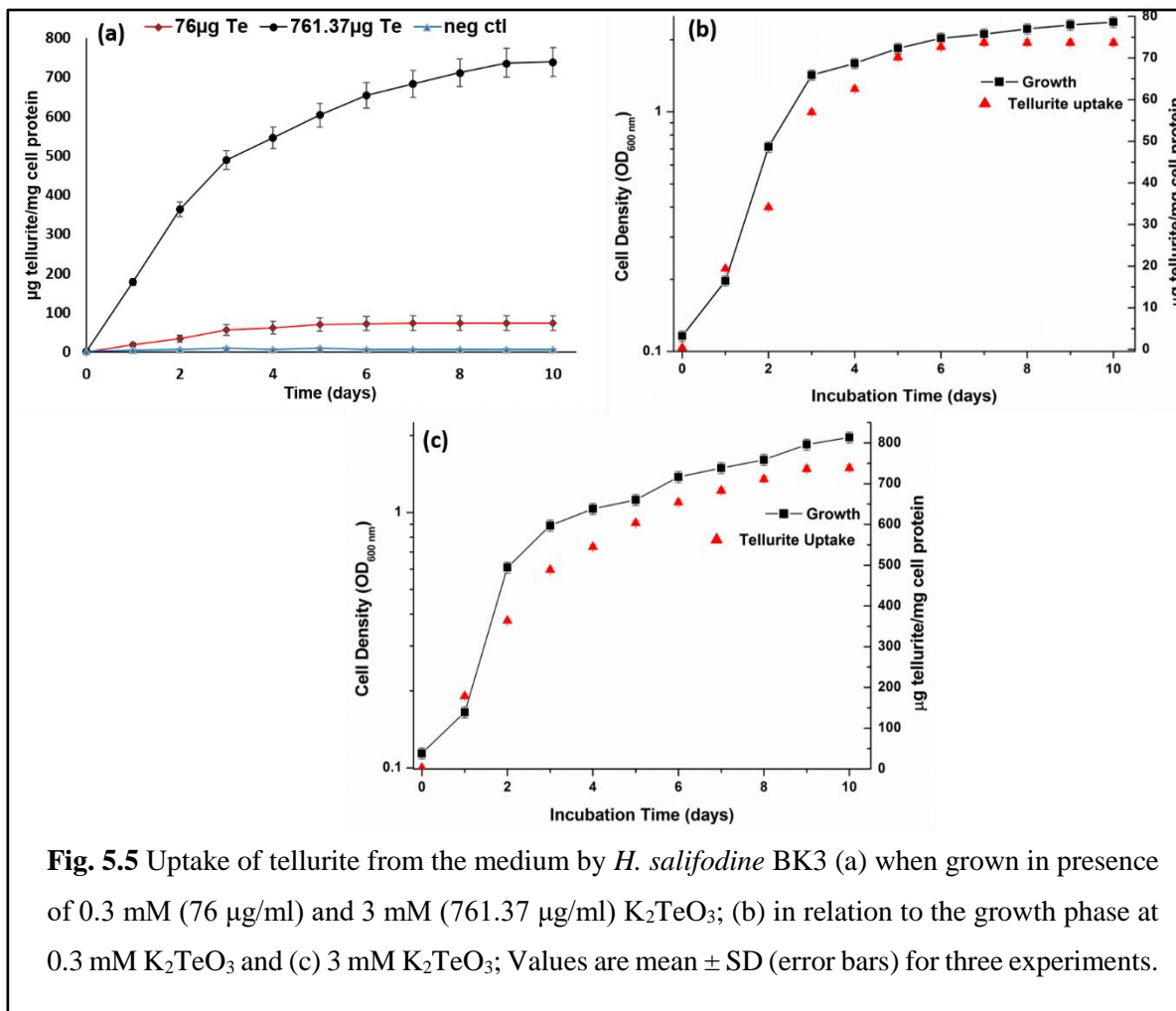


Fig. 5.5 Uptake of tellurite from the medium by *H. salifodine* BK3 (a) when grown in presence of 0.3 mM (76 µg/ml) and 3 mM (761.37 µg/ml) K₂TeO₃; (b) in relation to the growth phase at 0.3 mM K₂TeO₃ and (c) 3 mM K₂TeO₃; Values are mean ± SD (error bars) for three experiments.

5.3.2 Tellurium nanoparticles synthesis and characterisation

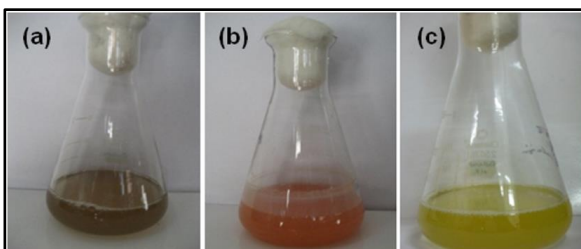


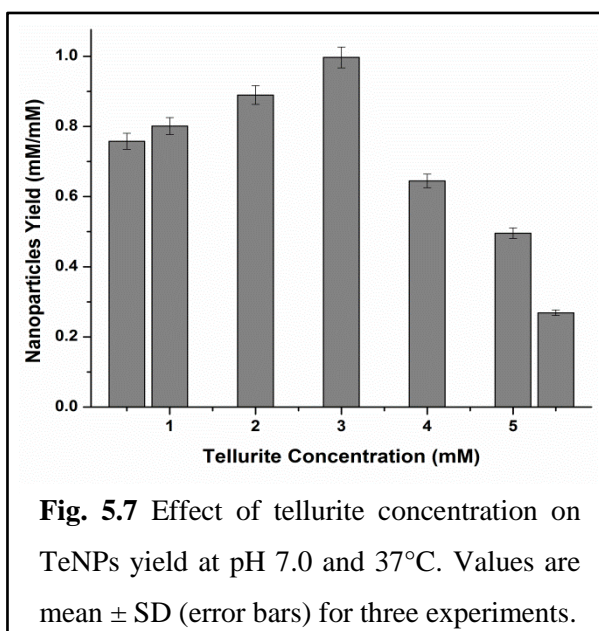
Fig. 5.6 Growth of *H. salifodinae* BK3 (a) in presence of K₂TeO₃ and (b) in absence of K₂TeO₃; (c) The media components did not result in reduction of TeO₃²⁻ in the absence of the culture.

Tellurium nanoparticles synthesis has been studied in various bacteria (Baesman et al, 2007; Zare et al, 2012; Basnayake et al, 2001), however, haloarchaea have not yet been explored for the same. *H. salifodinae* BK3 which appears orange-red turns black when grown in presence of K₂TeO₃. The black colouration of the culture in presence of K₂TeO₃ is indicative of the TeO₃²⁻ reduction, and TeNPs synthesis. Media

controls and culture supernatant did not result in reduction of tellurite, showing that the TeNPs synthesis is a culture-dependent phenomenon (Fig. 5.6). The TeNPs were found to be intracellular.

Process parameters such as K_2TeO_3 concentration, medium pH, and incubation temperature were optimised to obtain maximum yield of TeNPs. The haloarchaeon was grown at varying conditions as described in section 5.2.5, and following synthesis at these conditions, the nanoparticles were extracted and their yield determined.

K₂TeO₃ concentration



A concentration range of 0.5 mM to 5.5 mM K_2TeO_3 was tested to determine the optimum concentration for TeNPs synthesis. *H. salifodinae* BK3 exhibited maximum TeNPs synthesis in presence of 3 mM K_2TeO_3 with a yield of 0.997 mM/ mM K_2TeO_3 (Fig. 5.7a). The yield of TeNPs at 2 mM K_2TeO_3 was very similar to that of 3 mM K_2TeO_3 , with no significant difference ($p < 0.05$), although the growth at 2 mM K_2TeO_3 was better than at 3 mM K_2TeO_3 . The yield of TeNPs at lower concentrations

of K_2TeO_3 (0.5, and 1 mM) was found to be very similar. At concentrations of 4 mM, 5 mM and 5.5 mM, the yield decreased with the increase in tellurite concentrations. The yields obtained at these concentrations were significantly lower ($p > 0.05$) from that obtained at 3 mM K_2TeO_3 which may be attributed to the increase in toxicity at higher concentrations of K_2TeO_3 . Although the organism was able to grow and synthesise TeNPs at 5 mM and 5.5 mM K_2TeO_3 , both growth and TeNPs synthesis were negatively affected. Thus, a concentration of 3 mM K_2TeO_3 was used for TeNPs synthesis.

Medium pH

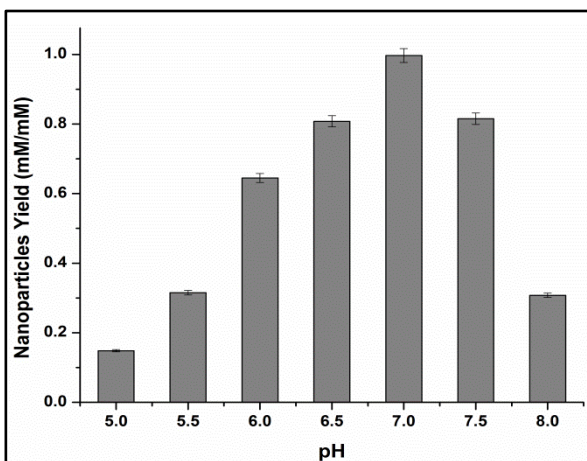


Fig. 5.8 Effect of pH on TeNPs yield at 37°C using 3 mM K_2TeO_3 precursor. Values are mean \pm SD (error bars) for three experiments.

The TeNPs synthesis by *H. salifodinae* BK3 was evaluated between pH 5.0- pH 8.0. Maximum yield of 0.997 mM/ mM K_2TeO_3 was obtained at pH 7.0 (Fig. 5.8). At pH of 5.0 and 5.5, the growth of haloarchaeal cultures in the absence of K_2TeO_3 was very poor, therefore the yield of TeNPs was significantly lower ($p < 0.05$) as compared to that at pH 7.0. The pH range for growth of *Halococcus* is 6.0-9.5, with the optimum at pH 7.0 (Grant, 2015). Thus, as the pH increased from 6.0 to 6.5, a concomitant

increase in yield was observed. Yield of TeNPs at pH 7.5 was 0.815 mM/ mM K_2TeO_3 , which was not significantly different ($p > 0.05$) from the yield obtained at pH 7.0. However, pH 8.0 significantly lowered the yield of TeNPs, which may be attributed to the pH changing to alkaline. Based on these results, TeNPs synthesis was carried out at pH 7.0.

Incubation Temperature

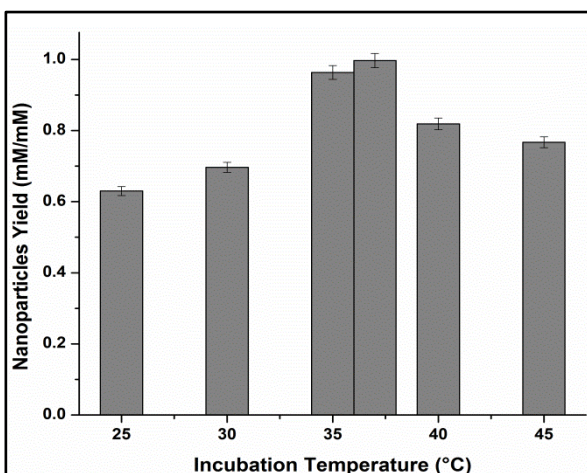


Fig. 5.9 Effect of temperature on TeNPs yield at pH 7.0 using 3 mM K_2TeO_3 . Values are mean \pm SD (error bars) for three experiments.

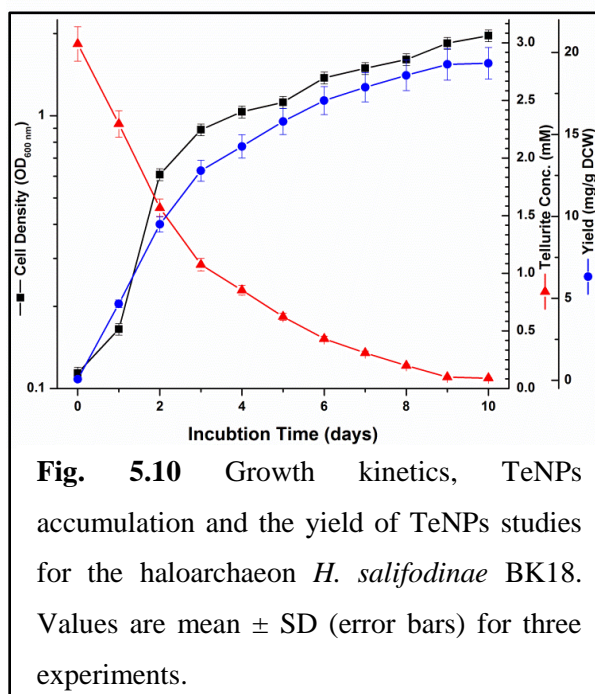
A temperature range of 25°C to 45°C was tested to determine the optimum temperature for TeNPs synthesis by *H. salifodinae* BK3. Maximum TeNPs synthesis was obtained at 35°C, and 37°C with a yield of ~ 0.98 mM/ mM K_2TeO_3 (Fig. 5.9). As the temperature increased from 25 to 37°C, the yield of TeNPs increased, albeit the difference in yield between 30, 35, and 37°C was insignificant ($p > 0.05$). The optimum range of temperature for growth of *Halococcus* is

30°C to 40°C (Grant, 2015). The haloarchaeal cultures exhibit slow growth at 45°C, and therefore, the yield of TeNPs was also lower. Thus, based on these results TeNPs synthesis was carried out at 37°C.

A summary of optimal parameters for TeNPs synthesis is represented in table 5.2.

Table 5.2 Summary of optimal parameters for maximal production of TeNPs

Parameters	Optimal Conditions
Time of K ₂ TeO ₃ addition	T= 0 hrs
pH	7.0
K ₂ TeO ₃ concentration	3 mM
Incubation temp	37°C



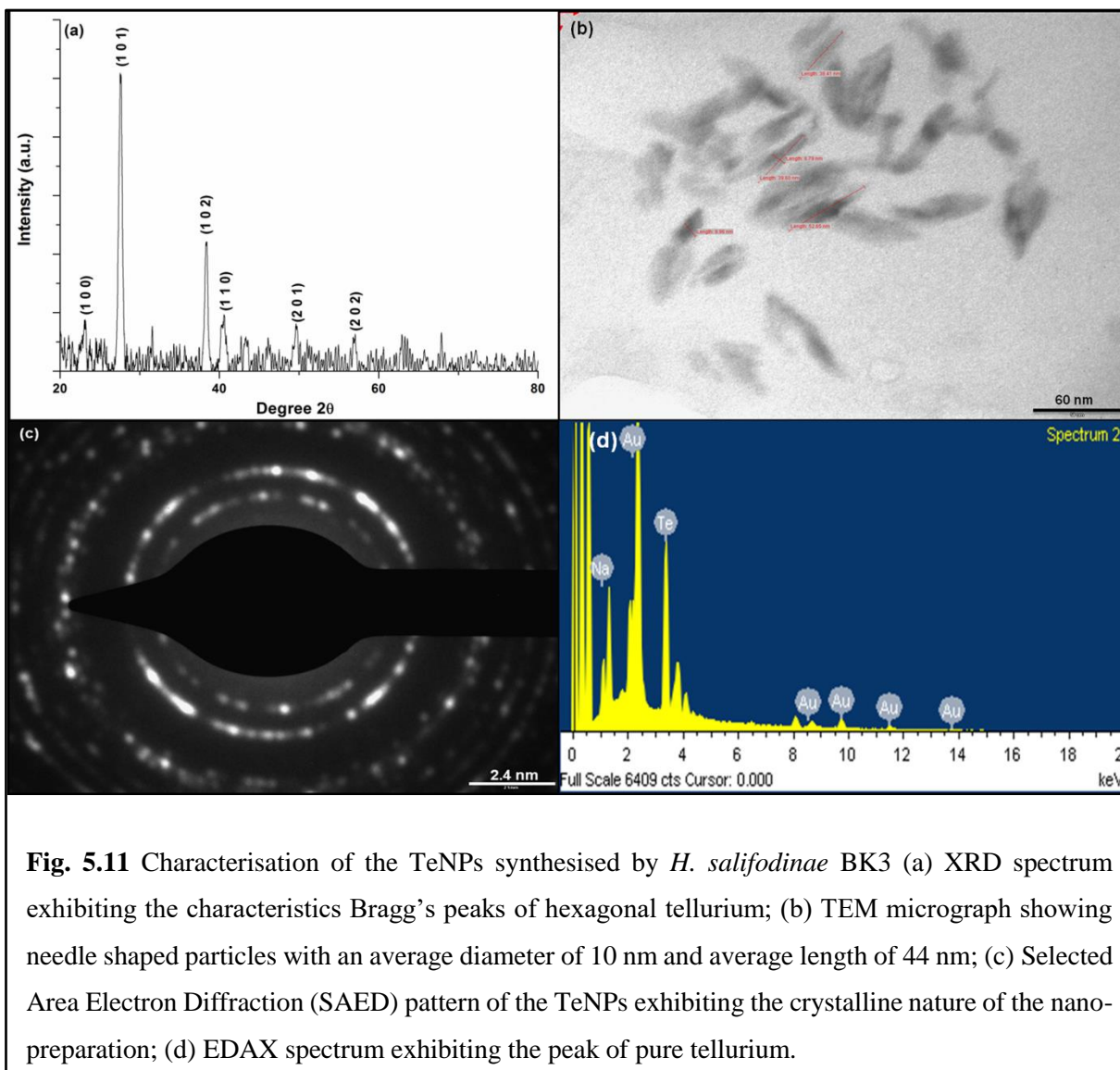
The time course of TeNPs accumulation, tellurite loss from the medium, and the growth is shown in Fig. 5.10. As mentioned in previous section (5.3.1), *H. salifodinae* BK3 exhibited a μ of 0.74 days⁻¹, in presence of 3 mM K₂TeO₃ and a doubling time of 22.48 hrs. *H. salifodinae* BK3 exhibited TeNPs accumulation from the early exponential phase. Both molar yield and the yield with respect to the biomass were estimated during the synthesis. Maximum yield (19.34 mg/g CDW; 0.97 mM/mM K₂TeO₃) was

obtained on day 10, exhibiting an efficiency of 97%. The loss of 3% tellurite is attributed to the residual tellurite in the medium, which remained un-utilised by the haloarchaeon. Table 5.3 summarises the various kinetic and yield parameters of TeNPs synthesis by *H. salifodinae* BK3.

Table 5.3 TeNPs synthesis kinetics and yield parameters.

Kinetics and Yield parameters	Values
μ (days ⁻¹)	0.74
t_d (hrs)	22.48
t_i (hrs)	14.4
Y (mg/g)	19.34
MY (mM/mM)	0.97
Efficiency (%)	97

X-Ray diffractometry was carried out to determine the crystalline nature of the ‘as-synthesised’ TeNPs. The XRD profile of *H. salifodinae* BK3 synthesised TeNPs (Fig. 5.11a) exhibited intense peaks at 2θ values of 20.14° , 27.56° , 38.44° , and 40.62° , corresponding to (1 0 0), (1 0 1), (1 0 2), and (1 1 0) sets of lattice planes for hexagonal tellurium (ICDD card no/file no 36-1452). The crystallite domain size as calculated by Debye-Scherrer formula using the line width of the (1 0 1) plane was 11.3 nm. The lattice parameters a and b were calculated for hexagonal system for the plane (1 0 1) and found to be 0.443 nm, and 0.597 nm, respectively. Morphological characterisation of the ‘as-synthesised’ TeNPs using TEM exhibited needle shaped nanoparticles with an average diameter of 10 nm, and length of 44 nm (Fig. 5.11b). The aspect ratio was found to be 1:4.4. Most of the studies on the TeNPs biosynthesis have reported the synthesis of tellurium nano-rods and needle shaped TeNPs, with the exception of tellurium nanospheres synthesised by *S. barnesii* (Borghese et al, 2004; Klonowska et al, 2005; Amoozegar et al, 2008; Zare et al, 2012; Baesman et al, 2007). SAED analysis revealed numerous diffraction rings which may be indexed to the hexagonal tellurium and co-relates to the XRD data (Fig. 5.11c). Elemental analysis by EDAX exhibited a peak at 3.6 keV corresponding to tellurium (Fig. 5.11d). The peaks due to sodium may be attributed to the media components, while the gold peak arises due to the gold coating.

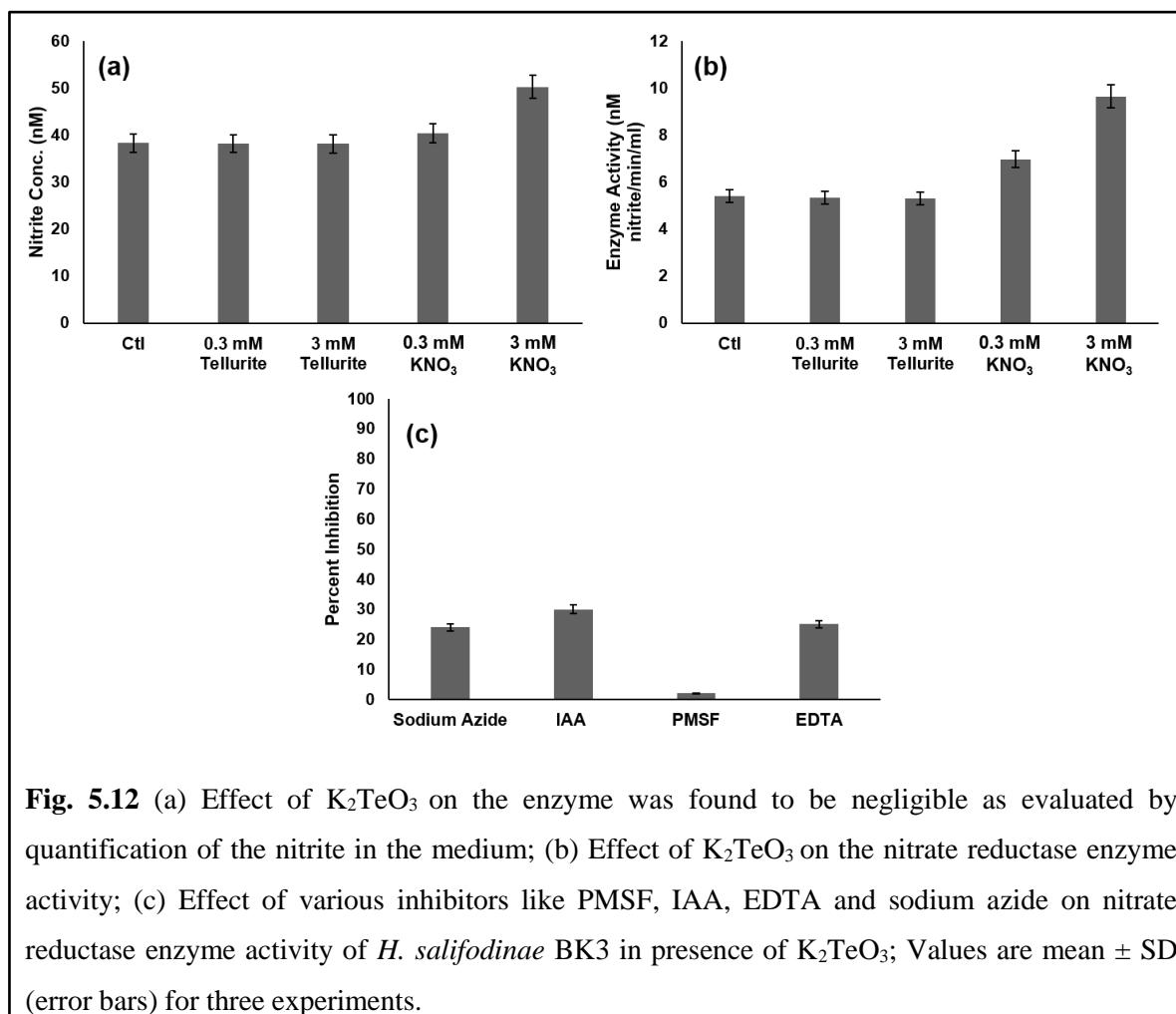


5.3.3 Mechanism of TeNPs synthesis

Nanoparticles synthesis is usually a result of the metal resistance mechanisms elucidated by microorganisms. The primary or the first defence against metal toxicity generally involves an increased efflux or a decreased influx of the metals. Tellurium resistance instead, entails either volatilisation or reductive precipitation of tellurite (Borghese et al, 2004; Klonowska et al, 2005). Certain gram-positive and gram-negative bacteria have exhibited low level of intrinsic resistance to TeO_3^{2-} (Turner et al, 1995). In these bacteria, various plasmid and chromosome mediated tellurite resistance (Te^R) determinants are shown to be responsible for tellurite resistance (Taylor et al, 1994; Turner et al, 1995; O'Gara et al, 1997; Cournoyer et al, 1998).

According to a model proposed by Taylor et al (1999), in *E. coli* the TeO_3^{2-} enters into the cell through the phosphate transporter, following which it is reduced by the inner membrane nitrate reductases (Avazeri et al, 1997). The TeO_3^{2-} that circumvents this initial line of defence may then get reduced to Te^0 by cellular reduced thiols or get converted enzymatically to volatile methyl or hydride compounds. As nitrate reductase (NR) was found to be involved in SNPs synthesis by *H. salifodinae* BK3, the role of NR in tellurite resistance and TeNPs synthesis was evaluated.

The nitrite content of the medium was estimated, after the growth of *H. salifodinae* BK3 in the presence and absence of 0.3 mM and 3 mM K_2TeO_3 (Fig. 5.12a). The nitrite content in presence of K_2TeO_3 was found to be similar to that of the control (cells grown in the absence of $\text{K}_2\text{TeO}_3/\text{KNO}_3$). In presence of 0.3 mM and 3 mM KNO_3 , the nitrite content was higher than the control (cells grown in the absence of $\text{K}_2\text{TeO}_3/\text{KNO}_3$). This increase is attributed to the increase in the substrate (NO_3^{2-}) for NR. Similarly, the NR activity (Fig. 5.12b) of the CFE of the cells grown in presence of 0.3 mM and 3 mM K_2TeO_3 was found to be 5.32 and 5.29 nM Nitrite/min/ml, respectively, similar to that of the control (5.40 nM Nitrite/min/ml). However, the activity for the CFE of the cells grown in presence of 0.3 mM and 3 mM KNO_3 was found to be higher than the control. The nitrite content and the enzyme activity, for cells grown in presence of K_2TeO_3 were similar to that of the control, which indicates that NR may not be involved in tellurite reduction. To further confirm this, inhibitor study was carried out using specific enzyme inhibitors such as PMSF, IAA, EDTA, and nitrate reductase inhibitor, sodium azide (as discussed in section 3.3.2). *H. salifodinae* BK3 grown in presence of 10 mM inhibitor exhibited growth similar to positive control (haloarchaeon grown in the absence of inhibitors), with the exception of IAA, which delayed the growth slightly. In presence of K_2TeO_3 and the inhibitors, *H. salifodinae* BK3 did not exhibit any change in nanoparticles synthesis. Further the NR enzyme activity was estimated in presence of 10 mM inhibitor and 3 mM K_2TeO_3 and compared to that of the cells grown only in the presence of 3 mM K_2TeO_3 . Sodium azide, a known inhibitor of NR, did not inhibit the enzyme and the activity was similar to that of the cells grown in presence of 3 mM K_2TeO_3 without the inhibitor (Fig. 5.12c). Thus, the enzyme NR was not involved in TeNPs synthesis and tellurite resistance in *H. salifodinae* BK3.



Tellurium reduction in certain bacteria such as *Mycobacterium avium*, *Streptococcus faecalis*, *E. coli*, and *Thermus thermophilus* HB8 is attributed to tellurite reductase activity (Cooper and Few, 1952; Terai et al, 1958; Thomas et al, 1963; Chiong et al, 1988a). Therefore, the tellurite reductase activity of the CFE of *H. salifodinae* BK3 was estimated by measuring the increase in absorbance at 500 nm, which indicates the generation of reduced tellurium, in presence and absence of NADH. NADH is a coenzyme that is essential for tellurite reductase activity (Chiong et al. 1988a; Pearion and Jablonski, 1999). The CFE of cells grown in the presence of 0.3 mM and 3 mM K₂TeO₃ exhibited an increase in the absorbance at 500 nm ($\Delta A_{500} \text{ min}^{-1}$), which was not observed when the assay was carried out in the absence of NADH (Fig. 5.13). Thus, the tellurite reductase activity of the CFE of *H. salifodinae* BK3 requires NADH for its function. The specific enzyme activity of the CFE for cells grown in presence of 0.3 mM and 3 mM K₂TeO₃ was 4.76 units/mg of protein and 11.39 units/mg of protein, respectively. Un-

induced cells (cells grown in the absence of K_2TeO_3) exhibited a specific activity of 0.22 units/mg of protein. This suggests that the ability to catalyse the reduction of TeO_3^{2-} to Te^0 is not a constitutive property of the haloarchaeon. Growth in presence of K_2TeO_3 induced the enzyme activity which was found to be dose-dependent, i.e., the activity increased with the increase in tellurite concentration. Similar inducible enzyme has been reported in *T. flavus* AT-62 whereas, the enzyme of *T. thermophiles* was found to be constitutive, and its activity did not exhibit any correlation with the tellurite concentration (Chiong et al, 1988a, b). To further understand the nature of the reducing moiety, the reaction was also carried out in presence of 1% SDS, β -mercaptoethanol, and after heat treatment of the CFE at 37°C, 70°C, and 100°C for 15 mins (Table 5.4). The tellurite reductase activity of the CFE of induced *H. salifodinae* BK3 was lost in the presence of SDS, suggesting that the reducing factor is proteinaceous. SDS binds to hydrophobic regions of proteins to perturb the secondary, tertiary, and quaternary structure producing a negatively charged linear polypeptide chain (Bhyuyan, 2009). The β -mercaptoethanol treated CFE of the induced *H. salifodinae* BK3 did not exhibit a decrease in enzyme activity. This is indicative of absence of disulphide linkages in the reducing factor, as β -mercaptoethanol treatment results in the cleavage of disulphide linkages present within the protein, resulting in the inactivation of the enzyme (Chang, 1997). A similar characteristic of proteinaceous tellurite reductase lacking disulphide linkages was reported in *T. flavus* (Chiong et al, 1988). 37°C treated CFE of induced haloarchaeal cells exhibited normal tellurite reductase activity, which was completely lost by heat treatment at 70°C for 15 mins. This suggests that the enzyme is heat labile. A heat labile tellurite reductase with similar characteristics was reported in *N. occultus* (Pearion and Jablonski, 1999), while the tellurite reductase of *T. flavus* AT-62 and *T. thermophiles* were found to be heat-stable (Chiong et al. 1988a,b). As *T. flavus* AT-62 and *T. thermophiles* are thermophiles, it follows that the tellurite reductase of these organisms' exhibit heat stability. Thus, the tellurite reductase of *H. salifodinae* BK3 required NADH for its activity, was proteinaceous without any disulphide linkages, and was heat labile.

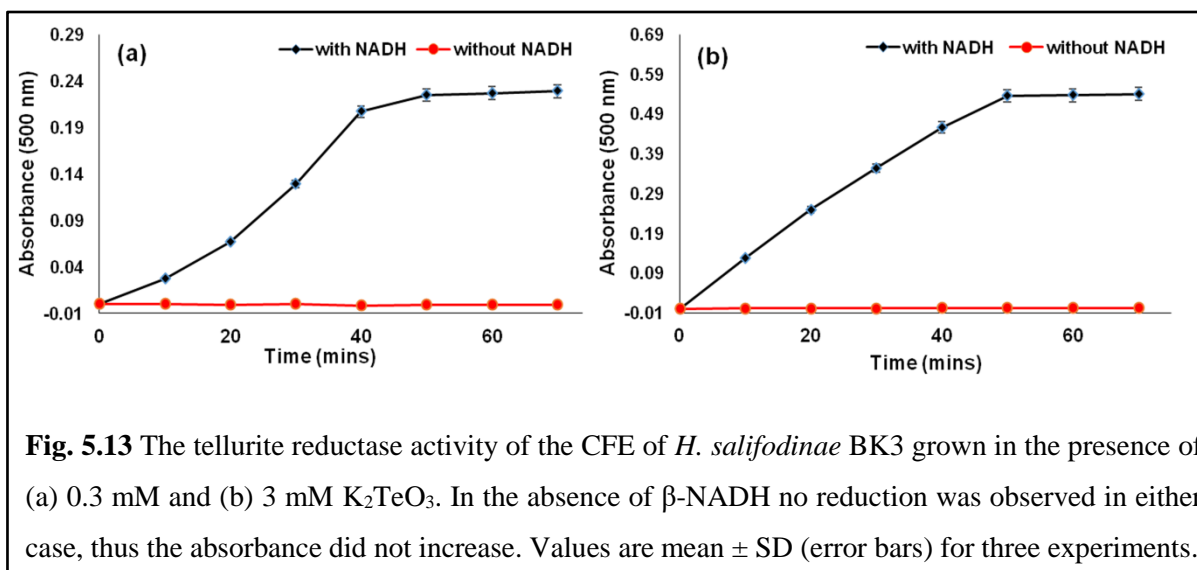


Table 5.4 Tellurite reductase activity of the cell free extract (CFE) of *H. salifodinae* BK3 at various conditions

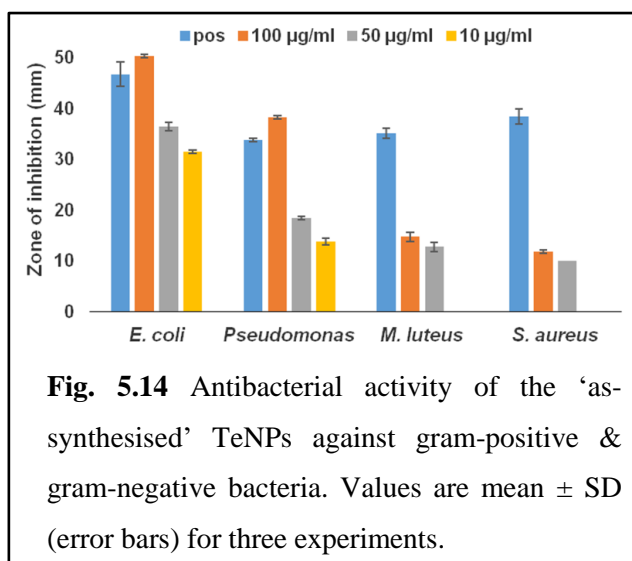
Assay Conditions	Activity (U/ mg of protein)
CFE (un-induced cells)	<0.0002
CFE _{0.3te}	0.001
CFE _{3te}	0.001
CFE (un-induced cells) + NADH	0.22
CFE _{0.3te} + NADH	4.76
CFE _{3te} + NADH	11.39
CFE _{0.3te} + NADH + 1% SDS	<0.0001
CFE _{3te} + NADH + 1% SDS	<0.0001
CFE _{0.3te} + NADH + β- mercapto ^a	4.75
CFE _{3te} + NADH + β- mercapto ^a	11.24
CFE _{0.3te} + NADH (37 ° C, 15 mins)	4.74
CFE _{3te} + NADH (37 ° C, 15 mins)	11.33
CFE _{0.3te} + NADH (80 ° C, 15 mins)	<0.0001
CFE _{3te} + NADH (80 ° C, 15 mins)	<0.0001
CFE _{0.3te} + NADH (100 ° C, 15 mins)	<0.0001
CFE _{3te} + NADH (100 ° C, 15 mins)	<0.0001

CFE_{0.3te}- CFE prepared from *H. salifodinae* BK3 exposed to 0.3 mM K₂TeO₃;

CFE_{3te}- CFE prepared from *H. salifodinae* BK3 exposed to 3 mM K₂TeO₃;

^a- 4 mM β- mercaptoethanol

5.3.4 Antimicrobial activity



The antibacterial properties of the biogenic TeNPs were evaluated against gram-negative *E. coli* ATCC 10536, *P. aeruginosa* MTCC 2581, and gram-positive *S. aureus* ATCC 6538P, and *M. luteus* NCIM 2170. The TeNPs exhibited excellent antimicrobial activity against gram-negative organisms as compared to gram-positives (Fig. 5.14; 5.15). In case of *E. coli* ATCC 10536 and *P. aeruginosa*

MTCC 2581, inhibition was observed at 10 $\mu\text{g/ml}$, and the ZoI increased with increase in TeNPs concentration. At 10 $\mu\text{g/ml}$ TeNPs, the growth of gram-positive *S. aureus* ATCC 6538P, and *M. luteus* NCIM 2170 remained unaffected, however ZoI were observed at higher concentrations of 50 $\mu\text{g/ml}$, and 100 $\mu\text{g/ml}$ TeNPs (Fig. 5.14). Tellurium and its compounds found historical applications as antimicrobial and therapeutic agents prior to the discovery of antibiotics (Cooper, 1971). More recently, tellurium is re-emerging as an antimicrobial agent and TeNPs have been reported to be better antibacterial agents as compared to sodium tellurite (Lin et al, 2012). The TeNPs, owing to their large surface-to volume ratio, exhibit antibacterial activity at lower concentrations as compared to the concentrations of sodium/potassium tellurite required to achieve a similar level of bactericidal effect. Similarly, the concentrations of SNPs required to achieve bacterial death is higher than that of TeNPs (Lin et al, 2012). At the same time the TeNPs were shown to be 3-4 times less toxic to human cells as compared to SNPs or tellurite. In order to determine whether TeNPs exhibited any strain specificity, the antibacterial activity of the TeNPs was evaluated against two different strains of *E. coli*, ATCC 10536 and NCIM 2574. However, no difference in the activity and thus no strain specificity was observed. The MIC for gram-negative organisms was found to be lower than that of gram-positive, confirming that the gram-negative organisms are more susceptible to the biogenic TeNPs (Table 5.5). Other studies have also reported biogenic TeNPs that exhibit better antibacterial activity against gram-negative bacteria at lower concentrations, as compared to

that against gram-positive bacteria (Zare et al. 2012; Lin et al. 2012). The exact mechanism of antimicrobial activity of TeNPs is not known, however it was proposed that dispersion of TeNPs in the bacterial growth medium results in its oxidation. TeO_3^{2-} is released that gains entry into the bacterial cell via the phosphate transporter, leading to generation of ROS, glutathione depletion, and/or damage of metabolic enzymes resulting in bacterial killing (Perez et al. 2007; Calderon et al. 2009; Lin et al. 2012). TeNPs have also been shown to have antifungal properties (Zare et al, 2013), and thus, biogenic TeNPs exhibit potential as antimicrobial agents.

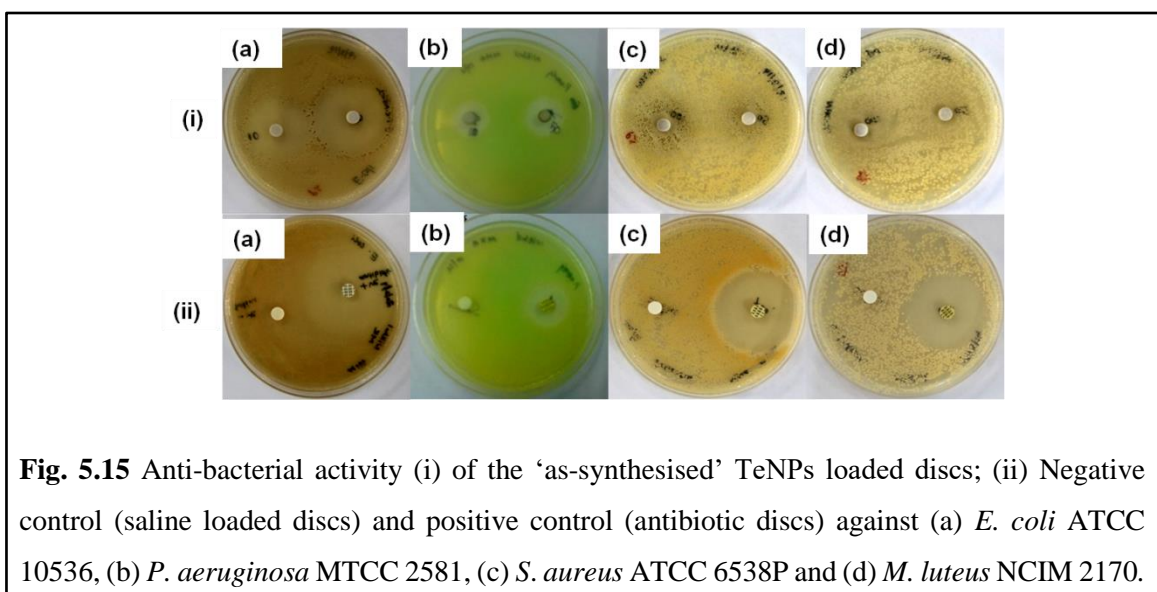


Fig. 5.15 Anti-bacterial activity (i) of the ‘as-synthesised’ TeNPs loaded discs; (ii) Negative control (saline loaded discs) and positive control (antibiotic discs) against (a) *E. coli* ATCC 10536, (b) *P. aeruginosa* MTCC 2581, (c) *S. aureus* ATCC 6538P and (d) *M. luteus* NCIM 2170.

Table 5.4 MIC of the TeNPs against gram-positive and gram-negative organisms.

Organism	MIC ($\mu\text{g/ml}$)
<i>E. coli</i> ATCC 10536	2.5
<i>E. coli</i> NCIM 2574	2.5
<i>P. aeruginosa</i> MTCC 2581	7.5
<i>S. aureus</i> ATCC 6538P	20
<i>M. luteus</i> NCIM 2170	17.5

5.4 Conclusion

In this study, *Halococcus salifodinae* BK3 was successfully used for the intracellular synthesis of tellurium nanoparticles. The needle shaped TeNPs were found to possess hexagonal crystalline facets, with lattice parameters $a = 0.443$ nm and $b = 0.597$ nm, a crystallite domain size of 11.3 nm and an aspect ratio of 1:4.4. The haloarchaeon was found to exhibit growth similar to that of the control in presence of 0.3 mM K_2TeO_3 and a slightly decreased growth in the presence of 3 mM K_2TeO_3 . The NADH-dependent tellurite reductase was involved in the detoxification of tellurite to black tellurium, conferring tellurite resistance to *H. salifodinae* BK3 and resulting in synthesis of TeNPs. The TeNPs were found to exhibit antibacterial activity against both gram-negative and gram-positive bacteria, with a better activity against gram-negative organisms.

CHAPTER 6

Biosynthesis of Antineoplastic Selenium Nanoparticles by the Moderate Halophilic Bacterium *Idiomarina* sp. PR58-8¹

6.1 Introduction

Selenium (Se) is an essential micronutrient, with 55 µg/day of recommended dietary allowance (RDA) for adults and children above 14 years of age. Se gets incorporated in various proteins (Allan et al. 1999) and has numerous health benefits (Fairweather-Tait et al. 2011; Rayman, 2012) as described in section 4.1. As discussed in detail (section 4.1) elemental Se nanoparticles (SeNPs) present an excellent alternative to selenocompounds for cancer therapy and prevention. They exhibit low toxicity towards non-cancerous cell and unique biological activity, while being cytotoxic towards cancer cells at lower concentrations (Chen et al. 2008; Estevez et al. 2014).

Although synthesis of these chemotherapeutic and/or chemopreventive SeNPs has been achieved by numerous physical and chemical methods (Lu et al. 2002; Jiang et al. 2003; Gedanken, 2004), the process is disadvantageous. Biological methods of nanofabrication employing microorganisms overcome these drawbacks resulting in nanoparticles capped with biomolecules (Mohanpuria et al. 2008). In view of this, numerous bacteria, fungi and archaea have been used for SeNPs synthesis (Tam et al. 2010; Sarkar et al. 2011; Srivastava et al. 2014). Here we report the intracellular synthesis and characterisation of SeNPs by a moderate halophilic marine bacterium, *Idiomarina* sp. PR58-8. The antiproliferative properties of these SeNPs against human cervical cancer cell line, HeLa and its mechanism is also reported.

6.2 Materials and Methods

6.2.1 Organism and culture maintenance

Idiomarina sp. PR58-8 was isolated in our laboratory previously by Seshadri et al. (2012), from the soil samples of the banks of Mandovi Estuary, Goa, India. The culture was stored as

¹ This work is published as: **Srivastava P**, Kowshik M (2016) Anti-neoplastic selenium nanoparticles from *Idiomarina* sp. PR58-8. *Enzyme and Microbial Technology* 2016 doi: 10.1016/j.enzmictec.2016.08.002

glycerol stocks at -80°C . Zobell marine broth 2216 (ZMB) was used for revival, enrichment, growth and sub-culturing.

6.2.2 MIC determination and growth kinetics studies

Idioamrina sp. PR58-8 was grown in ZMB 2216 medium in the presence of sodium selenite (Na_2SeO_3 ; 0.05- 12 mM) to determine the minimum inhibitory concentration (MIC). Na_2SeO_3 was prepared as a 1 M stock in SDW and filter sterilised. The cultures were incubated at 37°C , for 72 hrs under agitation (110 rpm). The minimum concentration of Na_2SeO_3 at which no growth was observed was designated as the MIC. Appropriate negative controls were also run simultaneously. Growth was indicated by brick-red colouration.

Further, the growth kinetics of *Idiomarina* sp. PR58-8 was determined in presence of 4 mM and 8 mM Na_2SeO_3 . In brief, ZMB 2216 was inoculated with the 1 % culture, supplemented with the requisite amount of Na_2SeO_3 , and the flasks were incubated at 37°C , 110 rpm. An aliquot of 1 ml was withdrawn every 4 hrs, till 60th hr, and the total protein content of the cells was estimated by Bradford's method using BSA as the standard (Bradford, 1976). The growth kinetics parameters such as specific growth rate (μ ; hrs^{-1}), lag time (t_l ; mins) and doubling time (t_d ; mins) were determined as described in section 2.2.2 The growth kinetics parameters of *Idiomarina* sp. PR58-8 grown in presence of Na_2SeO_3 were compared with that of control (culture grown in the absence of Na_2SeO_3).

6.2.3 Estimation of selenite content

The selenite concentration of the supernatant and cell pellet of *Idiomarina* sp. PR58-8 grown in presence of Na_2SeO_3 was estimated to determine the selenite uptake by the cells. The selenite concentration in the supernatant was determined according to Watkinson (1966) using 2,3-DAN with minor modifications. In brief, the culture was grown in the presence of 4 mM and 8 mM Na_2SeO_3 and an aliquot of 1 ml was withdrawn every 4 hrs starting from 0 hr. The aliquots were centrifuged and the supernatants were used for determination of selenite content, while the cell pellet was used to estimate the selenite uptake, as described previously in section 4.2.4.

6.2.4 Selenium nanoparticles synthesis and optimisation of process parameters

Idiomarina sp. PR58-8 was grown in ZMB 2216 in presence of requisite amounts of Na_2SeO_3 at 37°C, 110 rpm for 48 hrs. The SeNPs synthesis was indicated by brick-red colouration of the medium. Culture supernatant and medium controls were also incubated with the same concentration of Na_2SeO_3 and acted as negative controls. The SeNPs were extracted from the cells by wet heat sterilisation process in a laboratory autoclave at 121°C, 15 psi for 20 mins. The pellet obtained on centrifugation ($10,000 \times g$, 20 mins), was dialysed against deionised water for 12 hrs with change of water every 2 hrs. The dialysed samples were dried in a hot air oven at 70°C overnight, and the powder obtained was ground in a mortar and pestle. The nanopowder was used for characterisation studies. The molar yield and yield with respect to biomass were determined as described in section 4.2.4 and 3.2.4, respectively.

Conditions such as medium pH, incubation temperature and Na_2SeO_3 concentration were varied to determine the conditions for maximum yield of SeNPs. *Idiomarina* sp. PR58-8 was grown in ZMB 2216 at following conditions and the yield of SeNPs was determined as mentioned above.

pH	4.5	5.0	5.5	6.0	6.5	7.0	7.5	8.0
Na_2SeO_3 conc. (mM)	0.05	0.5	1.0	2.0	4.0	6.0	8.0	9.0
Temperature (°C)	20	25	30	35	37	40	45	

6.2.5 Characterisation of the SeNPs

XRD, crystallite domain size, UV-visible spectroscopic, TEM, and SAED analysis of the ‘as-synthesised’ SeNPs were carried out as described previously in section 3.2.5. Field emission gun- scanning electron microscope (FEG-SEM; JSM- 7600F) equipped with energy dispersive spectroscope (EDS) operated at 20 keV was used for determining the elemental composition of the SeNPs.

6.2.6 Thiol assay

Idiomarina sp. PR58-8 grown in the presence of 0 mM (control), 4 mM, and 8 mM Na_2SeO_3 was harvested by centrifugation at $10,000 \times g$ for 20 mins and the cell pellet was washed twice with 25 mM Tris-HCl buffer (pH 7.5). The pellet obtained was re-suspended in the same buffer

and subjected to sonication at 0°C for three cycles of 1 min each, at three RPS (40 W). The resulting suspension was centrifuged ($12,000 \times g$ for 45 mins at 4°C) to remove the cellular debris and the supernatant obtained was used as the cell-free lysate (CFL) for thiol assay. The T-SH, NP-SH, and, PB-SH were estimated using DTNB (Sigma) as described previously in section 3.2.6.

6.2.7 Mammalian cell culture

Human epidermal keratinocyte, HaCaT cell line and the human epithelial cervical adenocarcinoma, HeLa cell line were used for this study. They were maintained as described previously in section 4.2.7.

6.2.8 Cytotoxicity assay

MTT assay was employed to determine the cytotoxicity of SeNPs synthesised by *Idiomarina* sp. PR58-8 against HeLa and HaCaT cell lines. The assay was performed as described previously in section 4.2.8, using the *Idiomarina* sp. PR58-8 synthesised SeNPs (5- 100 µg/ml). The experiment was performed in triplicates on three different days. Selenium free cell material (ML2) and sodium selenite (SS) were also evaluated for their cytotoxicity towards HeLa and HaCaT cell lines. The cell viability (%) relative to unexposed controls was calculated using equation (7) given in section 4.2.8.

6.2.9 Detection of intracellular ROS

The ROS studies were carried out in HeLa cell line as described previously in section 4.2.9, with varying concentrations of SeNPs (5, 10, 15, 20, 25, 30 and 50 µg/ml). ML2 and SS were also evaluated for their ability to generate ROS in HeLa cell line. 1 µM hydrogen H₂O₂ was used as positive control. All the experiments were performed in triplicates on different days.

6.2.10 Determination of AI

Exponentially growing HeLa cells (2×10^5 cells/ well) were seeded in 6-well plates and allowed to grow for 24 hrs. The cells were then treated with varying concentration of SeNPs (0, 5, 10, 15, 20, 25, 30 and 50 µg/ml) for another 24 hrs. After trypsinisation the cells were washed with PBS and stained with AO/EB dye mixture as described previously in section

4.2.10. Post staining, the cells were observed immediately with the 40 × objective of the epi-fluorescence microscope (Olympus BX41) using the FITC and TRITC filters. A minimum of 300 cells were counted and the apoptotic and viable cells were differentiated based on the type of fluorescence and state of chromatin condensation. The experiments were performed in triplicates on different days. Apoptotic index (AI) was calculated using equation (8) given in section 4.2.10.

6.2.11 Western Blot analysis

HeLa cells treated with various concentrations of SeNPs (0, 10, 15, 20, and 25 µg/ml) at 37°C, for 24 hrs were washed three times in PBS (pH 7.5). The cells were trypsinised and then lysed with lysis buffer (0.1 % Triton X-100, 1 mM EDTA, 1 mM PMSF, 20 mM Tris-HCl, pH 7.4) for 25 mins. The total cellular proteins were obtained by centrifuging the cell lysates at 4°C (13,000 x g, 20 mins). The protein concentrations were quantified by Lowry's method using BSA as control (Lowry et al. 1951). The total cellular proteins were separated on SDS-PAGE, transferred to PVDF membranes and blocked with 5% non-fat milk in transfer buffer (Tris base, glycine, SDS and methanol) for 1 hr at RT. The membranes were then incubated overnight at 4°C with the corresponding primary antibodies diluted in 5% non-fat milk/ Tris-buffered saline containing Tween-20 (TBST) as follows: anti-caspase 3, 1:1000 (Biolegend), anti-hsp 70, 1:1000 (Biolegend) and anti-PARP, 1:1000 (BD Pharmingens). Following this the membranes were washed with TBST, and incubated for 1 h at room temperature with horse radish peroxidase conjugated secondary antibody at 1:2000 dilution, and specific proteins were visualised on X-ray films by enhanced chemiluminescence detection. β- Actin was used as the standard to check equal protein loading.

6.2.12. Statistical analysis

The statistical analysis was carried out as described in section 2.2.5.

6.3 Results and Discussion

6.3.1 Growth of *Idiomarina* sp. PR58-8 in presence of selenite oxyanion

Idiomarina sp. PR58-8 is a moderate halophile, isolated from the soil on the banks of the Mandovi Estuary, Goa, India, in our laboratory previously by Seshadri et al. (2012). It has an obligate requirement of 1% NaCl for growth and can tolerate up to 15% NaCl (Seshadri et al. 2012). The MIC for sodium selenite (Na_2SeO_3) was determined by observing the growth of *Idiomarina* sp. PR58-8 in various concentrations

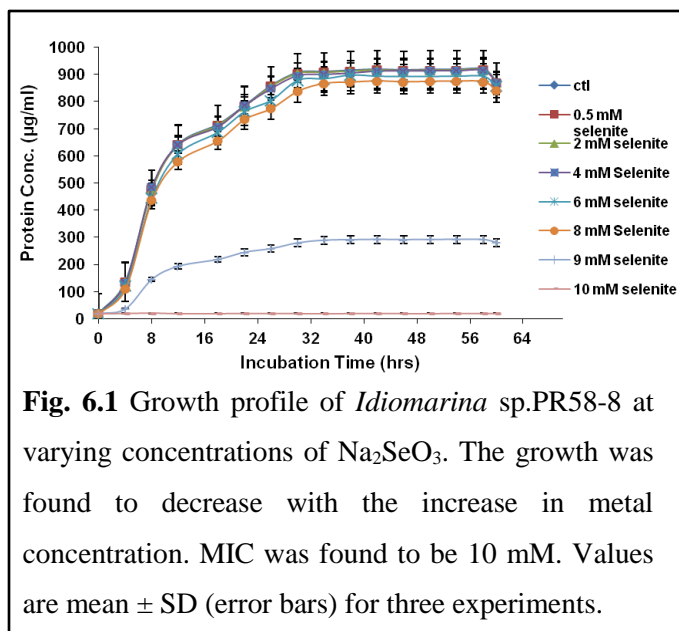


Fig. 6.1 Growth profile of *Idiomarina* sp. PR58-8 at varying concentrations of Na_2SeO_3 . The growth was found to decrease with the increase in metal concentration. MIC was found to be 10 mM. Values are mean \pm SD (error bars) for three experiments.

of Na_2SeO_3 . At concentrations up to 4 mM Na_2SeO_3 , *Idiomarina* sp. PR58-8 exhibited growth similar to that of un-exposed controls (in the absence of Na_2SeO_3). At 6 mM and 8 mM Na_2SeO_3 , the growth of the halobacteria was slightly affected (Fig. 6.1).

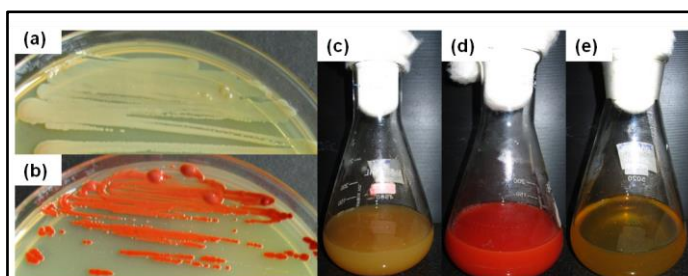


Fig. 6.2 *Idiomarina* sp. PR58-8 appears golden yellow when grown in Zobell marine agar (a) and Zobell marine broth (c). In presence of sodium selenite, it appears brick-red in color (b; d). Media controls with sodium selenite did not exhibit the brick-red coloration (e).

MIC of Na_2SeO_3 against *Idiomarina* sp. PR58-8 was found to be 10 mM. The culture appears as golden-yellow on ZMB 2216 medium containing plates, however in the presence of Na_2SeO_3 , the culture was found to become brick-red in colour (Fig. 6.2). Further, the effect of various concentrations of Na_2SeO_3 on the growth kinetics parameters was

evaluated (Fig. 6.3). The growth kinetics studies were carried out by determining the total protein content instead of direct optical density measurements as the profuse amounts of brick

red precipitate interfered with the UV-visible spectroscopy measurements. The growth kinetics parameters of *Idiomarina* sp. PR58-8 remained unaffected in presence of 4 mM Na₂SeO₃, exhibiting a specific growth rate (μ) of 1.050 hrs⁻¹ (Table 6.1). In presence of 8 mM Na₂SeO₃, the μ was 0.818 hrs⁻¹, which is slightly lower than the control (*Idiomarina* sp. PR58-8 grown in the absence of Na₂SeO₃), albeit the difference was insignificant ($p > 0.05$). The μ and the t_d in presence of 8 mM Na₂SeO₃ did not exhibit a significant difference ($p > 0.05$) as compared to the μ and the t_d of the cells grown in presence of 4 mM Na₂SeO₃. However, in a study on SeNPs synthesis by *Bacillus mycoides* SelTE01, selenium oxyanion (SeO₃²⁻) negatively affected the growth dynamics and final cell yield at concentration as low as 2 mM SeO₃²⁻ (Lampis et al. 2014).

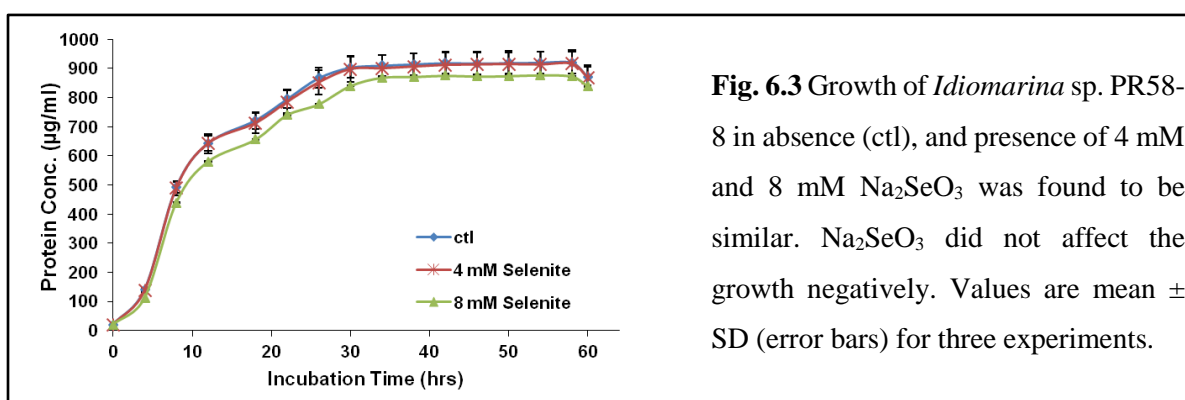


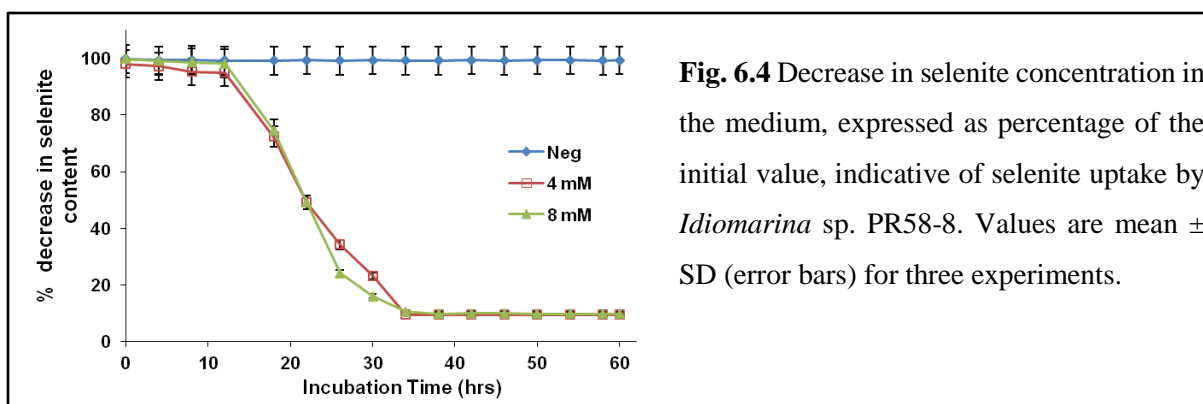
Fig. 6.3 Growth of *Idiomarina* sp. PR58-8 in absence (ctl), and presence of 4 mM and 8 mM Na₂SeO₃ was found to be similar. Na₂SeO₃ did not affect the growth negatively. Values are mean \pm SD (error bars) for three experiments.

Table 6.1 Growth kinetics parameters of *Idiomarina* sp. PR58-8 in presence of sodium selenite

Parameters	Control	4 mM Na ₂ SeO ₃	8 mM Na ₂ SeO ₃
Specific growth rate (h ⁻¹)	1.110	1.050	0.818
Doubling time (mins)	37.46	39.6	50.83
Lag time (mins)	30	40	75

The selenite loss from the medium and its uptake by cells was estimated in presence of 4 mM and 8 mM Na₂SeO₃. The selenite concentration of medium at 18th hour (mid-exponential phase) was 2.89 mM and 5.97 mM for cells grown in presence of 4 mM and 8 mM Na₂SeO₃, respectively, which decreased to 0.38 mM and 0.98 mM by the 38th hour (early stationary phase). Thus ~90% of selenite added in the medium was taken up by *Idiomarina* sp. PR58-8 (Fig. 6.4). The selenite concentration in the medium remained constant with no uptake by cells

during the lag, and the early log phase of the *Idiomarina* sp. PR58-8. The cells during this time adapt to growth in presence of selenite. The selenite content of the un-inoculated media controls remained constant throughout the experiment. Approximately 90% selenite provided to *Idiomarina* sp. PR58-8 was taken up indicating that nearly all the selenite lost from the medium was taken up by the cells in both the cases. These results differ from our previous findings, where the selenite uptake by the haloarchaeon, *H. salifodinae* BK18 was observed from early log phase and continued up to late stationary phase (Srivastava et al. 2014). The selenite uptake by the phototrophic bacterium *Rhodospirillum rubrum* on the other hand has been reported to commence at the beginning of the stationary phase (Kessi et al. 1999). This would suggest that Na_2SeO_3 may be added during the mid- exponential phase, however, *Idiomarina* sp. PR58-8 failed to grow and produce the brick-red colouration when selenite was added at the mid log phase. This may be due to the inability of the moderate halophile to adapt to the metal stress when the SeO_3^{2-} was added during active growth. Thus, for synthesis and further studies the Na_2SeO_3 was added to the medium during the time of inoculation at 0 hr. This is advantageous as the need of monitoring the growth phase of the culture for metal salt addition is circumvented.

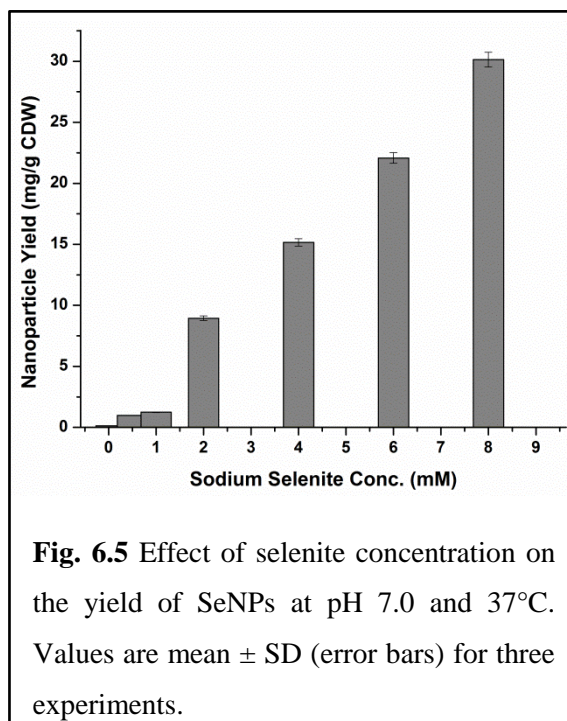


6.3.2 Selenium nanoparticles (SeNPs) synthesis and their characterisation

Selenium nanoparticles synthesis by a plethora of bacteria, yeast, and fungi has been reported, where the toxic oxyanions of selenium are converted to non-toxic red selenium (Tam et al. 2010; Hariharan et al. 2012; Lampis et al. 2014). Extremely halophilic bacteria *Bacillus selenitireducens*, *Selenihalanaerobacter shriftii*, and the slight halophile, *Sulfospirillum barnesii* were the first halophiles reported to synthesise SeNPs (Oremland et al. 2004). Here

we report the synthesis of selenium nanoparticles by moderate halophile *Idiomarina* sp. PR58-8. It exhibits golden yellow pigmentation, however, in presence of SeO_3^{2-} the culture turned brick-red in colour indicative of reduction of selenite to elemental selenium (Fig. 6.2). SeNPs synthesis was carried out at various medium pH, incubation temperature and Na_2SeO_3 concentration to determine the optimum conditions for synthesis.

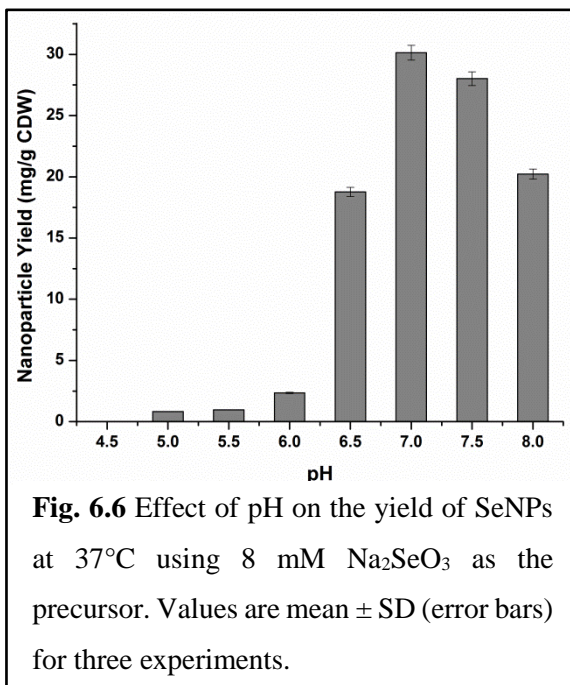
Na₂SeO₃ concentration



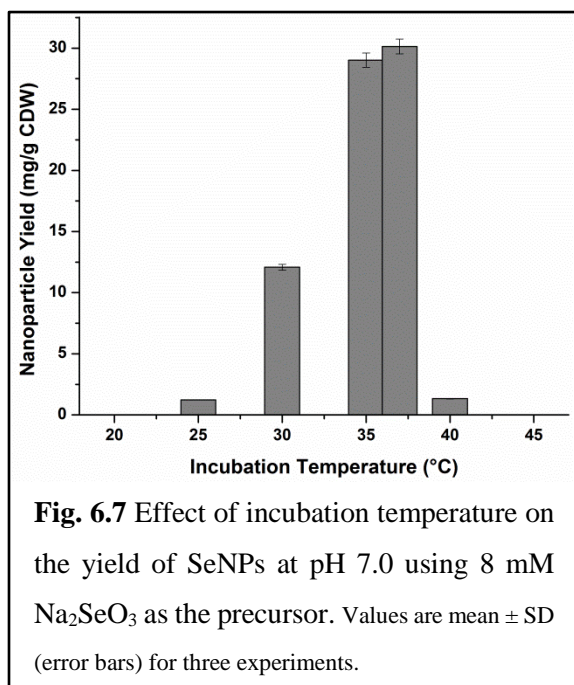
A concentration range of 0.05 mM to 9 mM Na_2SeO_3 was tested to determine the optimum concentration for SeNPs synthesis (Fig. 6.5). At concentrations lower than 2 mM Na_2SeO_3 , the yield of SeNPs obtained was very low and in the range of \sim 0.13- 1.2 mg/g CDW. The low yield may be attributed to the presence of low concentration of Na_2SeO_3 . At concentrations of 2 mM, and 4 mM Na_2SeO_3 (Fig. 6.5), the yield of SeNPs was 8.95 mg/g CDW, and 15.16 mg/g CDW, respectively. Although the growth of *Idiomarina* sp. PR58-8 was affected at 8 mM Na_2SeO_3 , maximum yield of 30.13 mg/g

CDW was obtained at this concentration. The yields obtained at 2 mM, 4 mM, and 6 mM Na_2SeO_3 were significantly lower ($p < 0.05$) as compared to the yield obtained at 8 mM Na_2SeO_3 . 9 mM Na_2SeO_3 negatively affected both growth and the SeNPs yield (0.018 mg/g CDW). This suggests that at concentrations above 8 mM Na_2SeO_3 , the oxyanion exerts its toxic effects on the moderate halophile which may be responsible for low yield. As maximum yield of SeNPs was obtained at 8 mM Na_2SeO_3 , this concentration was used for further studies on SeNPs synthesis.

Medium pH



The SeNPs synthesis was carried out at varying medium pH (4.5-8.0) to determine the optimum pH for maximum yield. The pH range for growth of *Idiomarina* sp. PR58-8 is 6.0-9.0, with the optimum at pH 7.0. At pH 7.0, maximum yield of 30.13 mg/g CDW was obtained (Fig. 6.6). *Idiomarina* sp. PR58-8 failed to grow at pH 4.5 even in the absence of Na₂SeO₃. The halophilic bacteria exhibited poor growth at pH of 5.0 and 5.5 in the absence of Na₂SeO₃, therefore, when grown in presence of 8 mM Na₂SeO₃ the yield of SeNPs was significantly lower ($p < 0.05$) as compared to that at pH 7.0. Thus, as the pH increased from 6.0 to 6.5, the yield also increased. Yield of SeNPs at pH 7.5 was 28.02 mg/g CDW, which was not significantly different ($p > 0.05$) than the yield obtained at pH 7.0. However, alkaline pH of 8.0 significantly lowered the yield of SeNPs. Based on these results, SeNPs synthesis was carried out at pH 7.0.



Incubation Temperature

A temperature range of 20°C to 45°C was tested to determine the optimum temperature for SeNPs synthesis by *Idiomarina* sp. PR58-8. The optimum range of temperature for growth of *Idiomarina* sp. PR58-8 is 30°C to 38°C. Maximum SeNPs synthesis was obtained at 35 and 37°C with a yield of 29.02 mg/g CDW, and 30.13 mg/g CDW, respectively (Fig. 6.7). The moderate halophile did not exhibit growth at 20°C even in the absence of

Na_2SeO_3 . As the temperature increased from 25°C to 37°C , the yield of SeNPs also increased and the difference in yield between 30 and 37°C was significant ($p < 0.05$). The halobacterial isolate exhibited slow growth at 45°C , and therefore, the yield of SeNPs was also lower. Thus, SeNPs synthesis by *Idiomarina* sp.PR58-8 was carried out at 37°C .

The SeNPs synthesis by *Idiomarina* sp.PR58-8 was carried out with 8 mM Na_2SeO_3 , at pH of 7.0 and a temperature of 37°C .

The time course of SeNPs accumulation (yield), selenite loss from the medium and the growth is shown in Fig. 6.8 (a, b). Both molar yield and the yield with respect to the biomass were estimated during the synthesis. Maximum yield was obtained at 38th hour exhibiting an efficiency of ~90% for both 4 mM and 8 mM Na_2SeO_3 . As the yield of SeNPs obtained in case of 8 mM Na_2SeO_3 was significantly higher ($p < 0.05$) as compared to that in presence of 4 mM Na_2SeO_3 , further synthesis was carried out using this concentration. Table 6.2 summarises the various yield parameters of SeNPs synthesis by *Idiomarina* sp. PR-58-8.

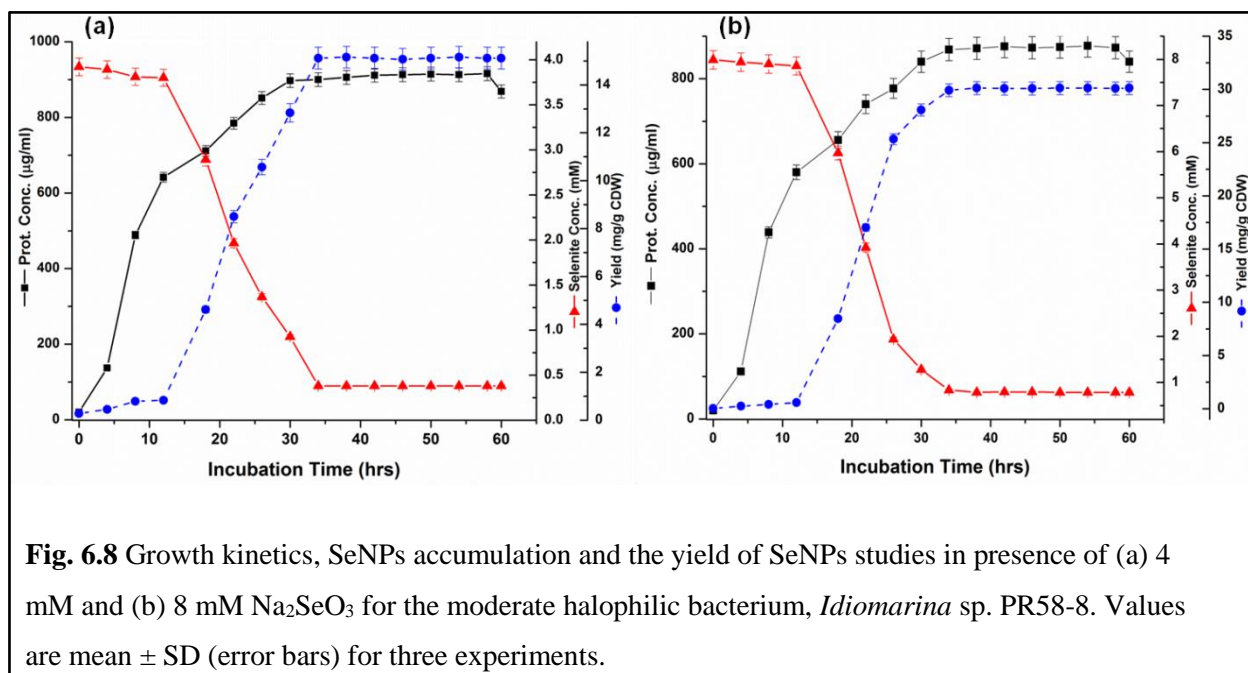
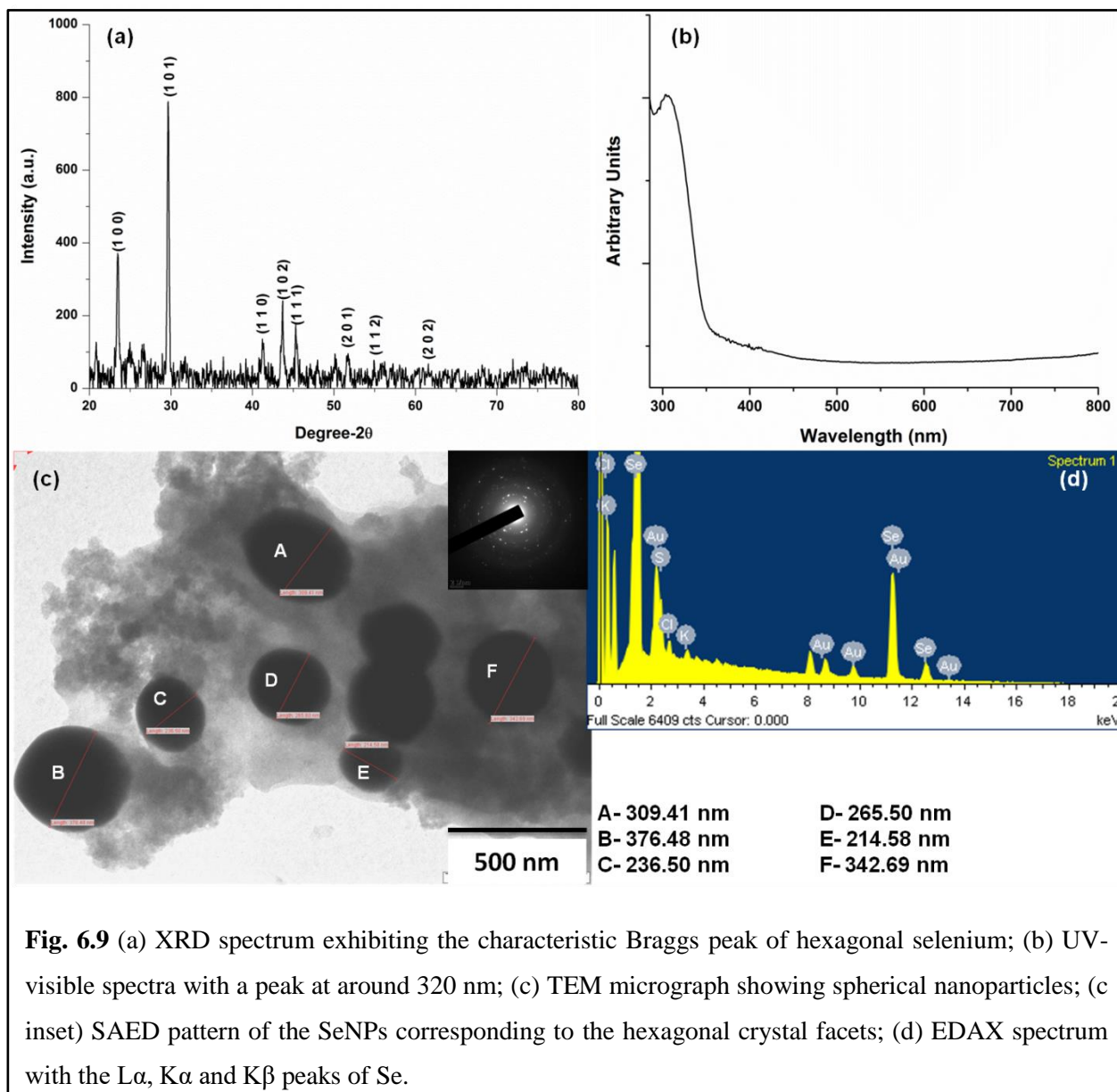


Table 6.2 The yield parameters of SeNPs synthesised by *Idiomarina* sp. PR58-8

Yield Parameters	4 mM Na ₂ SeO ₃	8 mM Na ₂ SeO ₃
Yield (mg/g CDW)	15.16	30.13
Molar Yield (mM/mM selenite)	0.907	0.902
Efficiency (%)	90.78	90.16

The crystallographic characterisation of the SeNPs was carried out using X-ray diffraction studies (Fig. 6.9a). The XRD spectra exhibited intense Bragg's peak at 2θ values of 23.46° , 29.66° and 43.72° , corresponding to the (1 0 0), (1 0 1) and (1 0 2) lattice planes of hexagonal selenium (ICDD- card no.06-0362). The crystallite domain size was calculated using the line width of (1 0 1) plane and was found to be 34.52 nm. The lattice parameters a and b , as calculated for hexagonal system were 4.366 \AA and 4.951 \AA , respectively which correspond well with the literature values of $a = 4.360 \text{ \AA}$ and $b = 4.956 \text{ \AA}$ (ICDD- card no.06-0362). The UV-visible spectra of the SeNPs (Fig. 6.9b) exhibited a strong peak at around 320 nm which may be attributed to the surface plasmon vibrations (Praharaj et al. 2004; Fesharaki et al. 2010). The morphological characterisation was achieved by transmission electron microscopy. Fig. 6.9c shows the TEM micrograph of the synthesised SeNPs. The nanoparticles were primarily spherical in shape and exhibited a size distribution of 150- 350 nm. A similar size distribution of 200- 400 nm was observed by Oremland et al. (2004) during the synthesis of spherical SeNPs by the halophilic bacteria *B. selenitireducens*, *S. shriftii* and *S. barnesii*. The red Se⁰ exists as α , β , or γ forms which may possess an eight-member ring structure, with Se-Se distance of 2.35 \AA and a bond angle of 105.7° . The other structural subsets include a six-member ring, and infinite α -helical chains with Se-Se distance of approximately 2.37 \AA and a bond angle of 103° . Oremland et al. (2004) attributed the spherical morphology of the SeNPs to the presence of both chain and ring structural aspects forming an inter-connected 3-dimensional net of Se⁰. This may explain the spherical morphology of the SeNPs synthesised by *Idiomarina* sp. PR58-8. The elemental analysis by EDS exhibited the presence of Se peaks at 1.5, 11.2 and 12.5 keV corresponding to the $L\alpha$, $K\alpha$, and $K\beta$ families of X-Rays, respectively (Fig. 6.9d). Peaks due to K and Cl may be attributed to the media components and peak due to Au, to the gold coating. The presence of Cl at the end of the Se chains, where it acts as dopant,

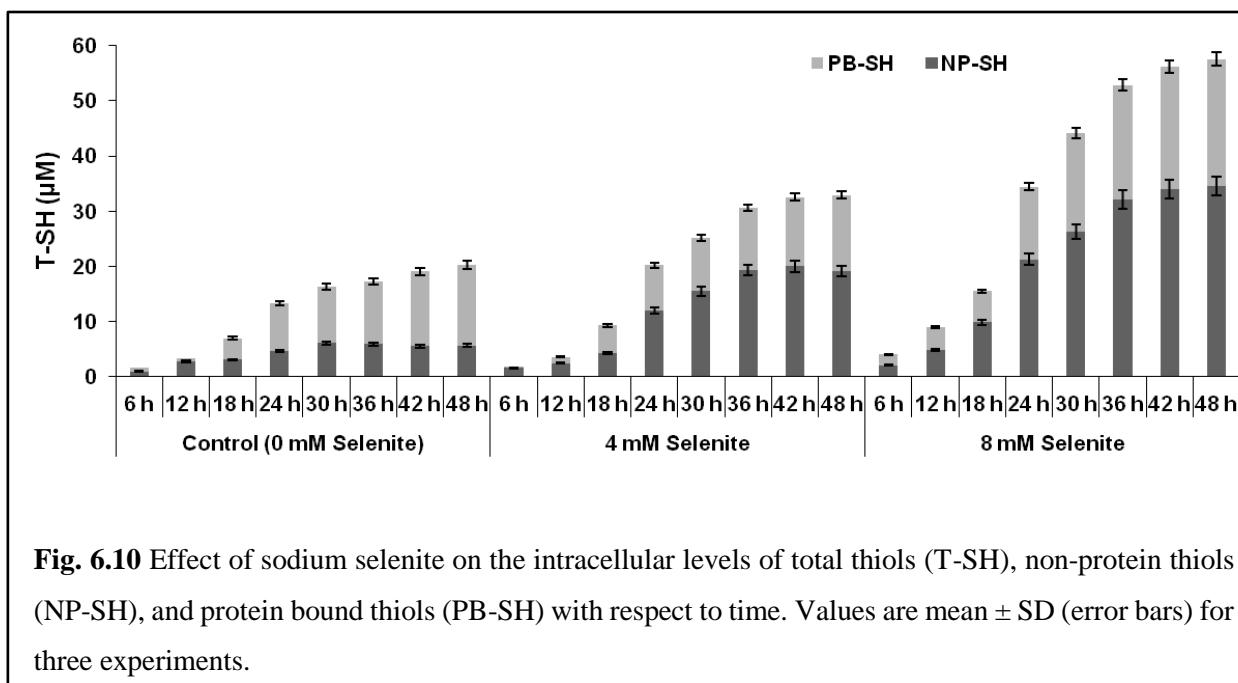
may be attributed to confer the 3-dimensional net-like structure of Se^0 . These Cl atoms allow the interaction between the Se chains, thus resulting in a spherical morphology (Kondakova et al. 2001). SAED pattern of the synthesised SeNPs showed characteristic diffraction rings that could be indexed to the hexagonal crystal phase (Fig. 6.9c inset).



6.3.3 Mechanism of SeNPs synthesis

Metal nanoparticles synthesis involves the metal-resistance mechanisms either inherent or acquired by the organism used for fabrication. Thiols, including the NP-SH like GSH, cysteine, and cystine; and PB-SH like PCs and MTs have been implicated in SeO_3^{2-} reduction and nanoparticle synthesis (Kessi and Hanselmann, 2004; Harrison et al. 2007; Debieux et al. 2011). GSH, the most abundant thiol in eukaryotes, cyanobacteria, and the α , β , and γ proteobacteria, has been proposed to be involved in Se metabolism (Kessi and Hanselmann, 2004). The mechanism of biological reduction of selenite was proposed by Kessi and Hanselmann (2004) based on studies in *E. coli* and *R. rubrum*. They suggested a multistep process where GSH donates an electron to SeO_3^{2-} to form seleno-diglutathione (GS-Se-SG) along with superoxide anion (O_2^-). GS-Se-SG in presence of NADPH and glutathione reductase/ thioredoxin reductase forms selenopersulphide (GS-Se⁻) which gets converted to reduced GSH and elemental Se⁰. The O_2^- formed is degraded by the enzymes involved in oxidative stress management. As *Idiomarina* sp. PR58-8 belongs to the γ - proteobacterium group, the involvement of thiols was investigated by determining the effect of metal on the thiol concentration.

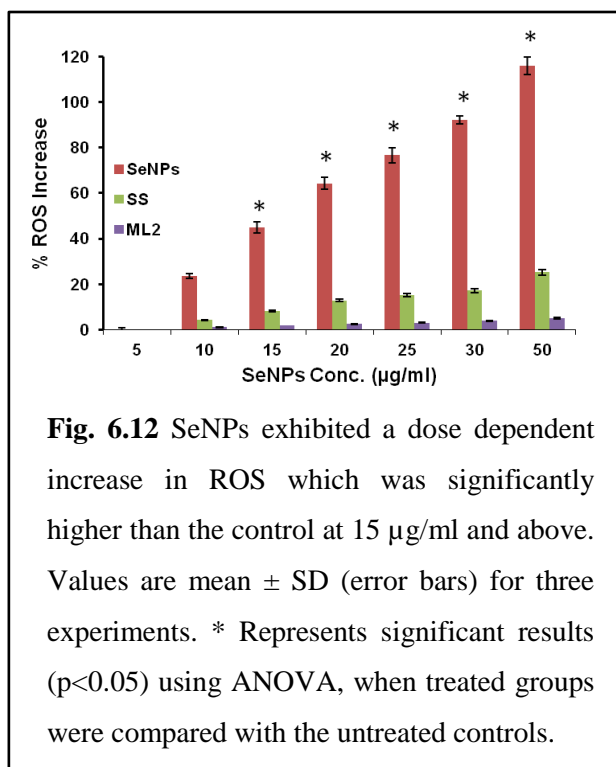
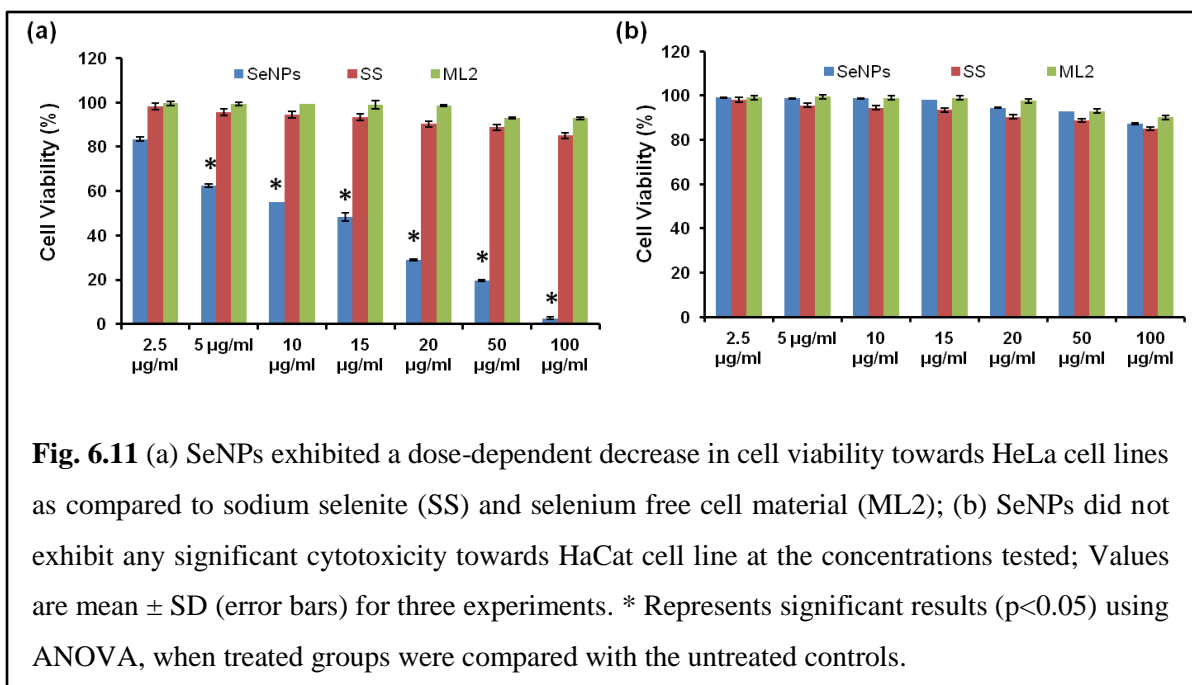
The intracellular thiol content of the bacterial cells exposed to varying concentrations of Na_2SeO_3 was determined over a period of 48 hrs. As compared to unexposed controls, the NP-SHs in selenite exposed *Idiomarina* sp. PR58-8 were significantly increased in a time dependent as well as dose dependent manner (Fig. 6.10). The T-SH and NP-SH content of the cells exposed to 4 mM Na_2SeO_3 exhibited a ~1.7 fold and a 4-fold increase, respectively, as compared to unexposed controls. Similarly, a 1.8-fold increase in T-SH and a 4.5-fold increase in NP-SH were observed for *Idiomarina* sp. PR58-8 grown in presence of 8 mM Na_2SeO_3 , as compared to untreated control. A similar increase in NP-SH in response to silver stress in this bacterium has been previously reported (Seshadri et al. 2012). Other fungi and bacteria have also been reported to exhibit an increase in NP-SH when exposed to metal stress (Guimaraes-Soares et al. 2007; Pages et al. 2008). At the same time PB-SHs levels were either lower or same in cells exposed to Na_2SeO_3 when compared to unexposed *Idiomarina* sp. PR58-8. The increase in NP-SH in selenite exposed bacterial cells suggests the involvement of GSH in selenite resistance/reduction.



6.3.4 Antineoplastic properties of SeNPs and its mechanism

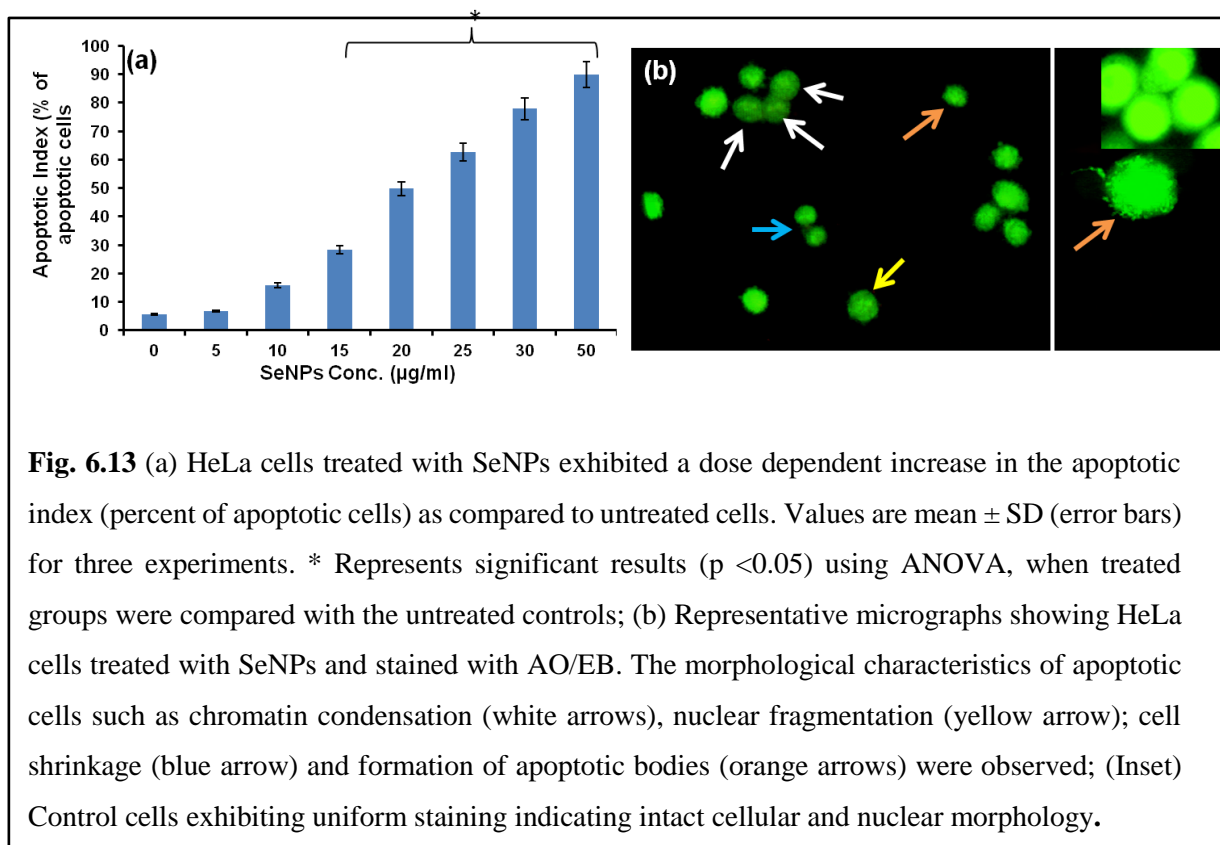
Previous studies have demonstrated the antioxidant, neuroprotective, anti-inflammatory, hepatoprotective, and apoptotic properties along with the anticancer properties of various organic and inorganic selenium compounds (Seng and Tiekink, 2012). Nano-preparations of Se present a safer alternative as they have been shown to exhibit anticancer properties at lower concentration and excellent biological activity (Luo et al. 2012; Srivastava et al. 2014). Thus, the SeNPs synthesised by *Idiomarina* sp. PR58-8 were evaluated for their antiproliferative properties against HeLa and HaCaT cell lines, where HeLa cells were treated as cancer cell line. HaCaT cell line was treated as substitute for normal primary culture. SeNPs exhibited dose-dependent cytotoxicity towards HeLa cell line (Fig. 6.11a) with only 3% viability at 100 μ g/ml. The cytotoxicity exerted by SeNPs was significantly higher ($p < 0.05$) in HeLa cells as compared to that in HaCaT. In fact, SeNPs did not exhibit the trend of dose dependent cell toxicity in HaCaT cell line (Fig. 6.11b). Selenium free cell material (ML2), and sodium selenite (SS) did not exhibit any significant cytotoxicity ($p < 0.05$) in both HeLa and HaCaT cell lines at the concentrations tested. The biosynthesised SeNPs thus exhibited selectivity towards malignant cell line, HeLa. This difference in susceptibility of the cancer cells to SeNPs

as compared to the normal cells may be attributed to the difference in the antioxidant enzyme regulation, particularly TR in cancer cells (Fang et al. 2005).



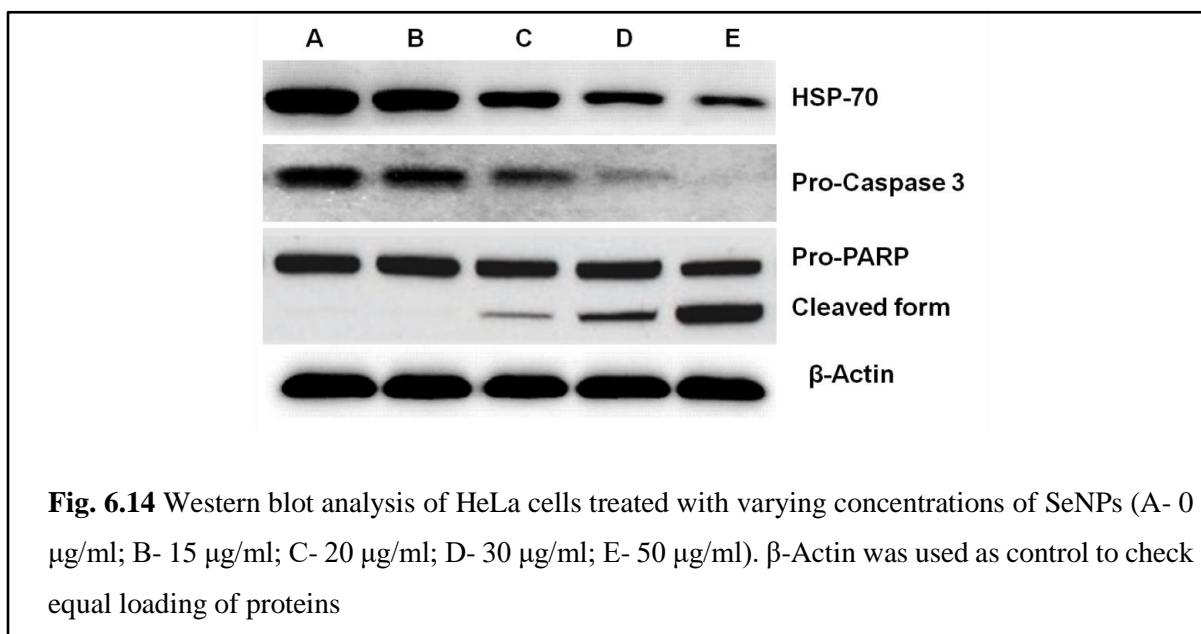
To elucidate the mechanism of SeNPs toxicity towards HeLa cells, ROS generated by these nanoparticles at varying concentrations was estimated using the fluorescent probe, 2', 7'-dichlorofluorescein diacetate (DCFH-DA). HeLa cells treated with SeNPs exhibited a dose dependent increase in ROS production (Fig. 6.12). A significant increase ($p < 0.05$) in ROS levels were observed in cells treated with 15, 20, 25, 30, and 50 µg/ml SeNPs, as compared to untreated controls. However, neither ML2, nor SS exhibited any significant increase ($p > 0.05$) in ROS production in

HeLa cell line, as compared to control. Increase in ROS production is an indication of mitochondrial dysfunction causing nucleic acid, proteins, and lipid damage, eventually leading to apoptotic cell death (Simon et al. 2000). To further understand the mechanism of cell death induced by SeNPs, the apoptotic index of the cells exposed and unexposed to nanoparticles was determined. SeNPs treatment exhibited a dose dependent increase in AI in HeLa cells (Fig. 6.13a). A significant increase ($p < 0.05$) in AI was observed in presence of 15, 20, 25, 30, and 50 $\mu\text{g/ml}$ SeNPs as compared to untreated controls. The cells treated with SeNPs exhibited morphological characteristics of apoptotic cells such as cell shrinkage, chromatin condensation, nuclear fragmentation, and formation of apoptotic bodies (Fig. 6.13b).



To further understand the mechanism of SeNPs cytotoxicity towards HeLa cell line, the expression of apoptotic markers, pro-caspase-3, poly(ADP-ribose) polymerase (PARP), and HSP-70 was determined by western blot analysis. Caspases are a group of intracellular proteases that exist as inactive pro-enzymes and are activated by proteolytic cleavage resulting in the deliberate disassembly of the cell into apoptotic bodies (Thornberry and Lazebnik,

1998). In response to a pro-apoptotic signal, such as UV-light or chemotherapy, proteins upstream of pro-caspase-3 cleave it resulting in generation of active form of caspase-3. HeLa cells treated with SeNPs exhibit a dose dependent decrease in expression of pro-caspase 3 as compared to untreated controls (Fig. 6.11), suggesting the activation of apoptotic pathway. This was confirmed by determining the expression of pro-PARP and cleaved PARP, as the activated form of caspase-3 catalyses the cleavage of pro-PARP. As seen in Fig. 6.14, the expression of pro-PARP was found to decrease with the increase in SeNPs concentration, while the cleaved-PARP was found to be upregulated. At the same time, HSP-70 was found to be down-regulated with the increase in SeNPs concentrations (Fig. 6.14). This further confirms the activation of apoptotic pathway, as HSP-70 is known to protect cells against caspase dependent apoptotic cell death (Sabirzhanov et al. 2012). A similar decrease in the expression levels of pro-caspase-3, and pro-PARP and an increased expression of cleaved PARP was observed in prostate cancer cell line, LNCaP, in response to chemically synthesised SeNPs treatment (Kong et al. 2011). Thus, the western blot analysis indicates the activation of caspase-dependent apoptosis in HeLa cells treated with the *Idiomarina* sp. PR58-8 synthesised SeNPs.



6.4 Conclusion

Selenium nanoparticles have gained attention due to their superior biocompatibility and activity at lower concentrations, with selectivity towards cancer cells. Such SeNPs have been synthesised by various chemical and biological methods. Here we report the intracellular synthesis of SeNPs by the moderate halophilic bacterium, *Idiomarina* sp PR-58-8. The hexagonal SeNPs exhibited a crystallite domain size of 34.52 nm, a spherical morphology with a size distribution of 150-350 nm and the characteristic $L\alpha$, $K\alpha$ and $K\beta$ peaks of Se. The marine bacterium exhibited an intrinsic resistance towards sodium selenite, as there was no significant effect on the growth even at a concentration of 8 mM. SeNPs synthesis at 4 mM and 8 mM Na_2SeO_3 exhibited an efficiency of 90.78% and 90.16%, respectively. Non-protein thiols were found to be upregulated in response to selenite stress and are indicative of their involvement in selenite resistance/reduction. The SeNPs were found to be cytotoxic towards HeLa (cancer) cell lines, whilst being non-cytotoxic towards HaCaT (model for normal cell line). SeNPs treatment of HeLa cells resulted in caspase mediated apoptotic cell death as evident from the ROS generation, apoptotic index and western blot studies. Thus, the SeNPS synthesised by *Idiomarina* sp. PR58-8 can be used as potential antineoplastic agents.

CHAPTER 7

Biosynthesis of Fluorescent Lead (IV) Sulphide Nanoparticles Synthesis by the Moderate Halophilic Bacterium *Idiomarina* sp. PR58-8**7.1 Introduction**

The IV-VI family lead based semiconductor nanoparticles have garnered great attention in the past decade due to their size tuneable optical and electronic properties. These intrinsic properties make them excellent materials for diode lasers, optical detectors, solar cells, photo-resistors, field-effect transistors, and biological applications (imaging and labelling) (Xiao et al. 2013; Patil et al. 2006). The most extensively studied lead based semiconductor nanoparticle is lead (II) sulphide nanoparticles (PbSNPs), which possesses a cubic crystallite lattice, large band gap energy, and a size smaller than the large exciton Bohr radius of the bulk PbS (Wise, 2000). However, there are very few reports on synthesis and application of lead (IV) sulphide nanoparticles (PbS₂NPs).

The bulk tetragonal β -PbS₂ was first synthesised by heating PbS with excess sulphur at temperatures above 650°C and a pressure of 30 kbars (Silvermann, 1966). The tetragonal β -PbS₂ nanoparticles were first obtained as a by-product of PbSNPs synthesis via the hydrothermal process using toxic precursors like thiourea, where the nanoparticles were embedded within the natural zeolite matrix. The formation of PbS₂NPs was attributed to the influence of the special ordered structure of the zeolite matrix that acted as crystallisation media (Roman-Zamorano et al. 2009). β -PbS₂ and Ga doped β -PbS₂ thin films obtained by chemical bath deposition method at extremely alkaline pH exhibited flower like morphology, a higher band gap as compared to the bulk, and p-type conductivity (Geethu et al. 2012). Similarly, the tetragonal PbS₂NPs prepared as thin films by photochemical deposition on glass and ITO coated glass substrates at extremely acidic pH and UV light irradiation, exhibited an oval morphology, and p- type conductivity (Shyju and Gopalakrishnan, 2013). Thus, the few studies till now on PbS₂NPs synthesis have been on chemical route of fabrication, employing high temperature, pressure, extreme pH, and toxic precursors. Biological routes of nanoparticle fabrication allow the process to occur at ambient temperature and pressure. Although synthesis of PbSNPs by bacteria, fungi, and viruses has been reported (Singh and Nara, 2013 Seshadri

et al. 2011; Bai and Zhang, 2009; Kowshik et al. 2002; Shenton et al. 1999), there are no reports on PbS₂NPs synthesis by microorganisms.

The lead based nanoparticles with a size distribution of 2-10 nm (quantum dots) find application in near-infrared imaging (Walling et al. 2009; Wolfbeis, 2015; Chen et al. 2016). These quantum dots exhibit size tuneable optical properties stemming from quantum confinement, negligible photo-bleaching due to narrow emission spectra, broad emission spectra that allows multi-photon excitation, high quantum yields (QY), and large Stokes' shift (Wegner and Hildebrandt, 2015). These properties make the QDs excellent candidates for bio-imaging and labelling applications, as the fluorescent dyes and proteins routinely used, present several shortcomings like, narrow excitation band, broad emission spectra, small stoke shifts, low QYs, and photo bleaching. A major drawback of QDs however, is their toxicity both *in-vitro* and *in-vivo* (Walling et al. 2009). To overcome the toxicity of the QDs and to make them water-soluble for biological applications, a hydrophilic coating of either thiolate ligand/silica/ other polymers may be applied (Bruchez et al. 1998; Chan and Nie, 1998). The microbially synthesised PbS₂NPs quantum dots would most likely be coated with a biomolecule making them hydrophilic and suitable for biological applications.

Here we report the intracellular synthesis of non-cytotoxic, biocompatible, tetragonal β -PbS₂ nanoparticles by the moderate halophile, *Idiomarina* sp. PR58-8. The nano-preparation was characterised by UV-visible spectroscopy, fluorescence spectroscopy, TEM, HR-TEM, SAED, and EDAX. The application of the 'as-synthesised' nanoparticles as bio-imaging agent is also demonstrated. To the best of our knowledge, this is the first report on synthesis of β -PbS₂ nanoparticles by microorganisms.

7.2 Materials and Methods

7.2.1 MIC determination and growth kinetics studies

Idiomarina sp. PR58-8 was grown in ZMB 2216 with varying concentrations of Pb(NO₃)₂ (0.05 mM- 10 mM) to determine the MIC. Pb(NO₃)₂ was prepared as a 1 M stock in SDW and filter sterilised. The cultures were incubated at 37°C, for 72 hrs under agitation (110 rpm). The minimum concentration of Pb(NO₃)₂ at which no growth was observed was designated as the MIC. Appropriate negative controls were also run simultaneously.

For growth kinetic studies, the bacterium was grown in presence of $\text{Pb}(\text{NO}_3)_2$ (0.05, 0.5, 1, and 5 mM). An aliquot of 1 ml was withdrawn every 4 hrs, till 60th hr, and the optical density was recorded at 600 nm on a UV-visible double beam spectrophotometer. The growth kinetics parameters such as specific growth rate (μ ; hrs^{-1}), lag time (t_l ; min), and doubling time (t_d ; min) were determined according to Berney et al. (2006), and Breidt et al. (1994) as described in section 2.2.2. *Idiomarina* sp. PR58-8 grown in the absence of $\text{Pb}(\text{NO}_3)_2$ served as positive control.

7.2.2 Lead uptake studies

Lead uptake by *Idiomarina* sp. PR58-8 was determined using FAAS, Shimadzu AA-700. Instrumental conditions for FAAS measurement are summarised in Table 7.1. An aliquot of 5 ml was withdrawn every 6 hrs from the culture grown in presence of 0.5 mM, and 5 mM $\text{Pb}(\text{NO}_3)_2$, up to 60th hr. The cells were separated from the supernatant, and both were digested in 20 ml of 50% nitric acid. Appropriate dilutions of the digested samples were prepared using deionised water and the samples were subjected to lead quantitation by FAAS. Appropriate controls were also run simultaneously.

Table 7.1 Instrumental conditions for FAAS measurements

Element	Lead
BGC mode	BCG-D2
Wavelength	283.3 nm
Lamp current	10 mA
Slit width	0.7 nm
Flame type	Air-C ₂ H ₂
C₂H₂ flow rate	2.0 L/min
Burner height	7 mm

7.2.3 PbS₂NPs synthesis and optimisation of process parameters

Idiomarina sp. PR58-8 was grown in ZMB 2216 with requisite amount of $\text{Pb}(\text{NO}_3)_2$ at 37°C, 110 rpm for 54 hrs to obtain PbS₂NPs. The cells were harvested by centrifugation (10,000 ×

g, 20 mins), washed twice with deionised water and lysed by sonication (Microson™ Sonicator) at 0°C for three cycles of 1 min each at three RPS (40 W). The cellular debris was separated by centrifugation at 10,000 × g, 40 mins. The resulting supernatant was centrifuged at 22,000 × g for 1 hr to harvest the nanoparticles. The preparation was washed twice with deionised water and subjected to dialysis against deionised water for 12 hrs, with change of water every 2 hrs. The samples were dried in a hot air oven at 70°C for 24 hrs and the powder obtained was ground in a mortar and pestle. Appropriate controls (un-inoculated medium + Pb(NO₃)₂ and culture supernatant + Pb(NO₃)₂) were run simultaneously.

For yield determination, the PbS₂NPs were quantified by FAAS as described above. One set of cell pellets, obtained after growth in presence of Pb(NO₃)₂ were dried and weighed to determine the respective cell dry weight (CDW). The yield per gram of CDW and the yield per mg of substrate added were determined as described in section 3.2.4.

Conditions such as medium pH, incubation temperature and Pb(NO₃)₂ concentration were varied to determine the conditions for maximum yield of PbS₂NPs. *Idiomarina* sp. PR58-8 was grown in ZMB 2216 at following conditions and the yield of PbS₂NPs was determined as mentioned above.

pH	5.0	5.5	6.0	6.5	7.0	7.5	8.0
Pb(NO₃)₂ conc. (mM)	0.05	0.5	1.0	3.0	5.0	7.0	
Temperature (°C)	25	30	35	37	40		

7.2.4 Characterisation of the PbS₂NPs

XRD, crystallite domain size, UV-visible spectroscopic, TEM, and SAED analysis of the ‘as-synthesised’ PbS₂NPs were carried out as described previously in section 3.2.5. The lattice parameters for the tetragonal crystal system were calculated using the formula:

$$\frac{1}{d^2} = \left(\frac{h^2+k^2}{a^2} \right) + \frac{l^2}{c^2}; \quad (9)$$

where (h k l) are Bragg’s diffraction planes.

The fluorescence (photoluminescence- PL) spectrum of the sample dispersed in deionised water, DMEM, and phosphate buffered saline (PBS; pH- 7.0) was recorded using a

spectrofluorimeter (Jasco FP-6300) with an excitation wavelength of 386 nm. Field emission gun- transmission electron microscope (FEG-TEM; Technai, G2-F30) operated at 300 kV, and a resolution point- 2 Å, and angstrom line- 1 Å was used to obtain high resolution TEM images and the SAED pattern. The nanoparticles were dispersed in deionised water by sonication and drop-coated on carbon-coated TEM grids for imaging. Elemental composition of the PbS₂NPs was determined as described in section 6.2.5. The band gap energy was calculated using the formula:

$$E = (hc)/\lambda \quad (10)$$

where E is the band gap energy in eV, hc=1.24 eV-μm and λ is the λ_{abs} obtained by UV-visible spectroscopy in μm.

The quantum yield was measured by the integrated photoluminescence intensities and absorbance values of the PbS₂NPs using the reference dye coumarin 153 (QY= 0.58 or 58%). Stokes' shift was estimated as follows:

$$\Delta\nu = \nu_{em} - \nu_{abs} \quad (11)$$

where, Δν is Stokes' shift in cm⁻¹, ν_{em} is the wavenumber of the emission maxima in cm⁻¹, and ν_{abs} is the wavenumber of the absorbance maxima in cm⁻¹.

7.2.5 Thiol assay

The moderate halophile, *Idiomarina* sp. PR58-8 was grown in the absence (0 mM/ control) and presence of 0.5 mM, and 5 mM Pb(NO₃)₂. The cells were separated from the supernatant to prepare the cell free lysate (CFL) as described in section 6.2.6 and used for thiol assay. The T-SH, NP-SH and PB-SH were estimated using DTNB according to Sedlak and Lindsay (1968) as described in section 6.2.6. The total protein content of the CFL was determined according to Bradford (1976).

7.2.6 Mammalian cell culture

Human epithelial cervical adenocarcinoma, HeLa cell line was used for this study. They were maintained as described previously in section 4.2.8.

7.2.7 Biocompatibility studies

MTT assay was performed as described previously in section 4.2.8, to determine the cytotoxicity of the PbS₂NPs (10- 50 µg/ml) towards HeLa cell line. The experiment was performed in triplicates on three different days. Lead free cell material (ML2) and lead nitrate (LN) were also evaluated for their cytotoxicity towards HeLa cell line. The cell viability (%) relative to un-exposed controls was calculated using equation (7) given in section 4.2.8.

The ROS studies were carried out in HeLa cell line as described previously in section 4.2.9, with varying concentrations of PbS₂NPs (10, 20, 30, 40 and 50 µg/ml). ML2 and LN were also evaluated for their ability to generate ROS in HeLa cell line. 1 µM hydrogen H₂O₂ was used as positive control. All the experiments were performed in triplicates on different days.

7.2.8 Nanoparticles internalisation and bio-imaging

Exponentially growing HeLa cells (5 x 10⁴ cells/well) maintained in CM were seeded onto 2 × 2 cm sterile glass slides placed in 6-well plates and supplemented with 2 ml CM. The cells were allowed to adhere onto the glass slides for 12 hrs, and incubated with the ‘as-synthesised’ nanoparticles (30 µg/ml) for another 4 hrs. Following this, the slides were washed with sterile PBS (pH 7.0) to remove the excess nanoparticles and other debris. The slides were then observed using the TRITC filter of the Olympus BX41 epi-fluorescence microscope. Quantitative fluorescence image analysis was carried out on the ImageJ software using the following formula:

$$CTCF = ID - (A - B) \quad (12)$$

where, CTCF is the corrected total cell fluorescence, ID is integrated density, A is area of selected cell, and B is the mean fluorescence of background readings.

7.2.9 Statistical analysis

The statistical analysis was carried out as described in 2.2.5

7.3 Results and Discussions

7.3.1 Growth of *Idiomarina* sp. PR58-8 in presence of lead nitrate

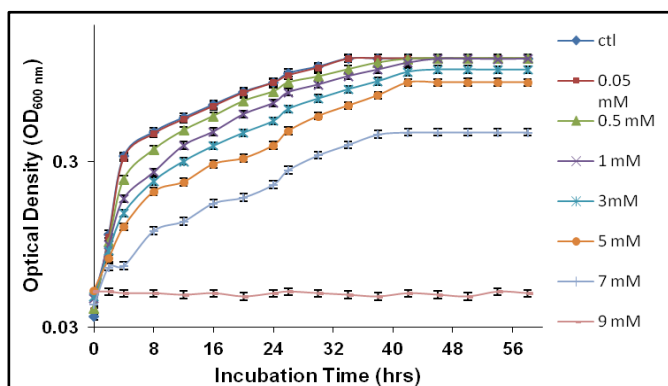


Fig. 7.1 Growth profile of *Idiomarina* sp. PR58-8 at varying concentrations of $\text{Pb}(\text{NO}_3)_2$. MIC of $\text{Pb}(\text{NO}_3)_2$ was found to be 9 mM. Values are mean \pm SD (error bars) for three experiments.

Idiomarina sp. PR58-8 possesses a high level of intrinsic resistance to silver ions (Seshadri et al. 2012) and selenium oxyanions. This marine bacterium was also found to tolerate up to 8 mM $\text{Pb}(\text{NO}_3)_2$ in ZMB 2216 (Fig. 7.1) with a simultaneous change in appearance from golden yellow to brown (Fig. 7.2). Growth at 0.05 and 0.5 mM $\text{Pb}(\text{NO}_3)_2$ was very similar to the control (0 mM $\text{Pb}(\text{NO}_3)_2$), however, as the concentration of

$\text{Pb}(\text{NO}_3)_2$ increased from 1 mM to 7 mM the growth decreased (Fig. 7.1). The MIC of $\text{Pb}(\text{NO}_3)_2$ was 9 mM, as the marine bacterium did not exhibit growth at this concentration.

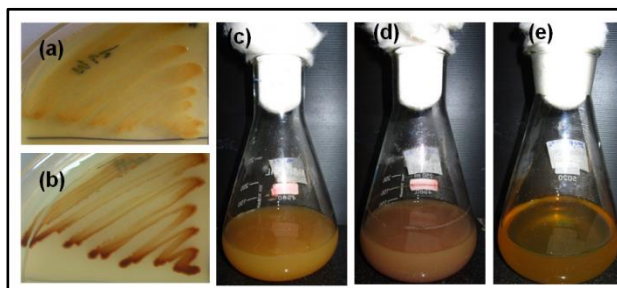


Fig. 7.2 *Idiomarina* sp. PR58-8 appears golden yellow when grown in ZMA (a) and ZMB (c). In presence of lead nitrate, it appears brown in colour (b; d). Media controls with lead nitrate did not exhibit the brown colouration (e).

Idiomarina sp. PR58-8 was grown in presence of varying concentrations of $\text{Pb}(\text{NO}_3)_2$ to determine the effect of metal salt on its growth kinetics. In the absence of $\text{Pb}(\text{NO}_3)_2$, *Idiomarina* sp. PR58-8 exhibited a specific growth rate (μ) of 1.11 hrs^{-1} , with a doubling time (t_d) of 37.46 mins, and a lag time (t_l) of 30 mins. The μ of the marine bacterium in presence of 0.05 mM and 0.5 mM $\text{Pb}(\text{NO}_3)_2$, was 1.057 hrs^{-1} and 0.896 hrs^{-1} , respectively, which was not significantly different ($p > 0.05$) as compared to the control. Similarly, the difference between the t_d and t_l of the cells grown in the presence of 0 mM (control), 0.05 mM, 0.5 mM $\text{Pb}(\text{NO}_3)_2$ was insignificant (Table 7.2). However, in presence of 1 mM, and 5 mM $\text{Pb}(\text{NO}_3)_2$, the specific

growth rates were 0.690 hrs^{-1} , and 0.463 hrs^{-1} , respectively, which were significantly lower ($p < 0.05$) than the control. The t_d and the t_l for cells grown in presence of 1 mM, and 5 mM $\text{Pb}(\text{NO}_3)_2$ were significantly higher ($p < 0.05$). Thus, higher concentrations of $\text{Pb}(\text{NO}_3)_2$ were found to negatively affect the growth of the marine bacterium (Fig. 7.3).

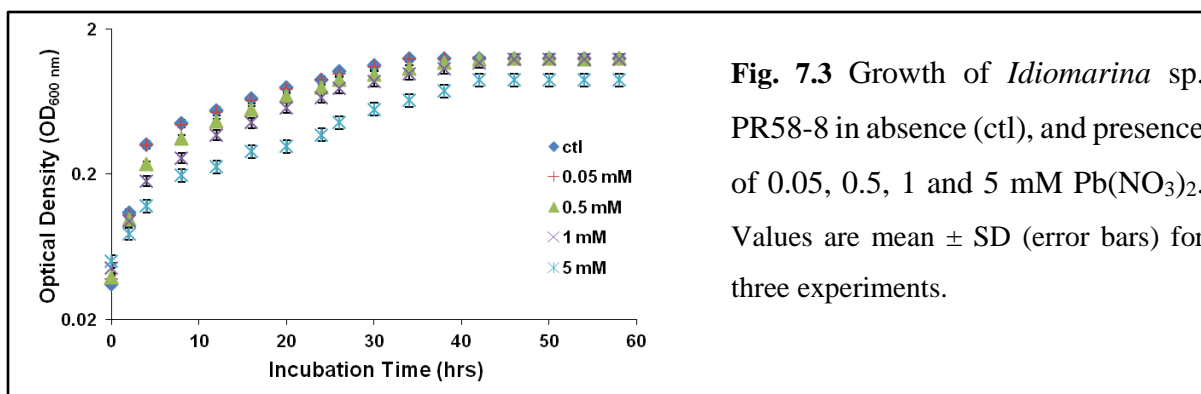


Fig. 7.3 Growth of *Idiomarina* sp. PR58-8 in absence (ctl), and presence of 0.05, 0.5, 1 and 5 mM $\text{Pb}(\text{NO}_3)_2$. Values are mean \pm SD (error bars) for three experiments.

Table 7.2 Growth kinetics parameters of *Idiomarina* sp. PR58-8 in absence (control) and in presence of lead nitrate.

Parameters	0 mM (ctl)	0.05 mM	0.5 mM	1 mM	5 mM
	$\text{Pb}(\text{NO}_3)_2$	$\text{Pb}(\text{NO}_3)_2$	$\text{Pb}(\text{NO}_3)_2$	$\text{Pb}(\text{NO}_3)_2$	$\text{Pb}(\text{NO}_3)_2$
μ (hrs^{-1})	1.110	1.057	0.896	0.690	0.463
t_d (mins)	37.46	39.34	46.41	60.26	89.81
t_l (mins)	30	30	45	60	120

μ - Specific growth rate; t_d - Doubling time; t_l - Lag time

Idiomarina sp. PR58-8 when grown in presence of $\text{Pb}(\text{NO}_3)_2$ exhibited intracellular accumulation of lead, and a concomitant loss from the medium, beginning from early exponential phase (6th hr) up to late stationary phase (42nd hr). For cells grown in presence of 0.5 mM (103.63 $\mu\text{g/ml}$) $\text{Pb}(\text{NO}_3)_2$, the Pb concentration in the medium at the 6th hr was 87.35 $\mu\text{g/ml}$, and only $\sim 1.7\%$ remained un-utilised in the medium by the 42nd hr. In case of cells grown in presence of 5 mM (1036.29 $\mu\text{g/ml}$) $\text{Pb}(\text{NO}_3)_2$, only 0.8% remained un-utilised by the

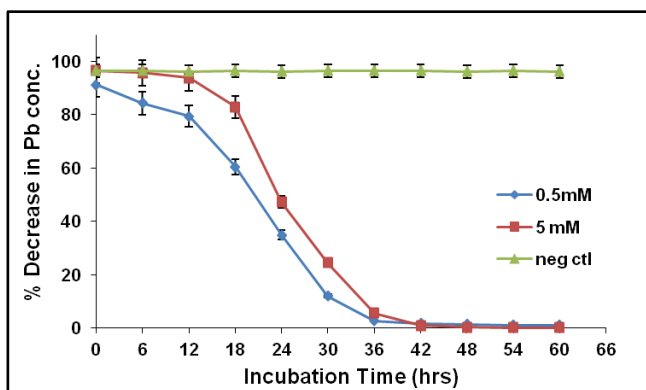


Fig. 7.4 Decrease in lead concentration in the medium, expressed as percentage of the initial value, indicative of lead uptake by *Idiomarina* sp. PR58-8; Values are mean \pm SD (error bars) for three experiments.

42nd hr. In both the instances, *Idiomarina* sp. PR58-8 accumulated ~ 91% lead by the 36th hr (Fig. 7.4). These findings are in contrast to the lead uptake exhibited by the yeasts associated with PbSNPs synthesis, *R. diobovatum*, and *Torulopsis* sp. (Seshadri et al. 20011; Kowshik et al. 2002c). Lead accumulation in both these yeasts was observed from mid exponential phase up to late stationary phase (Seshadri et al. 20011; Kowshik et al. 2002c). The effect of time of

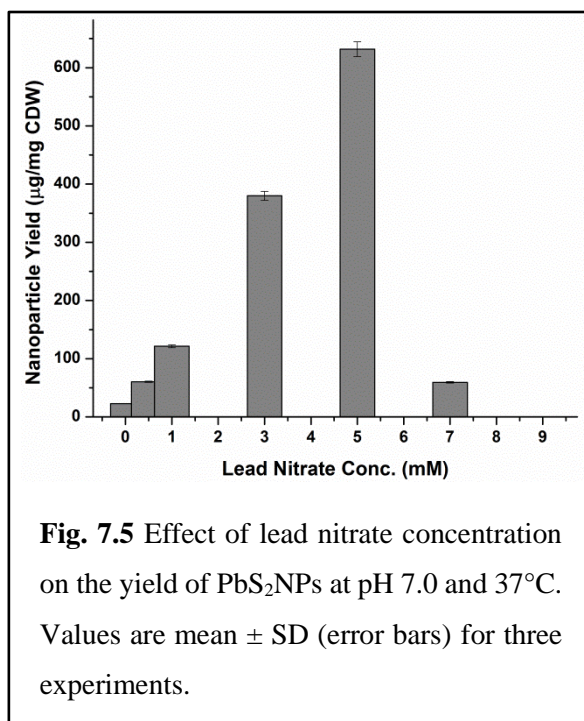
addition of $\text{Pb}(\text{NO}_3)_2$ on the growth of *Idiomarina* sp. PR58-8 was determined at 0th hr (time of inoculation) and 6th hr (early stationary phase). The addition of $\text{Pb}(\text{NO}_3)_2$ at 0th hr did not affect the growth of the marine bacterium and was accompanied with the change in culture colouration. However, when the $\text{Pb}(\text{NO}_3)_2$ was introduced in the early exponential phase, growth was retarded, with no associated colour change. These cells when transferred in fresh ZMB 2216 without $\text{Pb}(\text{NO}_3)_2$, resumed growth suggesting that the introduction of $\text{Pb}(\text{NO}_3)_2$ during the early exponential phase was bacteriostatic, and not bactericidal. Adaptation to growth in presence of $\text{Pb}(\text{NO}_3)_2$ added at the time of inoculation may be attributed to the intrinsic metal resistance mechanisms of the culture as well as the decreased availability of the Pb^{2+} to the bacterial cells. Fresh ZMB medium has a pH of 7.5, which decreases to ~6.0 in the early exponential phase. Solubility of lead complexes is higher at pH 6.0, which corresponds to increased concentrations of free Pb^{2+} , and more toxicity (Mager, 2011). Between pH 6.5 and 7.5, lesser Pb^{2+} are available and therefore addition of $\text{Pb}(\text{NO}_3)_2$ at the time of inoculation may not hinder the growth of *Idiomarina* sp. PR58-8. Thus, the $\text{Pb}(\text{NO}_3)_2$ was added simultaneously with the inoculum. This is an advantage exhibited by the marine bacterium over the yeasts, *Torulopsis* sp. and *R. diobovatum*, which require the addition of $\text{Pb}(\text{NO}_3)_2$ at mid-log phase for PbSNPs synthesis (Seshadri et al. 20011; Kowshik et al. 2002c), thereby circumventing the need for growth phase monitoring.

7.3.2 Lead (IV) sulphide nanoparticles (PbS₂NPs) synthesis and their characterisation

Growth of *Idiomarina* sp. PR58-8 in presence of Pb(NO₃)₂ was accompanied by the golden yellow culture turning brown in colour (Fig. 7.1). The culture supernatant and the media controls without inoculum failed to exhibit this colour change. Thus, the intracellular synthesis of the PbS₂NPs by *Idiomarina* sp. PR58-8 was found to be a culture dependent phenomenon. Although numerous bacteria, yeast, fungi and viruses have been reported to synthesise lead (II) sulphide nanoparticles both intracellularly and extracellularly (Singh and Nara, 2013; Seshadri et al. 2011; Bai and Zhang, 2009; Kowshik et al. 2002; Shenton et al. 1999), there are no reports on the microbial synthesis of PbS₂NPs synthesis. This is the first study on the synthesis of PbS₂NPs by a microorganism.

PbS₂NPs synthesis was carried out at various medium pH, incubation temperature and Na₂SeO₃ concentration to determine the optimum conditions for synthesis.

Pb(NO₃)₂ concentration

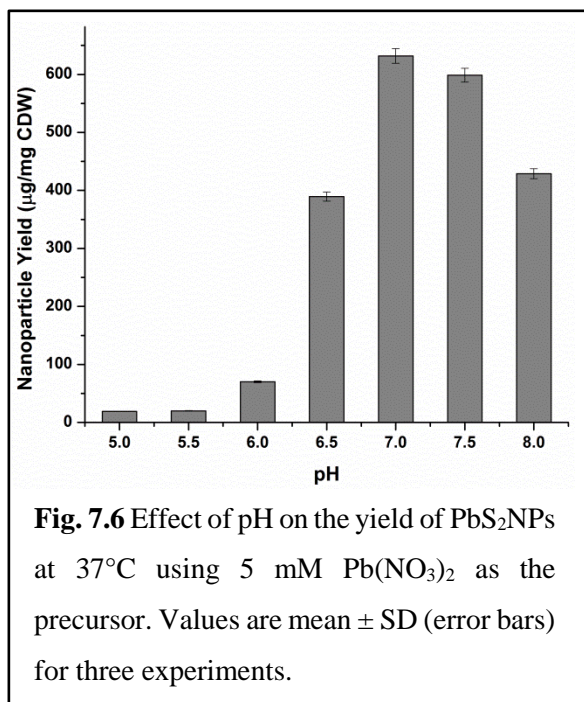


A concentration range of 0.05 mM to 9 mM Pb(NO₃)₂ was tested to determine the optimum concentration for PbS₂NPs synthesis (Fig. 7.5). At concentrations lower than 3 mM Pb(NO₃)₂, the yield of PbS₂NPs obtained was very low and in the range of ~ 22.73- 121.49 µg/mg CDW. The low yield may be attributed to the presence of low concentration of Pb(NO₃)₂. At concentrations of 3 mM, and 5 mM Pb(NO₃)₂ (Fig. 7.5), the yield of PbS₂NPs was 379.91 and 631.71 µg/mg CDW, respectively. Although the growth of *Idiomarina* sp. PR58-8 was affected at 5 mM

Pb(NO₃)₂, maximum yield was obtained at this concentration. The yields obtained at 1 mM, 3 mM, and 7 mM Pb(NO₃)₂ were significantly lower ($p < 0.05$) as compared to the yield obtained

at 5 mM $\text{Pb}(\text{NO}_3)_2$. As maximum yield of PbS_2NPs was obtained at 5 mM $\text{Pb}(\text{NO}_3)_2$, this concentration was used for further studies on PbS_2NPs synthesis.

Medium pH



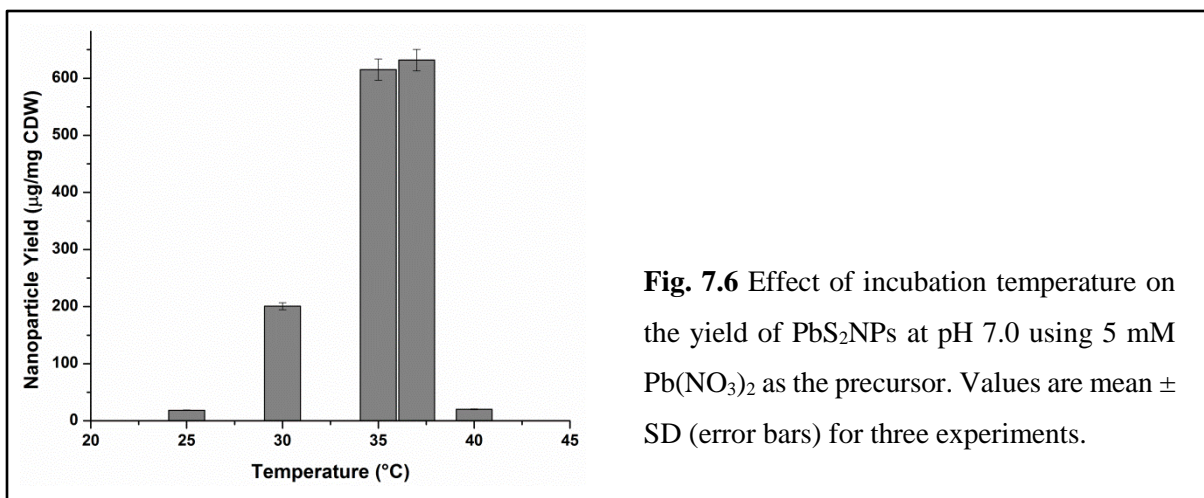
The PbS_2NPs synthesis was carried out at varying pH (5.0-8.0) to determine the optimum pH for maximum yield. The pH range for growth of *Idiomarina* sp. PR58-8 is 6.0-9.0, with the optimum at pH 7.0. At pH 7.0, maximum yield of 631.71 $\mu\text{g}/\text{mg}$ CDW was obtained (Fig. 7.6). The halophilic bacteria exhibited poor growth at pH of 5.0 and 5.5 in the absence of $\text{Pb}(\text{NO}_3)_2$, and the yield of PbS_2NPs was significantly lower ($p < 0.05$) as compared to that at pH 7.0. Thus, as the pH increased from 6.0 to 6.5, a corresponding increase in yield was observed. Yield of PbS_2NPs at pH 7.5 was

598.75 $\mu\text{g}/\text{mg}$ CDW, which was not significantly different ($p > 0.05$) from the yield obtained at pH 7.0. However, alkaline pH of 8.0 significantly lowered the yield of PbS_2NPs . Based on these results, PbS_2NPs synthesis was carried out at pH 7.0.

Incubation temperature

A temperature range of 25°C to 40°C was tested to determine the optimum temperature of growth for efficient PbS_2NPs synthesis by *Idiomarina* sp. PR58-8. The optimum range of temperature for growth of *Idiomarina* sp. PR58-8 is 30°C to 38°C. Maximum PbS_2NPs synthesis was obtained at 35 and 37°C with a yield of 615.09 and 631.71 $\mu\text{g}/\text{mg}$ CDW, respectively (Fig. 7.7). As the incubation temperature increased from 25°C to 37°C, the yield of PbS_2NPs also increased and the difference in yield between 30° and 37°C was significant ($p < 0.05$). The halobacterial isolate exhibited slow growth at 40°C, and therefore, the yield of

PbS₂NPs was also lower. Thus, further studies on PbS₂NPs synthesis by *Idiomarina* sp.PR58-8 was carried out at 37°C.

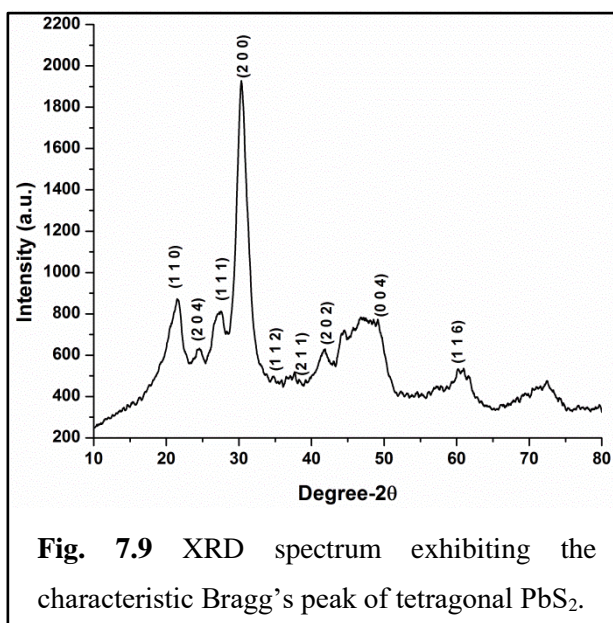
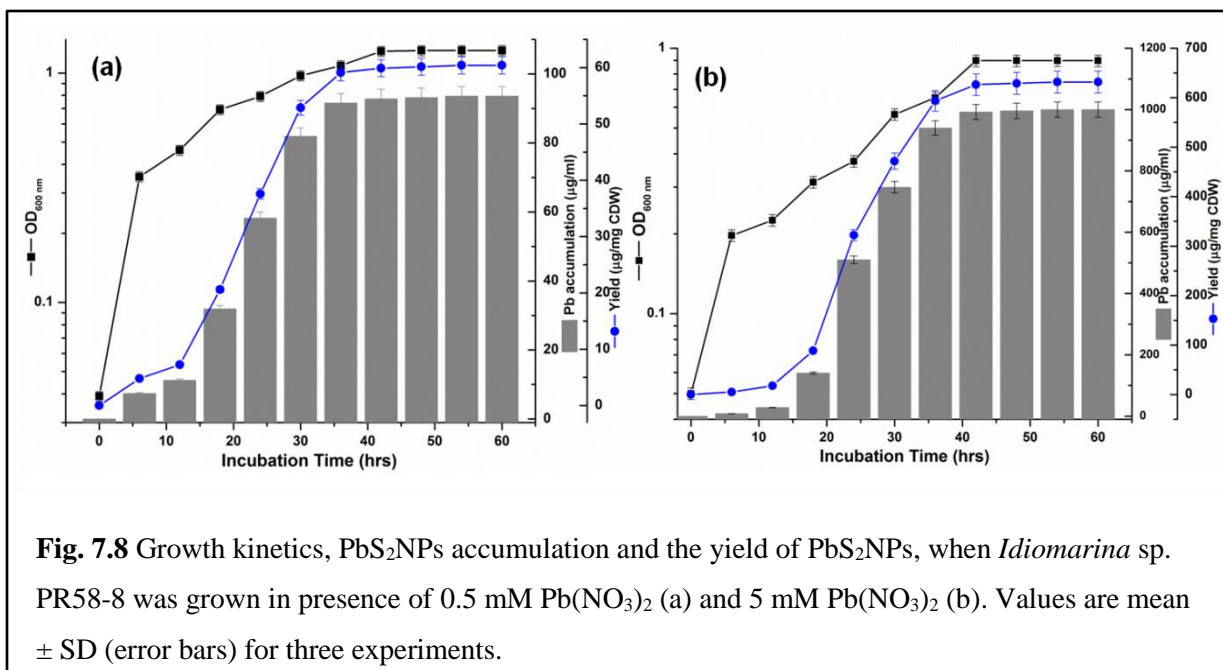


The PbS₂NPs by *Idiomarina* sp.PR58-8 was carried out with 5 mM Pb(NO₃)₂, at pH of 7.0 and an incubation temperature of 37°C.

Time course of lead uptake and nanoparticles yield were correlated to the growth phase of *Idiomarina* sp. PR58-8 (Fig. 7.8). Yield with respect to biomass and with respect to substrate added were estimated along with the efficiency of the process (Table 7.3). Maximum yield was obtained at 54th hr, with an efficiency of 90.3% in case of 0.5 mM Pb(NO₃)₂, and 96.5% in case of 5 mM Pb(NO₃)₂. The yield with respect to the biomass was 60.4 µg/mg CDW, and 631.71 µg/mg CDW for cells grown in presence of 0.5 mM, and 5 mM Pb(NO₃)₂, respectively. As the process was found to be more efficient at 5 mM Pb(NO₃)₂ with a significantly higher yield ($p < 0.05$) as compared to that in presence of 0.5 mM Pb(NO₃)₂, synthesis was carried out at 5 mM Pb(NO₃)₂.

Table 7.3 The yield parameters of PbS₂NPs synthesised by *Idiomarina* sp. PR58-8

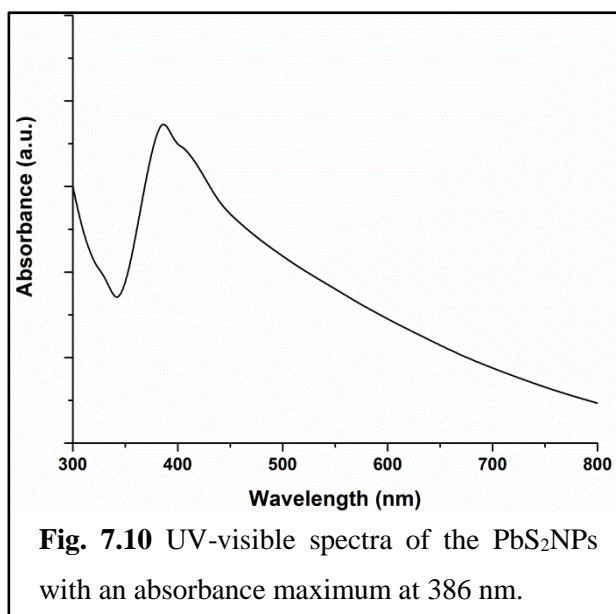
Yield Parameters	0.5 mM Pb(NO ₃) ₂	5 mM Pb(NO ₃) ₂
Yield (mg/g CDW)	15.16	30.13
Yield (mg/mg Pb)	0.907	0.965
Efficiency (%)	90.78	96.5



XRD spectra of the 'as-synthesised' nanoparticles exhibited characteristic peaks of tetragonal lead (IV) sulphide (PbS₂) corresponding to ICDD card no. 20-0596 (Fig. 7.9). This is the first report on PbS₂ nanoparticles synthesis by an organism. The studies to date about microbial lead sulphide nanoparticles fabrication have been on synthesis of cubic PbSNPs (Kowshik et al. 2002; Bai and Zhang, 2009; Seshadri et al. 2012). In fact, there are very few reports on

synthesis of tetragonal PbS₂ nanoparticles by chemical routes as well (Shyju and Gopalakrishanan, 2013; Geethu et al. 2012; Roman-Zamorano et al. 2009; Qadri et al. 1997). The α (hexagonal), and the β (tetragonal) PbS₂ phases are considered high pressure phases as their synthesis has a requirement of pressures higher than 20 Kbars and temperatures above 600°C (Pitcher et al. 2000). Synthesis of PbS₂ at atmospheric pressure using natural zeolite was attributed to the ability of the matrix to induce nucleation of the compressed lead sulphide

phases which is a function of the rigidity and order provided by the porous mineral (Roman-Zamorano et al. 2009). A similar nucleation, with biomolecules of bacterial origin acting as the centre, may be responsible for generation of β -PbS₂ nanoparticles by *Idiomarina* sp.PR58-8. Broadening of the peaks at the base are indicative of the particles being in nano-dimension. The crystallite domain size as calculated using the Debye-Scherrer formula for (2 0 2) peak was 2.38 nm. The formation of tetragonal lattice structure was attributed to the distortion in the cubic lattice of the lead sulphide nanocrystallites synthesised in the bi-continuous cubic phase of a lipid, when the size of the crystal decreased below 6 nm (Qadri et al. 1997). The lattice parameters for tetragonal system were $a = 4.45 \text{ \AA}$ and $c = 4.24 \text{ \AA}$, with an a/c ratio of 1.05, which corresponds to the a/c ratio obtained for tetragonal PbS nanocrystallites of ~ 3 nm size synthesised in the bi-continuous cubic phase of a lipid (Qadri et al. 1997) (35).



UV-visible spectroscopy of the ‘as synthesised’ PbS₂NPs exhibited an absorbance maximum (λ_{abs}) at 386 nm (Fig. 7.10) corresponding to an energy gap of ~ 3.22 eV. The PbS₂NPs thin films synthesised via the chemical routes exhibit a similar λ_{abs} at ~ 400 nm (Geethu et al. 2012). Roman-Zamorano *et al.* (2009) have reported that heating the PbS₂NPs at/above temperatures of 55°C , causes the λ_{abs} to shift from 240 nm to ~ 400 nm. On the other hand, the λ_{abs} of

the PbSNPs synthesised by *Torulopsis* sp. and *R. diobovatum* were 330 nm and 320 nm, respectively (Kowshik et al. 2002; Seshadri et al. 2011). The λ_{abs} of PbSNPs exhibit a blue shift as compared to bulk PbS, which has an absorption onset at 3020 nm, and a band gap of 0.41 eV at 298 K. This blue shift and the increase in the energy band gap is a result of the particle size becoming smaller than the excitonic Bohr radius of the bulk PbS (quantum confinement) (Wise, 2000). A similar phenomenon may be responsible for the increase in the energy band gap of the PbS₂NPs.

Morphological characterisation was achieved by transmission electron microscopy (TEM) and high resolution-TEM (HRTEM). TEM analysis indicated particles with spherical morphology and an average size of 6 nm (Fig. 7.11a). The HRTEM image of the PbS₂NPs (Fig. 7.11b) also exhibited nearly spherical particles with an average size of 6 nm, and interplanar spacing (*d*) of 0.318 nm which corresponds to the *d*-spacing of the (2 0 0) plane ($d_{(2\ 0\ 0)} = 0.307$ nm). Similar spherical shaped PbS₂NPs with an average size of ~ 10 nm stabilised in natural zeolite have been reported (Roman-Zamorano et al. 2009). The SAED pattern of the PbS₂NPs (Fig. 7.12a) can be indexed to the tetragonal PbS₂ crystallite planes of (2 0 0), (1 1 1), and (2 0 4). FFT (fast Fourier transform) analysis of the PbS₂NPs was also carried out to obtain the diffraction pattern and to measure the distances between the atomic planes (Fig. 7.12b). The small size distribution of the nano-preparation may be attributed to the kinetic constraints imposed by the strong binding conditions within the bacterial cells (Roman-Zamorano et al. 2009). Elemental composition of the PbS₂NPs as determined by EDAX confirmed the presence of Pb and S (Fig. 7.12c,d). The peaks of S overlaps with that of Pb and both the peaks appear at 2.3 KeV (Warner et al. 2005). Peaks due to C, O, and Cu may be attributed to the carbon coated copper grid used for SEM-EDS analysis.

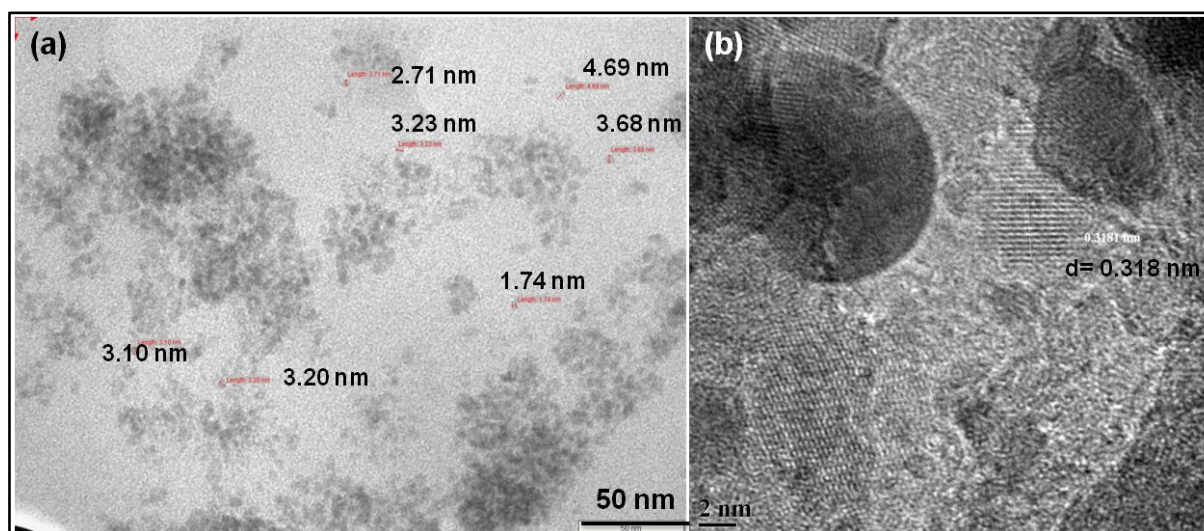


Fig. 7.11 (a) TEM micrographs of the PbS₂NPs exhibiting spherical particles with an average size of 6 nm. (b) HR-TEM micrograph showing spherical nanoparticles with interplanar spacing of 0.318 nm.

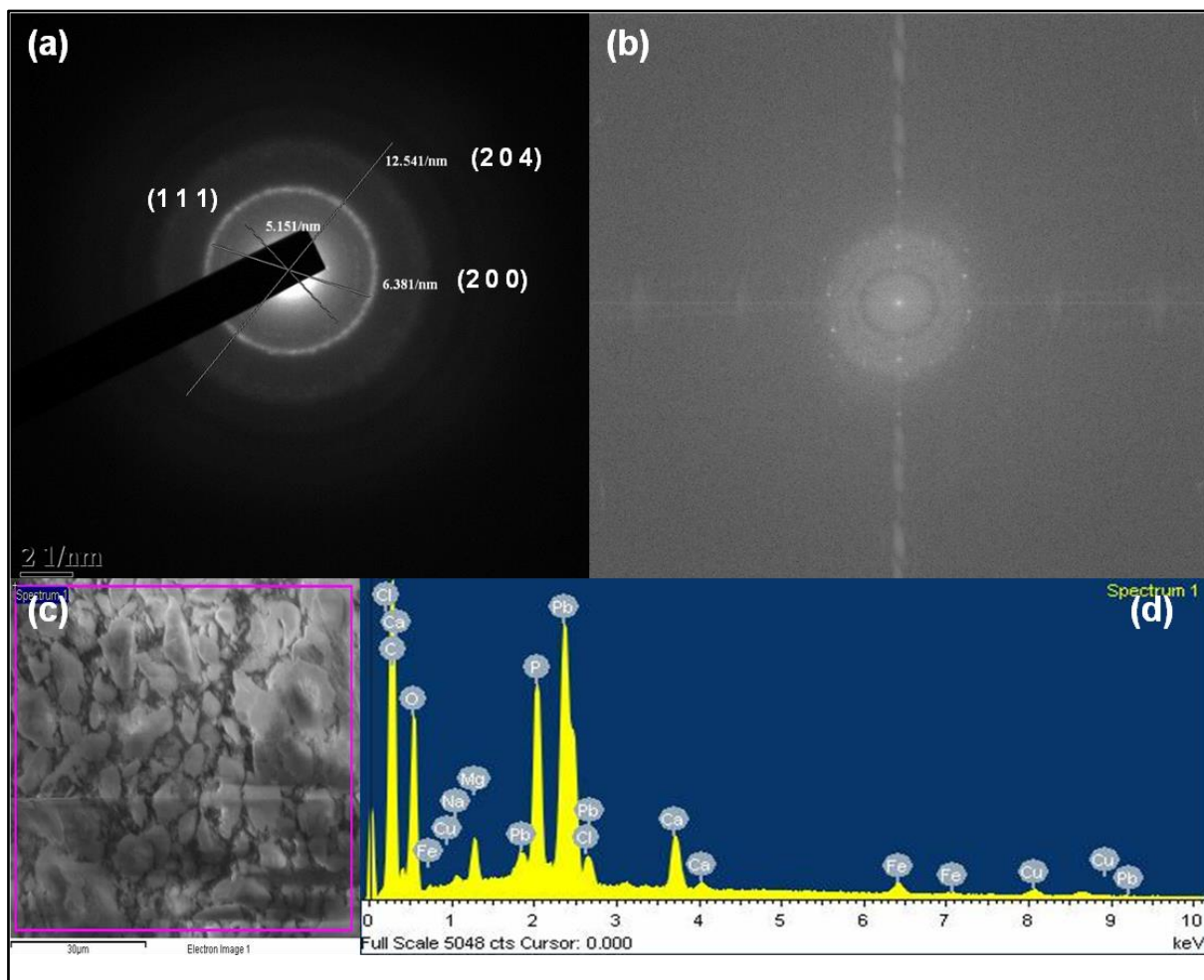


Fig. 7.12 (a) SAED pattern of the PbS₂NPs corresponding to the tetragonal crystal facets, where the three rings could be indexed to Bragg planes of (1 1 1), (2 0 4) and (2 0 0); (b) FFT of a single PbS₂NPs obtained during HR-TEM analysis; (c) SEM micrograph of the PbS₂NPs used for EDAX measurements; (d) EDAX spectrum with peaks of Pb. S peaks overlap with the Pb peak.

The photoluminescence spectra of the PbS₂NPs are shown in Fig. 7.13a. The emission maximum (λ_{em}) was obtained at 530 nm. The emission spectra of the ‘as-synthesised’ PbS₂NPs exhibited a Gaussian spectral line shape with a full width half maximum (FWHM) of 24.09 nm. Majority of the semi-conducting QDs exhibit Gaussian emission spectra with a FWHM of ~30 nm that confers multiplexing capability on to the QDs (Wolfbeis, 2015). The samples on storage exhibited similar fluorescence spectra as that of freshly synthesised PbS₂NPs (Fig. 7.13b). The lyophilised cellular material of *Idiomarina* sp. PR58-8 (ML2) did not exhibit a λ_{em} , instead luminescence was observed over a broad range (~340 nm to 500 nm), which disappeared on storage for 48 hrs or more (Fig. 7.14a). This luminescence may be attributed

to the presence of biomolecules such as NADH and tryptophan (Kowshik et al. 2002). However, after 48 hrs of storage at room temperature as is or in water/PBS, the luminescence disappeared due to the degradation of these biomolecules (Friedman and Cuq, 1988; Rover Junior et al. 1998). This is the first microbially synthesised PbS₂NPs exhibiting fluorescence that may have potential applications in bio-imaging. Most of the chemically synthesised PbS quantum dots have emissions in the near infrared region (NIR) (Truong et al. 2011; Hu et al. 2012; Chen et al, 2016), with the exception of PbS colloids synthesised by controlled precipitation in water and acetonitrile solutions that exhibit λ_{em} in the visible range (Nozik et al. 1985). These PbS colloids were shown to have a λ_{em} of 436 nm and/or 600 nm based on their size, with an excitation wavelength of 355 or 410 nm (Nozik et al. 1985). Since λ_{em} of the PbS₂NPs synthesised by *Idiomarina* sp. PR58-8 is in the visible range, it is advantageous as the routine, relatively inexpensive epi-fluorescence microscopes can be easily used for bio-imaging. The fluorescence spectra of the PbS₂NPs were also recorded in PBS (pH 7.0) and DMEM, where PBS was used to mimic the extracellular environment, while DMEM was used to mimic the *in-vitro* environment. Altering the solvent did not result in any change in the fluorescence spectra, thus, exhibiting the ability of these PbS₂NPs to retain their fluorescent property in varying environments (Fig. 7.14b).

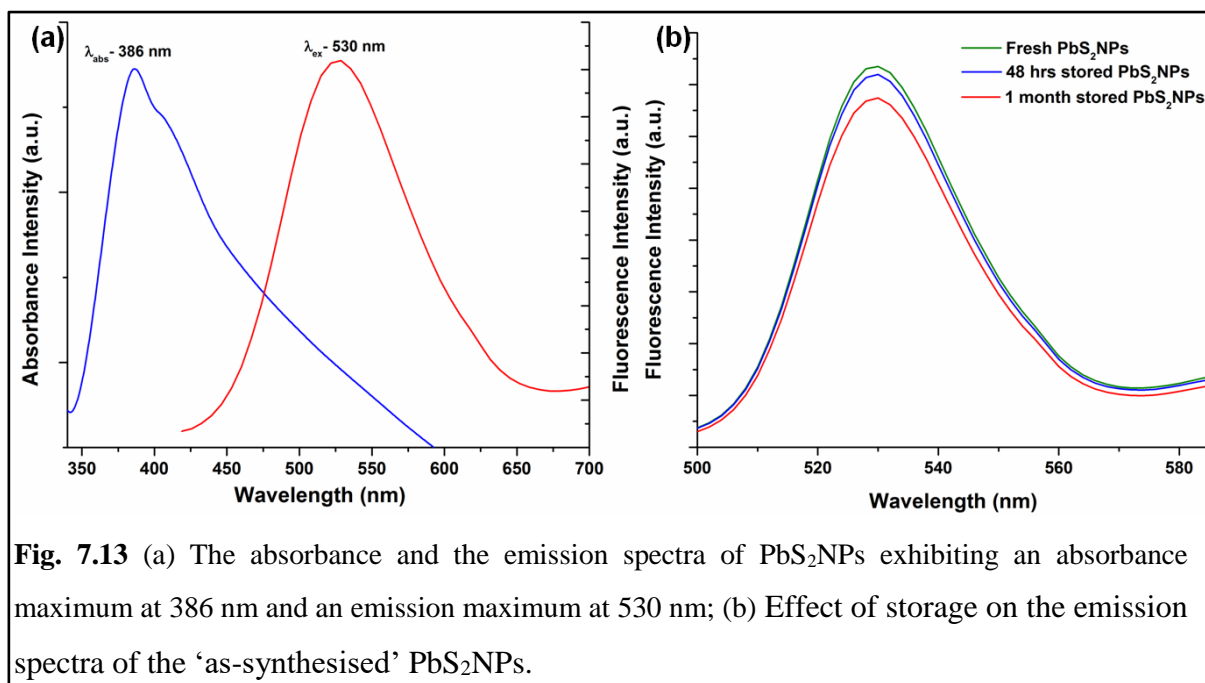


Fig. 7.13 (a) The absorbance and the emission spectra of PbS₂NPs exhibiting an absorbance maximum at 386 nm and an emission maximum at 530 nm; (b) Effect of storage on the emission spectra of the ‘as-synthesised’ PbS₂NPs.

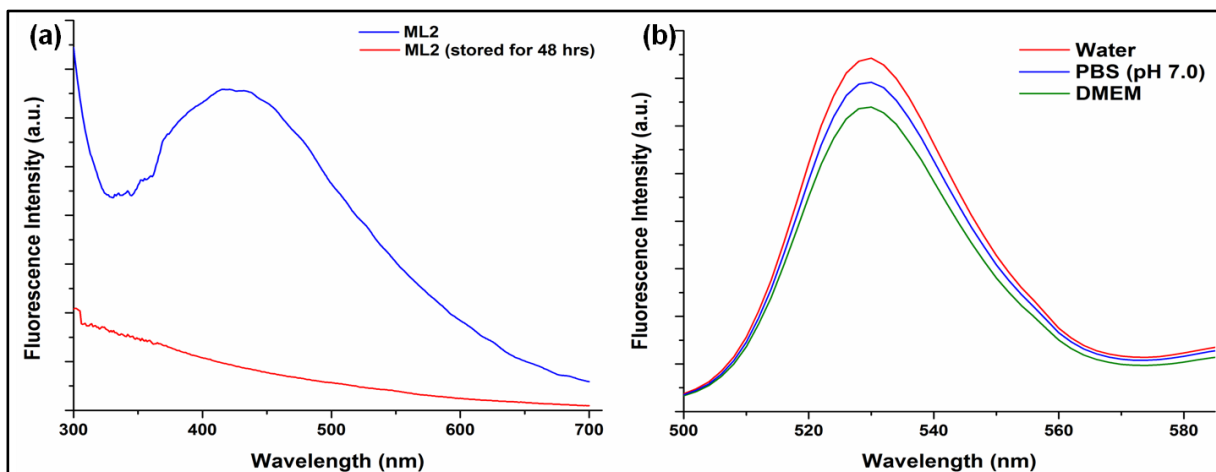


Fig. 7.14 (a) The photoluminescence spectra of the lyophilized *Idiomarina* sp. PR 58-8 exhibiting a broad peak, which disappeared on storage for 48 hrs; (b) The fluorescence spectra of PbS₂NPs synthesised by *Idiomarina* sp. PR58-8 in solvents such as water, PBS (pH 7.0) and DMEM.

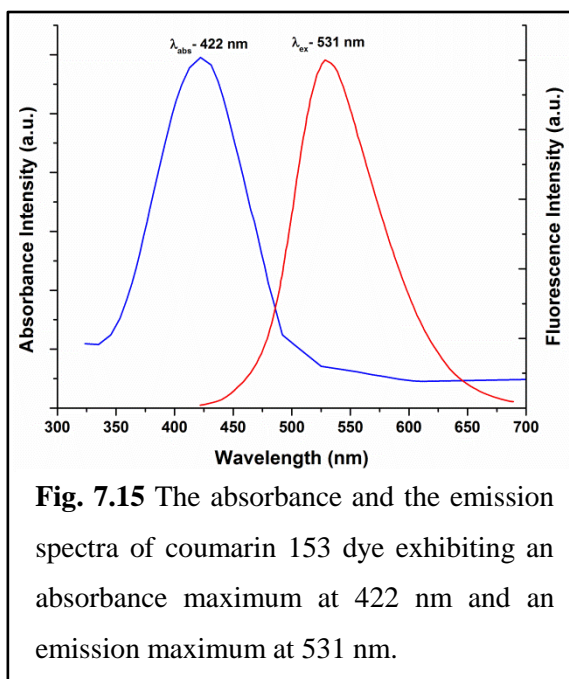


Fig. 7.15 The absorbance and the emission spectra of coumarin 153 dye exhibiting an absorbance maximum at 422 nm and an emission maximum at 531 nm.

The λ_{em} of the PbS₂NPs exhibited a relatively large Stokes' shift of 7038 cm⁻¹ (144 nm). Stokes' shift, defined as the red shift of the emission spectra with respect to the absorption spectra, is an important quantity that determines the optical properties of semiconductor nanoparticles (Bagga et al. 2005). Large Stokes' shift (5000- 10000 cm⁻¹) is a desirable property for an efficient fluorescent stain (He et al. 2015). Further, the fluorescence quantum yield (QY), an intrinsic property of fluorescent probes, was estimated using the reference dye, coumarin

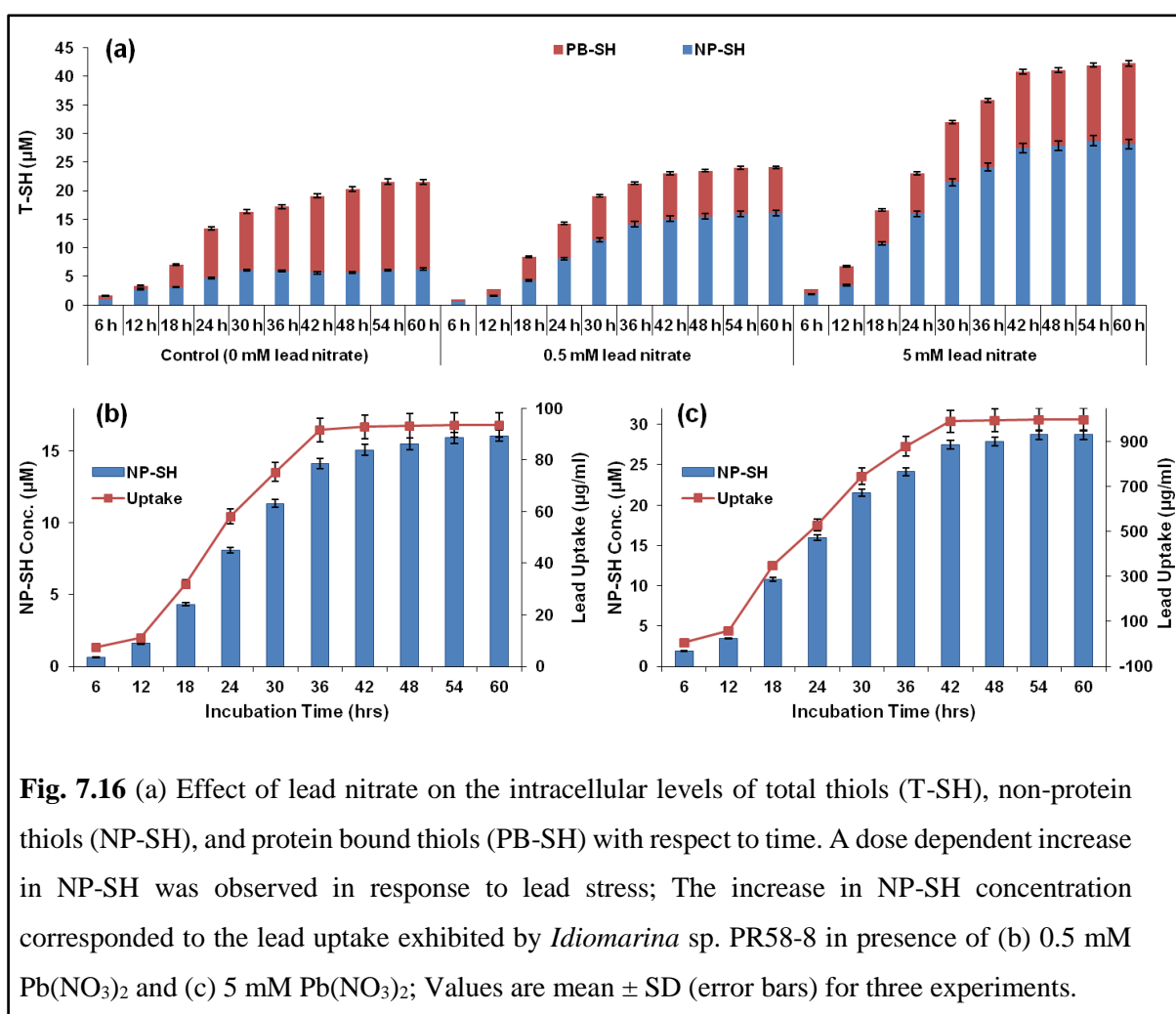
153 (QY=0.58) which has λ_{abs} at 422 nm and λ_{em} at 531 nm (Fig. 7.15). QY is defined as the ratio of the number of emitted photons to the absorbed photon. The QY of the synthesised PbS₂NPs was found to be 0.67 in all the three solvents. QY of PbS quantum dots synthesised by various chemical methods has been reported to be between 0.1 to 0.9 based on their size (Hinds et al. 2007; Spangler et al. 2016). Biological imaging requires sensitive fluorophores

with relatively large Stokes' shifts and acceptable QYs. The PbS₂NPs synthesised by *Idiomarina* sp. PR58-8, exhibited narrow symmetric emission spectra with Gaussian distribution; λ_{em} in the visible range with a large Stokes' shift and relatively high QY; were not affected by their micro-environment; and thus, present a superior fluorophore as compared to organic dyes, for bio-imaging applications.

7.3.3 Mechanism of PbS₂NPs synthesis

Pb²⁺ offers limited beneficial functions to both eukaryotes and prokaryotes, and is therefore, considered a toxin (Nies, 1999). Thus, microbes have evolved numerous mechanisms to overcome the stress exerted by the lead cation. Microorganisms may prevent the influx of Pb²⁺ by either precipitating it as insoluble phosphates, or by adsorption on the cell wall via EPS and/or other cell wall components. In case the Pb²⁺ is taken up by the microbial cell, it may be sequestered as phosphates or effluxed out of the cell via transporters viz., CadA, ZntA, and PbrA (Jaroslawiecka and Piotrowska-Seget, 2014). Pb²⁺ can also be rendered inactive by thiol compounds that include NP-SH like GSH, cysteine, and cystine; and PB-SH like PCs and MTs (Harrison et al. 2007; Naik and Dubey, 2013). In presence of metal ions such as that of lead, bacteria and fungi increase the cellular pools of thiols, thereby sequestering the toxic ions (Pages et al. 2008). *Idiomarina* sp. RR58-8, a γ proteobacteria, has G-SH as the most abundant thiol (Kessi and Hanselmann, 2004) and thus, the involvement of thiols in lead resistance and transformation was investigated. The intracellular thiol concentrations of the cells exposed to varying concentrations of Pb(NO₃)₂ were estimated over a period of 60 hrs. In untreated controls, at 6th hr NP-SH accounted for 88.3% while PB-SH accounted for 11.7% of the T-SH. However, at the 60th hr, the PB-SH had increased to 70.9% while the NP-SH decreased to 29.1%. Pb(NO₃)₂ exposed cells on the other hand exhibited a dose dependent and a time dependent increase in NP-SH. The NP-SH was found to be ~ 4 times higher in cells treated with 5 mM Pb(NO₃)₂ as compared to untreated controls, while the PB-SH decreased ~1.05 times as compared to controls at the 36th hr, with a concomitant intracellular lead accumulation of ~91%. The increase of T-SH is a function of the increase in NP-SH as is evident in Fig. 7.16a. A simultaneous increase in the intracellular lead and NP-SH concentration was observed at 18th hr suggesting a positive interdependence between the two. Although the lead uptake commences from early exponential phase (6th hr) during the growth of *Idiomarina* sp. PR58-

8, active uptake begins only around the 18th hr, at which time the concentration of NP-SH within the lead exposed cells also increased (Fig. 7.16b,c). As the lead uptake was found to continue till the late stationary phase (42nd hr), the increase in NP-SH concentration also exhibited a similar trend. A similar increase in NP-SH and concomitant decrease in PB-SH has been reported in response to various metals in bacteria and fungi (Guimaraes-Suares et al. 2008; Seshadri et al. 2011; Seshadri et al. 2012). The decrease in the PB-SH and the increase in NP-SH may be attributed to the presence of metal ions that causes the sulphur in the proteome to be redirected towards GSH synthesis (Fauchon et al. 2002). Our results suggest the involvement of NP-SH in lead resistance and synthesis of lead based nanoparticles.



7.3.4 Biocompatibility studies and application of PbS₂NPs

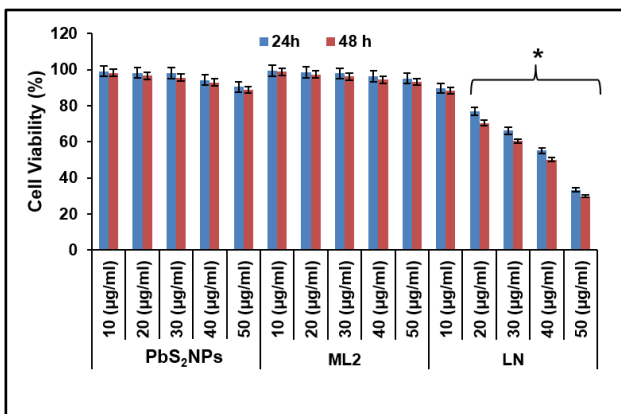


Fig 7.17 Effect of PbS₂NPs, lead free cell material (ML2) and lead nitrate (LN) on viability of HeLa cells. Values are mean \pm SD (error bars) for three experiments.

Biocompatibility and non-cytotoxicity are the prerequisites for a fluorophore to be used as bio-imaging agents. The biocompatibility of the PbS₂NPs was evaluated in HeLa cell line using MTT for 24 and 48 hrs. Even at the highest concentration of PbS₂NPs (50 µg/ml) tested, a viability of 90.31 %, and 88.77 %, was obtained for cells exposed for 24 hrs, and 48 hrs, respectively (Fig. 7.17). The nanoparticles exhibited no significant ($p > 0.05$) difference in viability as

compared to untreated controls at both the time points. Pb free cell material (ML2) did not exhibit any significant cytotoxicity at any of the concentrations tested. Pb(NO₃)₂, on the other hand exhibited a significantly higher ($p < 0.05$) toxicity towards HeLa cells at concentrations of 20 µg/ml and above (Fig. 7.17). Similar results have been reported for human leukemia (HI-60) cells treated with lead nitrate (Yedjou et al. 2010). This supports the biocompatible nature of PbS₂NPs as compared to Pb(NO₃)₂.

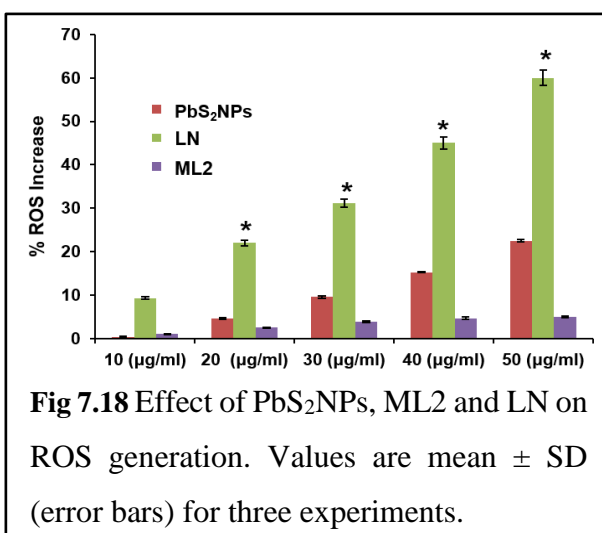


Fig 7.18 Effect of PbS₂NPs, ML2 and LN on ROS generation. Values are mean \pm SD (error bars) for three experiments.

Lead nitrate exerts its cytotoxicity by inducing oxidative stress through ROS generation followed by depletion of the anti-oxidative reserves (Flora et al. 2002). Thus, to further assess the biocompatibility of the PbS₂NPs, ROS assay was carried out. The 'as-synthesised' PbS₂NPs did not exhibit a significant increase ($p > 0.05$) in ROS generation up to 40 µg/ml as compared to

the untreated controls (Fig. 7.18). At 50 µg/ml, PbS₂NPs exhibited a significant increase (23%;

$p < 0.05$) in ROS generation as compared to untreated control. ML2 did not exhibit any significant increase ($p > 0.05$) in ROS production as compared to untreated control or PbS₂NPs treated cells. Pb(NO₃)₂ exhibited a dose-dependent increase in ROS (Fig. 7.18). At 10 µg/ml Pb(NO₃)₂ the increase in ROS was insignificant ($p > 0.05$) as compared to untreated control, which reached significance ($p < 0.05$) at concentrations of 20 µg/ml and above. Previous studies have shown that functionalising/capping agents play a major role in cytotoxicity of the lead based nanoparticles, where certain agents such as 3-mercaptopropylsulfonate and sodium 2,3-dimercaptopropylsulfonate were found to make the particles more toxic, while others viz., β-lactoglobulin, glutathione, and DNA rendered them non-toxic (Levina et al. 2005; Hu et al. 2012; Nakane et al. 2013; Chen et al. 2016). Pb in its divalent cationic form (Pb²⁺) easily replaces the divalent cations such as Ca²⁺, Mg²⁺, Fe²⁺, and sometimes the monovalent cations like Na⁺, present in the biological system, thereby disrupting various physiological functions (Lidsky and Schneider, 2003). Capping the PbS QDs with stabilising molecules such as GSH or β-lactoglobulin, prevents the release of Pb²⁺ thereby attenuating the cytotoxicity of the QDs (Chen et al. 2016). Pb in the PbS₂NPs synthesised by *Idiomarina* sp. PR58-8 is in +4 oxidation state (PbS₂) and most likely capped by a thiol containing bio-molecule. The capping agents stabilising the nanoparticles prevent the Pb⁺⁴ from exposure to the reducing moieties present in the biological environment and its reduction to Pb²⁺, thereby lowering its toxicity. Thus, PbS₂NPs synthesised by the *Idiomarina* sp. PR58-8 were found to be biocompatible and may be deemed safe for bio-imaging applications.

The HeLa cells grown in presence of 30 µg/ml PbS₂NPs were observed under the epifluorescence microscope using the TRITC filter to check for internalisation of the nanoparticles and bio-imaging. Fig. 7.19a shows cells with internalised PbS₂NPs that appear as red fluorescent particles. The particles were unable to penetrate the nucleus and appear uniformly distributed within the cytoplasm of the cell. Fig. 7.19c shows the image of the PbS₂NPs powder exhibiting red fluorescence, while the lyophilised cellular material, ML2 (Fig. 7.19e) did not exhibit any fluorescence. Figures 7.19b, d, and f show the phase-contrast images of the PbS₂NPs treated cells, PbS₂NPs, and ML2 respectively. Fig. 7.20 shows the CTCF of the cells stained with the PbS₂NPs where the background fluorescence was subtracted. The data indicates that fluorescence intensity is directly proportional to the size of the cell and the uniform distribution of the particles. Therefore, the PbS₂NPs synthesized by

Idiomarina sp. PR58-8 may be used as *in-situ* fluorescent probes. This is the first report on microbially synthesised PbS₂NPs with fluorescent properties with potential applications in bio-imaging. The ‘as-synthesised’ PbS₂NPs may also be used for targeted bio-labelling, where the nanoparticles can be functionalised to target specific subset of cells. As the PbS₂NPs synthesised by *Idiomarina* sp. PR58-8 are most likely capped with NP-SHs, the preparation can be suitably modified at –SH site by attaching various targeting ligands and antibodies for site-directed imaging. Thus, the ‘as-synthesised’ PbS₂NPs are versatile fluorophores that may be exploited for myriad applications in imaging and analysis.

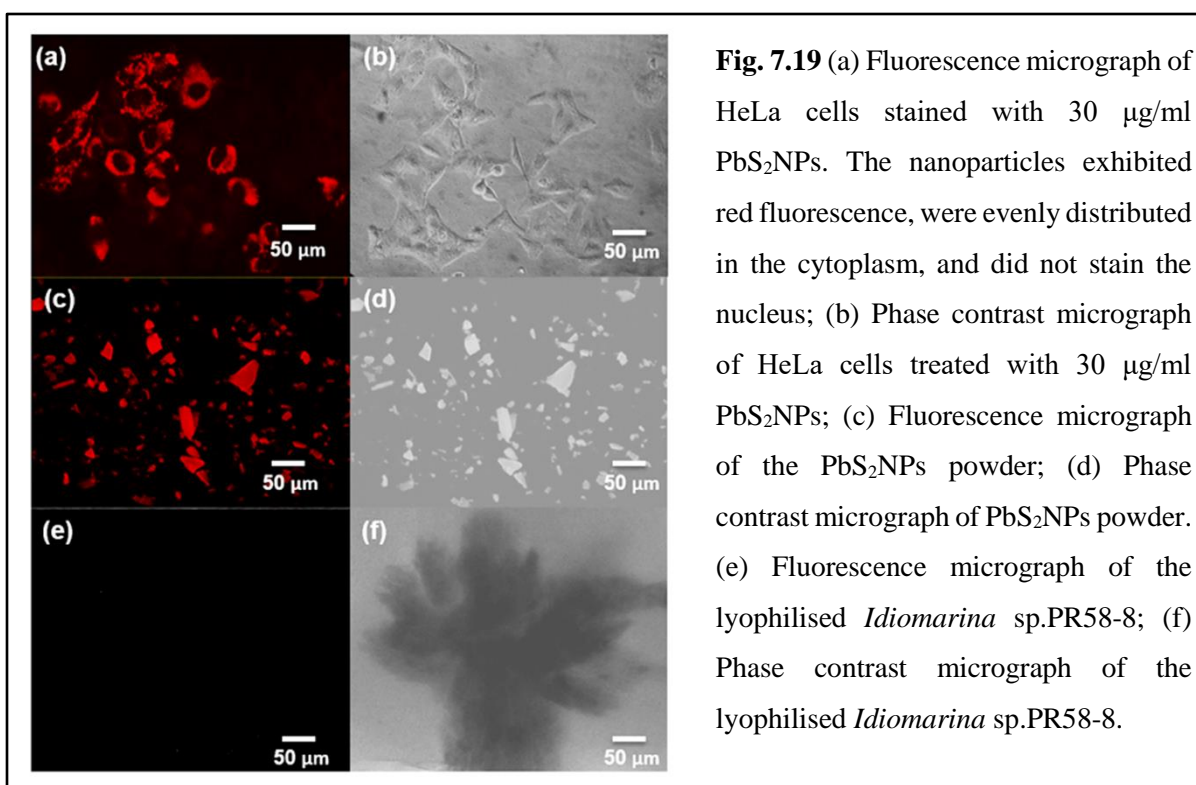


Fig. 7.19 (a) Fluorescence micrograph of HeLa cells stained with 30 μg/ml PbS₂NPs. The nanoparticles exhibited red fluorescence, were evenly distributed in the cytoplasm, and did not stain the nucleus; (b) Phase contrast micrograph of HeLa cells treated with 30 μg/ml PbS₂NPs; (c) Fluorescence micrograph of the PbS₂NPs powder; (d) Phase contrast micrograph of PbS₂NPs powder. (e) Fluorescence micrograph of the lyophilised *Idiomarina* sp. PR58-8; (f) Phase contrast micrograph of the lyophilised *Idiomarina* sp. PR58-8.

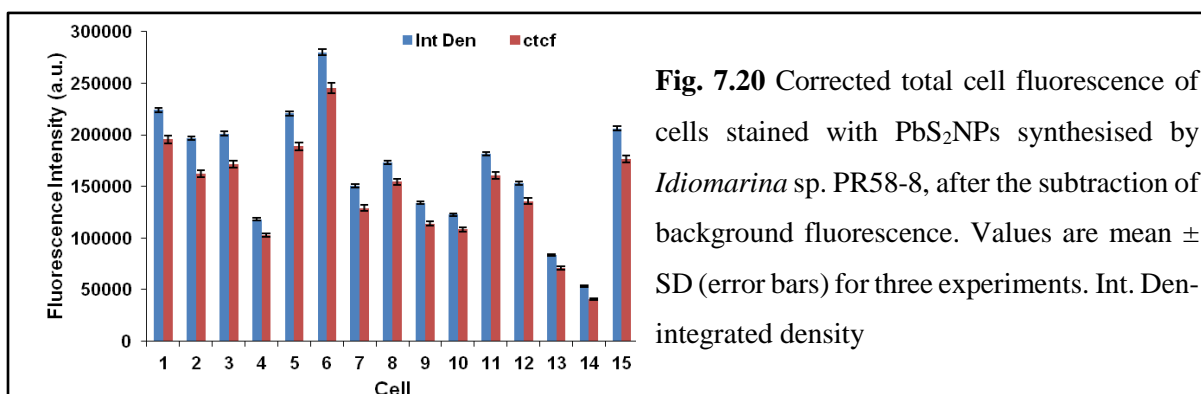


Fig. 7.20 Corrected total cell fluorescence of cells stained with PbS₂NPs synthesised by *Idiomarina* sp. PR58-8, after the subtraction of background fluorescence. Values are mean ± SD (error bars) for three experiments. Int. Den-integrated density

7.4 Conclusion

Lead based nanomaterials have been extensively reported for various optoelectronic applications due to their size tuneable properties. Amongst these, the studies on synthesis of tetragonal β -PbS₂ nanoparticles are very few with all of them employing toxic precursors, and extreme conditions of temperature, pressure, and pH. In this study, we report the intracellular synthesis of tetragonal PbS₂NPs by the marine bacterium *Idiomarina* sp. PR58-8, when grown in presence of 5 mM Pb(NO₃)₂ at ambient temperature, pressure and neutral pH. The nano-preparation exhibited a crystallite domain size of 2.38 nm, a spherical morphology and an average size distribution of 6 nm. The ‘as-synthesised’ PbS₂NPs exhibited an absorbance maximum at 386 nm and an emission maximum at 530 nm. The emission spectrum of the PbS₂NPs was narrow, symmetric with Gaussian distribution, and the nanoparticles exhibited a large Stokes’ shift with relatively high QY (67%). The fluorescence spectra remained unaffected by the micro-environment of the PbS₂NPs. The particles were found to be non-cytotoxic as evident from the MTT and ROS assay. The PbS₂NPs were internalised by the HeLa cells and were evenly distributed within the cytoplasm of the cell without penetrating the nucleus. Thus, these nanoparticles can be used for bio-imaging applications.

SUMMARY OF RESULTS AND CONCLUSIONS

The present work was carried out with the aim to identify and exploit haloarchaea and halophilic bacteria for metallic and metal sulphide nanoparticles synthesis. The haloarchaeal isolates *Halococcus salifodinae* BK3, *H. salifodinae* BK6, *H. salifodinae* BK7, *H. salifodinae* BK11, and *H. salifodinae* BK18, and the halophilic bacteria, *Halomonas aquamarina* MTCC 4661, *Halobacillus* sp. MTCC 6516, and *Idiomarina* sp. PR58-8 were screened for their ability to synthesise nanoparticles. At the onset, medium for growth for all the cultures was optimised. NTYE, SWYE, HB and modified Popescu media were used for the haloarchaea while ZMB 2216, NB + 2% NaCl, and 3.5% NTYE were used for halophilic bacteria. All the five haloarchaeal cultures exhibited optimum growth in NTYE, while optimum growth of *H. aquamarina* MTCC 4661 was obtained in NB + 2% NaCl; *Halobacillus* sp. MTCC 6516 in 3.5% NTYE; and *Idiomarina* sp. PR58-8 in ZMB 2216.

The cultures were exposed to increasing concentrations of metal salts to determine their minimum inhibitory concentration. Bio-availability of metals at high salinities is in the form of soluble chloro-complexes that are lipophilic. The cultures exhibited varying resistance towards the metal salts. *H. salifodinae* BK3 exhibited highest resistance towards K_2TeO_3 and Na_2SeO_3 as compared to $ZnSO_4$ and $AgNO_3$. *H. salifodinae* BK6 exhibited least susceptibility towards Na_2SeO_3 and most susceptibility towards $ZnSO_4/AgNO_3$. *H. salifodinae* BK7, BK11 and BK18 were found to possess high resistance towards Na_2SeO_3 , while $AgNO_3$ was toxic to these organisms. Amongst the halophilic bacteria used for this study, *Idiomarina* sp. PR58-8 exhibited a high level of intrinsic resistance towards $AgNO_3$, Na_2SeO_3 and $Pb(NO_3)_2$ as compared to *H. aquamarina* MTCC 4661 and *Halobacillus* sp. MTCC 6516 that exhibited low level of resistance towards most of the metal salts evaluated.

The MIC of each metal salt helped in determining the concentrations that could be used for biosynthesis of nanoparticles. The screening of the culture capable of nanoparticle synthesis was carried out employing UV-visible spectroscopy and/or XRD in combination with a visual change in culture colouration during growth in presence of metal salts. Amongst the halophilic archaea screened *H. salifodinae* BK3 exhibited the ability to synthesise SNPs, and TeNPs; *H. salifodinae* BK6 could synthesise SNPs; and *H. salifodinae* BK18 could synthesise SeNPs. Similarly, amongst the halophilic bacteria screened, only *Idiomarina* sp. PR58-8 could

successfully synthesise SeNPs and PbS₂NPs. Thus, these cultures were used for synthesis of metal and metal sulphide nanoparticles.

H. salifodinae BK3 and *H. salifodinae* BK6 synthesised SNPs when grown in presence of AgNO₃ in NTYE and HNB medium. The cultures exhibited retarded growth on first encounter with silver however on adaptation the isolates exhibited growth kinetics parameters similar to that of controls. Silver uptake by the haloarchaeal isolates was observed from mid-exponential phase to late stationary phase. A concentration dependent increase in NR activity in presence of silver nitrate and the negligible NR enzyme activity, along with inability of the haloarchaeal isolate to grow in presence of NR inhibitor, sodium azide, confirms the involvement of the enzyme in metal resistance, and silver nanoparticle synthesis. Thus, HNB was also used for SNPs synthesis. The growth of the isolates and SNPs synthesis was faster in this medium as compared to that in NTYE. The optimum yield of SNPs (~3.25 mg/g CDW) was obtained when 0.5 mM AgNO₃ was used as the precursor at 37°C and pH 7.0. The SNPs-BK3 and SNPs-BK6 exhibited the characteristic SPR at ~440 nm with an average particle size of 53 nm and 12 nm when synthesis was carried out using NTYE and HNB, respectively. The particles were predominantly spherical and exhibited fcc crystalline facet with lattice parameter of 2.16 Å. The ‘as-synthesised’ nanoparticles exhibited antimicrobial activities against both gram-positive and gram-negative organisms, with a better activity at lower concentrations towards Gram-negative bacteria. Thus, these SNPs may find applications as antibacterial agents.

H. salifodinae BK18 when grown in presence of Na₂SeO₃ exhibited a brick-red colouration indicating the reduction of SeO₃²⁻ to Se⁰, and SeNPs synthesis. At 4 mM Na₂SeO₃, the growth profile was similar to that of unexposed controls. The haloarchaeon exhibited selenite uptake from early exponential phase up to late stationary phase. The optimum yield of SeNPs (0.697 mM/ mM Na₂SeO₃) was obtained when 4 mM Na₂SeO₃ was used as the precursor at 37°C and pH 7.0. The ‘as-synthesised’ nanorods exhibited a hexagonal crystal nature, a crystallite domain size of 28.27 nm, with an aspect ratio of 13:1, and lattice parameters of a=4.36 Å and b=4.39 Å. EDAX analysis confirmed the presence of elemental selenium. The increase in the nitrate reductase enzyme activity in presence of Na₂SeO₃ and its inability to grow in the presence of the enzyme inhibitor sodium azide implies the involvement of nitrate reductase in detoxification of the selenite. The nano-preparation exhibited toxicity towards human cervical

cancer cell line, HeLa, while being non-cytotoxic towards the normal primary cell substitute, human epidermal keratinocyte cell line, HaCaT. This indicates the ability of the SeNPs to select cancer cells over normal cells. ROS and AI were found to increase in a dose dependent manner in SeNPs treated HeLa cells, suggesting the activation of apoptosis. Western blot analysis of SeNPs treated HeLa cells exhibited a concomitant decrease in the expression of HSP-70, pro-caspase 3, and pro-PARP, along with an increase in cleaved PARP expression which suggests the activation of caspase-dependent apoptotic pathway. Thus, these SeNPs may find application as potential chemotherapeutic agents.

H. salifodinae BK3 could synthesise TeNPs as was evident from the change in culture colouration to black which indicates reduction of TeO_3^{2-} to Te^0 . At 0.3 mM K_2TeO_3 , the growth of haloarchaeon was very similar to that of control, while at 3 mM K_2TeO_3 the growth was slightly decreased and tellurite uptake was observed from early exponential phase to late stationary phase. The maximum yield of TeNPs (0.997 mM/ mM K_2TeO_3) was obtained when 3 mM K_2TeO_3 was used as the precursor at 37°C and pH 7.0. The needle shaped TeNPs exhibited a hexagonal crystalline structure, with lattice parameters of $a= 4.43 \text{ \AA}$ and $b= 5.97 \text{ \AA}$, a crystallite domain size of 11.3 nm and an aspect ratio of 1:4.4. The tellurite resistance and reduction in *H. salifodinae* BK3 entailed an inducible, heat labile NADH-dependent tellurite reductase enzyme. This enzyme was found to lack any disulphide linkages. The ‘as-synthesised’ TeNPs exhibited antimicrobial activities against both gram-positive and gram-negative organisms, with a better activity at lower concentrations towards gram-negative bacteria. The nano-preparation did not exhibit any strain specificity. Thus, these nanoparticles may be used as potential antibacterial agents.

Idiomarina sp. PR58-8 exhibited brick-red colouration when grown in presence of Na_2SeO_3 , indicating the reduction of SeO_3^{2-} to Se^0 . Growth in presence of 4 mM Na_2SeO_3 was similar to that of control, while at 8 mM Na_2SeO_3 a slight decrease in growth kinetics parameters was observed. Selenite uptake was noted from the mid-exponential phase to the early stationary phase. The optimum yield of SeNPs (30.13 mg/g CDW) was obtained with 8 mM Na_2SeO_3 , at 37°C and pH 7.0. The spherical SeNPs exhibited a hexagonal crystal structure with lattice parameters of $a= 4.366 \text{ \AA}$ and $b= 4.951 \text{ \AA}$, a crystallite size of 34.52 nm and an average size distribution of 250 nm. The up-regulation of non-protein thiols in a dose dependent manner in

response to selenite stress is indicative of their involvement in selenite resistance/reduction and SeNPs synthesis. The nano-preparation exhibited selectivity towards cancer cells exerting their toxicity in a dose dependent manner. The increase in ROS and AI in HeLa cells treated with SeNPs suggests the involvement of apoptosis in cell death. Western blot analysis confirmed the activation of caspase-dependent apoptotic pathway. Thus, the ‘as-synthesised’ SeNPs may be used as potential chemotherapeutic agents.

Idiomarina sp. PR58-8 exhibited intracellular synthesis of PbS₂NPs during growth in presence of Pb(NO₃)₂. At 0.05 mM and 0.5 mM Pb(NO₃)₂ the marine bacterium exhibited growth profile similar to that of control, whilst higher concentrations of 1 mM and 5 mM Pb(NO₃)₂ negatively affected its growth. The bacterium exhibited lead uptake from early exponential phase to late stationary phase. The transformation of Pb(NO₃)₂ to nano-particulate PbS₂ entailed the non-protein thiols. Optimum yield of PbS₂NPs (631.71 µg/mg CDW) was obtained with 5 mM Pb(NO₃)₂, at 37°C, and pH 7.0. The spherical nanoparticles exhibited a tetragonal crystalline facet with a crystallite size of 2.38 nm, a/c ratio of 1.05, interplanar spacing d= 0.318 nm and an average size of 6 nm. The absorbance maximum was found at 386 nm corresponding to an energy band gap of ~3.22 eV, and the emission maximum was at 530 nm. The emission spectrum of the PbS₂NPs was narrow, symmetric with Gaussian distribution, and the nanoparticles exhibited a large Stokes’ shift with relatively high QY (67%). Storage or change in the micro-environment of the nanoparticles did not alter the emission spectrum of the PbS₂NPs. The nanoparticles were found to be bio-compatible as evident from the MTT and ROS assays. The PbS₂NPs were internalised by the HeLa cells with even distribution within the cytoplasm of the cell without penetrating the nucleus, and may thus be used for bio-imaging applications.

Thus, some of the important conclusions that may be drawn from the present work are as follows:

1. This is the first study to demonstrate nanoparticle synthesis by haloarchaea. *H. salifodinae* BK3 and *H. salifodinae* BK6 exhibited synthesis of silver nanoparticles; *H. salifodinae* BK18 exhibited synthesis of selenium nanoparticles; and *H. salifodinae* BK3 exhibited synthesis of tellurium nanoparticles. In all these instances, nitrate/tellurite reductase enzyme was found to be responsible for metal reduction and

nanoparticles synthesis. This represents a metal resistance mechanism that was not reported earlier in haloarchaea.

2. Amongst the three halophilic bacteria screened, only *Idiomarina* sp. PR58-8 exhibited ability to synthesise selenium and lead (IV) sulphide nanoparticles. In both the instances non-protein thiols were found to be responsible for nanoparticle synthesis and metal transformation.
3. All the nanoparticles obtained in this study were through intra-cellular synthesis by the organisms.
4. The nanoparticle synthesis was obtained only when the metal precursor was added at the time of inoculation. Addition of the metal salts during active growth was found to be bacteriostatic to the organisms used in this study. However, when these cells were transferred to fresh medium, growth resumed. Addition of metal salts at the time of inoculation eliminates the need for monitoring of growth phase during nanoparticle synthesis.
5. The SNPs and TeNPs exhibited antibacterial activities against both, Gram-positive and Gram-negative bacteria. However, a higher activity at lower concentration was observed against Gram-negative bacteria, in both the cases.
6. SeNPs synthesised by *Idiomarina* sp. PR58-8 and *H. salifodinae* BK18 exhibited cytotoxicity towards HeLa cells via caspase-dependent apoptotic pathway. They also exhibited selectivity towards cancer cell line. The SeNPs synthesised by *Idiomarina* sp. PR58-8 exhibited cyto-toxicity at lower concentration.
7. This is the first report on the synthesis of PbS₂NPs by a microorganism and also the first report on microbial synthesis of lead based nanoparticles exhibiting fluorescent properties.
8. The PbS₂NPs exhibited an emission maximum in the visible range, with a large Stokes' shift and relatively high quantum yield (67%), which makes these particles excellent candidates for bio-imaging applications.

It can be gleaned from the findings of the present work that the microbially synthesised metal sulphide and metallic nanoparticles may find application either as antibacterial, anticancer or bio-imaging agents. The present work tends to the advancement of knowledge and paves way for future research.

FUTURE SCOPE OF WORK

1. This study demonstrates the various mechanisms involved in transformation of metal precursor to metal sulphide or metallic nanoparticles. Future work on isolation, extraction and purification of the NADH-dependent nitrate reductase, NADH-dependent tellurite reductase and non-protein thiols involved in metal transformation would enable *ex-vivo* synthesis of nanoparticles.
2. The SNPs and TeNPs obtained during the course of this work exhibited excellent anti-bacterial activities against both gram-positive and gram-negative bacteria, with better activity against gram-negative bacteria. These nano-preparations may therefore find applications as anti-microbial agents, in textile industries to manufacture self-cleaning textiles, as topical creams for wound healing, and in conjugation with antibiotics against multidrug-resistance bacteria as the SNPs have lower propensity to induce resistance in microbes. However, future work on the *in-vivo* compatibility and toxicity, both short-term and long-term of these nanoparticles needs to be evaluated before any commercial application.
3. The SeNPs exhibited effective anticancer activity and selectivity towards cancer cells *in-vitro*. *In vivo* studies using animal models would help in establishing the dosage and time course required for achieving anticancer activity. At the same time, the *in-vivo* studies on the chemopreventive properties would add to the future applications of the 'as-synthesised' SeNPs.
4. The PbS₂NPs synthesised in this work exhibited characteristics of an excellent candidate for bio-imaging applications. As the nano-preparation is most likely capped with a NP-SH, the nanoparticles can be suitably modified at –SH site by attaching various targeting ligands and antibodies. These nanoparticles may then not only be exploited for site-directed imaging, but also for targeted drug-delivery.
5. As the nanoparticles synthesis by the organisms used for this study is an intracellular phenomenon, these microbes may be exploited for remediation of metal polluted effluents with high salinity, arising from agro-food, petroleum, leather industries, etc.

REFERENCES

- Abdulah R, Miyazaki K, Nakazawa M, Koyama H (2005) Chemical forms of selenium for cancer prevention. *J Trace Elem Med Biol* 19:141-150
- Adhikari S, Fernando SD, Novotny M (2006) Nanoparticles production from glycerin via electrospray and size measurement techniques. *T ABASE* 49:1269-1272
- Afkar E, Lisak J, Saltikov C, Basu P, Oremland RS, Stolz JF (2003) The respiratory arsenate reductase from *Bacillus selenitireducens* strain MLS10. *FEMS Microbiol Lett* 226:107-112
- Ahmad A, Mukherjee P, Senapati S, Mandal D, Khan MI, Kumar R (2003) Extracellular biosynthesis of silver nanoparticles using the fungus *Fusarium oxysporum*. *Colloids Surf B Biointerfaces* 28:313-318
- Ahmad A, Mukherjee P, Mandal D, Senapati S, Khan MI, Kumar R, Sastry M (2002) Enzyme mediated extracellular synthesis of CdS nanoparticles by the fungus, *Fusarium oxysporum*. *J Am Chem Soc* 124:12108-12109
- Allan CB, Lacourciere GM, Stadtman TC (1999) Responsiveness of selenoproteins to dietary selenium. *Ann Rev Nutr* 19:1-16
- Allen M, Willits D, Young M, Douglas T (2003) Constrained synthesis of cobalt oxide nanomaterials in the 12-subunit protein cage from *Listeria innocua*. *Inorg Chem* 42:6300-6305
- Amarnath K, Mathew NL, Nellore J, Siddarth CRV, Kumar J (2011) Facile synthesis of biocompatible gold nanoparticles from *Vitis vinifera* and its cellular internalization against HBL-100 cells. *Cancer Nano* 2:121. doi:10.1007/s12645-011-0022-8
- Amoozegar MA, Ashengroph M, Malekzadeh F, Reza Razavi M, Naddaf S, Kabiri M (2008) Isolation and initial characterisation of the tellurite reducing moderately halophilic bacterium, *Salinicoccus* sp. strain QW6. *Microbiol Res* 163:456-465
- Amy NK, Garrett R (1974) Purification and characterisation of the nitrate reductase from the diatom *Thalassiosira pseudonana*. *Plant Physiol* 54:629-637
- Anil Kumar S, Abyaneh MK, Gosavi SW, Kulkarni SK, Pasricha R, Ahmad A, Khan MI (2007) Nitrate reductase-mediated synthesis of silver nanoparticles from AgNO₃. *Biotechnol Lett* 29:439-445
- Appanna VD, Gazso LG, Pierre MS (1996) Multi-metal tolerance in *Pseudomonas fluorescence* and its biotechnological significance. *J Biotechnol* 52:75-80

- Arthur JR, McKenzie RC, Beckett GJ (2003) Selenium in the immune system. *J Nutr* 133:1457S-1459S
- Auld DS (1995) Removal and replacement of metal ions in metallopeptidases. *Methods Enzymol* 248: 228-242
- Avazeri C, Turner RJ, Pommier J, Weiner JH, Giordano G, Vermiglio A (1997) Tellurite and selenate reductase activity of nitrate reductases from *Escherichia coli*: correlation with tellurite resistance. *Microbiology* 143:1181-1189
- Avery SV (2001) Metal toxicity in yeast and the role of oxidative stress. *Adv Appl Microbiol* 49:111–142
- Babu MMG, Sridhar J, Gunasekaran P (2011) Global transcriptome analysis of *Bacillus cereus* ATCC 14579 in response to silver nitrate stress. *J Nanobiotechnology* 9:49 (doi: 10.1186/1477-3155-9-49)
- Baesman SM, Bullen TD, Dewald J, Zhang D, Curran S, Islam FS, Beveridge TJ, Oremland RS (2007) Formation of tellurium nanocrystals during anaerobic growth of bacteria that use Te oxyanions as respiratory electron acceptors. *Appl Environ Microbiol* 73:2135-2143
- Bagga A, Chattopadhyay PK, Ghosh S (2007) Stokes shift in quantum dots: Origin of dark exciton. In: *Physics of semiconductor devices. Proceedings of the 14th International Workshop on the Physics of Semiconductor Devices, Mumbai, India.*
- Bai H, Zhang Z, Guo Y, Jia W (2009a) Biological synthesis of size-controlled cadmium sulfide nanoparticles using immobilised *Rhodobacter sphaeroides*. *Nanoscale Res Lett* 4:713-723
- Bai HJ, Zhang ZM (2009c) Microbial synthesis of semiconductor lead sulfide nanoparticles using immobilized *Rhodobacter sphaeroides*. *Mater Lett* 63:764-766
- Bai HJ, Zhang ZM, Gong J (2006) Biological synthesis of semiconductor zinc sulfide nanoparticles by immobilized *Rhodobacter sphaeroides*. *Biotechnol Lett* 28:1135–1139
- Bai HJ, Zhang ZM, Guo Y, Yang GE (2009b) Biosynthesis of cadmium sulfide nanoparticles by photosynthetic bacteria *Rhodospseudomonas palustris*. *Colloids Surf B Biointerfaces* 70:142–146
- Bansal V, Rautaray D, Ahmad A, Sastry M (2004) Biosynthesis of zirconia nanoparticles using the fungus *Fusarium oxysporum*. *J Mater Chem* 14:3303-3305

- Bansal V, Rautaray D, Bharde A, Ahire K, Sanyal A, Ahmad A, Sastry M (2005) Fungus-mediated biosynthesis of silica and titania particles. *J Mater Chem* 15:2583-2589
- Bao H, Hao N, Yang Y, Zhao D (2010a) Biosynthesis of biocompatible cadmium telluride quantum dots using yeast cells. *Nano Res* 3:481-489
- Bao H, Lu Z, Cui X, Qiao Y, Guo J, Anderson JM, Li CM (2010b) Extracellular microbial synthesis of biocompatible CdTe quantum dots. *Acta Biomater* 6:3534-3541
- Basavaraja S, Balaji SD, Lagashetty A, Rajasab AH, Venkataraman A (2008) Extracellular biosynthesis of silver nanoparticles using the fungus *Fusarium semitectum*. *Mater Res Bull* 43:1164-1170
- Basnayake RST, Bius JH, Akpolat OM, Chasteen TG (2001) Production of dimethyl telluride and elemental tellurium by bacteria amended with tellurite or tellurate. *Appl Organomet Chem* 15:499-510
- Bazylinski DA, Frankel RB (2004) Magnetosome formation in prokaryotes. *Nature Rev Microbiol* 2:217-230
- Bera RK, Das AK, Raj CR (2010) Scope of network polysilanes in the synthesis of fluorescent silver and gold nanoparticles/ nanoclusters- modulations of their optical properties in the presence of Hg (II) ions. *Chem Mater* 22:4505-4511
- Berney M, Weilenmann HU, Ihssen J, Bassin C, Egli T (2006) Specific growth rate determines the sensitivity of *Escherichia coli* to thermal, UVA, and solar disinfection. *Appl Environ Microbiol* 72:2586-2593
- Bharde A, Rautaray D, Bansal V, Ahmad A, Sarkar I, Yusuf MS, Sanyal M, Sastry M (2006) Extracellular biosynthesis of magnetite using fungi. *Small* 1:135-141
- Bhattacharya R, Mukherjee P (2008) Biological properties of "naked" metal nanoparticles. *Adv Drug Deliv Rev* 60:1289-306
- Bhuyan AK (2010) On the mechanism of SDS-induced protein denaturation. *Biopolymers* 93:186-199
- Bindhu MR, Umadevi M (2014) Silver and gold nanoparticles for sensor and antibacterial applications. *Spectrochim Acta A Mol Biomol Spectrosc* 128:37-45
- Bini E (2010) Archaeal transformation of metals in the environment *FEMS Microbiol Ecol* 73:1-16
- Bjornberg A, Martensson US, Paulsson KM (1986) Method for producing selenium salts. U.S. Patent 4,605,544

- Bochiwal C (2009) Adaptation of low-salt tolerant Haloarchaea in estuarine environments. University of Essex, UK
- Bonifas J, Hennen J, Dierolf D, Kalmes M, Blömeke B (2010) Evaluation of cytochrome P450 1 (CYP1) and N-acetyltransferase 1 (NAT1) activities in HaCaT cells: implications for the development of in vitro techniques for predictive testing of contact sensitizers. *Toxicol in Vitro* 24:973-980
- Borghese R, Baccolini C, Francia F, Sabatino P, Turner RJ, Zannoni D (2014) Reduction of chalcogen oxyanions and generation of nanoprecipitates by the photosynthetic bacterium *Rhodobacter capsulatus*. *J Hazard Mater* 269:24-30
- Borrelly GPM, Harrison MD, Robinson AK, Cox SG, Robinson NJ, Whitehall SK (2002) Surplus zinc is handled by Zym1 metallothionein and Zhf endoplasmic reticulum transporter in *Schizosaccharomyces pombe*. *J Biol Chem* 277:30394-30400
- Boukamp P, Petrussevska RT, Breitkreutz D, Hornung J, Markham A, Fusenig NE (1988) Normal keratinization in a spontaneously immortalised aneuploid human keratinocyte cell line. *J Cell Biol* 106:761-771
- Bradford MM (1976) A rapid and sensitive method for the quantitation of microgram quantities of protein utilizing the principle of protein-dye binding. *Anal Biochem* 72:248-254
- Breidt F, Romick TL, Fleming HF (1994) Rapid method for the determination of bacterial growth kinetics. *J Rapid Methods Autom Microbiol* 3:59-68
- Brelle MC, Zhang JZ, Nguyen L, Mehra RK (1999) Synthesis and ultrafast study of cysteine- and glutathione-capped Ag₂S semiconductor colloidal nanoparticles. *J Phy Chem* 103:10194-10201
- Bruchez, MJr, Moronne M, Gin P, Weiss S, Alivisatos AP (1998) Semiconductor nanocrystals as fluorescent biological labels. *Science* 281:2013-2016
- Burda C, Chen X, Narayanan R, El-Sayed MA (2005) Chemistry and properties of nanocrystals of different shapes. *Chem Rev* 105:1025-1102
- Byrne RH (2002) Inorganic speciation of dissolved elements in seawater: the influence of pH on concentration ratios. *Geochem T* 3:11-16
- Calderon IL, Arenas FA, Perez JM, Fuentes DE, Araya MA, Saavedra CP, Tantalean JC, Pichuantes SE, Youderian PA, Vasquez CC (2006) Catalases are NAD(P)H-dependent tellurite reductases. *PLoS One* 1:e70. doi:10.1371/journal.pone.0000070

- Castro ME, Cottet L, Castillo A (2014) Biosynthesis of gold nanoparticles by extracellular molecules produced by the phytopathogenic fungus *Botrytis cinerea*. *Mater Lett* 115:42-44
- Catauro M, Raucci MG, De Gaetano F, Marotta A (2004) Antibacterial and bioactive silver-containing $\text{Na}_2\text{O} \times \text{CaO} \times \text{SiO}_2$ glass prepared by sol-gel method. *J Mater Sci Mater Med* 15:831-837
- Chan WCW, Nie S (1998) Quantum dot bioconjugates for ultrasensitive nonisotopic detection. *Science* 281:2016-2018
- Chang JY (1997) A two-stage mechanism for the reductive unfolding of disulfide-containing proteins. *J Biol Chem* 272:69-75
- Chapman PM, Wang F (2001) Assessing sediment contamination in estuaries *Environ Toxicol Chem* 20:3-12
- Chasteen TG, Bentley R (2003) Biomethylation of selenium and tellurium: microorganisms and plants. *Chem Rev* 103:1-25
- Chatellier X, Fortin D, West MM, Leppard GG, Ferris FG (2001) Effect of the presence of bacterial surfaces during the synthesis of Fe oxides by oxidation of ferrous ions. *Eur J Mineral* 13:705-714
- Chen H, Lesnyak V, Bigall NC, Gaponik N, Eychmüller A (2010) Self-assembly of TGA-capped CdTe nanocrystals into three-dimensional luminescent nanostructures. *Chem Mater* 22:2309-2314
- Chen J, Kong Y, Wang W, Fang H, Wo Y, Zhou D, Wu Z, Li Y, Chen S (2016) Direct water-phase synthesis of lead sulfide quantum dots encapsulated by β -lactoglobulin for *in vivo* second near infrared window imaging with reduced toxicity. *Chem Commun* 52:4025-4028
- Chen T, Wong YS, Zheng W, Bai Y, Huang L (2008) Selenium nanoparticles fabricated in *Undaria pinnatifida* polysaccharide solutions induce mitochondria-mediated apoptosis in A375 human melanoma cells. *Colloid Surf B Biointerfaces* 67:26-31
- Chen WQ, Zheng RS, Zhang SW (2013) Liver cancer incidence and mortality in China, 2009. *Chin J Cancer* 32:162-169
- Chen X, Schluesener HJ (2008) Nano-silver: A nanoparticle in medical application. *Toxicol Lett* 176:1-12

- Cheraghian G, Hendraningrat L (2016) A review on applications of nanotechnology in the enhanced oil recovery part B: effects of nanoparticles on flooding. *Int Nano Lett* (2016) 6:1. doi:10.1007/s40089-015-0170-7
- Cherian MG, Chan HM (1993) Biological functions of metallothionein- an overview. In Suzuki KT, Imura N, Kimura M (Eds) *Metallothionein III. Biological roles and medical implications*. Burkhäuser Verlag Basel pp. 87-110
- Cherin P, Unger P (1967) The crystal structure of trigonal selenium. *Inorg Chem* 6:1589-1591
- Chiong M, Barra R, González E, Vásquez C (1988a) Resistance of *Thermus* spp. to potassium tellurite. *Appl Environ Microbiol* 54:610-612
- Chiong M, Gonzalez E, Barra R, Vaeasquez C (1988b) Purification and biochemical characterization of tellurite-reducing activities from *Thermus thermophilus* HB8. *J Bacteriol* 170:3269-3273
- Chou LYT, Ming K, Chan WCW (2011) Strategies for the intracellular delivery of nanoparticles. *Chem Soc Rev* 40:233-245
- Chowdhury S, Basu A, Kundu S (2014) Green synthesis of protein capped silver nanoparticles from phytopathogenic fungus *Macrophomina phaseolina* (Tassi) Goid with antimicrobial properties against multidrug-resistant bacteria. *Nanoscale Res Lett* 9:365. doi:10.1186/1556-276X-9-365
- Cobbett CS, Goldbrough P (2002) Phytochelatins and metallothioneins: Roles in heavy metal detoxification and homeostasis. *Annu Rev Plant Biol* 53:159-82
- Combs GF Jr (2005) Current evidence and research needs to support a health claim for selenium and cancer prevention. *J Nutr* 135:343-347
- Cooper P, Few A (1952) Uptake of potassium tellurite by a sensitive strain of *Escherichia coli*. *J Biochem (Tokyo)* 51:552-557
- Cooper WC (1971) *Tellurium*. Van Nostrand Reinhold, New York, USA
- Correa-Llanten DN, Munoz-Ibacache SA, Castro ME, Munoz PA, Blamey JM (2013) Gold nanoparticles synthesized by *Geobacillus* sp. strain ID17 a thermophilic bacterium isolated from Deception Island, Antarctica. *Microb Cell Fact* 12:75. doi:10.1186/1475-2859-12-75
- Cournoyer B, Watanabe S, Vivian A (1998) A tellurite resistance genetic determinant from phytopathogenic pseudomonads encodes a thiopurine methyltransferase: evidence of a widely-conserved family of methyltransferases. *Biochim Biophys Acta* 1397:161-168

- Curcic MG, Stankovic MS, Mrkalic EM, Matovic ZD, Bankovic DD, Cvetkovic DM, Dacic DS, Markovic SD (2012) Antiproliferative and proapoptotic activities of methanolic extracts from *Ligustrum vulgare* L. as an individual treatment and in combination with palladium complex. *Int J Mol Sci* 13:2521-2534
- Dameron CT, Reese RN, Mehra RK, Kortan AR, Carroll PJ, Steigerwald ML, Brus LE, Winge DR (1989) Biosynthesis of cadmium sulphide quantum semiconductor crystallites. *Nature* 338:596-597
- Dameron CT, Winge DR (1990) Peptide-mediated formation of quantum semiconductors. *Trends Biotechnol* 8:3-6
- Danilcauk M, Lund A, Saldo J, Yamada H, Michalik J (2006) Conduction electron spin resonance of small silver particles. *Spectrochimica Acta Part A* 63:189-191
- DasSarma S (1989) Mechanisms of genetic variability in *Halobacterium halobium*: the purple membrane and gas vesicle mutations. *Can J Microbiol* 35:65-72
- DasSarma S, Arora P (1997) Genetic analysis of gas vesicle gene cluster in haloarchaea. *FEMS Microbiol. Lett.* 153:1-10
- DasSarma S, Arora P, Lin F, Molinari E, Yin LR (1994) Wild-type gas vesicle formation requires at least ten genes in the *gvp* gene cluster of *Halobacterium halobium* plasmid pNRC100. *J Bacteriol* 176:7646-7652
- DasSarma S, Damerval T, Jones JG, Tandeau de Marsac N (1987) A plasmid encoded gas vesicle protein gene in a halophilic archaebacterium. *Mol Microbiol* 1:365-370
- DasSarma S, DasSarma P (2012) Halophiles. In: eLS. John Wiley & Sons, Ltd. Chichester. doi: 10.1002/9780470015902.a0000394.pub3
- DasSarma S, DasSarma P (2015a) Gas vesicle nanoparticles for antigen display. *Vaccines* 3:686-702
- DasSarma S, Karan R, DasSarma P, Barnes S, Ekulona F, Smith B (2013) An improved genetic system for bioengineering buoyant gas vesicle nanoparticles from Haloarchaea. *BMC Biotechnol* 13:112. doi:http://www.biomedcentral.com/1472-6750/13/112
- DasSarma P, Negi VD, Balakrishnan A, Kim JM, Karan R, Chakravorty D, DasSarma S (2015b) Haloarchaeal gas vesicle nanoparticles displaying *Salmonella* antigens as a novel approach to vaccine development. *Procedia Vaccinol* 9:16-23
- De Gusseme B, Hennebel T, Christiaens E, Saveyn H, Verbeken K, Boon N, Verstraete W (2011) Virus disinfection in water by biogenic silver immobilized in polyvinylidene fluoride membranes. *Water Res* 45:1856-1864

- Debieux CM, Dridge EJ, Mueller CM, Splatt P, Paszkiewicz K, Knight I, Florance H, Love J, Titball RW, Lewis RJ, Richardson DJ, Butler CS (2011) A bacterial process for selenium nanosphere assembly. *Proc Natl Acad Sci USA* 108:13480-13485
- Deepak V, Kalishwaralal K, Ram Kumar Pandian S, Gurunathan S (2011) An insight into the bacterial biogenesis of silver nanoparticles, industrial production and scale-up. In: Rai M, Durán N (Eds) *Metal nanoparticles in microbiology*. Springer-Verlag Berlin Heidelberg, pp. 17-35
- Dhanjal S, Cameotra SS (2010) Aerobic biogenesis of selenium nanospheres by *Bacillus cereus* isolated from coalmine soil. *Microb Cell Fact* 9:52. doi:10.1186/1475-2859-9-52
- Domenech B, Bastos-Arrieta J, Alonso A, Macanas J, Munoz M, Muraviev DN (2012) Bifunctional polymer-metal nanocomposite ion exchange materials. In: Kilislioglu A. (Ed.) *Ion exchange technologies*. InTech DOI: 10.5772/51579
- Dong Y, Zhang H, Hawthorn L, Ganther HE, Ip C (2003). Delineation of the molecular basis for selenium induced growth arrest in human prostate cancer cells by oligonucleotide array. *Can Res* 63:52-59
- Donmez G, Aksu Z (2001) Bioaccumulation of copper(II) and nickel(II) by the non-adapted and adapted growing *Candida* sp. *Water Res* 35:1425-1434
- Douglas T, Strable E, Willits D, Aitouchen A, Libera M, Young M (2002) Protein engineering of a viral cage for constrained nanomaterials synthesis. *Adv Mater* 14:414-418
- Douglas T, Young M (1998) Host-guest encapsulation of materials by assembled virus protein cages. *Nature* 393:152-155
- Douglas T, Dickson DP, Betteridge S, Charnock J, Garner CD, Mann S (1995) Synthesis and structure of an iron(III) sulphide-ferritin bioinorganic nanocomposite. *Science* 269:54-57
- Drexler KE (1981) *Molecular engineering: An approach to the development of general capabilities for molecular manipulation*. *Proc Natl Acad Sci U S A* 78:5275-5278
- Drexler KE (1986) *Engines of creation: Coming era of nanotechnology*. New York: Anchor Books/Doubleday
- Duran N, Marcato PD, Alves OL, De Souza GIH, Esposito E (2005) Mechanistic aspects of biosynthesis of silver nanoparticles by several *Fusarium oxysporum* strains. *J Nanobiotechnology* 3:8. doi: 10.1186/1477-3155-3-8

- Duran N, Marcato PD, De Souza GIH, Alves OL, Esposito E (2007) Antibacterial effect of silver nanoparticles produced by fungal process on textile fabrics and their effluent treatment. *J Biomed Nanotechnol* 3:203-208
- Ehrlich HL (1997) Microbes and metals. *Appl Microbiol Biotechnol* 48:687-692
- El-Rafie HM, El-Rafie HM, Zahran MK (2013) Green synthesis of silver nanoparticles using polysaccharides extracted from marine macro algae. *Carbohydr Polym* 96:403-410
- Estevez H, Garcia-Lidon JC, Luque-Garcia JL, Camara C (2014) Effects of chitosan-stabilized selenium nanoparticles on cell proliferation, apoptosis and cell cycle pattern in HepG2 cells: comparison with other selenospecies. *Colloid Surf B Biointerfaces* 122:184-193
- Estrader M, Lopez-Ortega A, Estrade S, Golosovsky IV, Salazar-Alvarez G, Vasilakaki M, Trohidou KN, Varela M, Stanley DC, Sinko M, Pechan MJ, Keavney DJ, Peiro F, Surinach S, Baro MD, Nogues J (2013) Robust antiferromagnetic coupling in hard-soft bi-magnetic core/shell nanoparticles. *Nat Commun* 4:2960. doi: 10.1038/ncomms3960.
- Etezad SM, Khajeh K, Soudi M, Ghazvini PTM, Dabirmanesh B (2009) Evidence on the presence of two distinct enzymes responsible for the reduction of selenate and tellurite in *Bacillus* sp. STG-83. *Enzyme Microb Tech* 45:1-6
- Fahey RC (2001) Novel thiols of prokaryotes. *Annu Rev Microbiol* 55:333-356
- Fairweather-Tait SK, Bao Y, Broadley MR, Collings R, Ford D, Hesketh JE, Hurst R (2011) Selenium in human health and disease *Antioxid Redox Signal* 14:1337-1383
- Fang J, Lu J, Holmgren A (2005) Thioredoxin reductase is irreversibly modified by curcumin: a novel molecular mechanism for its anticancer activity. *J Biol Chem* 280:25284-25290
- Farrar WE (1985) Antibiotic Resistance in Developing Countries. *J Infect Dis* 152:1103-1106
- Fauchon M, Lagniel G, Aude J, Lombardio L, Soulrue P, Petat C, Marguerie G, Sentenac A, Werner M, Labarre J (2002) Sulphur sparing in the yeast proteome in response to sulfur demand. *Mol Cell* 9:713-723
- Fayaz AM, Girilal M, Venkatesan R, Kalaichelvan PT (2011) Biosynthesis of anisotropic gold nanoparticles using *Maduca longifolia* extract and their potential in infrared absorption. *Colloids Surf B Biointerfaces* 88:28-291
- Feng QL, Wu J, Chen GQ, Cui FZ, Kim TN, Kim JO (2008) A mechanistic study of the antibacterial effect of silver ions on *Escherichia coli* and *Staphylococcus aureus*. *J Biomed Mater Res* 52:662-668

- Fesharaki PJ, Nazari P, Shakibaie M, Rezaie S, Banooee M, Abdollahi M, Shahverdi AR (2010) Biosynthesis of selenium nanoparticles using *Klebsiella pneumoniae* and their recovery by a simple sterilization process. *Braz J Microbiol* 41:461-466
- Flora G, Gupta D, Tiwari A (2012) Toxicity of lead: A review with recent updates. *Interdiscip Toxicol* 5:47-58
- Freshney RI (2005) In: A manual of basic techniques, Ed. John Wiley Inc publication, New York 5:199-216
- Friedman M, Cuq JL (1988) Chemistry, analysis, nutritional value, and toxicology of tryptophan in food. A review. *J Agric Food Chem* 36:1079-1093
- Friedman M, Cuq JL (1988) Chemistry, analysis, nutritional value, and toxicology of tryptophan in food. A review. *J Agric Food Chem* 36:1079-1093
- Furno F, Morley KS, Wong, B, Sharp BL, Arnold PL, Howdle SM, Bayston R, Brown PD, Winship PD (2004) Silver nanoparticles and polymeric medical devices: a new approach to prevention of infection? *J Antimicrob Chemother* 54: 1019-1024
- Gadd GM (1992) Metals and microorganisms: a problem of definition. *FEMS Microbiol Lett* 100:197-204
- Gadd GM (2007) Geomycology: biogeochemical transformations of rocks, minerals, metals and radionuclides by fungi, bioweathering and bioremediation. *Mycol Res* 111:3-49
- Gadd GM (2010a) Geomicrobiology of eukaryotic microorganisms. *Geomicrobiol J* 27:491-519
- Gadd GM (2010b) Metals, minerals and microbes: geomicrobiology and bioremediation. *Microbiology* 156:609-643
- Gangula A, Podila R, Ramakrishna M, Karanam L, Janardhana C, Rao AM (2011) Catalytic reduction of 4-nitrophenol using biogenic gold and silver nanoparticles derived from *Breynia rhamnoides*. *Langmuir* 27:15268-15274
- Gao F, Lu Q, Meng X, Komarneni S (2008) Synthesis of nanorods and nanowires using biomolecules under conventional- and microwave-hydrothermal conditions. *J Mater Sci* 15:27-38
- Gao F, Yuan Q, Gao L, Cai P, Zhu H, Liu R, Wang Y, Wei Y, Huang G, Liang J, Gao X (2014) Cytotoxicity and therapeutic effect of irinotecan combined with selenium nanoparticles. *Biomaterials* 35:8854-8866

- Garcia I, Gallo J, Marradi M, Penades S (2011) Glyconanoparticles: New nanomaterials for biological applications. In: Narain R (Ed.) Engineered carbohydrate-based materials for biomedical applications: Polymers, surfaces, dendrimers, nanoparticles, and hydrogels. John Wiley and Sons, Inc. pp. 213-259
- Ge W, Zamri D, Mineyama H, Valix M (2011) Bioaccumulation of heavy metals on adapted *Aspergillus foetidus*. Adsorption 17:901-910
- Gedanken A (2004) Using sonochemistry for the fabrication of nanomaterials. Ultrason sonochem 11:47-55
- Geethu R, Jacob R, Shripathi T, Okram GS, Ganesan V, Tripathi S, Fatima A, Sreenivasan PV, Urmila KS, Pradeep B, Philip RR (2012) Optoelectronic and thermoelectric properties in Ga doped - PbS₂ nanostructured thin films. Appl Surf Sci 258:6257-6260
- Gericke M, Pinches A (2006) Biological synthesis of metal nanoparticles. Hydrometallurgy 83:132-140
- Ghorbani HR, Safekordi AA, Attar H, Sorkhabadi SMR (2011) Biological and non-biological methods for silver nanoparticles synthesis. Chem Biochem Eng Q 25:317-326
- Glaeser H, Coblenz A, Kruczek R, Ruttke I, Ebert-Jung A, Wolf K (1991) Glutathione metabolism and heavy metal detoxification in *Schizosaccharomyces pombe*. Curr Genet 19:207-213
- Gleiter H (2000) Nanostructured materials: basic concepts and microstructure. Acta Mater 48:1-29
- Graham D, Faulds K, Thompson D, McKenzie F, Stokes R, Dalton C, Stevenson R, Alexander J, Garside P, McFarlane (2009) Functionalized nanoparticles for bioanalysis by SERRS. Biochem Soc Trans 37:697-701
- Grant WD, Kamekura M, McGenity TJ, Ventosa A (2001) Class III. Halobacteria class. nov. In: Boone DR, Castenholz RW, Garrity GM (Eds) Bergey's manual of systematic bacteriology. Vol I Springer Verlag, New York pp. 294-301
- Greenwood NN, Eamshaw A (1997) Chemistry of elements. 2nd edn. Pergamon Press, Oxford, Ch 16
- Grill E, Loeffler S, Winnacker EL, Zenk MH (1989) Phytochelatins, the heavy-metal-binding peptides of plants, are synthesized from glutathione by a specific γ -glutamylcysteine dipeptidyl transpeptidase (phytochelatinsynthase). Proc Natl Acad Sci USA 86:6838-6842

- Guimaraes-Soares L, Pascoal C, Cassio F (2007) Effects of heavy metals on the production of thiol compounds by the aquatic fungi *Fontanospora fusiramosa* and *Flagellosporacurta*. *Ecotoxicol Environ Saf* 66:36-43
- Guo L, Nie J, Du B, Peng A, Tesche B, Kleinermanns K (2007) Thermoresponsive polymer-stabilized silver nanoparticles. *J Colloid Interface Sci* 319:175-181
- Gurunathan S, Kalishwaralal K, Vaidyanathan R, Venkataraman D, Pandian SR, Muniyandi J, Hariharan N, Eom SH (2009) Biosynthesis, purification and characterization of silver nanoparticles using *Escherichia coli*. *Colloids Surf B Biointerfaces* 74:328-335
- Hall SR, Shenton W, Engelhardt H, Mann S (2001) Site-specific organization of gold nanoparticles by biomolecular templating. *Chem Phy Chem* 2:184-186
- Halladay JT, Jones JG, Lin F, MacDonald AB, DasSarma S (1993) The rightward gas vesicle operon in *Halobacterium* plasmid pNRC100: identification of the *gvpA* and *gvpC* gene products by use of antibody probes and genetic analysis of the region downstream of *gvpC*. *J Bacteriol* 175:684-692
- Hamilton SJ (2004) Review of selenium toxicity in the aquatic food chain. *Sci Total Environ* 326:1-31
- Hariharan H, Al-dhabi NA, Karuppiyah P, Rajaram SK (2012) Microbial synthesis of selenium nanocomposite using *Saccharomyces cerevisiae* and its antimicrobial activity against pathogens causing nosocomial infection. *Chalcogenide Lett* 9:509-515
- Harley SM (1993) Use of a simple, colorimetric assay to demonstrate conditions for induction of nitrate reductase in plants. *Am. Biol. Teach* 55:161-164
- Harrison JJ, Ceri H, Turner RJ (2007) Multimetal resistance and tolerance in microbial biofilms. *Nat Rev Microbiol* 5:928-938
- Hayashi Y, Mutoh N (1994) Cadystin (phytochelatin) in fungi. In: Winkelmann G, Winge DR (Eds.) *Metal ions in Fungi*. Marcel Dekker, New York, pp.311-337
- He B, Nie H, Chen L, X, Hu R, Qin A, Zhao Z, Tang BZ (2015) High fluorescence efficiencies and large stokes shifts of folded fluorophores consisting of a pair of alkenyl-tethered, π -stacked oligo-*p*-phenylenes. *Org Lett* 17: 6174-6177
- He S, Guo Z, Zhang Y, Zhang S, Wang J, Gu N (2007) Biosynthesis of gold nanoparticles using the bacteria *Rhodospseudomonas capsulata*. *Mater Lett* 61: 3984–3987
- Heatley MK (1995) Association between the apoptotic index and established prognostic parameters in endometrial adenocarcinoma. *Histopathology* 27:469-472

- Hennebel T, De Gusseme B, Boon N, Verstraete W (2009) Biogenic metals in advanced water treatment. *Trends Biotechnol* 27:90-98
- Hinds S, Myrskog S, Levina L, Koleilat G, Yang J, Kelley SO, Sargent EH (2007) NIR-emitting colloidal quantum dots having 26% luminescence quantum yield in buffer solution. *J Am Chem Soc* 129:7218-7219
- Hofmeister H (1999) *Fivefold twinning* in nanosized particles and nanocrystalline thin films - ubiquitous metastable structures. *Mater Sci Forum* 325:312-314
- <http://www.prochimia.com/nanoparticles/>
- <https://nanohub.org/resources/13842> (2012)
- <https://www.tumblr.com/search/haloarchaea>
- Hu EL, Shaw DT (1999) Synthesis and assembly. In: Siegel RW, Hu EL (Eds) *Nanostructure science and technology*. Springer Netherlands, pp. 342-354
- Hu R, Law WC, Lin G, Ye L, Liu J, Liu J, Reynolds JL, Yong KT (2012) PEGylated phospholipid micelle-encapsulated near-infrared Pbs Quantum dots for *in vitro* and *in vivo* bioimaging. *Theranostics* 2:723-733
- Huang J, Wang L, Shi C, Dai Y, Gu C, Liu J (2014) Selective detection of picric acid using functionalized reduced graphene oxide sensor device. *Sensors Actuat B Chem* 196:567-573
- Huber R, Sacher M, Vollmann A, Huber H, Rose D (2000) Respiration of arsenate and selenate by hyperthermophilic archaea. *Syst Appl Microbiol* 23:305-314
- Hunter WJ (2007) An *Azospira oryzae* (syn *Dechlorosoma suillum*) strain that reduces selenate and selenite to elemental red selenium. *Curr Microbiol* 54:376-381
- Hunter WJ, Kuykendall LD (2007) Reduction of selenite to elemental red selenium by *Rhizobium* sp. strain B1. *Curr Microbiol* 55:344-349
- Hunter WJ, Manter DK (2009) Reduction of selenite to elemental red selenium by *Pseudomonas* sp. strain CA5. *Curr Microbiol* 58:493-498
- Hutter E, Fendler JH (2004) Exploitation of Localized Surface Plasmon Resonance. *Adv Mater* 16:1685-1706
- Hwang ET, Lee JH, Chae YJ, Kim YS, Kim BC, Sang B-I, Gu MB (2008) Analysis of the toxic mode of action of silver nanoparticles using stress-specific bioluminescent bacteria. *Small* 4:746-750

- Ingle A, Rai M, Gade A, Bawaskar M (2009) *Fusarium solani*: a novel biological agent for the extracellular synthesis of silver nanoparticles. *J Nanopart Res* 11:2079-2085
- Iravani S, Korbekandi H, Mirmohammadi SV, Zolfaghari B (2014) Synthesis of silver nanoparticles: chemical, physical and biological methods. *Res Pharm Sci* 9:385-406
- Iskandar F (2009) Nanoparticle processing for optical applications – A review. *Powder Technol* 20:283-292
- Issa B, Obaidat IM, Albiss BA, Haik Y (2013) Magnetic nanoparticles: surface effects and properties related to biomedicine applications. *Int J Mol Sci* 14:21266-21305
- Jaroslwiecka A, Piotrowska-Seget Z (2014) Lead resistance in micro-organisms. *Microbiology* 160:12-25
- Jasenec A, Barasa N, Kulkarni S, Shaik N, Moparathi S, Konda V, Caguiat J (2009) Proteomic profiling of L-cysteine induced selenite resistance in *Enterobacter* sp. YSU. *Proteome Sci* 7:30. doi:10.1186/1477-5956-7-30
- Jens Baumgartner J, Bertinetti L, Widdrat M, Hirt AM, Faivre D (2013) Formation of magnetite nanoparticles at low temperature: From superparamagnetic to stable single domain particles. *PLoS ONE* 8(3): e57070. doi:10.1371/journal.pone.0057070
- Jeong UY, Xia YN (2005) Synthesis and crystallization of monodisperse spherical colloids of amorphous selenium. *Adv Mater* 17:102-106
- Jha AK, Prasad K, Kulkarni AR (2009a) Synthesis of TiO₂ nanoparticles using microorganisms. *Colloids Surf B Biointerfaces* 71:226-229
- Jha AK, Prasad K, Prasad K (2009b) A green low-cost biosynthesis of Sb₂O₃ nanoparticles. *Biochem Eng J* 43:303-306
- Jiang ZY, Xie ZX, Xie SY, Zhang XH, Huang RB, Zheng LS (2003) High purity trigonal selenium nanorods growth via laser ablation under controlled temperature. *Chem Phys Lett* 368:425-429
- Jianping X, Jim YL, Daniel ICW, Yen PT (2007) Identification of active biomolecules in the high-yield synthesis of single-crystalline gold nanoplates in algal solutions. *Small* 3:668-672
- Johnson JA, Saboungi ML, Thiyagarajan P, Csencsits R, Meisel D (1999) Selenium nanoparticles: A small-angle neutron scattering study. *J Phy Chem B* 103:59-63
- Jones JG, Young DC, DasSarma S (1991) Structure and organization of the gas vesicle gene cluster on the *Halobacterium halobium* plasmid pNRC100. *Gene* 102:1017-1022

- Jung GY, Kim JR, Park JY, Park S (2002) Hydrogen production by a new chemoheterotrophic bacterium *Citrobacter* sp Y19. *Int J Hydrogen Energy* 27: 260-610
- Kalimuthu K, Suresh Babu R, Venkataraman D, Bilal M, Gurunathan S (2008) Biosynthesis of silver nanocrystals by *Bacillus licheniformis*. *Colloids Surf B* 65:150-153
- Kamekura M (1993) Lipids of extreme halophiles. In: Vreeland RH, Hochstein LI (Eds.) *The biology of halophilic bacteria*. CRC Press, Boca Raton pp. 135-161
- Kang MK, Kim JW, Kwak MG, Yoon HO, Kim YS (2011) Synthesis of Cu nanoparticles with self-assembled monolayers via inert-gas condensation. *J Nanosci Nanotechnol* 11:6020-6024
- Kang S, Herzberg M, Rodrigues DF, Elimelech M (2008) Antibacterial effects of carbon nanotubes: Size does matter. *Langmuir* 24:6409-6413
- Kango S, Kalia S, Celli A, Njuguna J, Habibi Y, Kumar R (2013) Surface modification of inorganic nanoparticles for development of organic-inorganic nanocomposites- A review. *Prog Polym Sci* 38:1232-1261
- Kannan N, Mukunthan KS, Balaji S (2011) A comparative study of morphology, reactivity and stability of synthesized silver nanoparticles using *Bacillus subtilis* and *Catharanthus roseus* (L.) G. Don. *Colloids Surf B Biointerfaces* 86:378-83
- Kapoor S, Lawless D, Kennepohl P, Meisel D, Serpone N (1994) Reduction and aggregation of silver ions in aqueous gelatin solutions. *Langmuir* 10:3018-3022
- Kathiresan K, Alikunhi NM, Pathmanaban S, Nabikhan A, Kandasamy S (2010) Analysis of antimicrobial silver nanoparticles synthesized by coastal strains of *Escherichia coli* and *Aspergillus niger*. *Can J Microbiol* 56:1050-1059
- Kathiresan K, Manivannan S, Nabeel MA, Dhivya B (2009) Studies on silver nanoparticles synthesized by a marine fungus, *Penicillium fellutanum* isolated from coastal mangrove sediment. *Coll Surf B* 71:133-137
- Kaur A, Gupta U (2009) A review on applications of nanoparticles for the preconcentration of environmental pollutants. *J Mater Chem* 19:8279-8289
- Kaur A, Pan M, Meislin M, Facciotti MT, El-Gewely R, Baliga NS (2006) A systems view of haloarchaeal strategies to with stand stress from transition metals. *Genome Res* 16:841-854
- Kessi J, Hanselmann KW (2004) Similarities between the abiotic reduction of selenite with glutathione and the dissimilatory reaction mediated by *Rhodospirillum rubrum* and *Escherichia coli*. *J Biol Chem* 279:50662-50669

- Kessi J, Ramuz M, Wehrli E, Spycher M, Bachofen R (1999) Reduction of selenite and detoxification of elemental selenium by the phototrophic bacterium *Rhodospirillum rubrum*. *Appl Environ Microbiol* 65:4734-4740
- Kim JS, Kuk E, Yu KN, Kim JH, Park SJ, Lee HJ, Kim SH, Park YK, Park YH, Hwang CY, Kim YK, Lee YS, Jeong DH, Cho MH (2007) Antimicrobial effects of silver nanoparticles. *Nanomedicine* 3:95-101
- Kim SH, Lee HS, Ryu DS, Choi SJ, Lee DS (2011) Antibacterial activity of silver-nanoparticles against *Staphylococcus aureus* and *Escherichia coli*. *Korean J Microbiol Biotechnol* 39:77-85
- Kitching M, Ramani M, Marsili E (2015) Fungal biosynthesis of gold nanoparticles: Mechanism and scale up. *Microbial Biotechnol* 8:904-917
- Klaus-Joerger T, Joerger R, Olsson E, Granqvist CG (2001) Bacteria as workers in the living factory: metal-accumulating bacteria and their potential for materials science. *Trends Biotechnol* 19:15-20
- Klonowska A, Heulin T, Vermeglio A (2005) Selenite and tellurite reduction by *Shewanella oneidensis*. *Appl Environ Microbiol* 71:5607-5609
- Knap AK, Pratt RF (1991) Inactivation of the RTEM-1 cysteine beta-lactamase by iodoacetate. The nature of active-site functional groups and comparisons with the native enzyme. *Biochem J* 273:85-91
- Kneer R, Kutchan TM, Hochberger A, Zenk MH (1992) *Saccharomyces cerevisiae* and *Neurospora crassa* contain heavy metal sequestering phytochelatin. *Arch Microbiol* 157:305-310
- Kondakova OA, Zyubin AS, Dembovsky SA, Kurnakov NS (2001) quantum-chemical modeling of chlorine-doped and hypervalent defects participation in reconstruction of the a-Se structure. *J Optoelectron Adv Mater* 3:847-853
- Kong L, Yuan Q, Zhu H, Li Y, Guo Q, Wang Q, Bi X, Gao X (2011) The suppression of prostate LNCaP cancer cells growth by selenium nanoparticles through Akt/Mdm2/AR controlled apoptosis. *Biomaterials* 32:6515-6522
- Konishi Y, Ohno K, Saitoh N, Nomura T, Nagamine S, Hishida H, Takahashi Y, Uruga T (2007) Bioreductive deposition of platinum nanoparticles on the bacterium *Shewanella algae*. *J Biotechnol* 128:648-653
- Kowshik M, Ashtaputre S, Kharrazi S, Vogel W, Urban J, Kulkarni SK, Paknikar KM (2002b) Extracellular synthesis of silver nanoparticles by a silver-tolerant yeast strain MKY3. *Nanotechnology* 14:95-100

- Kowshik M, Deshmukh N, Vogel W, Urban J, Kulkarni SK, Paknikar KM (2002a) Microbial synthesis of semiconductor CdS nanoparticles, their characterisation, and their use in the fabrication of an ideal diode. *Biotechnol Bioeng* 78:583-588
- Kowshik M, Vogel W, Urban J, Kulkarni SK, Paknikar KM (2002c) Microbial synthesis of semiconductor PbS nanocrystallites. *Adv Mater* 14:815-818
- Kumar DS, Srikantawamy S (2012) Influence and effects of industries on geochemical behaviour of heavy metals in soil. *J Env Sci Comp Sci Eng Technol* 2:1-12
- Kurimella VR, Kumar KR, Sanasi PD (2013) A novel synthesis of tellurium nanoparticles using iron (II) as a reductant. *Int J Nanosci Nanotech* 4:209-221
- Kushner DJ (1985) The halobacteriaceae. In: *The bacteria*. vol. 8. Academic Press, New York, pp. 171-214
- Lamas DG, Juarez RE, Lascalea GE, Walsoe NE (2001) Synthesis of compositionally homogeneous, nanocrystalline ZrO₂-35 mol% CeO₂ powders by gel combustion. *J Mater Sci Lett* 20:1447-1449
- Lampis S, Zonaro E, Bertolini C, Bernardi P, Butler C, Vallini G (2014) Delayed formation of zero-valent selenium nanoparticles by *Bacillus mycoides* SeITE01 as a consequence of selenite reduction under aerobic conditions. *Microb Cell Fact* 13:35. doi:10.1186/1475-2859-13-35
- Lan WJ, Yu SH, Qian SH, Wan Y (2007) Dispersability, stabilisation, and chemical stability of ultrathin tellurium nanowires in acetone: Morphology change, crystallization, and transformation into TeO₂ in different solvents. *Langmuir* 23:3409- 3417
- Law WC, Yong KT, Roy I, Ding H, Hu R, Zhao W, Prasad PN (2009) Aqueous- phase synthesis of highly luminescent CdTe/ZnTe core/Shell quantum dots optimised for targeted bioimaging. *Small* 5:1302-1310
- Lee SW, Mao C, Flynn CE, Belcher AM (2002) Ordering of quantum dots using genetically engineered viruses. *Science* 296:892-895
- Lee SY, Royston E, Culver JN, Harris MT (2005) Improved metal cluster deposition on a genetically engineered tobacco mosaic virus template. *Nanotechnology* 16-S435-441
- Lengke M, Fleet M, Southam G (2006) Biosynthesis of silver nanoparticles by filamentous cyanobacteria from a silver (I) nitrate complex. *Langmuir* 10:1021-1030

- Levina L, Sukhovatkin V, Musikhin S, Cauchi S, Nisman R, Bazett-Jones DP, Sargent EH (2005) Efficient infrared-emitting PbS quantum dots grown on DNA and stable in aqueous solution and blood plasma. *Adv Mater* 17:1854-1857
- Li S, Shen Y, Xie A, Yu X, Zhang X, Yang L, Li C (2007) Rapid, room-temperature synthesis of amorphous selenium/protein composites using *Capsicum annuum L* extract. *Nanotechnol* 18: 9 doi:10.1088/0957-4484/18/40/405101
- Li X, Xu H, Chen ZS, Chen G (2011) Biosynthesis of nanoparticles by microorganisms and their applications. *J Nanomater* 2011:16. doi:10.1155/2011/270974
- Lidsky TI, Schneider JS (2003) Lead neurotoxicity in children: basic mechanisms and clinical correlates. *Brain* 126:5-19
- Lin IWS, Lok CN, Che CM (2014) Biosynthesis of silver nanoparticles from silver (I) reduction by the periplasmic nitrate reductase c-type cytochrome subunit NapC in a silver-resistant *E. coli*. *Chem Sci* 5:3144-3150
- Lin ZH, Lee CH, Chang HY, Chang HT (2012) Antibacterial activities of tellurium nanomaterials. *Chem Asian J* 7:930-934.
- Lin ZH, Yang Z, Chang HT (2008) Preparation of fluorescent tellurium nanowires at room temperature. *Cryst Growth Des* 8:351-357
- LiPuma JJ, Rathinavelu S, Foster BK, Keoleian JC, Makidon PE, Kalikin LM, Baker JR Jr (2009) In Vitro activities of a novel nanoemulsion against *Burkholderia* and other multidrug-resistant cystic fibrosis-associated bacterial species. *Antimicrob Agents Chemother* 53:249-255
- Liu ZP, Hu ZK, Xie Q, Yang BJ, Wu J, Qian YT (2003) Surfactant assisted growth of uniform nanorods of crystalline tellurium. *J Mater Chem* 13:159-162
- Losi ME, Frankenberger WT (1997) Reduction of selenium oxyanions by *Enterobacter cloacae* SLD1a-1: isolation and growth of the bacterium and its expulsion of selenium particles. *Appl Environ Microbiol* 63:3079-3084
- Lowry OH, Rosebrough NJ, Farr AL, Randall RJ (1951) Protein measurement with the folin phenol reagent. *J Biol Chem* 193:265-275
- Lu J, Jiang C (2001) Antiangiogenic activity of selenium in cancer chemoprevention: metabolite-specific effects. *Nutr Cancer* 40:64-73
- Lu J, Xie Y, Xu F, Zhu L (2002) Study of the dissolution behavior of selenium and tellurium in different solvents- a novel route to Se, Te tubular bulk single crystals. *J Mater Chem* 12:2755-2761

- Luo H, Wang F, Bai Y, Chen T, Zheng W (2012) Selenium nanoparticles inhibit the growth of HeLa and MDA-MB-231 cells through induction of S phase arrest. *Colloid Surf B Biointerfaces* 94:304-308
- Luo Y, Wang C, Qiao Y, Hossain M, Ma L, Su M (2012) In vitro cytotoxicity of surface modified bismuth nanoparticles. *J Mater Sci Mater Med* 23:2563-2573
- Madern D, Ebel C, Zaccai G (2000) Halophilic adaptation of enzymes. *Extremophiles* 4:91-98
- Mafune F, Kohno J, Takeda Y, Kondow T, Sawabe H (2001) Formation of gold nanoparticles by laser ablation in aqueous solution of surfactant. *J Phys Chem B* 105:5114-5120
- Mager EM (2011) Lead, In. Wood CM, Farrell AP, Brauner CJ (Eds) Homeostasis and toxicology of non-essential metals, Fish physiology, vol. 31B Academic Press, New York pp. 185-236.
- Majidi S, Zeinali Sehgig F, Samiei M, Milani M, Abbasi E, Dadashzadeh K, Akbarzadeh A (2016) Magnetic nanoparticles: Applications in gene delivery and gene therapy. *Artif Cells Nanomed Biotechnol* 44:1186-1193.
- Malarkodi C, Annadurai G (2013) A novel biological approach on extra-cellular synthesis and characterisation of semiconductor zinc sulphide nanoparticles. *Appl Nanosci* 3:389-395
- Malki L, Yanku M, Borovok I, Cohen G, Mevarech M, Aharonowitz Y (2009) Identification and characterisation of gshA, a gene encoding the glutamate-cysteine ligase in the halophilic archaeon *Haloflex volcanii*. *J Bacteriol* 191:5196-5204
- Mallick K, Witcomb MJ, Scurell MS (2004) Polymer stabilized silver nanoparticles: a photochemical synthesis route. *J Mater Sci* 39:4459-4463
- Manayani DJ, Thomas D, Dryden KA, Reddy V, Siladi ME, Marlett JM, Rainey GJA, Pique ME, Scobie HM, Yeager M, Young JAT, Manchester M, Schneemann A (2007) A viral nanoparticle with dual function as an anthrax antitoxin and vaccine. *PLoS Pathog* 3:e142. doi: 10.1371/journal.ppat.0030142.
- Mandilas C, Daskalos E, Karagiannakis G, Konstandopoulos AG (2013) Synthesis of aluminium nanoparticles by arc plasma spray under atmospheric pressure. *Mat Sci Eng B* 178:22-30
- Mani K, Salgaonkar BB, Braganca JM (2012) Culturable halophilic archaea at the initial and crystallization stages of salt production in a natural solar saltern of Goa, India. *Aquat Biosyst* 8:15. doi:10.1186/2046-9063-8-15

- Manivannan S, Alikunhi NM, Kandasamy K (2010) *In vitro* synthesis of silver nanoparticles by marine yeasts from coastal mangrove sediment. *Adv Sci Lett* 3:1-6
- Manjunath S, Thiagarajan P (2014) Exploring the mechanism for mycobiosynthesis of silver nanoparticles from *Aspergillus* spp. and optimisation of synthesis parameters. *Micro Nano Lett* 9:600-604
- Mann S (1993) Molecular tectonics in biomineralisation and biomimetic materials chemistry. *Nature* 365:499-505
- Mao C, Flynn CE, Hayhurst A, Sweeney R, Qi J, Georgiou G, Iverson B, Belcher AM (2003) Viral assembly of oriented quantum dot nanowires. *Proc Natl Acad Sci U S A* 100:6946-6951
- Marks LD (1994) Experimental studies of small particle structures. *Rep Prog Phys* 57:603-649
- Marshall MJ, Beliaev AS, Dohnalkova AC, Kennedy DW, Shi L, Wang Z, Boyanov MI, Lai B, Kemner KM, McLean JS, Reed SB, Culley DE, Bailey VL, Simonson CJ, Saffarini DA, Romine MF, Zachara JM, Fredrickson JK (2006) c-Type cytochrome-dependent formation of U(IV) nanoparticles by *Shewanella oneidensis*. *PLoS Biol.* 4:e268. doi:10.1371/journal.pbio.0040268
- Martin DD, Ciulla RA, Roberts MF (1999) Osmoadaptation in archaea. *Appl Environ Microbiol* 65:1815-1825
- Matsumura Y, Yoshikata K, Kunisaki S, Tsuchido T (2003) Mode of bacterial action of silver zeolite and its comparison with that of silver nitrate. *Appl Environ Microbiol* 69:4278-4281
- May M, Heebner G (2005) Putting molecule-scale biology to work. *Science AAS* http://www.sciencemag.org/site/products/adv_20051028.xhtml
- Mayers B, Xia Y (2002a) Formation of tellurium nanotubes through concentration depletion at the surfaces of seeds. *Adv Mater* 14:279-282
- Mayers B, Xia Y (2002b) One dimensional nano structures of trigonal tellurium with various morphologies can be synthesised using a solution phase- approach. *J Mater Chem* 12:1875-1881
- Messing GL, Zhang SC, Jayanthi GV (1993) Ceramic powder synthesis by spray-pyrolysis. *J Am Ceram Soc* 76:2707-2726
- Miao X, Ling L, Shuai X (2013) Sensitive detection of glucose in human serum with oligonucleotide modified gold nanoparticles by using dynamic light scattering technique. *Biosens Bioelectron* 41:880-883

- Michaud D, Faye L, Yelle S (1993) Electrophoretic analysis of plant cysteine and serine proteinases using gelatin-containing polyacrylamide gels and class-specific proteinase inhibitors. *Electrophoresis* 14:94-98
- Mie G (1908) Beiträge zur Optik trüber Medien, speziell kolloidaler Metallösungen. *Ann Phys* 25:377-445 American translation at <http://diogenes.iwt.uni-bremen.de/vt/laser/papers/SAND78-6018-Mie-1908-translation.pdf>
- Miersch J, Tschimedbalshir M, Barlocher F, Grams Y, Pierau B, Schierhorn A, Krauss GJ (2001) Heavy metals and thiol compounds in *Mucor racemosus* and *Articulospora tetracladia*. *Mycol Res* 105:883-889
- Mishra RR, Prajapati S, Das J, Dangar TK, Das N, Thatoi H (2011) Reduction of selenite to red elemental selenium by moderately halotolerant *Bacillus megaterium* strains isolated from Bhitarkanika mangrove soil and characterization of reduced product. *Chemosphere* 84:1231-1237
- Mitchell GP, Mirkin CA, Letsinger RI (1999) Programmed assembly of DNA functionalised quantum dots. *J Am Chem* 121:8122-8123
- Mohanpuria P, Rana NK, Yadav SK (2008) Biosynthesis of nanoparticles: technological concepts and future applications. *Nanopart Res* 10:510-517
- Mokhtari N, Daneshpajouh S, Seyedbagheri, Atashdehghan R, Abdi K, Sarkar S, Minaian S, Shahverdi HR, Shahverdi AR (2008) Biological synthesis of very small silver nanoparticles by culture supernatant of *Klebsiella pneumoniae*: the effects of visible-light irradiation and the liquid mixing process. *Mater Res Bull* 44:1415-1421
- Molina RC, Burra R, Pérez-Donoso JM, Elías AO, Muñoz C, Montes RA, Chasteen TG, Vásquez CC (2010) Simple, fast, and sensitive method for quantification of tellurite in culture media. *Appl Environ Microbiol* 76:4901-4904
- Monroe S, Polk R (2000) Antimicrobial use and bacterial resistance. *Curr Opin Microbiol* 3:496-501
- Morones JB, Elechiguerra JL, Camacho A, Holt K, Kouri JB, Ramírez JP, Yacaman MJ (2005) The bactericidal effect of silver nanoparticles. *Nanotechnology* 16:2346-2353
- Mukherjee P, Roy M, Mandal BP, Dey GK, Mukherjee PK, Ghatak J, Tyagi AK, Kale SP (2008) Green synthesis of highly stabilized nanocrystalline silver particles by a non-pathogenic and agriculturally important fungus *T. asperellum*. *Nanotechnology* 19:75103-75110

- Mukherjee SG, O'Claonadh N, Casey A, Chambers G (2012) Comparative in vitro cytotoxicity study of silver nanoparticle on two mammalian cell lines. *Toxicol In Vitro* 26:238-251
- Mulvaney P (1996) Surface plasmon spectroscopy of nanosized metal particles. *Langmuir* 12:788-800
- Munger K, Germann UA, Lerch K (1987) The *Neurospora crassa* metallothionein gene. Regulation of expression and chromosomal location. *J Biol Chem* 262:7363-7367
- Musarrat J, Dwivedi S, Singh BR, Al-Khedhairi AA, Azam A, Naqvi A (2010) Production of antimicrobial silver nanoparticles in water extracts of the fungus *Amylomyces rouxii* strain KSU-09. *Biores Technol* 101: 8772-8776
- Muthukannan R, Karuppiyah B (2011) Rapid synthesis and characterization of silver nanoparticles by novel *Pseudomonas* sp. "ram bt-1" *J Ecobiotechnol* 3:24
- Myung S, Solanki A, Kim C, Park J, Kim KS, Lee K-B (2011), Graphene-encapsulated nanoparticle-based biosensor for the selective detection of cancer biomarkers. *Adv Mater* 23:2221-2225
- Naik MM, Dubey SK (2013) Lead resistant bacteria: lead resistance mechanisms, their applications in lead bioremediation and biomonitoring. *Ecotoxicol Environ Saf* 98:1-7
- Nakane Y, Tsukasaki Y, Sakata T, Yasuda H, Jin T (2013) Aqueous synthesis of glutathione-coated PbS quantum dots with tunable emission for non-invasive fluorescence imaging in the second near-infrared biological window (1000-1400 nm). *Chem Commun (Camb)* 49:7584-7586
- Narayanan KB, Sakthivel N (2010) Biological synthesis of metal nanoparticles by microbes. *Adv Colloid Interface Sci* 156:1-13. doi: 10.1016/j.cis.2010.02.001
- Naumov AV (2010) Selenium and tellurium: state of the markets, the crisis, and its consequences. *Metallurgist* 54:3-4
- Nepijko SA, Hofmeister H, Sack-Kongehl H, Schlogl R (2000) Multiply twinned particles beyond the icosahedron. *J Cryst Growth* 213:129-134
- Newton GL, Javor B (1985) gamma-Glutamylcysteine and thiosulfate are the major low-molecular-weight thiols in halobacteria. *J Bacteriol* 161:438-441
- Ng WV, Kennedy SP, Mahairas GG, Berquist B, Pan M, Shukla HD, Lasky SR, Baliga NS, Thorsson V, Sbrogna J, Swartzell S, Weir D, Hall J, Dahl TA, Welti R, Goo YA, Leithauser B, Keller K, Cruz R, Danson MJ, Hough DW, Maddocks DG, Jablonski PE, Krebs MP, Angevine CM, Dale H, Isenbarger TA, Peck RF, Pohlschroder M,

- Spudich JL, Jung KW, Alam M, Freitas T, Hou S, Daniels CJ, Dennis PP, Omer AD, Ebhardt H, Lowe TM, Liang P, Riley M, Hood L, DasSarma S (2000) Genome Sequence of *Halobacterium* species NRC-1. PNAS 97: 12176-12181
- Nies DH (1999) Microbial heavy metal resistance. Appl Microbiol Biotechnol 51:730-750
- Nozik AJ, Williams F, Nenadovic MT, Rajh T, Micic OI (1985) Size quantitation in small semiconductor particles. J Phys Chem 89:397-399
- O’Gara JP, Gomelsky M, Kaplan S (1997) Identification and molecular genetic analysis of multiple loci contributing to high level tellurite resistance in *Rhodobacter sphaeroides*. Appl Environ Microbiol 63:4713-4720
- Ogi T, Honda R, Tamaoki K, Saitoh N, Konishi Y (2011) Direct room-temperature synthesis of a highly dispersed Pd nanoparticle catalyst and its electrical properties in a fuel cell. Powder Technol 205:143-148
- Olenin AY, Krutyakov YA, Kudrinskii AA, Lisichkin GV (2008) Formation of surface layers on silver nanoparticles in aqueous and water-organic media. Colloid J 70:71-76
- Olshavsky MA, Allcock HR (1997) Small scale system for *in-vivo* drug delivery. Chem Mater 9:1367
- Oremland RS, Herbel MJ, Blum JS, Langley S, Beveridge TJ, Ajayan PM, Sutto T, Ellis AV, Curran S (2004) Structural and spectral features of selenium nanospheres produced by Se- respiring bacteria. Appl Environ Microbiol 70:52-60
- Oremland RS, Stolz JF (2000) Dissimilatory reduction of selenate and arsenate in nature, p. 199-224. In Lovley DR (ed.), Environmental metal-microbe interaction. ASM Press, Washington DC
- Oren A (2008) Microbial life at high salt concentrations: phylogenetic and metabolic diversity. Saline Syst 4:2 (doi: 10.1186/1746-1448-4-2)
- Oren A (2012) The function of gas vesicles in halophilic archaea and bacteria: Theories and experimental evidence. Life 3:1-20. doi:10.3390/life3010001
- Ortiz DF, Ruscitti T, McCue KF, Ow DW (1995) Transport of metal-binding peptides by HMT1, a fission yeast ABC-type vacuolar membrane protein. J Biol Chem 270:4721-4728
- Oza G, Pandey S, Shah R, Sharon M (2012) A mechanistic approach for biological fabrication of crystalline gold nanoparticles using marine algae, *Sargassum wightii*. Eur J Exp Biol 2:505-512

- Pages D, Rose J, Conrod S, Cuine S, Carrier P, Heulin T, Achouak W (2008) Heavy metal tolerance in *Stenotrophomonas maltophilia*. PLOS One 3:e1539. doi: 10.1371/journal.pone.0001539
- Pandian SRK, Deepak V, Kalishwaralal K, Gurunathan S (2011) Biologically synthesized fluorescent CdS NPs encapsulated by PHB. Enzyme MicrobTechnol 48:319-325
- Park BK, Jeong S, Kim D, Moon J, Lim S, Kim JS (2007) Synthesis and size control of monodisperse copper nanoparticles by polyol method. J Colloid Interface Sci 311: 417-424
- Park TJ, Lee SY, Heo NS, Seo TS (2010) In vivo synthesis of diverse metal nanoparticles by recombinant *Escherichia coli*. Angew Chem Int Ed Engl 49:7019-7024
- Patil RS, Pathan HM, Gujar TP, Lokhande CD (2006) Characterisation of chemically deposited nanocrystalline PbS thin films. J Mater Sci 41:5723-5725
- Paul S, Paul D, Fern GR, Ray AK (2011) Surface plasmon resonance imaging detection of silver nanoparticle-tagged immunoglobulin. J R Soc Interface 8:1204–1211
- Pearion CT, Jablonski PE (1999) High level, intrinsic resistance of *Natronococcus occultus* to potassium tellurite. FEMS Microbiol Lett 174:19-23
- Penas E, Martinez-Villaluenga C, Frias J, Sanchez-Martinez MJ, Perez-Corona MT, Madrid Y, Camara C, Vidal-Valverde C (2012) Se improves indole glucosinolate hydrolysis products content, Se-methylselenocysteine content, antioxidant capacity and potential anti-inflammatory properties of sauerkraut. Food Chem 132:907-914
- Pereira F, Kerkar S, Krishnan KP (2013) Bacterial response to dynamic metal concentrations in the surface sediments of a solar saltern (Goa, India). Environ Monit Assess 185:3625-3636
- Perez JM, Calderon IL, Arenas FA, Fuentes DE, Pradenas GA, Fuentes EL, Sandoval JM, Castro ME, Elias AO, Vasquez CC (2007) Bacterial toxicity of potassium tellurite: unveiling an ancient enigma. PLoS ONE 2: e211. doi:10.1371/journal.pone.0000211
- Phillips K, ZaidanIII F, Elizondo OR, Lowe KL (2012) Phenotypic characterization and 16S rDNA identification of culturable non-obligate halophilic bacterial communities from a hypersaline lake, La Sal del Rey, in extreme South Texas (USA). Aquat Biosyst 8:5. doi:10.1186/2046-9063-8-5
- Pitcher MW, Cates E, Raboin L, Bianconi PAA (2000) Synthetic analogue of the biomineralization process: formation of novel lead sulphide phases. Chem Mater 12:1738-1742

- Popescu G, Dumitru L (2009) Biosorption of some heavy metals from media with high salt concentrations by halophilic archaea. *Biotechnol Biotechnol (SE)* 23:791-795
- Praharaj S, Nath S, Panigrahi S, Basu S, Ghosh SK, Pande S, Jana S, Pal T (2006) Room temperature synthesis of coinage metal (Ag, Cu) chalcogenides. *Chem Commun* 36:3836-3838
- Prasad K, Jha AK, Prasad K (2007) *Lactobacillus* assisted synthesis of titanium nanoparticles. *Nanosclae Res Lett* 2:248-250
- Prasad KS, Vyas P, Prajapati V, Patel P, Selvaraj K (2012). Biomimetic synthesis of selenium nanoparticles using cell-free extract of *Microbacterium* sp. ARB05. *Micro Nano Lett* 7:1-4
- Qadri SB, Yang JP, Skelton EF, Ratna BR (1997) Evidence of strain and lattice distortion in lead sulfide nanocrystallites. *Appl Phys Lett* 70:1020-1021
- Rai M, Yadav A, Gade A (2009) Silver nanoparticles as a new generation of antimicrobials. *Biotechnol Adv* 27:76-83
- Rajakumar G, Rahuman AA, Roopan SM, Khanna VG, Elango G, Kamaraj C, Zahir AA, Velayutham K (2012) Fungus-mediated biosynthesis and characterization of TiO₂ nanoparticles and their activity against pathogenic bacteria. *Spectrochim Acta A Mol Biomol Spectrosc* 91:23-29
- Rajeshkumar S, Malarkodi C, Paulkumar K, Vanaja M, Gnanajobitha G, Annadurai G (2014) Algae mediated green fabrication of silver nanoparticles and examination of its antifungal activity against clinical pathogens. *Int J Metals* 2014:8. doi:10.1155/2014/692643
- Ramamurthy CH, Sampath KS, Arun kumar P, Suresh Kumar M, Sujatha V, Premkumar K, Thirunavukkarasu C (2013) Green synthesis and characterisation of selenium nanoparticles and its augmented cytotoxicity with doxorubicin on cancer cells. *Bioprocess Biosyst Eng* 36:1131-1139
- Ramezani F, Ramezani M, Talebi S (2010) Mechanistic aspects of biosynthesis of nanoparticles by several microbes. *Nanocon* 10:12-14
- Rao CNR, Cheetham AK (2001) Science and technology of nanomaterials: current state and future prospects. *J Mater Chem* 11:2887-2894
- Rao NP, Lee HJ, Kelkar M, Hansen DJ, Heberlein JVR, McMurry PH, Girshick SL (1997) Nanostructured materials production by hypersonic plasma particle deposition. *Nanostruct Mater* 9:129-132

- Ratheesh Kumar CS, Joseph MM, Gireesh Kumar TR, Renjith KR, Manju MN, Chandramohanakumar N (2010) Spatial variability and contamination of heavy metals in the inter-tidal systems of a tropical environment. *Int J Environ Res* 4:691-700
- Ratke L, Voorhees PW (2002) Growth and coarsening: Ostwald ripening in material processing. Springer-Verlag Berlin Heidelberg pp. 298
- Rausser WE (1995) Phytochelatins and related peptides: structure, biosynthesis, and function. *Plant Physiol* 109: 1141-1149
- Raveendran S, Chauhan N, Nakajima Y, Toshiaki H, Kurosu S, Tanizawa Y, Tero R, Yoshida Y, Hanajiri T, Maekawa T, Ajayan PM, Sandhu A, Kumar DS (2013a) Ecofriendly route for the synthesis of highly conductive graphene using extremophiles for green electronics and bioscience. *Part Part Syst Charact* 30:573-578
- Raveendran S, Dhandayuthapani B, Nagaoka Y, Yoshida Y, Maekawa T, Kumar DS (2013c) Biocompatible nanofibers based on extremophilic bacterial polysaccharide, Mauran from *Halomonas maura*. *Carbohydr Polym* 92:1225-1233
- Raveendran S, Girija AR, Balasubramanian S, Ukai T, Yoshida Y, Maekawa T, Kumar DS (2014) Green approach for augmenting biocompatibility to Quantum Dots by extremophilic polysaccharide conjugation and nontoxic bioimaging. *ACS Sustainable Chem Eng* 2:1551-1558
- Raveendran S, Poulouse AC, Yoshida Y, Maekawa T, Kumar DS (2013b) Bacterial exopolysaccharide based nanoparticles for sustained drug delivery, cancer chemotherapy and bioimaging. *Carbohydr Polym* 91:22-32
- Ravindra P (2009) Protein-mediated synthesis of gold nanoparticles. *Mat Sci Eng B* 163:93-98
- Rayman MP (2005) Selenium in cancer prevention: a review of the evidence and mechanism of action. *Proc Nutr Soc* 64:527-542
- Rayman MP (2012) Selenium and human health. *Lancet* 379:156-1268
- Reddy LH, Arias JL, Nicolas J, Couvreur P (2012) Magnetic nanoparticles: design and characterization, toxicity and biocompatibility, pharmaceutical and biomedical applications. *Chem Rev* 112:5818-5878
- Redwood MD, Deplanche K, Baxter-Plant VS, Macaskie LE (2008) Biomass-supported palladium catalysts on *Desulfovibrio desulfuricans* and *Rhodobacter sphaeroides*. *Biotechnol Bioeng* 99:1045-1054

- Reese RN, White CA, Winge DR (1992) Cadmium sulfide crystallites in Cd-(γ -EC)_nG peptide complexes from tomato. *Plant Physiol* 98:225-229
- Reidy B, Haase A, Luch A, Dawson K, Lynch I (2013) Mechanisms of silver nanoparticle release, transformation and toxicity: A critical review of current knowledge and recommendations for future studies and applications. *Materials* 6:2295-2350
- Ribble D, Goldstein NB, Norris DA, Shellman YG (2005) A simple technique for quantifying apoptosis in 96-well plates. *BMC Biotechnol* 5:12. doi: 10.1186/1472-6750-5-12.
- Rikiishi H (2007) Apoptotic cellular events for selenium compounds involved in cancer prevention. *J Bioenerg Biomembr* 39:91-98
- Roman-Zamorano JF, Flores Acosta M, Arizpe-Chavez H, Castillon-Barraza FF, Farias MH, Ramirez-Bon R (2009) Structure and properties of lead and lead sulfide nanoparticles in natural zeolite. *J Mater Sci* 44:4781-4788
- Rosenholm JM, Zhang J, Linden M, Sahlgren C (2016) Mesoporous silica nanoparticles in tissue engineering—a perspective. *Nanomedicine (Lond)* 11:391-402.
- Ross SM (1994) Retention, transformation and mobility of toxic metals in soils. In: Ross SM (Ed.) *Toxic metals in soil-plant systems*. John Wiley & Sons Chichester UK pp. 63–152
- Rover Junior L, Fernandes JC, de Oliveira Neto G, Kubota LT, Katekawa E, Serrano SH (1998) Study of NADH stability using ultraviolet-visible spectrophotometric analysis and factorial design. *Anal Biochem* 260:50-55
- Rover Junior L, Fernandes JC, de Oliveira Neto G, Kubota LT, Katekawa E, Serrano SH (1998) Study of NADH stability using ultraviolet-visible spectrophotometric analysis and factorial design. *Anal Biochem* 260:50-55
- Sabirzhanov B, Stoica BS, Hanscom M, Piao CS, Faden AI (2012) Over-expression of HSP70 attenuates caspase-dependent and caspase-independent pathways and inhibits neuronal apoptosis. *J Neurochem* 123:542-554
- Salamanca-Buentello F, Persad DL, Court EB, Martin DK, Daar AS, Singer PA (2005) Nanotechnology and the developing world. *PLoS Med* 2:e97
- Salvadori MR, Ando RA, Oller do Nascimento CA, Corre B. Intracellular biosynthesis and removal of copper nanoparticles by dead biomass of yeast isolated from the wastewater of a mine in the Brazilian Amazonia. *PLoS One* 9:e87968. doi:10.1371/journal.pone.0087968

- Sangappa M, Thiagarajan P (2014) Exploring the mechanism for mycobiosynthesis of silver nanoparticles from *Aspergillus* spp. and optimisation of synthesis parameters. IET Micro Nano Lett 9:600. doi: 10.1049/mnl.2014.0176
- Sarikaya M, Tamerler C, Jen AK, Schulten K, Baneyx F (2003) Molecular biomimetics: nanotechnology through biology. Mat Mater 2:577-585
- Sarkar J, Dey P, Saha S, Acharya K (2011) Mycosynthesis of selenium nanoparticles. Micro Nano Lett 6:599-602
- Sarkar R, Kumbhakar P, Mitra AK (2010) Green synthesis of silver nanoparticles and its optical properties. Dig J Nanomater Biostruct 5:491-496
- Sathiyarayanan G, Kiran GS, Selvin J (2013) Synthesis of silver nanoparticles by polysaccharide bioflocculant produced from marine *Bacillus subtilis* MSBN17. Coll Surf B 102:13-20
- Schneegurt MA (2012) Media and conditions for the growth of halophilic and halotolerant bacteria and archaea. In: Vreeland RH (Ed) Advances in understanding the biology of halophilic microorganisms. Dordrecht Springer, pp. 35-58
- Schrofel A, Kratosova G, Bohunicka G, Dobrocka E, Vavra I (2011) Biosynthesis of gold nanoparticles using diatoms-silica-gold and EPS-gold bionanocomposite formation. J Nanopart Res 13:3207-3216
- Schrofel A, Kratosova G, Safarik I, Safarikovs M3, Raska I, Shor LM (2014) Applications of biosynthesized metallic nanoparticles - a review. Acta Biomater 10:4023-4042
- Sedlak J, Lindsay RH (1968) Estimation of total, protein-bound, and nonprotein sulfhydryl groups in tissue with Ellman's reagent. Anal Biochem 25:192-205
- Senapati S, Ahmad A, Khan MI, Sastry M, Kumar R (2005) Extracellular biosynthesis of bimetallic Au-Ag alloy nanoparticles. Small 1:517-520
- Seng HL, Tiekink ERT (2012) Anti-cancer potential of selenium- and tellurium-containing species: opportunities abound! Appl Organomet Chem 26:655-662
- Seshadri S, Prakash A, Kowshik M (2012) Biosynthesis of silver nanoparticles by marine bacterium, *Idiomarina* sp. PR58-8. Bull Mater Sci 35:1201-1205
- Seshadri S, Saranya K, Kowshik M (2011) Green synthesis of lead sulfide nanoparticles by the lead resistant marine yeast, *Rhodospiridium diobovatum*. Biotechnol Prog 7:1464-1469

- Shah R, Oza G, Pandey S, Sharon M (2012) Biogenic fabrication of gold nanoparticles using *Halomonas salina*. *J Microbiol Biotech Res* 2:485-492
- Shahverdi AR, Minaian S, Shahverdi HR, Jamalifar H, Nohi A (2007) Rapid synthesis of silver nanoparticles using culture supernatants of Enterobacteria: A novel biological approach. *Process Biochem* 42:919-923
- Shakibaie M, Khorramizadeh MR, Faramarzi MA, Sabzevari O, Shahverdi AR (2010) Biosynthesis and recovery of selenium nanoparticles and the effects on matrix metalloproteinase-2 expression. *Biotechnol Appl Biochem* 56: 7-15
- Shankar SS, Rai A, Ahmad A, Sastry M (2004) Biosynthesis of silver and gold nanoparticles from extracts of different parts of the geranium plant. *Appl Nanosci* 1:69-77
- Sharma VK, Yngard RA, Lin Y (2008) Silver nanoparticles: Green synthesis and their antimicrobial activities. *Adv Colloid Interface Sci* 145: 83-96
- Shenton W, Douglas T, Young M, Stubbs G, Mann S (1999) Inorganic–organic nanotube composites from template mineralization of Tobacco mosaic virus. *Adv Mater* 11:253-256
- Shisler JL, Senkevich TG, Berry MJ, Moss B (1998) Ultraviolet-induced cell death blocked by a selenoprotein from a human dermatropic pox virus. *Science* 279:102-105
- Shokovit ER (1976) Flocculation of dissolved organic and inorganic matter during the mixing river water and seawater. *Geochim Cosmochim Acta* 40:831-845
- Shukla HD, DasSarma S (2004) Complexity of gas vesicle biogenesis in *Halobacterium* sp. strain NRC-1: identification of five new proteins. *J Bacteriol* 186:3182-3186
- Shyju TS, Gopaiakrishnan R (2013) Studies on lead sulphide thin films deposited by photochemical method. *Proceedings of the International Conference on Advanced Nanomaterials & Emerging Engineering Technologies* pp. 340-343
- Silverman MS (1966) High-pressure (70-kbar) synthesis of new crystalline lead dichalcogenides. *Inorg Chem* 5:2067-2069
- Simkiss K, Wilbur KM (1989) *Biom mineralization: cell biology and mineral deposition*. pp. 137 Academic Press, San Diego, California
- Simon H-U, Haj-Yehia A, Levi-Schaffer F (2000) Role of reactive oxygen species (ROS) in apoptosis induction. *Apoptosis* 5:415-418

- Singaravelu G, Arockiamary JS, Ganesh Kumar V, Govindaraju K (2007) A novel extracellular synthesis of monodisperse gold nanoparticles using marine alga, *Sargassum wightii* Greville. *Coll Surf B* 57:97-101
- Singh N, Nara S (2013) Biological synthesis and Characterisation of lead sulphide nanoparticles using bacterial isolates from heavy metal rich sites. *Int J Agric Food Sci* 4:16-23
- Sinha A, Khare SK (2011) Mercury bioaccumulation and simultaneous nanoparticle synthesis by *Enterobacter* sp. cells. *Bio esource Technol* 102:4281-4284
- Soini Y, Paakko P, Lehto V-P (1998) Histopathological evaluation of apoptosis in cancer. *Am J Pathol* 153:1041-1053
- Sondi I, Salopek-Sondi B (2004) Silver nanoparticles as antimicrobial agent: a case study on *E. coli* as a model for Gram-negative bacteria. *J Colloid Interface Sci* 275: 177-182
- Spangler LC, Lu L, Kiely CJ, Berger BW, McIntosh S (2016) Biomineralization of PbS and PbS–CdS core–shell nanocrystals and their application in quantum dot sensitized solar cells. *J Mater Chem A* 4:6107-6115
- Speiser DM, Abrahamson SL, Banuelos G, Ow DW (1992) Brassica juncea produces a phytochelatin-cadmium-sulfide complex. *Plant Physiol* 99:817-821
- Sperling RA, Parak WJ (2010) Surface modification, functionalization and bioconjugation of colloidal inorganic nanoparticles. *Phil Tran R Soc A* 368:1333-1383
- Srivastava N, Mukhopadhyay M (2013) Biosynthesis and structural characterisation of selenium nanoparticles mediated by *Zooglea ramigera*. *Powder Technol* 244:26-29
- Srivastava P, Braganca JM, Kowshik M (2014) In vivo synthesis of selenium nanoparticles by *Halococcus salifodinae* BK18 and their anti-proliferative properties against HeLa cell line. *Biotechnol Prog* 30:1480-1487
- Srivastava P, Kowshik M (2013) Mechanisms of metal resistance and homeostasis in haloarchaea. *Archaea* 2013:16. doi:10.1155/2013/732864
- Stolz JF, Oremland RS (1999) Bacterial respiration of selenium and arsenic. *FEMS Microbiol Rev* 23:615-627
- Summers AO, Jacoby GA (1977) Plasmid-determined resistance to tellurium compounds. *J Bacteriol* 129:276-281

- Sun C, Lee JS, Zhang M (2008) Magnetic nanoparticles in MR imaging and drug delivery. *Adv Drug Deliv Rev* 60:1252-265
- Sun D, Liu Y, Yu Q, Qin X, Yang L, Zhou Y, Chen L, Liu J (2014) Inhibition of tumor growth and vasculature and fluorescence imaging using functionalized ruthenium-thiol protected selenium nanoparticles. *Biomaterials* 35: 1572-1583
- Sundquist AR, Fahey RC (1989) The function of γ -glutamylcysteine and bis- γ -glutamylcysteine reductase in *Halobacterium halobium*. *J Biol Chem* 264:719-725
- Sweeney RY, Mao C, Gao X, Burt JL, Belcher AM, Georgiou G, Iverson BL (2004) Bacterial biosynthesis of cadmium sulphide nanocrystals. *Chem & Biol* 11:1553-1559
- Tabak HH, Lens P, van Hullebusch ED, Dejonghe W (2005) Developments in bioremediation of soils and sediments polluted with metals and radionuclides. 1. Microbial processes and mechanisms affecting bioremediation of metal contamination and influencing metal toxicity and transport. *Rev Environ Sci Biotechnol* 4:115-156
- Takahashi T (1982) Comparative x-ray-photoemission study of monoclinic, trigonal, and amorphous selenium. *Phys Rev B: Condens Matter* 26:5963-5964
- Tam K, Ho CT, Lee JH, Lai M, Chang CH, Rheem Y, Chen W, Hur HG (2010) Growth mechanism of amorphous selenium nanoparticles synthesised by *Shewanella sp. HN-41*. *Biosci Biotech Bioch* 74:696-700
- Tan L, Jia X, Jiang XF, Zhang YY, Tang H, Yao SZ, Xie Q (2009) In vitro study on the individual and synergistic cytotoxicity of Adriamycin and selenium nanoparticles against Bel7402 cells with a quartz crystal microbalance. *Biosens Bioelectron* 24:2268-2272
- Tang SC, Lo IM (2013) Magnetic nanoparticles: essential factors for sustainable environmental applications. *Water Res* 47:2613-2632
- Tang Z, Zhang Z, Wang Y, Glotzer SC, Kotov NA (2006) Self-assembly of CdTe nanocrystals into free-floating sheets. *Science* 314:274-278
- Taylor DE (1999) Bacterial tellurite resistance. *Trends Microbiol* 7:111-115
- Terai T, Kamamura Y (1958) Tellurite reductase from *Mycobacterium avium*. *J Bacteriol* 75:535-539
- Thakkar KN, Mhatre SS, Parikh YR (2010) Biological synthesis of metallic nanoparticles. *Nanomed Nanotech Biol Med* 6:275-262

- Thomas JW, Appleman MD, Tucker FL (1963) Reduction of tellurite by whole cells, protoplasm and cell-free extracts of *Streptococci*. Bacteriological Proceedings 124
- Thornberry NA, Lazebnik Y (1998) Caspases: enemies within. Science 281:1312-1316
- Tidke PR, Gupta I, Gade AK, Rai M (2014) Fungus-mediated synthesis of gold nanoparticles and standardisation of parameters for its biosynthesis. IEEE Trans Nanobioscience 13:397-402
- Tien DC, Tseng KH, Liao CY, Huang JC, Tsung TT (2008) Discovery of ionic silver in silver nanoparticle suspension fabricated by arc discharge method. J Alloys Compd 463:408-411
- Torres SK, Campos VL, Leon CG, Rodriguez-Llamazares SM, Rojas SM, Gonzalez M, Smith C, Mondaca MA (2012) Biosynthesis of selenium nanoparticles by *Pantoea agglomerans* and their antioxidant activity. J Nanopart Res 14:1236 doi:10.1007/s11051-012-1236-3
- Tran QH, NguyenVQ, Le AT (2013) Silver nanoparticles: synthesis, properties, toxicology, applications and perspectives. Adv Nat Sci: Nanosci Nanotechnol 4:20 doi:10.1088/2043-6262/4/3/033001
- Truong L, Moody IS, Stankus DP, Nason JA, Lonergan MC, Tanguay RL (2011) Differential stability of lead sulfide nanoparticles influences biological responses in embryonic zebrafish. Arch Toxicol 85:787-798
- Turner R, Weiner J, Taylor D (1992) Use of diethyldithiocarbamate for quantitative determination of tellurite uptake by bacteria. Anal Biochem 204:292-295
- Turner RJ, Weiner JH, Taylor DE (1995) The tellurite-resistance determinants *tehA* and *tehB* have different biochemical requirements. Microbiology 141:3133-3140
- Turner RJ, Weiner JH, Taylor DE (1999) Tellurite-mediated thiol oxidation in *Escherichia coli*. Microbiology 145:2549-2557
- Ufimtsev VB, Osvensky VB, Bublik VT, Sagalova TB, Jouravlev OE (1997) Structure, homogeneity and properties of thermoelectric materials based on ternary solid solutions of bismuth and antimony chalcogenides. Adv Perform Mater 4:189-197
- Underwood S, Mulvaney P (1994) Effect of the solution refractive index on the color of gold colloids. Langmuir 10: 3427-3430
- Vaidyanathan R, Gopalram S, Kalishwaralal K, Deepak V, Pandian SR, Gurunathan S (2010) Enhanced silver nanoparticle synthesis by optimization of nitrate reductase activity. Colloids Surf B Biointerfaces 75:335-41

- Valodkar M, Jadeja RN, Thounaojam MC, Devkar RV, Thakore S (2011) Biocompatible synthesis of peptide capped copper nanoparticles and their biological effect on tumor cells. *Mater Chem Phys* 128:83-89
- van Keulen G, Hopwood DA, Dijkhuizen L, Sawers RG (2005) Gas vesicles in actinomycetes: old buoys in novel habitats. *Trends Microbiol* 13:350-354
- Vance ME, Kuiken T, Vejerano EP, McGinnis SP, Hochella MF Jr, Rejeski D, Hull MS (2015) Nanotechnology in the real world: Redeveloping the nanomaterial consumer products inventory. *Beilstein J Nanotechnol* 6:1769-1780
- Vasiliev A, Gulliver E, Khinast J, Riman R (2009) Highly dispersible polymer-coated silver nanoparticles. *Surf Coat Technol* 203:2841-2844
- Vekariya KK, Kaur J, Tikoo K (2012) ER α signaling imparts chemotherapeutic selectivity to selenium nanoparticles in breast cancer. *Nanomed Nanotech Biol Med* 8:1125-1132
- vo-Dinh T (2008) Nanobiosensing using plasmonic nanoprobe. *IEEE J Sel Topics Quantum Electron* 14:198-205
- Walker CW, Houston CW (1981) Toxicity of cadmium to bacteria. *Biotechnol Lett* 3:437-442
- Walling MA, Novak JA, Shepard JRE (2009) Quantum dots for live cell and in vivo imaging. *Int J Mol Sci* 10:441-491
- Wang G, Kennedy SP, Fasiludeen S, Rensing C, DasSarma S (2004) Arsenic resistance in *Halobacterium* sp. strain NRC-1 examined by using an improved gene knockout system. *J Bacteriol* 186:3187-3194
- Wang H, Zhang Q, Cai B, Li H, Sze KH, Huang ZX, Wu HM, Sun H (2006) Solution structure and dynamics of human metallothionein-3 (MT-3). *FEBS Lett* 580:795-800
- Wang T, Yang L, Zhang B, Liu J (2010) Extracellular biosynthesis and transformation of selenium nanoparticles and application in H₂O₂ biosensor. *Colloids Surf B Biointerf* 2010:94-102
- Warner JH, Watt AAR, Tilley RD (2005) Controlling PbS nanocrystal aggregation in conducting polymers. *Nanotechnology* 16:2381-2384
- Watkinson JH (1966). Fluorimetric determination of selenium in biological material with 2,3-diaminonaphthalene. *Anal Chem* 38:92-97
- Wegner KD, Hildebrandt N (2015) Quantum dots: bright and versatile *in vitro* and *in vivo* fluorescence imaging biosensors. *Chem Soc Rev* 44:4792-4834

- Weiner RM, Devine R, Powell D, Dagasan L, Moore R (1985) *Hyphomonas oceanitis* sp. nov., *Hyphomonas hirschiana* sp. nov., and *Hyphomonas jannaschiana* sp. nov. Int J Syst Bacteriol 35:237-243
- Whanger PD (2004) Selenium and its relationship to cancer: an update. Br J Nutr 91:11-28
- Wierucka M, Biziuk M (2014) Application of magnetic nanoparticles for magnetic solid-phase extraction in preparing biological, environmental and food samples. Trends Anal Chem 59:50-58
- Winge DR, Nielson KB, Gray WR, Hamer DH (1985) Yeast metallothionein sequence and metal binding properties. J Biol Chem 260:14464-14470
- Wise FW (2000) Lead salt quantum dots: the limit of strong quantum confinement. Acc Chem Res 33:773-780
- Wolfbeis OA (2015) An overview of nanoparticles commonly used in fluorescent bioimaging. Chem Soc Rev 44: 4743-4768
- Wong KKW, Mann S (1996) Biomimetic synthesis of cadmium sulphide-ferritin nanocomposites. 8:928-932
- Xi G, Peng Y, Yu W, Qian Y (2005) Synthesis, characterisation, and growth mechanism of tellurium nanotubes. Cryst Growth Des 5:325-328
- Xia L, Liu X, Zeng J, Yin C, Gao J, Liu J, Qiu G (2008) Mechanism of enhanced bioleaching efficiency of *Acidithiobacillus ferrooxidans* after adaptation with chalcopyrite. Hydrometallurgy 92:95-101
- Xiao G, Wang Y, Ning J, Wei Y, Liu B, Yu WW, Zou G, Zou B (2013) Recent advances in IV–VI semiconductor nanocrystals: synthesis, mechanism, and applications. RSC Adv 3:8104-8130
- Xin R, Ren F, Leng Y (2010) Synthesis and characterization of nano-crystalline calcium phosphates with EDTA-assisted hydrothermal method. Mater Design 31:1691-1694
- Yan AG, Liu XH, Qiu GZ, Wu HY, Yi R, Zhang N, Xu J (2008) Solvothermal synthesis and characterisation of size-controlled Fe₃O₄ nanoparticles. J Alloys Compd 458:487-491
- Yanke LJ, Bryant RD, Laishley EJ (1995) Hydrogenase (I) of *Clostridium pasteurianum* functions a novel selenite reductase. Anaerobe 1:61-67
- Yao G, Pei H, Li J, Zhao Y, Zhu D, Zhang Y, Lin Y, Huang Q, Fan C (2015) Clicking DNA to gold nanoparticles: poly-adenine-mediated formation of monovalent DNA-gold

- nanoparticle conjugates with nearly quantitative yield. *NPG Asia Mater* 7:e159. doi:10.1038/am.2014.131
- Yedjou CG, Milner JN, Howard CB, Tchounwou PB (2010) Basic apoptotic mechanisms of lead toxicity in human leukemia (HL-60) cells. *Int J Environ Res Public Health* 7:2008-2017
- Yi H, Nisar S, Lee SY, Powers MA, Bentley WE, Payne GF, Ghodssi R, Rubloff GW, Harris MT, Culver JN (2005) Patterned assembly of genetically modified viral nanotemplates via nucleic acid hybridization. *Nano Lett* 5:1931-1936
- Yong P, Rowson NA, Farr JP, Harris IR, Macaskie LE (2002) Bioreduction and biocrystallization of palladium by *Desulfovibrio desulfuricans* NCIMB 8307. *Biotechnol Bioeng* 80:369-79
- Yurkov V, Jappe J, Vermeglio A (1996) Tellurite resistance and reduction by obligately aerobic photosynthetic bacteria. *Appl Environ Microbiol* 62: 4195-4198
- Zafrilla B, Martínez-Espinosa RM, Alonso MA, Bonete MJ (2010) Biodiversity of Archaea and floral of two inland saltern ecosystems in the Alto Vinalopó Valley, Spain. *Saline Syst* 6:10. doi:10.1186/1746-1448-6-10
- Zare B, Babaie S, Setayesh N, Shahverdi AR (2013) Isolation and characterisation of a fungus for extracellular synthesis of small selenium nanoparticles. *Nanomed J* 1:13-19
- Zare B, Faramarzi MA, Sepehrizadeh Z, Shakibaie M, Sassan R, Ahmad RS (2012) Biosynthesis and recovery of rod-shaped tellurium nanoparticles and their bactericidal activities. *Mater Res Bull* 47:3719-3725
- Zare B, Sepehrizadeh Z, Faramarzi MA, Soltany-Rezaee-Rad M, Rezaie S, Shahverdi AR (2013) Antifungal activity of biogenic tellurium nanoparticles against *Candida albicans* and its effects on squalene monooxygenase gene expression. *Biotechnol Appl Biochem* 61: 395-400
- Zeng H (2009) Selenium as an essential micronutrient: roles in cell cycle and apoptosis. *Molecules* 14:1263-1278
- Zhang JS, Wang XF, Xu TW (2008) Elemental selenium at nano size (nano-Se) as a potential chemopreventive agent with reduced risk of selenium toxicity: comparison with Se-methylselenocysteine in mice. *Toxicol Sci* 101:22-31
- Zheng D, Hu C, Gan T, Dang X, Hu S (2010) Preparation and application of a novel vanillin sensor based on biosynthesis of Au-Ag alloy nanoparticles. *Sensors Actuat B Chem* 148:247-252

Zheng JS, Zheng SY, Zhang YB, Yu B, Zheng WJ, Yang F, Chen TF (2010) Sialic acid surface decoration enhances cellular uptake and apoptosis-inducing activity of selenium nanoparticles. *Colloid Surf B Biointerfaces* 83:183-187

Media and Buffer composition

NaCl Tryptone Yeast Extract (NTYE)	g/L	Modified Popescu et al. (2009)	g/L
Solar Salt	250	Sodium Chloride	200
Potassium Chloride	5	Potassium Chloride	20
Magnesium Sulfate	20	Magnesium Sulfate	10
Yeast Extract	3	Magnesium Chloride	30
Tryptone	5	Calcium Chloride	0.2
		Yeast Extract	5
Salt Water Yeast Extract (SWYE)	g/L	Zobell Marine Broth 2216	g/L
Sodium Chloride	194	Peptic digest of animal tissue	5
Magnesium Chloride	16	Yeast extract	1
Magnesium Sulfate	24	Ferric citrate	0.1
Calcium Chloride	1	Sodium chloride	19.45
Potassium Chloride	5	Magnesium chloride	8.8
Sodium Bicarbonate	0.2	Sodium sulphate	3.24
Sodium Bromide	0.5	Calcium chloride	1.8
Yeast Extract	5	Potassium chloride	0.55
		Sodium bicarbonate	0.16
Halophilic Broth (Himedia M591)	g/L	Potassium bromide	0.08
Sodium Chloride	250	Strontium chloride	0.034
Caesin acid hydrolysate	10	Boric acid	0.022
Yeast Extract	10	Sodium silicate	0.004
Proteose peptone	5	Sodium fluorate	0.0024
Trisodium citrate	3	Ammonium nitrate	0.0016
Potassium Chloride	2	Disodium phosphate	0.008
Magnesium Sulfate	25		
Popescu et al. (2009)	g/L	Nutrient Broth amended with 2% NaCl (NB + 2% NaCl)	g/L
Sodium Chloride	175	Peptone	10
Magnesium Chloride	50	Beef extract	10
Potassium Sulfate	5	Sodium chloride	5+20
Calcium Chloride	0.1		
Yeast Extract	5		

Appendix I

3.5% NTYE	g/L
Sodium Chloride	35
Potassium Chloride	5

Magnesium Sulfate	20
Yeast Extract	3
Tryptone	5

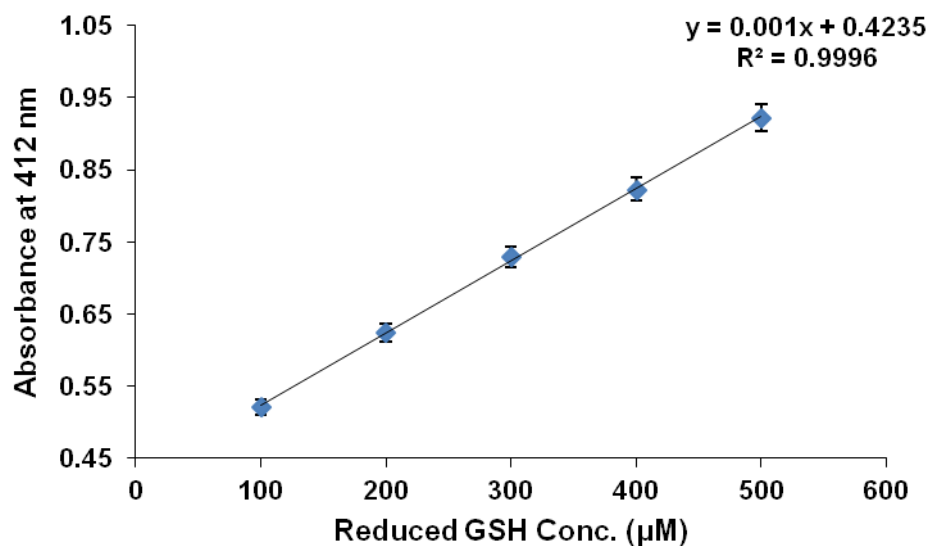
Cell lysis buffer	-/L
0.1 % Triton X-100	0.01 ml/L
1 mM EDTA	0.292 g/L
1 mM PMSF	0.174 g/L
20 mM Tris-HCl	3.152 g/L

Transfer buffer (for WB)	g/L
25 mM Tris-HCl	3.02
192 mM Glycine	14.4
10% Methanol	100

TN buffer	g/L
50 mM Tris	7.88
4 M NaCl	233.76

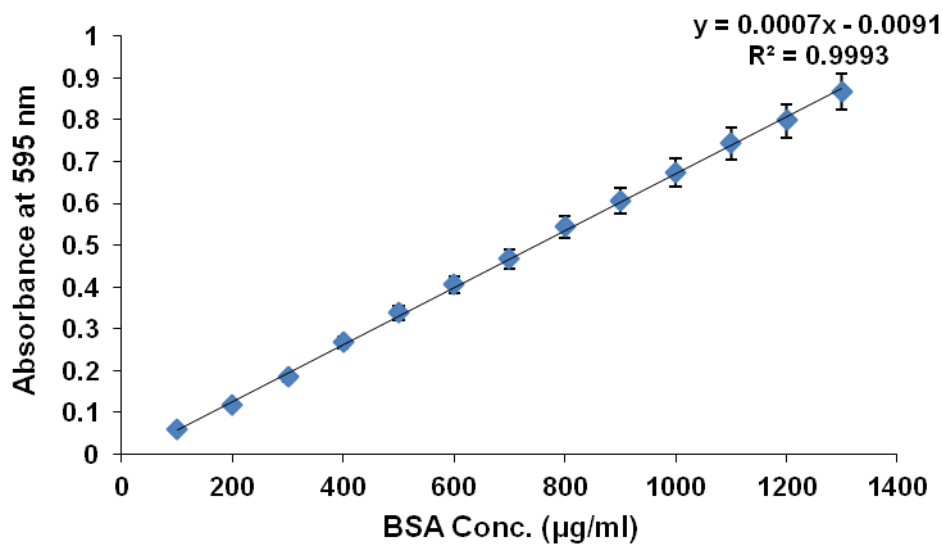
TBST buffer (for WB)	-/L
Tris	2.4 g/L
NaCl	8.8 g/L
Tween-20	0.1 ml/L

Calibration curve of reduced glutathione (GSH) for estimation of thiols in *Halococcus salifodinae* BK3 and *H. salifodinae* BK6

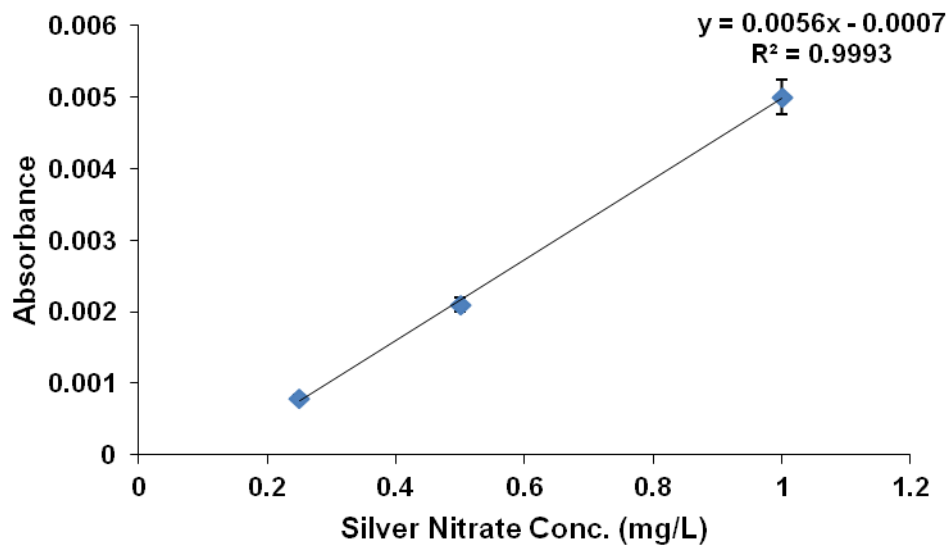


Values are mean \pm (standard error) for three independent experiments.

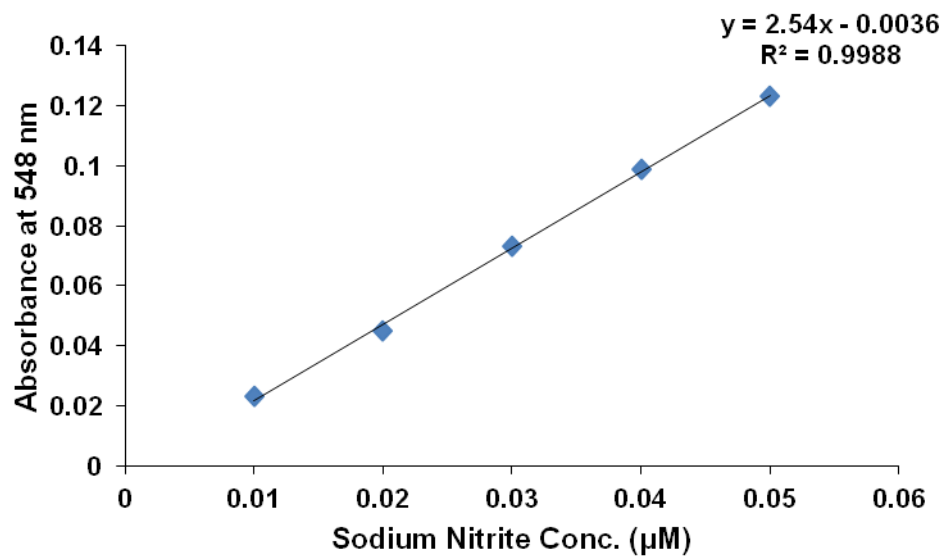
Calibration curve of bovine serum albumin (BSA) for estimation of proteins by Bradford's method (Bradford, 1976)



Values are mean \pm (standard error) for three independent experiments.

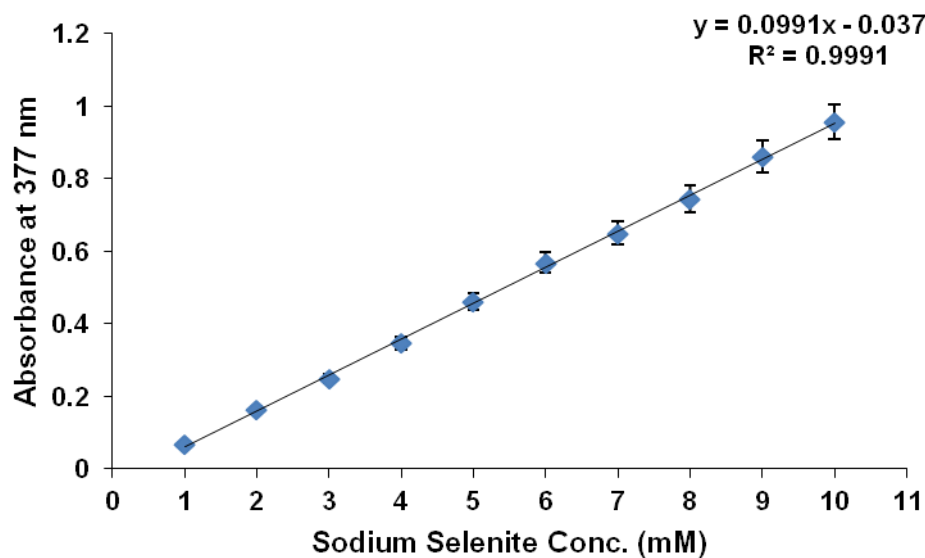
Calibration curve of silver nitrate (AgNO₃) for estimation of Ag by FAAS

Values are mean \pm (standard error) for three independent experiments.

Calibration curve of sodium nitrite for estimation of nitrite concentration

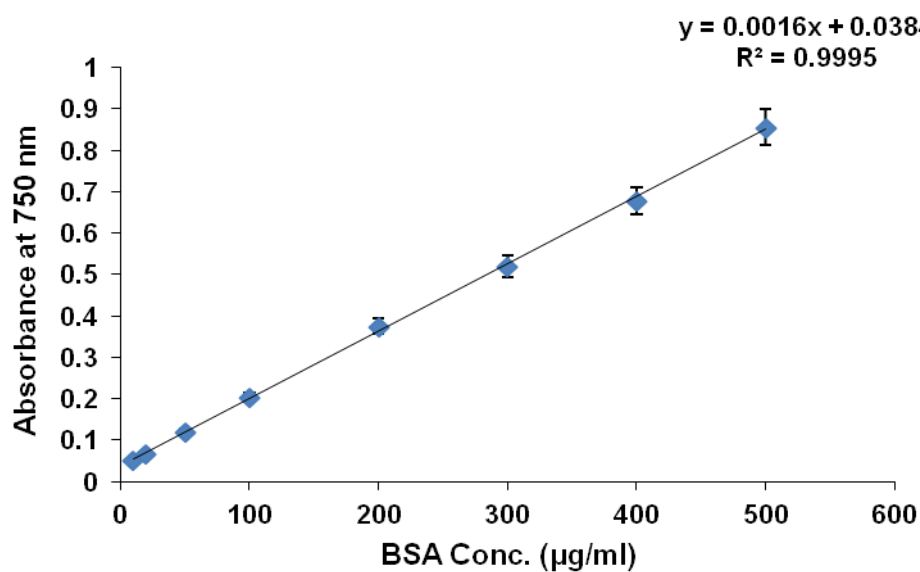
Values are mean \pm (standard error) for three independent experiments.

Calibration curve of sodium selenite for estimation of selenite using 2,3-diaminonaphthalene
(2,3-DAN)



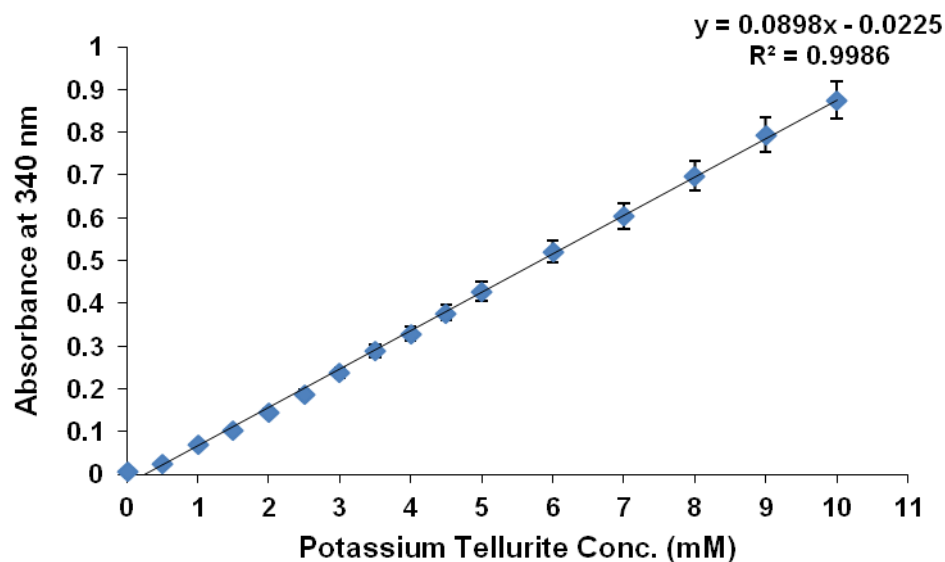
Values are mean \pm (standard error) for three independent experiments.

Calibration curve of BSA for estimation of protein concentration in cell lines by Lowry's
method



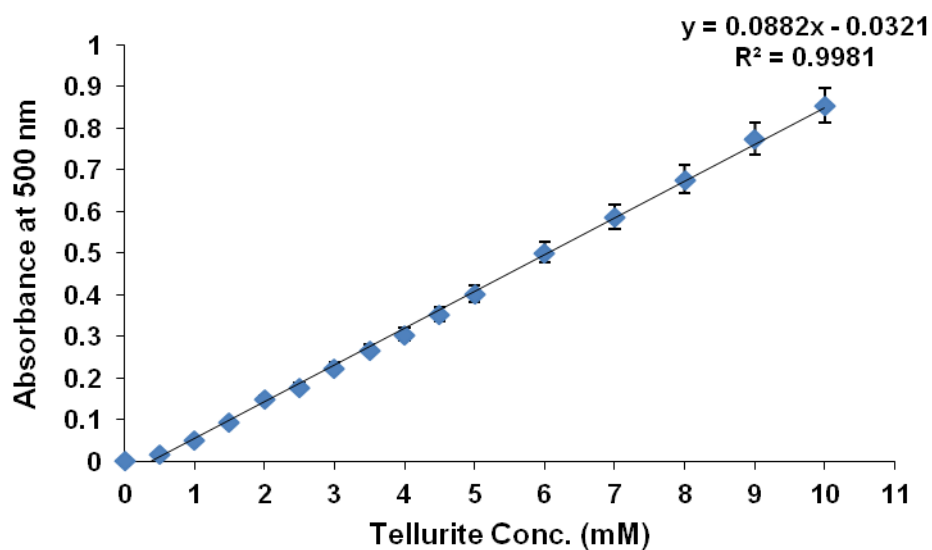
Values are mean \pm (standard error) for three independent experiments.

Calibration curve of potassium tellurite (K_2TeO_3) for estimation of tellurite using diethyldithiocarbamate (DDTC)

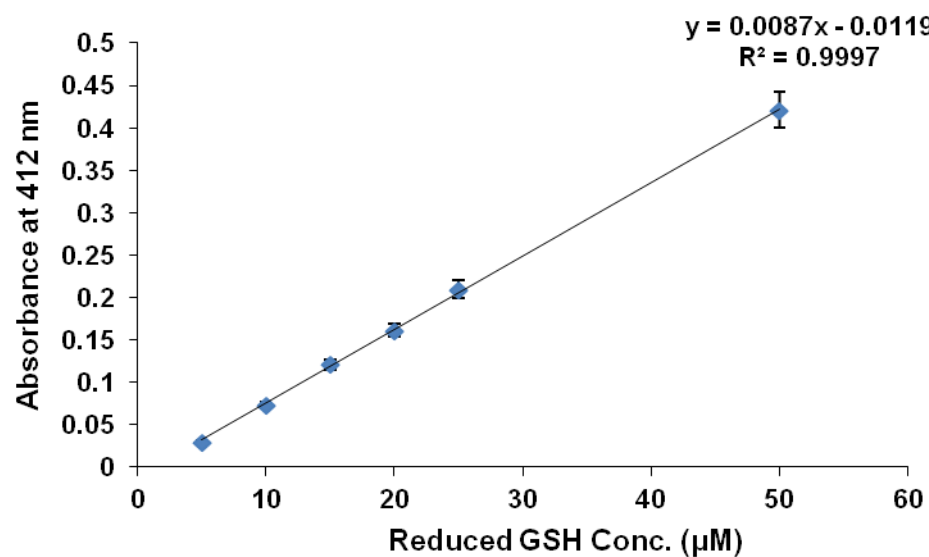


Values are mean \pm (standard error) for three independent experiments.

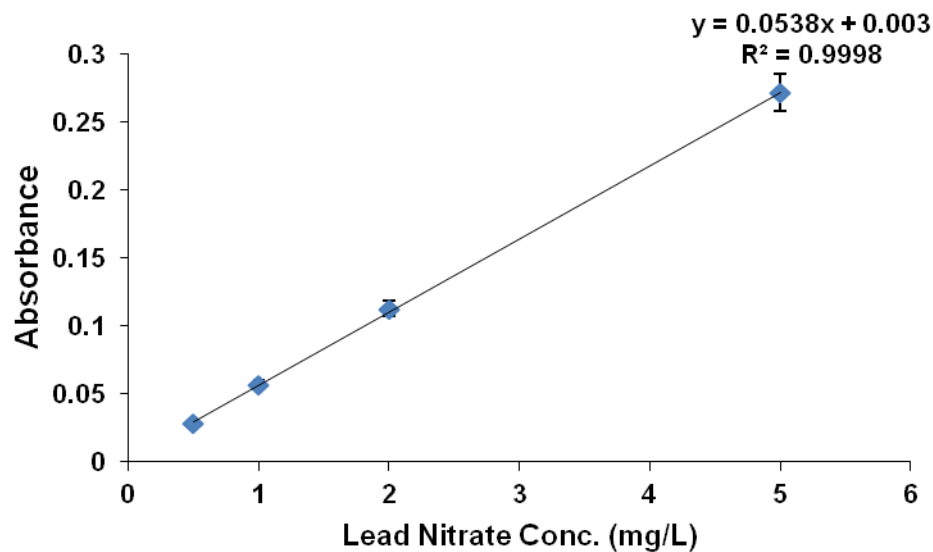
Calibration curve of reduced tellurium for estimation of TeNPs yield



Values are mean \pm (standard error) for three independent experiments.

Calibration curve of reduced GSH for estimation of thiols in *Idiomarina* sp. PR58-8

Values are mean \pm (standard error) for three independent experiments.

Calibration curve of lead nitrate ($\text{Pb}(\text{NO}_3)_2$) for estimation of Pb(II) by FAAS

Values are mean \pm (standard error) for three independent experiments.

LIST OF PUBLICATIONS

Publications related to this thesis

1. **Pallavee Srivastava** & Meenal Kowshik, Mechanisms of Metal Resistance and Homeostasis in Haloarchaea, *Archaea*, doi.org/10.1155/2013/732864, 2013.
2. **Pallavee Srivastava**, Judith Braganca, Sutapa Roy Ramanan, Meenal Kowshik, Synthesis of silver nanoparticles using haloarchaeal isolate *Halococcus salifodinae* BK3, *Extremophiles*, 17(5):821-31, 2013.
3. **Pallavee Srivastava**, Judith Braganca, Sutapa Roy Ramanan, Meenal Kowshik, Green synthesis of silver nanoparticles by haloarchaeon *Halococcus salifodinae* BK6, *Advanced Materials Research*, 938:236-241, 2014.
4. **Pallavee Srivastava**, Judith Braganca, Meenal Kowshik, *In-vivo* synthesis of selenium nanoparticles by *Halococcus salifodinae* BK18 and their anti-proliferative properties against HeLa cell line, *Biotechnology Progress*, 30(6): 1480-1487, 2014.
5. **Pallavee Srivastava**, Edarapalli V R Nikhil, Judith Braganca, Meenal Kowshik, Anti-bacterial TeNPs biosynthesized by haloarchaeon *Halococcus salifodinae* BK3, *Extremophiles*, 19(4):875-884, 2015.
6. **Pallavee Srivastava**, Meenal Kowshik, Biosynthesis of nanoparticles from halophiles. In: Dinesh K. Maheshwari, Meenu Saraf (Eds), **Halophiles: Biodiversity and sustainable development**, Vol. 6, pp: 145-159, Springer International Publishing, Switzerland, 2015. (Book Chapter)
7. **Pallavee Srivastava**, Meenal Kowshik, Anti-neoplastic selenium nanoparticles from *Idiomarina* sp. PR58-8, *Enzyme and Microbial Technology*, 2016. DOI:dx.doi.org/10.1016/j.enzmictec.2016.08.002

Other publications:

1. Kshipra Naik, **Pallavee Srivastava**, Ketaki Deshmukh, M Monsoor S, Meenal Kowshik, Nanomaterial-based approaches for prevention of biofilm-associated infections on medical devices and implants, *Journal of Nanoscience and Nanotechnology*, 15:10108-10119, 2015.

LIST OF WORKSHOPS AND CONFERENCES ATTENDED

1. **Pallavee Srivastava**, Judith M. Braganca and Meenal Kowshik (2012) *In vivo* synthesis of silver nanomaterial by haloarchaeon (**Poster presentation** at International Conference on Supramolecules and Nanomaterials- Research and Applications ICSNA- 2013, Ahmedabad, Gujarat, 6th- 8th February, 2012) organised by Dept. of Chemistry, Gujarat University and GUJCOST, DST (Govt. of Gujarat), India.
2. **Pallavee Srivastava** and Meenal Kowshik (2012) Biosynthesis of silver nanoparticles by halophilic archaeon. (**Oral Presentation** at UGC Sponsored National Seminar, Nanomaterials: Synthesis, Characterisation and Applications during 2nd and 3rd February, 2012) organised by Department of Chemistry, Smt. Parvatibai Chowgule College of Arts and Science, Margao – Goa.
3. Attended the International Conference on Nanoscience and Technology (ICONSAT-2012) held in Hyderabad during January 20-23, 2012.
4. **Pallavee Srivastava**, Judith M. Braganca, Sutapa Roy Ramanan Meenal Kowshik (2013) Green synthesis of silver nanoparticles by haloarchaeon *Halococcus salifodinae* BK6 (**Oral presentation** at International Conference on Nano Materials: Science, Technology and Applications, ICNM'13, Chennai, Tamil Nadu), organised by B.S. Abdur Rahman University, India, Deakin University, Australia and Universiti Teknologi MARA, Malaysia from 5th-7th December, 2013.
5. **Pallavee Srivastava**, EVR Nikhil, Judith M. Braganca, Sutapa Roy Ramanan Meenal Kowshik (2014) Tellurium nanoparticles biosynthesised by haloarchaeon *Halococcus salifodiane* BK3 (**Poster presentation** at Indo-UK international workshop on advanced materials and their applications in nanotechnology (AMAN) at BITS Pilani K K Birla Goa Campus), organised by BITS Pilani K K Birla Goa Campus and University of Leeds, UK, from 17th-19th May, 2014.
6. **Pallavee Srivastava**, Meenal Kowshik (2015) Selenium nanoparticles biosynthesised by marine bacterium *Idiomarina* sp. PR58-8 (**Poster presentation** at the 2nd AMAN at BITS Pilani K K Birla Goa Campus), organised by BITS Pilani K K Birla Goa Campus and University of Leeds, UK, from 11th -12th January, 2016. (Won 2nd prize for poster.)

Brief Biography of the Candidate

Name	Ms. Pallavee Srivastava
Education	M.Sc. (Bio-Medical Genetics), VIT University (2010) B.Sc. (Microbiology, Chemistry), Govt. Coll. of Arts Science and Commerce, Khandola, Goa (2005)
Email	pallavee.srivastava@gmail.com

Work experience:

Ms. Pallavee Srivastava joined BITS Pilani K K Birla Goa campus as JRF, and SRF in the third year, on a Ministry of Earth Science (MoES) sponsored project entitled “**Biological Synthesis of Metal Sulfide and Metallic Nanoparticles using Halophilic Archaeobacteria**” (MoES/11-MRDF/1138/P/10-PCIII), from 28/03/2011 to 31/03/2014. She extended this work to include synthesis of nanoparticles using halophilic bacteria as part of her Ph.D. thesis. She has published 4 research articles; 1 review article; and 1 book chapter as first author in Internal Journals and Publication House. She has also published a review article as second author. She has presented her work at various conferences either as poster or oral presentation. She was the recipient of second prize for her poster entitled ‘Selenium nanoparticles biosynthesised by marine bacterium *Idiomarina* sp. PR58-8’ at the 2nd Indo-UK workshop on Advanced Materials and their Applications in Nanotechnology (AMAN 2016) held at BITS Pilani K K Birla Goa Campus, organised by BITS Pilani K K Birla Goa Campus, jointly with University of Leeds, UK on 11th and 12th January, 2016.

Brief Biography of the Supervisor

Prof. Meenal Kowshik received her M.Sc. in Microbiology from Goa University in 1997. She worked on the biological synthesis of metallic and metal sulphide nanoparticles using yeasts at Agharkar Research Institute, and obtained her Ph.D. degree from Pune University (1999-2003). Subsequently, she joined Birla Institute of Technology and Science, Pilani K K Birla Goa Campus, and is currently working as Associate Professor in the Department of Biological Sciences. Her research interests include studies on bio-functionalisation of silver base nanocomposites for anti-microbial applications; synthesis of bio-compatible nanomaterials for tissue engineering; application of nanomaterials in molecular biology research; interactions of nanomaterials and microorganisms with respect to nanomaterial synthesis as well as toxicity, with special emphasis on halophilic archaeobacteria. She has received research grants from Department of Science and Technology for three projects and one from Ministry of Earth Sciences. She has been a co-investigator on four other projects sanctioned by DBT, DRDO and UGC. She has published 38 research papers in international and national journals of repute; has three patents to her credit and has delivered several invited talks at international and national conferences.